5-28-2021

Integrating vibratory membrane-based water recovery systems for sustainable food and beverage production

Michael Vincent O. Laurio
Rowan University

INTEGRATING VIBRATORY MEMBRANE-BASED WATER RECOVERY SYSTEMS FOR SUSTAINABLE FOOD AND BEVERAGE PRODUCTION

by

Michael Vincent O. Laurio

A Dissertation

Submitted to the
Department of Chemical Engineering
College of Engineering
In partial fulfillment of the requirement
For the degree of
Doctor of Philosophy
at
Rowan University
April 30, 2021

Dissertation Advisor: C. Stewart Slater, Ph.D.

Committee Members:
Mariano J. Savelski, Ph.D.
Kirti M. Yenkie, Ph.D.
Robert P. Hesketh, Ph.D.
Ramon Christian P. Eusebio, Ph.D.

Dedication

For Mom and Dad

Acknowledgments

I would like to acknowledge Dr. C. Stewart Slater, for being my graduate advisor and mentor in my dissertation and for the opportunity to work on this project. He has continuously encouraged me by always challenging me in my research, by being rigorous yet kind and understanding, and by sharing useful academic and life lessons.

I would also like to thank Dr. Kirti Yenkie, Dr. Robert Hesketh, Dr. Mariano Savelski, and Dr. Ramon Christian Eusebio, for sharing their extensive knowledge in guiding my research. I would like to thank the Rowan Engineering Clinic students, Adam Niznik, Sommer Vandergrift, Steven Husar, Carly Jankowski, Jacquelyn Shaeffer, Matt Raaze, Ben Kayhart, Liam Callahan, and David Aguirre, who helped in the experimental work and data gathering. I also thank the Rowan Engineering faculty, staff, and alumni – Dr. John Schmalzel, Kim Johnston, Robert McClernan, and Christian Wisniewski; and Chip Johnson and Landon Graham of New Logic Research, Inc. for all the assistance.

I would also like to thank Nestlé-USA and the U.S. Environmental Protection Agency for the support. I would also like to thank the University of the Philippines Los Baños, and the Engineering Research and Development for Technology, DOST for giving me the opportunity and financial support to pursue my doctoral studies abroad.

Lastly, I would like to thank my family, relatives, and friends, who in one way or another shared their support and encouragement.

Abstract

Michael Vincent O. Laurio
INTEGRATING VIBRATORY MEMBRANE-BASED WATER RECOVERY SYSTEMS FOR SUSTAINABLE FOOD AND BEVERAGE PRODUCTION
2020-2021
C. Stewart Slater, Ph.D.
Doctor of Philosophy

A vibratory nanofiltration (NF) system was investigated for the preconcentration of coffee extracts for soluble coffee production. The simulated coffee extracts studied contained mostly suspended and colloidal organic components that, although were effectively rejected by the NF membrane (>99% turbidity rejection), affected the vibratory NF performance. The vibratory NF operation improved permeate flux, rejection efficiencies, and reduced flux decline from those observed in crossflow (CF) operation. Further, the effects of applied transmembrane pressure (TMP) and vibrational frequency (F) at corresponding displacement (d) were investigated and modeled. A semi-empirical resistance-in-series model was employed to characterize the mass transfer mechanism, osmotic pressure effects, and fouling resistances that affected the vibratory NF performance. Response surface methodology (RSM), in conjunction with a Box-Behnken experimental design, was also employed to develop statistical models and determine optimal operating conditions (TMP = 3.79 MPa, F = 54.7 Hz, d = 3.18 cm). Lastly, scale-up design, economic, and environmental assessment for a 3% feed coffee extract corresponded to a 7-module i84 VSEP filtration system recovering 3.79 x 10^5 L of reusable water per day, a capital cost of $2,100,000 with estimated annual savings of $481,900 per year, a payback period of 10 years, and a potential to reduce the environmental emissions of the process by approximately 40%.

Table of Contents

Table of Contents (Continued)

Table of Contents (Continued)

Table of Contents (Continued)

Table of Contents (Continued)

Table of Contents (Continued)

List of Figures

Figure Page

List of Figures (Continued)

Figure Page

List of Figures (Continued)

Figure Page

List of Figures (Continued)

Figure | Page

List of Figures (Continued)

Figure Page

List of Figures (Continued)

Figure Page

List of Tables

Table Page

List of Tables (Continued)

List of Tables (Continued)

Table | Page

Chapter 1

Introduction

1.1 Background of the Study

Membrane processes are gaining importance in shaping food and beverage industries towards sustainable production. Common among these are conventional crossflow (CF) pressure-driven membrane processes (PDMPs) like microfiltration (MF), ultrafiltration (UF), nanofiltration (NF), and reverse osmosis (RO) that can selectively separate suspended, colloidal, and dissolved components in many food and beverage process streams [1]. These processes operate under mild conditions that also mitigate the effect on food product quality and minimizes operating costs. This advantage makes them suitable in many food applications like microbial removal from alcohol fermentation broths [2], [3], fractionation of dairy products [4], [5], recovery of high-value organic food compounds, and other macromolecules via porous MF and UF membranes [6], [7]; wastewater reclamation from dairy effluents [8], [9], and concentration of syrups [10] via RO membranes; and vegetable oil processing [11]–[13], fruit juice and wine purification [14]–[16], fractionation of dairy products [17], [18], extraction and concentration of sugar solutions [19], [20] via NF membranes. Downstream, these membrane operations increase the potential to reclaim reusable water and recover important food components from process waste streams [21], [22].

One of the potential applications of membrane separation is in the soluble coffee industry, where membrane-based water recovery can potentially address the effects of the production steps on product quality, wastewater generation, and energy consumption. The soluble coffee process is considered water- and energy-intensive, as it consumes large amounts of water to extract coffee components from roasted ground beans into coffee extract solutions; and uses high energy phase-change operations to remove the water to produce the dried powdered soluble coffee product. Essentially, all the water used in coffee extraction and removed from the evaporation and dehydration end up as wastewater that requires treatment. At the end of the process, this is equivalent to about 7.5 of water is used per kilogram of soluble coffee powder [23]. In addition, thermal dewatering operations have several disadvantages associated with the product quality and sustainability index of the soluble coffee industry. During the process, thermal operations degrade the flavor and aroma of soluble coffee by about 70% of that of conventionally roasted coffee due to the losses in phenolic compounds and generation of Maillard reaction byproducts [24]. As such, developments in the soluble coffee industry have, so far, focused on configuring thermal dewatering operations by operating at lower boiling temperatures (vacuum evaporation), or in the absence of heat (freeze dehydration); integrating coffee aroma recovery routes [25]–[27]; and by employing chemical enrichment methods in improving the quality of instant coffee [24]. However, while product quality is essential in soluble coffee production, the process continues to rely on energy-intensive phase-change separations in its thermal dewatering operations [23]. Currently, the industry shares the highest energy footprint (~15 MJ kg^{-1} soluble coffee) among powdered food and beverage products, with thermal dewatering operations contributing to a considerable fraction of energy consumption [28].

Membrane processes, NF in particular, is a low-energy alternative suitable for water removal and recovery operations in food and beverage processes. The membrane process has been investigated in the concentration of apple and pear juices [29], sea buckthorn tea [14], red wine [16], lactic acid whey [18], and alternative sweeteners [30]. When integrated into the soluble coffee process, NF can potentially positively impact sustainable processing. The membrane process has been studied on soluble coffee waste streams for caffeine recovery from spent coffee grounds [7] and decaffeination. [31]. As an alternative to thermal evaporation, NF has also been regarded as an attractive alternative in concentrating coffee extracts prior to spray- or freeze-drying [32], [33]. When integrated as an alternative or supplement to thermal evaporation, membrane processes offer an energy reduction of up to about 30% [10]. However, like most membrane operations, NF is susceptible to concentration polarization and membrane fouling, i.e., the accumulation of solute deposits on or near the membrane surface, resulting in decreased flow through rates and rejection of components [32]. In particular, initial studies on coffee extract concentration using CF NF were observed to have low and unstable permeate fluxes with considerable flux decline, limiting the final coffee extract concentrations to 35% wt/wt [32]. Like most food and beverage streams, coffee extracts are complex streams that contain a variety of foulants – organic, biological, and colloidal solids – that, under poor operating conditions, such as low feed CF velocities, high feed concentrations, etc., cause flux to drastically decline irreversibly, increase operating costs, and reduce membrane lifetime. And while conventional crossflow (CF) configuration can be improved by increasing CF velocities to prevent concentration polarization, membrane fouling may only be alleviated to a limited extent [34], [35]. Overall, when poorly managed, membrane fouling makes NF and other membrane operations inefficient and economically unattractive.

Novel dynamic filtration systems are among the approaches that substantially improve the performance of CF operation by generating surface shear rates at magnitudes substantially larger than those generated in conventional CF systems [8], [35]–[38]. By employing mechanical motion on the membrane support, surface shear rates effectively enhance permeate fluxes while keeping inlet flows and transmembrane pressures (TMP) to a minimum, thus, conserving energy during the operation [38]. The Vibratory Shear-Enhanced Process (VSEP) (New Logic Research, Inc., Minden, NV, USA) is one of the dynamic membrane systems that employ torsional oscillations at resonant frequencies of up to 60 Hz [39]. The oscillatory vibrations impart high membrane surface shear rates (20,000 s^{-1} to 160,000 s^{-1}) that overcome those generated from crossflow velocities (< 30,000 s^{-1}) [40] and considerably reduce membrane fouling [2], [41]. On the other hand, while mechanical vibration at increasing resonant frequencies increase the power consumption of the system by about 2 to 10 times of the pump power requirement, the flux enhancement from higher membrane surface shear rates makes the specific energy demand per volume of permeate recovered more economical than that of CF operation by about 18% [42]. This mechanism is energy-efficient in improving permeate fluxes and separation efficiencies [43], making operating and maintenance costs less expensive [44] than CF operation. In addition, the high-flux operation provides a smaller process design, which positively impacts on lowering investment costs [43]. Further, in terms of design, its space-efficient vertical module design allows scale-up systems to handle larger processing volumes [39]. Among its successes over CF filtration in food, beverages, and drinking water production include the concentration of milk proteins and dairy wastewater treatment [5], [45], clarification and yeast recovery of alcoholic beverages

[2], [3], and water treatment from high salt seawater and freshwater sources [46]–[49]. Overall, when employed for coffee extract preconcentration, the vibratory membrane process can further the potential of membrane-based water recovery alternatives in the soluble coffee process.

1.2 Motivation of the Study

The initiative to propose water recovery options for the soluble coffee industry started with investigations on soluble coffee wastewater reclamation, proposed by Wisniewski et al. [50]–[53]. Accordingly, recovering about 378,500 L of water per day for reuse in the factory cooling tower reduces operating costs for feed water consumption and wastewater treatment and discharge by about 22.5% and impacts 27.8% emission reduction from the current process [51]. A dynamic membrane-based preconcentration of coffee extract to supplement thermal evaporation, explored in this dissertation, is another attractive option that may advance the potential of making the soluble coffee process greener through water reuse, energy reduction, and wastewater minimization. In contrast with thermal evaporation and drying, membrane-based water removal minimizes the damage or loss in the quality of food products [54], [55]. Membrane processes also consume less energy and operating costs as the separation of water is not driven by a phase-change mechanism [10]. More importantly, commercial membranes developed to date have high rejection efficiencies that allow the recovery of water that may be qualified for direct reuse in ancillary plant operations, reducing freshwater consumption and wastewater generation [51], [56]. Base case calculations detailed in Chapter 4 estimate a potential energy reduction of 4.87×10^7 MJ from steam consumption alone when a membrane-based water recovery system is integrated upstream to partially replace thermal evaporation.

However, CF filtration studies on coffee extract filtration observed a strong influence of membrane fouling that limits its implementation [32]. By employing vibratory shear enhancement, this dissertation intends to alleviate fouling and investigate the extent to which the membrane operation can be used for both water recovery and coffee constituent concentration. Currently, there are no studies related to vibratory filtration applications in coffee extract preconcentration. However, soluble coffee wastewater reclamation by vibratory NF indicates a potential flux enhancement of about 4.5 times than that of CF operation [52]. Nonetheless, coffee extracts have considerably higher solids concentration that may affect the vibratory operation to a greater extent than those of process waste streams. Although parallel experimental studies strongly suggest the process fit for this application, the effectiveness of the dynamic vibratory filtration system is still dictated by various membrane separation mechanisms. Such mechanisms may differ greatly between process streams in terms of constituents involved, concentration levels, and the variety of operating constraints that limit process application. Thus, a parametric investigation of the vibratory membrane performance on coffee extract preconcentration is still necessary to establish the suitable operating conditions, like the applied TMP, feed concentration, vibratory settings, etc., as detailed in Chapter 5.

Apart from experimental work, understanding the multiple factors affecting membrane separation can certainly help develop predictive models and incorporate parameters for more realistic scenarios. Preferably, a detailed numerical solution based on the governing momentum and solute mass balance equations with pertinent boundary conditions may be used to model membrane processes [57]. However, this method can be difficult for design purposes due to certain inherent complexities and rigorous computational requirements. More importantly, the unique dynamic nature of the vibratory membrane system impacts more complex fluid flow and mass transport analyses that likely challenges conventional approaches for evaluating the interplay of vibration with other operating factors in predicting performance. Thus, a very limited number of mathematical modeling studies for vibratory membrane systems have been reported to date [58]–[60]. While so far, no universally accepted model exists for describing conventional and dynamic membrane systems, alternative modeling approaches may be employed. One approach proposed in this study (Chapter 6) simultaneously correlated the performance of the vibratory membrane system with osmotic pressure effects, concentration polarization, and fouling resistance. Another approach was employed with the aid of experimental design and statistical analyses by response surface methodology (RSM), as discussed in Chapter 7. In place of detailed parametric studies, RSM is a useful tool not only for correlating a variety of operating factors with membrane performance, but also for process optimization. One way or another, the models developed in this dissertation can be useful in managing membrane fouling in vibratory systems and optimizing and developing alternative approaches for its scale-up. Overall, these alternative techniques can be implemented to promote membrane integration to broader food and beverage sectors, likewise to other industries of significance.

While experimental studies serve to determine the operational aspect of the membrane operation in coffee extract preconcentration, factors beyond parametric evaluation should also be equally considered [51], [61]. For instance, despite flux and separation enhancement, the dynamic operating nature of the vibratory membrane system can impose additional maintenance and higher capital costs [43]. In addition, although the benefits from using the system as a nonthermal dewatering alternative and as a water recovery route present environmental merits, the extent by which the operation can be integrated into the soluble coffee process should balance its economic metrics. This limited information on the environmental and economic impacts of system design prevents the translation of parallel studies on complex systems such as coffee extracts [51]. As a crucial element in sustainable food and beverage production, this dissertation evaluated the potential of integrating the process into soluble coffee production by comparing it with a base case scenario. Chapter 8 demonstrates the benefits and limitations of the vibratory NF process by using laboratory-scale filtration experiments to establish scale-up parameters and operating conditions as bases for economic and environmental assessment.

1.3 Objectives

The general objective of the study is to assess the viability of vibratory nanofiltration as a supplementary operation to thermal evaporation in preconcentrating coffee extracts for soluble coffee production and develop predictive models for its performance. Specifically, this dissertation aims to:

1. Evaluate a base case scenario for soluble coffee production in terms of mass and energy flows, operating cost, and environmental emissions;
2. Assess the performance of crossflow and vibratory nanofiltration operations in concentrating coffee extracts;
3. Determine the effects of operating conditions such as feed coffee extract concentration, applied TMP, and vibratory amplitude on nanofiltration performance;
4. Develop model equations in terms of operating conditions that could predict nanofiltration performance, and mass transfer mechanisms occurring in crossflow and vibratory membrane operations;
5. Determine scale-up parameters for the design and operation of a commercial scale vibratory nanofiltration system; and
6. Perform a techno-economic and environmental assessment of water recovery from an alternative membrane-based coffee extract preconcentration scenario in comparison with current operations.

Chapter 2

Literature Review

This Chapter details the background information in establishing the role of membrane processes in improving the sustainability index of food and beverage industries, particularly the soluble coffee industry. Likewise, in proposing a membrane-based preconcentration, water recovery alternative, this section introduces the role of water usage and water removal in food and beverage production and its implications in energy consumption and wastewater generation. The soluble coffee industry is a water- and energy-intensive process due to the large consumption of water for coffee extraction, which is essentially completely removed via thermal evaporation and freeze- or spray-drying to produce the dried soluble coffee powdered product. In turn, the water removed from the coffee extract ends up as wastewater that requires treatment. The use of membrane technology is gaining importance not only in the water and wastewater treatment industry, but also in food and beverage production. Membrane processes offer several advantages over conventional thermal dewatering methods. It operates under mild operating conditions of temperature and pressure, therefore preserving the functional properties of heat-sensitive food products. As a competitive process, understanding the membrane selection criteria, separation mechanism, and the influence of operating conditions on the performance of the membrane operation is fundamental. However, despite their potential, membrane processes are commonly challenged by concentration polarization and membrane fouling. While several approaches can help minimize membrane fouling, dynamic membrane systems like the vibratory shear-enhanced filtration system investigated in this study are among the most effective. This chapter discusses how module vibrations generate membrane surface shear rates that are considerably higher than those of conventional membrane systems and how these enhance flow-through rates and alleviate membrane fouling. Finally, beyond the improvement in performance from vibratory membrane operations, this Chapter also discusses the various implications of the scaled-up operation, especially when integrated into a process. When integrated into plant operations, it is essential to assess the impacts of the process intensification from a life cycle analytical perspective. Thus, background information on the conduct of life cycle assessment is provided towards the end of this Chapter.

2.1 Water Removal in Food and Beverage Production

Water is essential in food and beverage production. In processing, it is used in cleaning, heat exchange, and flow operations; and as a food and beverage component that initiates various chemical, biological, and enzymatic reactions [62]. Water also has an important role in the quality of food, dictating its longevity and stability that make them available in any part of the world. Dewatering operations do not only serve for this purpose in the food and beverage industry, but fundamentally address the following tasks: size and volume reduction, separation and concentration of food components, and food preservation. In this light, apart from adding water to food and beverages, water removal operations or "dewatering" have become one of the essential stages in food and beverage production. Among several dewatered products, the powdered food and beverage industry is one of the major industries utilizing various dewatering operations. Many food products in the market are found in powdered forms such as milk and cheese, instant tea and coffee, fruit and vegetable juices, wheat flour, ground garlic, and other powdered premixes used as food flavoring. From granular products to fine powdered products, this industry grows tremendously and continually draws off large volumes of water through various dewatering methods.

Figure 1

Generalized Process Flow for Powdered Food and Beverage Production

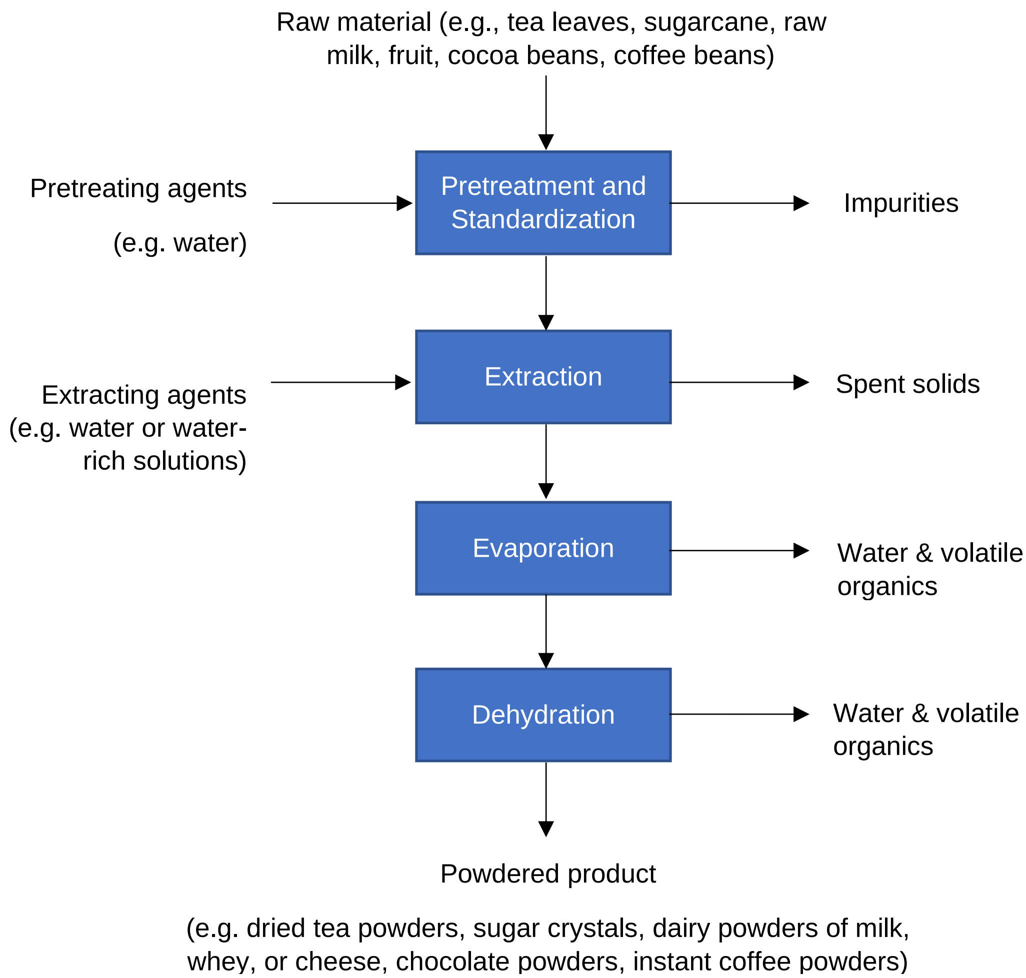

Figure 1 shows a typical process flow for producing powdered food and beverages. In general, the raw materials undergo a series of treatments such as standardization and extraction, heat treatment, and evaporative concentration. Also, the water that is used in stages of pretreatment, purification, extraction, etc., is also removed completely in the last stages. Most food and beverage powder industries rely on spray or freeze dehydration to remove significant amounts of moisture and water.

One important advantage of water removal is on the separation and concentration of food components. Extraction or separation of food components is fundamental for the preparation of ingredients, removal of food impurities, and for the retrieval of high-value compounds, such as essential oils and enzymes [63]. Water in food and beverage production is not only accounted to the water used in the various processing stages, but also in the water content of food. In addition to this, water is used as cleaning agent to remove contaminating materials such as crop residues, soil, or excess fluids; and, in extracting food components such as juice and coffee extracts end up diluting the product. Because of this, dewatering operations are considered common to any food and beverage industry. For example, bulk of the operations in sugar refining are centered on the removal of the water content of the sugar cane juice until the sugar concentration is high enough for solid crystals to form. Similarly, powdered, and concentrated juice extracts, milk, and dairy products, as well as coffee also rely largely on dewatering operations to meet food quality standards.

The water removed from food and beverage products contributes to the reduction of post-processing costs through size and volume reduction. Dried goods such as tomatoes, raisins, mangoes, fish, and beef, as well as powdered products such as milk, spices, sugar, tea leaves, and coffee lose significant amounts of weight from the removal of water content. The mass of dried tomatoes, for example, is only about 5% of the weight of raw tomatoes after removing most of its water content. Mangoes, on the other hand, contain 83% water and is reduced to 10 to 15% before they are exported to different countries. In addition, the shrinkage resulting from the drying of these goods contribute to volume reduction, which results to lesser storage cost. Powdered beverages present more convenience in handling and packaging than those in liquid form because they are easier to contain. Without dewatering, we can say that majority of the cost of packaging, storage, handling, and transportation of these goods may be attributed to their water content alone.

Among the three, perhaps prolonging the shelter life of food and beverages is the most important reason and advantage in dewatering food and beverage products to make them accessible for consumers not only locally, but even for those away from site of production. Though water plays a significant role on the texture, appearance, and flavor of fruits, vegetables, meat, and other products; water also catalyzes the deterioration of quality of food and food products. Moisture increases the potency of food spoilage through chemical, enzymatic, and microbial pathways [64]. These reactions decrease the quality of food and also pose risks of food-borne diseases coming from microorganisms such as molds, yeasts, lactic acid bacteria, *Salmonella, Clostridium botulinum, E. coli*, etc. [65]. However, food spoilage is not solely dictated by moisture as shown in Table 1.

Table 1

Typical Water Content of Some Foods and their Shelf Life

Food	Water (%)	Shelf life (week)	Food	Water (%)	Shelf life (week)
Cucumber	95 – 96	1	Hard cheese	30 - 50	6
Tomatoes	93 – 95	1	White bread	34	1
Cabbage	90 – 92	3	Jam	30 - 35	52
Orange juice	86 – 88	2	Honey	15 - 23	104
Apples	85 – 87	8	Wheat	10 - 13	32
Cow milk	86 – 87	1	Nuts	4 - 7	24
Eggs, whole	74	3	Dried onion	4 - 5	52
Chicken, broiled	68 – 72	3 days	Milk powder	3 - 4	52
Raw fish	60 – 65	1 day	Canola oil	0.1	104

Note: Adapted from Tucker [65]

Most high moisture foods such as fruits, vegetables, juices, and fresh milk deteriorate more easily than honey, wheat, nuts, and powdered milk, thus, showing the relevance of the physical water content of food with shelf life in this context. However, the relation between these two criteria does not mathematically show an inverse proportion. For example, between honey and wheat, it can be observed that honey containing 23% water is perfectly stable than the latter despite having half as high water. The same goes with jam preservatives and powdered milk, which have the same shelf lives despite the observable difference in water content. For intermediate-to-high moisture products, cabbage, despite of having 92% moisture, has longer shelf life than broiled chicken. Cow's milk deteriorates faster than orange juice despite having equal water contents. Relative to the water content of foods, studies have found that preservation is more accurately controlled by the food's water activity, shown in Table 2.

Table 2

Typical Water Activities of Selected Food and Food Products

Water Activity	Products
> 0.95	Fresh fruits and vegetables, milk, meat, fish
0.90 - 0.95	Semi-hard cheeses, salted fish, bread
0.85 - 0.90	Hard cheese, sausage, butter
0.80 - 0.85	Concentrated fruit juices, jelly, moist pet food
0.70 - 0.80	Jams and preserves, prunes, dry cheeses, legumes
0.50 - 0.70	Raisins, honey, grains
0.40 - 0.50	Almonds
0.20 - 0.40	Non-fat milk powder
< 0.2	Crackers, roasted ground coffee, sugar

Note: Adapted from Berk [64]

Water activity is a measure of the percentage of free water available for microbial processes, chemical reactions, or enzyme activity. It is measured as the ratio between the water vapor pressure of food and the vapor pressure of pure water at the same temperature [64], [65]. Under ambient conditions where the food moisture is in equilibrium with air, water activity is also called as equilibrium relative humidity [66]. Solute-water interactions, as well as the pH and temperature of the food also affect the parameter [66]. As temperature increases, water-solute interactions in food become lower that increases the water activity, while the pH dictates the type of microorganisms that thrive on the food material. The ability of micro-organisms to grow on food reduces with decreased water activity. Bacterial growth does not occur at water activity levels below 0.9; for the growth of molds and yeasts, the water activity is between 0.8 and 0.9; and enzymatic reactions require water activity levels of 0.85 or higher. In this light, food and beverage products undergo various water removal operations to maintain a water activity of 0.8 or less to prolong their shelf life.

2.1.1 *Water Removal Methods in Food and Beverage Production*

Water removal operations are fundamental in food and beverage production. These operations may be attained using mechanical operations where water removal is done by physical means; or by thermal operations where water in the food product undergo phase change by thermo-physical factors. Between the two approaches, thermal operations are conventionally practiced in food and beverage production due to the extent of water removal that enable food industries to produce highly concentrated or essentially dried food products. Table 3 lists the common water removal methods used in food and beverage production, as discussed herein.

Table 3

Common Thermal Water Removal Operations in Food and Beverage Production

Water Removal Method	Remarks	Food/Beverage Products
Evaporation	- partial removal of water by boiling liquid food products - relatively expensive and requires large area for operations - may result in thermal damage to product quality, and losses in volatile flavor and aroma components	Concentrated liquid products, e.g., fruit juice, condensed milk, coffee; vegetable pastes, seasonings, and sauces; jams and marmalades
Drying	- complete removal of water from food products	Dried fruits, vegetables, and meat products; salt, bouillon cubes
Freeze-dehydration	- removal of water at relatively low temperatures - achieves extremely low water activity for food preservation - highly expensive	Powdered beverages, e.g., milk, fruit juice, instant coffee; granulated flavor enhancers

2.1.1.1 Evaporation. Evaporation uses heat to partially remove water and other volatile components from bulk liquid foods like milk, fruit and vegetable juices and sugar solutions by boiling off water vapor. This operation is performed in virtue of preservation, size and volume reduction, but most commonly to pre-concentrate food prior to succeeding stages of food processes. For example, in crystallization, a portion of water is removed until the product reaches super-saturated concentration of solute. After which, the super-saturated solution is cooled down until solid crystals of solute are formed. In the coffee process discussed herein, evaporators are used to pre-concentrate coffee extracts from percolators before they are finally dried by spray- or freeze-drying. As a pretreatment operation, evaporation withdraws the largest volume of water among the dewatering operations at about a hundred tons of water per hour [63], [64], [67].

As an industrial operation, evaporation consists of three functional sections: a heat exchanger to transfer heat from a hot fluid, commonly steam, to the food extract; an evaporator section where water from the food extract is converted to vapor; and vapor separator where water vapor leaves and passes off to a condenser or other equipment [65]. A large factor considered in the design of evaporators is dictated by the latent heat of vaporization, i.e., the amount of heat needed by water in a solution for it to be converted into vapor phase. In its simplest sense, evaporation can be done under atmospheric conditions and at standard boiling point in an open pan. However, the increase in concentration of solids during evaporation tend to increase the boiling point of water; and the stagnant films generated from viscous flow further aggravates the heat requirement and economy of the operation. Attention to the design and operation of the equipment, as well as careful planning of energy use are employed to substantially improve the economics of evaporation. One effective approach is by multi-stage evaporation where the vapor is reused as heating medium for succeeding stages [65]. Thermocompression of vapor in which water vapor from a single-effect is adiabatically compressed and reused as heating agent, has also improved the energy efficiency of the operation by up to 90% [64]. Different types of evaporators have also been designed for various total solids concentrations, as shown in Table 4.

Table 4

Typical Total Solids Concentrations for Various Types of Evaporators

Evaporator Type	Total Solids Inlet (% w/w)	Total Solids Outlet (% w/w)
Vacuum pans	60 - 70	80 - 85
Shell and tube, multistage		
Rising film	5 - 25	40 - 75
Falling film	5 - 25	40 - 75
Plates, multistage	5 - 25	40 - 75
Wiped/thin film	40 - 50	70 - 90
Centrifugal thin film	5 - 25	40 - 60

Note: Adapted from Santonja, et al. [68]

Evaporators vary as shell and tube, plate, or thin-film types. Shell and tube evaporators consist of a vessel or shell that contains a bundle of tubes, where a thin film of feed liquor is introduced, while being heated by steam supplied at the shell side of the evaporator. This type of evaporator is suitable for moderately viscous fluids or for heat-sensitive streams such as dairy products, syrups, fruit juices, and can achieve a desired concentration of up to 40 - 75% solids by weight. These are also suitable for large-scale production, with limited floor space requirement. On the other hand, plate evaporators consist of evenly space plates in which thin film of feed liquor and steam are introduced alternately. Climbing films, falling films, or a combination of both are employed to meet the production rate and the desired degree of concentration. Unlike shell-and-tube evaporators, plate evaporators have higher heat transfer coefficients and are suitable for heat-sensitive foods of higher viscosity (0.3 - 0.4 N s m^{-2}), e.g., yeast extract, coffee extract, milk, whey protein, pectin and gelatin concentrates, high-solids corn syrups, liquid egg, fruit juice concentrates, and meat extracts [64]. They can also be used as final evaporators for pre-concentrated feeds such as fruit purees and vegetable oils. Lastly, wiped-film evaporators are designed with high-speed rotors or agitators to keep the film thickness between 0.25 mm to 1.25 mm while being heated through a jacket of steam or hot oil. The thin film promotes higher heat transfer rates than the latter evaporator types, while the agitation also prevents the feed from burning onto the hot surface. Thinner films (~ 0.1 mm) are also produced in centrifugal evaporators, in which the liquor is fed from a central pipe to the undersides of rotating hollow cones [65]. These thin-film evaporators are suitable in handling highly viscous (~ 20 N s m^{-2}) and heat-sensitive fluids that are susceptible to foaming, e.g., fruit pulps, tomato paste, honey, cocoa, coffee, and dairy products.

2.1.1.2 Drying. Another dewatering method in the food and beverage industry is drying. In this operation, water is removed by evaporation from a solid or liquid food, with the purpose of obtaining a solid product of sufficiently low water content. Drying is also one of the most effective preservation methods because it reduces the water content, hence water activity of food to a level well below the threshold for microbial growth. In this operation, pre-heated air commonly acts as the drying medium, employed by convection, conduction on heated surfaces, or by alternative heating methods through radiation or dielectric heating, as listed in Table 5.

Table 5

Typical Drying Methods Used in Food and Beverage Production

Drying Method	Operating Temperature (°C)	Initial Moisture (%)	Final Moisture (%)	Food Applications
Solar drying	-	-	-	Fish, tomatoes, raisins, apricots
Contact drying				
Roller drum drying	-	-	-	Gelatin, potato powder, infant foods, corn syrup
Vacuum drying	-	-	-	Chocolate crumb, juices, meat extract, fruit pieces, vegetable extracts
Hot air drying				
Bin drying	40 - 45	10 - 15	3 - 6	Vegetables
Tray drying	60 - 80		15 - 20	Fruits and vegetables
Belt drying		50 - 60	10 - 15	Breakfast cereals, biscuits
Trough drying		50 - 60	15 - 20	Peas, diced fruits and vegetables
Rotary dryers	-	-	-	Sugar, cocoa beans, nuts
Fluidized bed drying	50 - 140 50 - 70	 ~25%	 12 - 15%	 Cereal grains and oil seeds Sugar production, peas, sliced/diced fruits and vegetables, extruded foods, powders
Pneumatic drying	-	Free moisture	-	Gravy powder, potato powder, soup powder, flour
Spray drying	40 - 250	40 - 60	0.4	
	130 - 240			Powdered milk
	< 60			Herbs production
	40 - 80			Decaffeinated coffee
	250			Instant coffee

Note: Adapted from Berk [64]

Simplest among the drying methods, are solar or sun drying and contact drying. Solar drying is the oldest method that dehydrates food products by direct solar radiation. This method is commonly applied to fish in most tropical regions, but is also practiced on fruits such as raisins, and tomatoes. Contact drying is a food dehydration method that uses conduction to transfer heat using drums or rollers. Though simple, these methods are characterized by the high drying time and heat transfer areas that limit them on small-scale operations. Larger scale food and beverage industries rely on hot air drying, in which, air is indirectly preheated via fin tube heat exchangers, or directly using combustion gases into the dryer. In this operation, hot air is blown into the drying chamber in four modes: parallel or co-current, counter-current, center-exhaust, and crossflow. This method is suitable for coarse-to-fine sized solid foods, but may also be employed to dehydrate liquid beverages into powdered form [65]. In one configuration, pre-heated air pass through food materials contained in meshed bins, trays, troughs, or belt conveyors. These dryers are often used in coarse products such as fruits and vegetables, breakfast cereals, and biscuits.

Agitation and fluidization increase the drying rate especially for small-to-fine food products by use of rotating drums, fluidized beds, and pneumatic dryers [69]. Rotary drum dryers consist of cylindrical shells that rotate at 4 to 5 rpm while the heated air and food is fed to the unit. The rotation improves drying by exposing higher surface areas, resulting in lower drying time. Grains, flours, cocoa beans, sugar, and salt crystals are among the food materials dried in rotary dryer. On the other hand, in fluidized bed dryers, pre-heated air is blown through a bed of food material at high velocities, causing them to be suspended or fluidized. This type of drying method is highly suitable for small, particulate foods (about 20 μm to 10 mm in diameter) such as grains, herbs, peas, beans, coffee, sugar, yeast, desiccated coconut, extruded foods, and tea. Fine food particles such as flour and grains may also be dried in pneumatic systems (or pneumatic dryers) that employ a stream of hot, dry air. Overall, the products subjected in these systems are found to dry rapidly because of the efficient heat and mass transfer, thus making this method highly suitable for large-scale drying applications.

Powdered beverages formed from liquid beverages and food extracts, e.g., milk, fruit juices, coffee, etc., are produced via spray drying. Solutions or slurries go through an atomizers or spray nozzles that disperse the fluid into small droplets. The atomizers are pressure nozzles operating at 700 kPa to 2000 kPa with fluid velocities ranging from 50 m s^{-1} to 200 m s^{-1} before they are released into large drying chambers [69]. The sudden change in volume between the nozzle and the drying chamber results to the dispersion of small droplets at about 10 μm to 200 μm in diameter. At this size, the effective surface area for heat and mass transfer increases, thus drying the food at significantly faster rates, hence short drying time (1 s to 30 s) that reduces thermal damages on food even at 250 °C to 300 °C [67], [69]. Thus, spray dryers are highly suitable for heat-sensitive food components or high-value ingredients that are unstable or volatile during thermal processing. These products include flavors, lipids, carotenoids, and nutritive products such as probiotics, anti-oxidants, and bioactive products [70].

2.1.1.3 Freeze Dehydration. Freeze dehydration, or freeze drying, is the removal of water via sublimation from a frozen material under high vacuum. This operation involves three stages: pre-freezing the food in a chamber under vacuum (about 611.73 Pa and 0.01 °C); primary drying through the sublimation ice crystals leaving the food dry; and secondary drying of residual moisture via desorption [54]. In the absence of heat, this drying and preservation method is widely applied to heat-sensitive biological materials. In the food industry, freeze drying is employed to concentrate aroma-rich liquid beverages, including fruit juices, coffee, tea, and selected alcoholic beverages [65]. Due to the low-temperature operation, thermal damages and losses of volatile aroma are completely avoided. This advantage makes freeze dehydration competitive over thermal approaches like evaporation and drying, with food applications ranging from coarse to fine food materials, and from highly viscous to dilute food solutions as well. However, among water removal operations, freeze drying is the most expensive in terms of capital and operating costs associated to the energy requirement. Freeze drying methods require twice as much the energy used in conventional drying method that increases costs by four to eight times. As a result, currently, it is only feasible in the case of high added-value products and whenever the superior quality of the product justifies the higher production cost [65].

2.1.2 *Thermal Losses from Conventional Water Removal Operations*

Dewatering operations are indispensable in any food industry because of their importance in food product quality in terms of concentration, preservation, and handling. However, most of the dewatering methods commonly employ heat, which can contribute to thermal damage and loss of food components. Physical and chemical changes on the appearance, composition, and taste of food products from Maillard browning, pigment losses, loss of fresh taste, and protein denaturation, have been reported to affect food quality [65]. In addition to thermal damage is the loss of volatile flavor components that affect the aroma, fragrance, or essence of the food product. For example, the aroma of coffee is completely lost after 15% of water from coffee extracts is evaporated [69]. The same goes with grapes, plums, peaches, apricots, strawberries that lose significant amounts of volatile aroma and flavor when about 50% to 80% of the juice is evaporated. Hot air drying, on the other hand, result to food shrinkage, poor rehydration, and unfavorable effects on color, texture, flavor, and most importantly, nutritive value are still likely to occur [71]. These effects become more significant at higher concentrations, thus presenting a huge disadvantage of evaporation in food processes. Though thermal damage may be drastically reduced by operating at low temperature and under vacuum, this approach results in longer residence times and larger heat transfer areas. While freeze-drying has been found to be an alternative in removing water without the risks of thermal damages, its application is only limited to high-value food and biological products due to its relatively higher costs. At present, 85% of food industries still rely on convective drying methods, and all these industries rely on evaporation as pre-concentration method [72].

2.1.3 *Energy Consumption of Conventional Water Removal Operations*

The energy consumption of evaporation, drying, and freeze dehydration is arguably one of the factors that influence food and beverage processes. In 2007, the U.S. Environmental Protection Agency reported that the food and beverage industry is fifth among the top industrial consumers with 59% of usage associated to energy-intensive process heating and drying operations [28], [73]. As shown in Figure 2, more than half of the energy consumption in food industries are those required by manufacturing processes. Boilers, which are used to generate steam for supplying process heat to different unit operations such as sterilization, pasteurization, evaporation, and dehydration share about one third of the total energy consumption of food industries [28]. Cold operations such as freezing consume 16% of energy used in food processes, while only 12% is consumed by motor drives related to mechanical operations.

Figure 2

Energy Consumption of End Users in the Food Industry

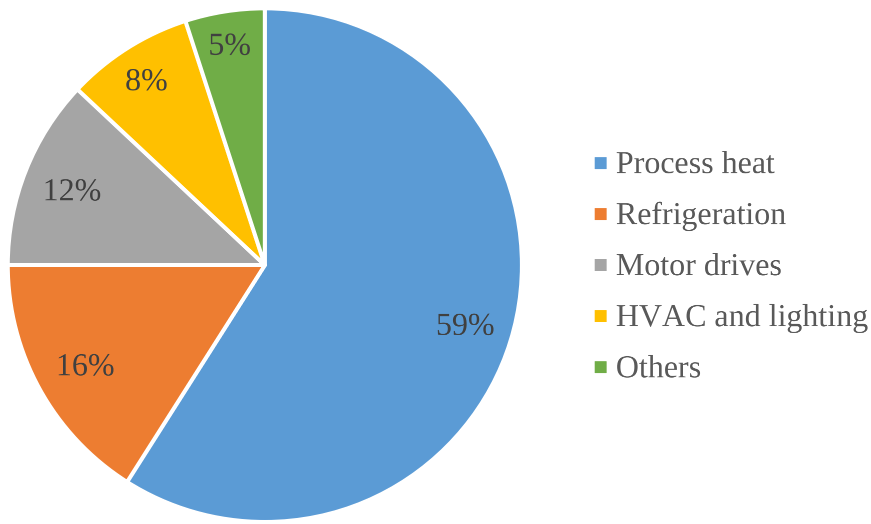

Note: Adapted from Compton et al. [73]

Despite the limited data on the fraction of energy consumed by dewatering operations in food and beverage production, thermal removal of water by phase change has always been regarded as energy intensive. Apart from the sensible heat required to increase the temperature of the food, additional heat is also required to overcome the latent heat of water for it to undergo phase change from liquid to vapor phase [69]. This explains why thermal dewatering operations considerably consumes larger energy than electro-motors and pumps.

Apart from the heat requirements, the energy efficiency of these operations also dictate the overall energy consumption of water removal. For example, the energy efficiency of drying can be as low as 40% as shown in Table 6.

Table 6

Energy Efficiency of Industrial Dryers

Dryer Type	Energy Efficiency (%)
Tray, batch	85
Tunnel	35 - 40
Spray	50 - 56
Conveyor	40 - 60
Fluidized bed, standard	40 - 80
Drum	85
Rotary	75 - 90
Vacuum Rotary	< 70
Freeze	< 10

Note: Adapted from Vaishampayan & Costa [74]

As shown, for spray drying which is commonly used in powdered food production, with only 50% - 56% energy efficiency, 44% of the heat supplied ends up as waste heat [69], [74]. For freeze dryers, 90% of energy supplied ends up as waste heat. Drying alone has been found to consume 20% - 25% of the energy used by the food processing industry or 10% - 25% of the energy used in all industries in developed countries, and 8% of global consumption [75]. With an approximated energy requirement of 8,110 kJ per kilogram of water evaporated, the energy consumption for drying is significantly higher than the heat of evaporation of water at standard temperature and pressure, which is only at 2,500 kJ kg^{-1} [76]. As a result, pre-concentration steps usually precede dehydration processes to partially remove water from wet food by evaporation until it reaches a concentration at which drying operation is economical.

As a preconcentration step, evaporation has lower energy consumption per volume of water removed. A single effect evaporator has an estimated energy requirement ranging from 2,600 kJ kg^{-1} to 3,100 kJ kg^{-1} water removed but with the consideration of multiple effect evaporation and vapor recompression, the energy requirement averages to 2,700 kJ kg^{-1} and can further be reduced to 260 kJ kg^{-1} to 310 kJ kg^{-1} with additional capital cost consideration [77]. However, in general, the volume of water removed via evaporation is greater than that of drying. Also, the additional water that is used in several stages of processing like cleaning, pretreatment, or as extracting agent increase the volume of water to be dewatered in a later stage. In wet milling of corn, for example, the evaporation of steepwater, i.e., water from extraction of starch, gluten, and other components, consumes approximately 18% of energy, while the combined energy used in dewatering and drying of starch consumes 30% [78]. In sugar production, the pretreatment stages of cleaning and extraction dilutes the sugar content of the juice to as low as 7% which is then concentrated to 60% prior to crystallization. After sugar crystals are obtained, additional water is used to separate it from impurities before it is further dried down to a moisture of 0.5 to 2%. At around 430 kJ/kg cane processed, evaporation alone consumes approximately 24% of energy in sugar milling [79]. For dairy and feed powders that utilize vacuum evaporation and spray drying, energy requirements ranging between 6,000 to 20,000 kJ kg^{-1} of product has been reported [80]. These findings show that even at a lower energy consumption, given the volume of water evaporated, this operation is still considered energy intensive.

In gaining an insight on how thermal dewatering operations impact energy consumption in food production, Figure **3** compares the energy used in dried and concentrated food products against those that did not undergo dewatering.

Figure 3

Energy Requirement of Selected Dried Food Products and Concentrated Beverages

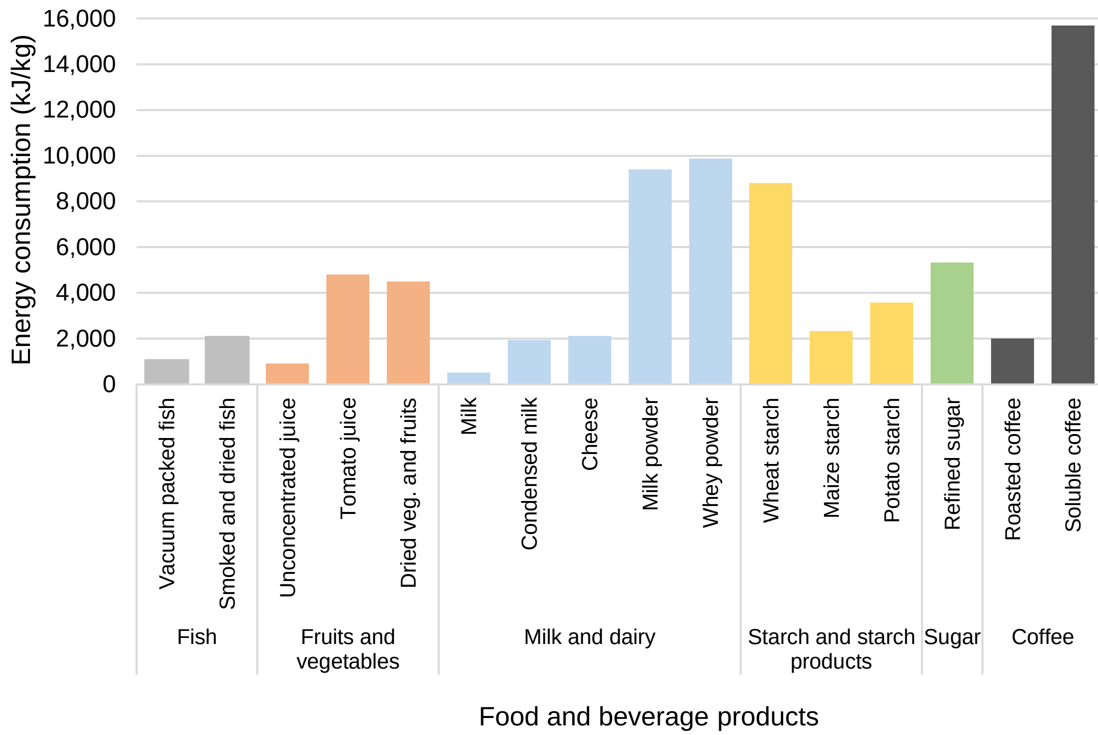

Note: Adapted from Wang [28]

As shown in the Figure, the energy consumed in drying and concentrating food and beverage products may range from about 2,000 to more than 10,000 kJ kg^{-1} depending on the type of product [28]. Dried fish, for example, has the lowest energy consumption of about 2,077 kJ kg^{-1} of product but is twice the energy consumed in vacuum-packed refrigerated fish products. Higher difference is observed between unconcentrated juice

(900 kJ kg^{-1}) and tomato juice (4,789 kJ kg^{-1}), which is concentrated by means of evaporation. The energy requirement of condensed milk (1,936 kJ kg^{-1}) is almost four times higher than that of energy required to process sterilized milk (524 kJ kg^{-1}), while producing milk powders significantly require up to 9,385 kJ kg^{-1} product. Highest among these products is spray-dried coffee which consumes about 15,675 kJ kg^{-1} soluble coffee, which is more than seven times higher than that consumed in roasted coffee production. As will be discussed in the succeeding section, the higher energy demand in soluble coffee production over coffee roasting is attributed to the thermal steps of extracting coffee extract components and removal of water by evaporation and spray- or freeze-dehydration steps.

Overall, water removal is a challenge in the food and beverage industry. Currently most of the common methods of removing water from food and beverages rely on thermal operations, however, these methods entail disadvantages that deteriorates the quality of the final product, as well as the energy efficiency of the food industry. While several modifications have been considered in improving the evaporation and drying of products, most developments, if not costly, are more complex and may still need more research. It is for these reasons that alternative methods to thermal dewatering are being studied and developed. Among the technologies that have potential and are gaining popularity are membrane separation processes, as discussed in the succeeding sections of this study.

2.2 Soluble Coffee Production

Coffee is an important commodity and probably is commonly present in every household, or food establishment nowadays. It is one of the most widespread commodities that is consumed by millions of people on a daily basis. One of the reasons for its demand is its dietary benefits from antioxidants that are claimed to boost the immune system, help prevent cancer, enhance cardiovascular health, etc. [81], [82]. Further, coffee is a popular beverage consumed daily by people for its caffeine value, a stimulant that helps in maintaining alertness and help prevent the onset of tiredness. These several claimed benefits help make coffee the second most traded commodity worldwide, next to oil. With about 145 million bags or 10 million tons of coffee produced yearly, this industry has a global income of about $ 68.5 billion with a total consumer spending of $74.2 billion [83]. Despite this overwhelming demand, the commodity is exported globally as it is only ideally grown in the tropical regions, otherwise known as the "coffee belt". The coffee belt consists of countries along the equator including Central and South America, Southeast Asia, Africa and Arabia, and Australia. The top exporters of green coffee, Colombia exports about 22.8% of green coffee, followed by Brazil that exports 22.4% [84]. In Asia, the top producers of green coffee are Vietnam and Indonesia that shares 10.3% and 6.4% of the global production, respectively [84].

The soluble coffee industry contributes to making coffee available to consumers outside the coffee belt region, and further, globally. Soluble coffee, or "instant" coffee is a green coffee derivative that was processed by brewing coffee beans using hot water, and then dehydrating the coffee extract into powders or granules. As a powdered beverage, instant coffee products are a convenient way to reconstitute the coffee beverage, along with its benefits, in a form that can be easily prepared by dissolving in water. In addition, the ways of distribution of instant coffee beverage products are numerous, ranging from large, family packages to small, one-dose sachets. Recent studies also show that fortification with nutritive components is highly compatible with the reconstitution properties of instant coffee products that further promotes their health benefits [81]. As a result of these advantages, about 15% of the global production of green coffee is shared by the instant coffee industry. This large production allocation equates to about $10.4 billion annual income that is also projected to grow by 5% annually.

2.2.1 *Soluble Coffee Process*

The added health benefits and commercial convenience from soluble coffee products result in its high demand worldwide that drives agricultural production and the soluble coffee industry. In meeting the global demand for soluble coffee products, dewatering operations play an important role in the manufacturing process. The process has four important stages, roasting and grinding, extraction, preconcentration and dehydration [85], as schematically presented in Figure 4. The process starts with the green coffee beans that have been processed after harvest for pulping, hulling, and sorting. The sorted green coffee beans are initially roasted to develop the flavor and aroma of the coffee product. To further release the components influencing the flavor and aroma of the coffee product, the roasted coffee beans are ground into smaller size. This method not only make the surface area of the coffee grounds, but also pretreats them by making soluble solids and volatile substances available for extraction. The ground beans are then processed in percolation batteries where water at 175 °C and under pressure, is passed in several cycles to extract soluble coffee compounds. This step yields coffee extracts with solids concentrations of about 15% to 25% by weight. The coffee extract is then separated from the spent coffee grounds for water removal.

Figure 4

Simplified Soluble Coffee Process Flow Chart

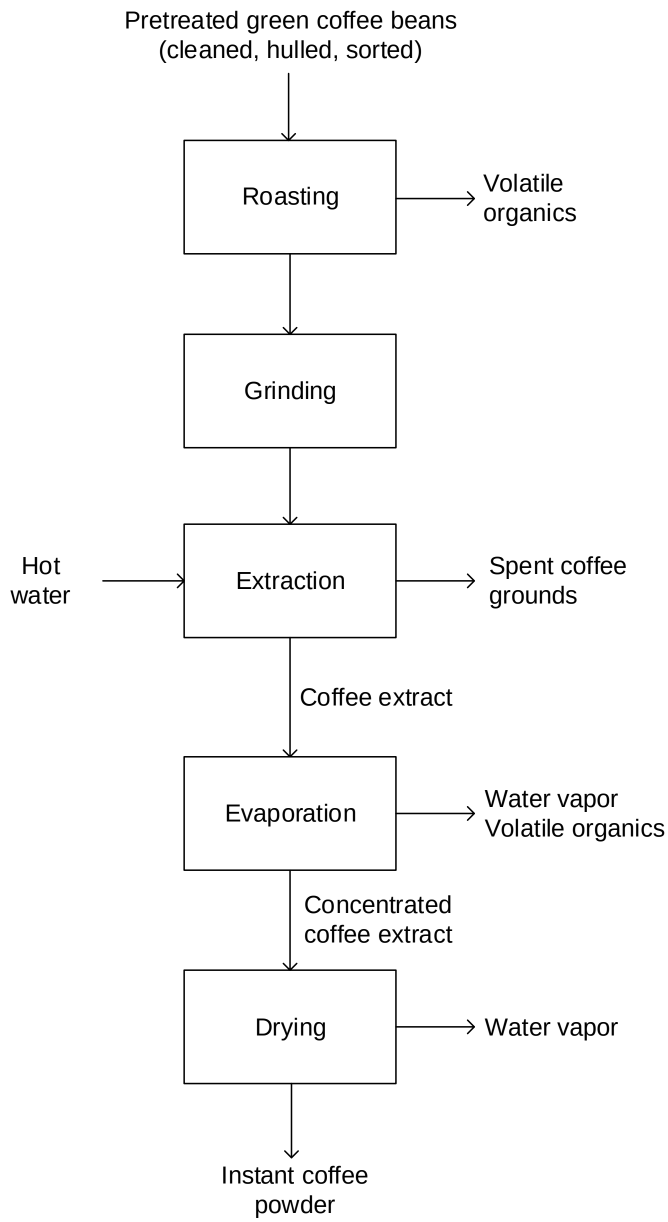

Water removal operations consists of two steps: (a) preconcentration by evaporation and (b) final dehydration by freeze- or spray drying. In the preconcentration step, the extract passes through vacuum evaporators at 50 °C and 7.3 kPa [23] to obtain a more concentrated coffee extract with around 40% to 60% solids by weight [54], [86]. The goal of this step is to reduce the time and energy needed for final dehydration. As a thermal operation, a fraction of the volatile compounds is either lost thermally by evaporation or from Maillard reaction byproducts [24]. These losses can include caffeine, phenolic compounds, chlorogenic acids, and other essential compounds that attribute the appearance, aroma, and taste of coffee [54], [55]. These components are reintroduced in the latter stages of the process to produce the desirable flavor profile [24], [81]. The concentrated coffee extract, then, undergoes final dehydration.

In the final step, two methods of drying are commonly employed by soluble coffee industries: spray drying or freeze drying. Solutions or slurries go through an atomizers or spray nozzles that disperse the fluid into small droplets that facilitates high drying rates, typically resulting in short drying time (1 - 30 s) with reduced thermal damages on food even at 250 - 300 °C [67], [69]. On the other hand, freeze dehydration, or freeze drying, is employed under vacuum at about 611.73 Pa and 0.01 °C to facilitate the removal of moisture from the concentrated coffee extract slurry [54]. In contrast to thermal evaporation, both dehydration methods employ low to freezing temperatures that help reduce deterioration of flavor and aroma. The final product after this step are essentially dried powders at about 2.5% moisture that prevents microbial activity and spoilage [87].

2.2.2 *Water and Energy Footprint of Soluble Coffee Production*

The extensive water and energy use in the manufacture of instant coffee is especially interesting because instant coffee powder finished products contain no water at all. As with any food and beverage process, the water consumed in instant coffee manufacture is directed to various ancillary plant operations such as cooling, steam production, equipment operations, intermediate production steps, and cleaning and sterilization. But, apart from these applications, a large volume of the water used in the process also goes to percolation columns used in extracting the essential components from the coffee grounds. The mass ratio of coffee grounds to water processed in the extraction step is roughly 1:3 [85]. At the end of the process, this is equivalent to about 7.5 kg of water is used per kilogram of soluble coffee powder [23].

Apart from its water consumption, the soluble coffee process is also considered energy-intensive due to the different thermal operations that are employed in the process. As discussed in the previous sections, the soluble coffee production is composed of four important thermal stages: roasting, extraction, concentration, and dehydration. Okada, et al. [23], investigated on the energy consumption and energy efficiencies of these stages in a spray-dried coffee production plant, as shown in Table 7.

Table 7

Consumption and Efficiency of Energy Usage in Spray-Dried Coffee Production

Energy Use	Energy Consumption (kJ kg^{-1} instant coffee)	Energy Efficiency (%)	Conservable Energy from Losses (%)
Overall Energy Usage			
Thermal operations	51,400	56.34	69.5
Electricity	2,720		
Unit Operations			
Coffee roasting	3,720	67.20	46.2
Extraction	8,500	22.12	72.4
Concentration	7,450	82.70	89.0
Spray drying	21,100	36.90	68.0

Note: Adapted from Okada, et al. [23]

As can be seen from the Table, the consumption of energy by thermal operations was much higher than electricity by about 18 times. In the first stage, the energy used for roasting and grinding green coffee beans was found to be the lowest energy consumption in the production process at about 3,720 kJ kg^{-1} instant coffee. On the other hand, the energy used in coffee extraction comes from heating water to 110 °C and was reported to consume 8,500 kJ kg^{-1} instant coffee, while that consumed in pre-concentration of coffee extract by triple-stage vacuum evaporation at 55 °C and 50 mmHg was at 7,450 kJ kg^{-1} instant coffee. The highest energy consumption among the four stages is spray-drying which uses more than 50% of total energy for thermal operations. In the absence of energy conservation measures, it is also shown that not all the energy supplied in soluble coffee production is efficiently used in each stage. In coffee roasting, for example, energy losses have been reported for heat discarded in the air during the processes. On the other hand, the highest energy loss is in coffee extraction because of its low energy efficiency of about 22%, and the residual heat from the steam condensate and spent coffee grounds is not recovered. Next to this, one of the thermal operations with the lowest energy efficiency is spray drying (only about 37%) with energy losses from steam condensate and residual heat discarded in air. The energy efficiency of vacuum evaporation is seen to be improved by employing multi-stage operation. With the use of triple-effect evaporator, the energy efficiency of this pre-concentration step was highest at about 89%.

Conservation measures have been proposed to potentially recover 69.5% of energy losses obtained from these operations. This can be obtained by recovering steam condensates from boiler operations. However, despite the high energy efficiency of the pre-concentration step, the vapors from the evaporator may be condensed but will still have an acidic pH of 3.7. Because of the low pH, the water cannot be used directly in boilers or in other ancillary plant operations, thus generating wastewater that requires treatment before reuse or disposal [50], [52]. This generation further increases the water footprint of the industry. A typical soluble coffee spent wastewater is characterized by low pH, with dark color, influenced by the presence of highly organic components in dissolved and suspended or colloidal forms. Wastewaters such as these are commonly treated to meet municipal sewage treatment requirements, or industrial effluent standards for disposal, while 70% of which is reused as agricultural fertilizer or irrigation source [88]. However, conventional wastewater treatment systems, though efficient, may still not be an effective management approach considering the large volume of wastewater that is processed downstream and disposed to the environment. Also, residual pollutants from excess spent wastewaters used as fertilizer and irrigation water tend to accumulate in the environment through surface run off.

2.3 Process Intensification via Membrane Processes

Over the past three decades, membrane separation processes has gained importance in different fields of application such as, food processing, water purification, seawater desalination, and wastewater treatment and reuse [89]. Membranes are semi-permeable materials that act as barriers to selectively separate phases of particulates, colloidal, and dissolved materials in fluids. As shown in Figure 5, membranes restrict the transport of fluid components, thereby, producing a permeate stream that has less concentration of the rejected components. The rejected components, on the other hand, are collected from a more concentrated stream, commonly designated as the retentate.

Figure 5

Simplified Schematic Illustration of Membrane Separation.

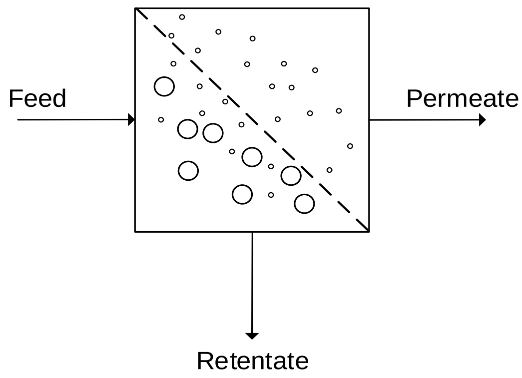

Simplest among these processes are pressure-driven membrane processes (PDMPs). These include microfiltration (MF), ultrafiltration (UF), nanofiltration (NF), and reverse osmosis (RO) that are categorized based on the pore size of the membranes used in the operations and applied operating pressures as shown in Table 8. While there may be an overlap in the nominal size ranges depending on the literature source, the Table below presents a typical range of those values. The mechanism of membrane separation has the same principle as that of conventional filtration. The difference, however, is that while conventional filtration is suitable in separating visible, and coarse particles (> 0.1 mm), membrane filtration is more suitable in separating finer particulates that may be present as microorganisms, suspended and colloidal solids, and dissolved organics and inorganics (salts) [90]. Particulates are commonly separated in MF where pore size ranges from 0.05 μm to 0.1 μm, while molecular separation is commonly employed by UF membranes with pore diameters ranging between 5 nm and 0.05 μm. Narrower pore-sized membranes offer higher rejection of smaller components such as solutes, and salts. NF membranes have mean pore size of approximately 1 to 5 nm that is able to reject molecules with molecular weight below 2,000 Da. RO membranes, are dense membranes that can reject molecular weights below 100 Da.

Table 8

Typical Pore Size and Transmembrane Pressure for Various Membrane Types

Membrane Type	Pore Size	Molecular Weight Cut-off	Transmembrane Pressure
	(μm)	(Da)	(MPa)
Microfiltration	0.05 – 0.1	> 100,000	< 0.3
Ultrafiltration	0.005 – 0.05	2,000 – 150,000	0.3 – 0.7
Nanofiltration	0.001 – 0.005	100 – 2,000	0.7 – 3.0
Reverse Osmosis	< 0.001	< 100	1.0 – 7.6

Note: Adapted from Berk [91]

Hydraulic pressure generally serves as the driving force for flow across membranes in PDMPs; whereas the degree and selectivity of rejection depends on the permeability of the filter medium used. The permeate flux of a solvent, commonly water, (J_v) through the membrane varies proportionally with the transmembrane pressure or TMP, i.e., the pressure drop (ΔP) across the feed and permeate sides of the membrane, and the hydraulic permeability (A_w) of the membrane. The membrane hydraulic permeability is a constant parameter dictated by membrane structure and its interaction with water. This relationship is mathematically shown in Equation 1.

$$J_v = A_w \Delta P \tag{1}$$

Porous membranes like MF and UF commonly have higher hydraulic permeabilities and are operated under low TMPs. However, non-porous membranes like NF and RO have relatively lower hydraulic permeabilities and must be operated at larger

TMPs. In addition, the small molecular size and concentration of components rejected in dense membranes such as these exert osmotic pressure difference across the membrane ($\Delta\pi$) that further decrease the TMP across the membrane, as shown in Equation 2.

$$J_v = A_w(\Delta P - \Delta\pi) \tag{2}$$

Membranes provide an attractive separation process because of the low operating costs and energy requirements, the high product quality and yields, and the minimal amounts of chemical additives. Overall, the simplicity of the process as well as the effectiveness of various membrane types to separate streams opens opportunities for a wide range of industrial application. In addition, membrane systems do not require high temperatures for operation, allowing temperature sensitive materials to be processed with this type of separation. These industries include chemical, pharmaceutical, water supply, wastewater treatment, and the focused of this study, the food and beverage industry.

2.3.1 *Membrane Separation in Food and Beverage Production*

The use of membrane technology as a processing and separation method has been well-known in water and wastewater treatment applications. However, as an efficient separation method offering several advantages over conventional separation operations such as in water removal, it is recently gaining importance in other industrial applications. In food and beverage production, membrane technologies have been found as potential alternatives for the clarification of cloudy fluids such as vegetable oils as alternative to centrifugation and sedimentation, preservation by removal of microorganisms as alternative to sterilization or addition of preservatives, pre-concentration of beverages as alternative to evaporation, and purification of drinking water as alternative to distillation [44], [92]. As an alternative to thermal evaporation, membrane filtration operates under mild operating conditions of temperature and pressure, thus conserving the functional properties of heat-sensitive food products. As a competitive process, membrane separation is known to have high separation efficiency, and makes use of simple equipment that is easy to scale-up without the necessity for additional processing steps [93].

The proper selection of membrane is among the important operating consideration in membrane operations as membranes differ in specifications including pore size, selectivity, operational limits, etc. A size selectivity chart for food and beverage applications of various pressure-driven membrane processes is presented in Figure 6. On the other hand, a list of various food and beverage industries employing membrane processes is shown in Table 9.

Figure 6

Approximate Pore Sizes and Selectivity of Membrane Processes

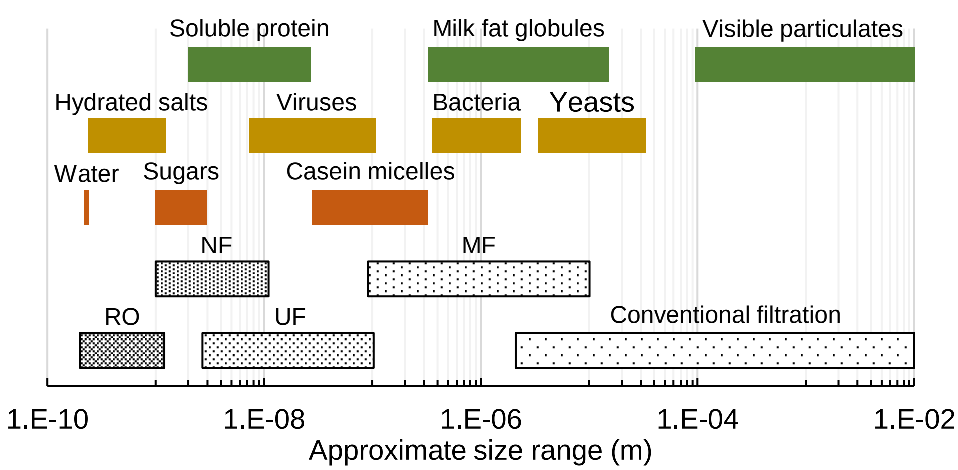

Note: Adapted from Dewettinck & Le [44]

The earliest food applications of membrane filtration were intended for the separation of ultrafine particles that can be found the processing of dairy products such as cheese, whey, and milk. UF and MF membranes were used to fractionate skimmed milk into whey protein and casein micelles in cheese production, and separation of fat globules from milk, thus were considered as a more practical clarification method than sedimentation [44]. A wide range of microorganisms can also be effectively removed using UF and MF membranes. This microbial removal method has been termed as cold sterilization, an alternative preservation method that does not employ heat and the addition of preservatives [92]. This method became the basis for other applications such as in recovering yeast from beer after fermentation, and the clarification of wine, juices from fruits and vegetables, sugarcane juice, and aqueous soy extracts, along with the removal of microbial contaminants. These membranes are permeable to water and other liquid and dissolved components such as salts, sugars and based on this, MF and UF may be employed in dewatering or concentrating food slurries containing suspensions.

Most dissolved components, and liquids such as water, are processed using NF and RO membranes. RO was first developed in the objective of purifying water without undergoing thermal processes. Water desalination by RO produces ultrapure water from seawater with above 99% salt rejection, and today, this process provides 1% of the world's drinking water [89]. NF is a more novel process in producing water-rich permeate, but compared to RO, this membrane technology is semi-permeable to certain solutes [94]. Despite this, NF operates at relatively lower pressure than RO, thus making it a low-cost water and wastewater treatment alternative. Overall, the efficiencies of both membrane types in producing water-rich streams expands the applications of RO and NF in food and beverage industries, as summarized in Table 9.

Table 9

Membrane Separation Technologies Applied in Food and Beverage Production

Industry	Technology	Applications
Dairy	MF	Cold pasteurization of milk and cheese products
		Fractionation of skimmed milk to micellar casein and serum proteins
		Separation of fat globules from whole milk
		Bacteria and fat removal from cheese brine
	UF	Concentration of cheese whey and derivatives
	NF	Desalination and lactose removal from milk
		Pre-concentration of milk
	Electrodialysis	Desalination and lactose removal
	RO	Pre-concentration of milk and other dairy liquids
Brewery	MF	Clarification and recovery of beer from yeast
		Removal of microorganisms prior to bottling
	RO	Purification of brewing water
	Dialysis	Alcohol removal from fermented beer
Wine	MF	Clarification of wine
	NF and RO	Concentration of sugar content from grapes extract
		Concentration of wine components such as alcohol
	Electrodialysis	Tartaric acid stabilization, removal of potassium and calcium ions
Fruits & vegetable juices	MF and UF	Juice clarification and microbial removal
	MF and RO	Fruit juice concentration
	NF	Removal of fertilizer nitrates and nitrites
	Electrodialysis	Deacidification of sour fruit juices
Sugar	MF and UF	Clarification of sugarcane juice, and effluent
	NF	Concentration of sugar syrups
	RO	Pre-concentration prior to crystallization
Soy	MF	Clarification and removal of microorganisms
	UF	Concentration of aqueous soy extracts
	NF	Partial desalination

Note: Adapted from Cassano [92]; Dewettinck & Le [44]

In the context of energy consumption, membrane separation has relatively low energy consumption compared to other water removal processes as shown in Table 10.

Table 10

Energy Consumption of Industrial Water Removal Operations

Method or equipment	Energy Required for Water Removal ($kJ\ kg^{-1}$ of water removed)
Membrane filtration	50 – 150
Osmotic dehydration	200 – 500
Evaporation, single effect	2,600
Evaporation, double effect	1,300
Spray dryer	4,000 - 6,000
Drum dryer	5,000
Tunnel dryer	4,000
Freeze dryer	Up to 100,000

Note: Adapted from Vaishampayan & Costa [74]

In general, this non-thermal water removal method is about 10% to almost 100% less energy intensive [95]. Since the operation is based on the use of permselective barriers under a given TMP, the mechanism of separation is induced by the solubilization (in the case of RO and NF) and diffusion (in the cases of RO, NF, UF, and MF) of specific feed components without the consideration of phase change. Thus, in contrast with thermal dewatering methods, the energy consumption of membrane separation methods is lower because of the absence of heating and phase change requirements. With the current available technology, however, membrane separation has limited applicability to replace convective- and freeze-dehydration. Nevertheless, as a pre-concentration alternative, the reduction in energy consumption is still highly favorable considering the volume of water removed in thermal evaporation.

2.3.2 *Membrane-Based Preconcentration of Coffee Extracts*

Thermal dewatering operations in soluble coffee production have several disadvantages associated with the loss of product quality and low sustainability index. Particularly during the evaporation of coffee extracts, the thermal conditions considerably degrade the flavor and aroma of soluble coffee by about 70% of that of conventionally roasted coffee due to the losses in phenolic compounds and generation of Maillard reaction byproducts [24]. Thus, developments in the soluble coffee industry have, so far, focused on configuring thermal dewatering operations at lower boiling temperatures (vacuum evaporation), or in the absence of heat (freeze dehydration); integrating coffee aroma recovery routes [25]–[27]; and employing chemical enrichment methods in improving the quality of instant coffee [24]. However, while product quality is essential in soluble coffee production, the process continues to rely on energy-intensive phase-change separations in its thermal dewatering operations [23]. The industry currently shares the highest energy footprint (~ 15.7 MJ kg^{-1} soluble coffee) among powdered food and beverage products [28]. Thermal dewatering operations contribute to a considerable fraction of the energy used in the process. Also, a large volume of water used in the extraction step ends up as wastewater that requires treatment before disposal, a large portion of which is withdrawn from evaporators. From a sustainability standpoint, these increase not only the operating cost of the process, but also result in a large water- and energy footprint of the soluble coffee industry.

The use of membrane as an alternative to, or in combination with evaporation could potentially address several disadvantages of the thermal operation. In particular, NF, as a low-energy alternative to RO, is suitable for water removal operations, while efficiently rejecting colloidal and dissolved solids, such as organics solutes, more than those achieved by UF. This allows the recovery of water reusable for plant operations that not only reduces the need for fresh water in the process, but also the amount of wastewater generated. When integrated as an alternative to evaporation, the membrane process also offer an energy reduction of about 30% [10]. Because of these benefits, NF has been investigated in the concentration of food and beverages including apple and pear juices [29], sea buckthorn tea [14], red wine [16], lactic acid whey [18], and alternative sweeteners [30].

Despite its potential, only few studies have investigated the integration of NF and other membrane technologies in the soluble coffee process. NF has been studied mostly on waste streams for caffeine recovery from spent coffee grounds [7], decaffeination [31], and as a water reclamation option for soluble coffee wastewater [50], [52]. Vincze and Vatai [33] first proposed the nanofiltration (NF) of coffee extract as a low energy preconcentration alternative to evaporation prior to the final dehydration step without significant losses in quality, e.g., caffeine content. With an initial total solids concentration of about 14 g L^{-1}, the highest flux of about 50 L m^{-2} h^{-1} was obtained at 42°C under a pressure 20 bar, and a corresponding solids rejection of 98.75%. The final concentration of the coffee extract was increased from 14 g L^{-1} to 45 g L^{-1}; however, this final concentration was still low. Pan, et al. [32] further added that coffee extracts could be theoretically concentrated up to 39% wt/wt via crossflow (CF) NF, while producing a water-rich permeate stream. While this concentration is still considered low for commercial operation, these studies presented that NF can potentially supplement evaporation in preconcentrating coffee extracts if membrane fouling can be minimized.

2.3.3 *Membrane Fouling in Conventional Filtration Systems*

Despite the potential of membrane separation in food and beverage production, most membrane processes are susceptible to membrane fouling. Over time, in their prolonged use, membrane surfaces accumulate different types of contaminants or foulants that negatively impacts the effective permeability of the membrane. Membrane fouling is common in conventional filtration systems such as dead-end (DE), and crossflow (CF) membrane filtration systems, shown in Figure 7.

Figure 7

Conventional Filtration Flow Configuration: (a) Dead-End Filtration and (b) Crossflow Filtration

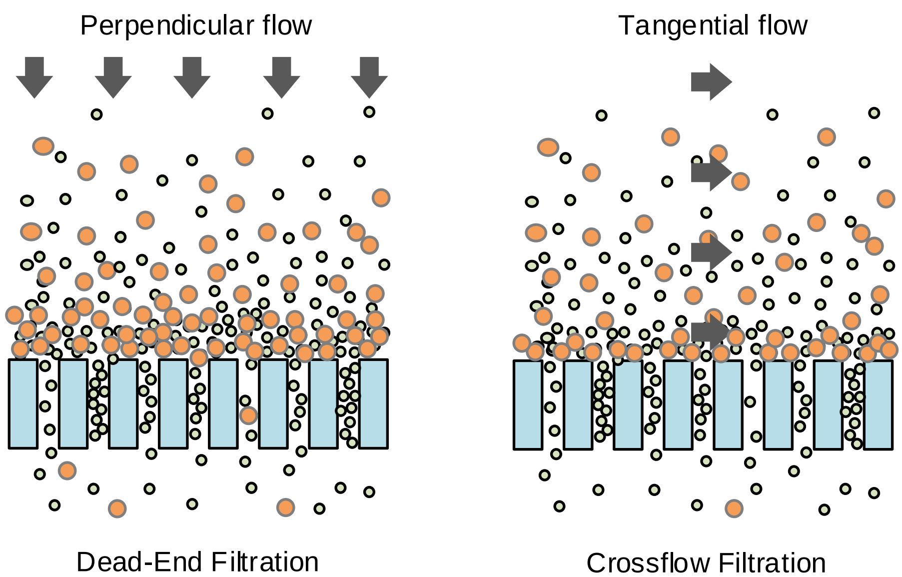

In DE filtration, the feed flows perpendicular to the membrane surface. This allows the permeation of components through the membrane as the fluid is forced towards the membrane at a certain TMP. However, it is because of this flow configuration that foulants accumulate on the membrane surface and form a cake layer that eventually reduces the filtration performance and cause permeate flux to drop at a much faster rate. Moreover, the foulants forced perpendicularly towards the membrane surface cause stronger fouling that, even after membrane cleaning, can reduce the permeation ability of the membrane. CF filtration improves the performance of membrane filtration and reduces membrane fouling as the feed flows tangentially over the membrane. In this manner, the tangential flow imparts shear on the membrane surface, sweeping the foulants off the membrane surface. Increasing the CF velocity of the feed enhances the permeate flux., at the expense of energy from the pump driving the flow.

Even so, conventional CF membrane filtration systems are still susceptible to membrane fouling. An illustration of this phenomenon in CF operation is shown in Figure 8. Membrane fouling is inevitable even with increased feed velocity in CF filtration systems as it is caused not only by the nature of constituents found in the feed that can serve as foulants, but also by several factors including the operating conditions of the membrane system that tend to polarize high concentrations of solutes on the membrane surface. Thus, under poor operating conditions, such as low feed CF velocities, high feed concentrations, and even exceedingly high operating pressures, membrane fouling often leads to the decline of throughput rates and rejection efficiencies as foulants continue to accumulate on the membrane surface causing the formation of a concentrated gel layer, or worst, irreversibly block membrane pores [48].

Figure 8

Simplified Illustration of Membrane Fouling as a Result of an Increased Solids Concentration Near the Membrane Surface during Conventional Crossflow Filtration.

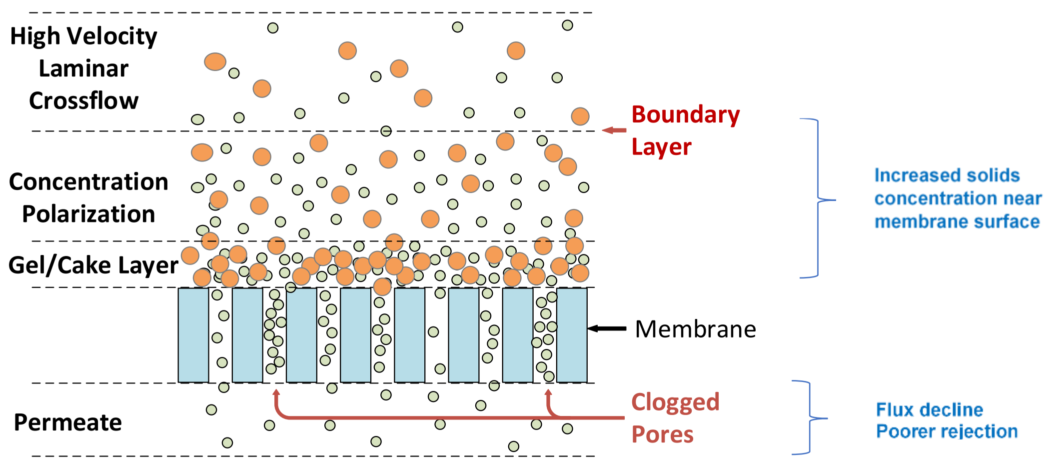

Food and beverage process streams, unlike water supply and wastewater streams, are more concentrated and contain a highly complex variety of foulants – organic, biological, and colloidal solids. Thus, food and beverage streams are highly viscous that tend to limit fluid velocities on the membrane surface and result in concentration polarization. In concentrating milk proteins, for example, concentration polarization lead to non-Newtonian flow behavior near the membrane surface as surface concentrations increase viscosities exponentially [5]. For coffee extract preconcentration, these foulants may be organic components like caffeine (4.5% to 5.1%), lipids (1.5% to 1.6%), chlorogenic acids (5.2% to 7.4%), saccharides (7.2% to 11.7%), proteins (16.0% to 21.0%), and humic acids (15%) [96]; mineral components (9 to 10%) [97] and other soluble, colloidal, and suspended components. In concentrating coffee extracts, Pan, et al. [32] reported a flux decline of about 80% of the initial permeate flux after six hours of operation, and a limiting maximum concentration of coffee extracts under conventional crossflow NF up to approximately 35% to 39% wt/wt. Also, as the feed coffee extract becomes more concentrated, fouling becomes more prominent and uncontrollable that increased CF velocities and high operating pressure would increase the operating cost of the process [52]. This drawback can result in increased energy consumption, system downtime, higher membrane area requirement, increased capital costs, and maintenance expenses [98] that limits the application of NF as a dewatering alternative in the soluble coffee process.

2.3.4 *Shear-Enhanced Dynamic Filtration Systems*

Overall, membrane fouling makes NF and other membrane operations inefficient and economically unattractive. Thus, efforts have been made to overcome or alleviate the negative impacts of fouling in membrane systems. Membrane cleaning has been common to most membrane-based industries as part of regular maintenance operations to extend the usage of membranes. Chemical and enzymatic solutions degrade membrane foulants and restore the original permeability of membranes [99] However, this approach is only effective at a certain extent where fouling is reversible, i.e., foulants are only adsorbed on the surface. Irreversibly fouled membranes, where complete pore blockage is observed, will continually degrade in performance even with regular cleaning. Additionally, the cleaning regiments increase the operating costs, and may pose a concern with product contamination, due to their introduction into the system.

The hydrodynamic flow in membrane systems is an important aspect in managing fouling and in optimizing the operation. In doing so, the generation of local shear zones on the membrane surface has been found to be effective in preventing foulants from accumulating on the membrane surface [35]. As stated earlier, increasing CF velocities is one approach applied to induce local shear zones on the membrane surface. However, this approach enhances flow and prevents membrane fouling only at a limited extent [34], [35]. Also, the energy consumed by the pump increases drastically with the turbulent flow of the feed. Dynamic filtration systems (Figure 9), on the other hand, generate surface shear rates at magnitudes substantially larger than conventional CF systems [8], [35]–[38].

Figure 9

Dynamic Shear-Enhanced Filtration

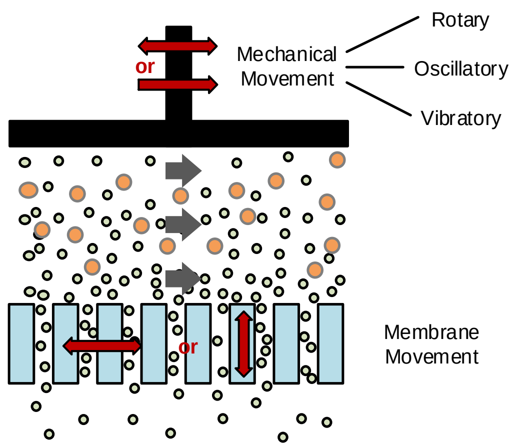

Dynamic Filtration

Approximately, maximum membrane surface shear rates under dynamic membrane systems can reach up to 160,000 s^{-1}, whereas high CF velocities from conventional membrane operations can only approach surface shear rates of up to about 30,000 s^{-1} [40]. Shear rates are effectively enhanced by employing mechanical motion on the membrane support, while keeping inlet flows and TMPs to a minimum and conserving energy during the operation [38].The mechanical movements are imparted via rotating disk, impeller, or cylinder; or with the membrane module oscillating or vibrating. Jaffrin [37], [43] reviewed various types of dynamic shear-enhanced filtration systems. Among these systems are Couette flow type rotating cylindrical membranes that were first commercialized for blood plasma separation. However, since the system has only been used in the medical field, its application was only limited to small scale application, rather than in an industrial setting [43]. On the contrary, rotating multi-disk filtration systems have been employed in yeast suspensions, oil/water emulsions, mineral suspensions, and fermentation broths [43]. These systems consist of circular membrane disk modules mounted on a shaft that rotates at certain speed. The rotation imparts about 120,000 s^{-1} at a maximum speed of 3,450 rpm. On the other hand, oscillating membrane systems consist of a membrane module that are mounted on a torsional shaft that spins back-and-forth at resonant frequencies of about 60 Hz. These are also considered as vibratory membrane systems based on the azimuthal oscillations of the membrane module. Such systems consist of a stack of circular membranes, or cylindrical hollow fiber membranes that have been investigated for water treatment [100], volatile organic compounds removal from spent surfactant solutions [101], and yeast recovery [2].

In food and beverage production, both rotating filtration and vibratory filtration systems were found effective in various dairy processing applications. Particularly dynamic filtration was used to recover proteins from casein micelle, and in the fractionation of milk proteins [5], [41], [102]. In soy milk processing, dynamic UF was investigated to concentrate soy trypsin inhibitors to enrich soy milk [103]. Vibrating and rotating filtration systems were also used to clarify rough or cloudy raw liquors like freshly brewed beer [3] and raw fermented wine [104]. Overall, these systems substantially improve the permeate flux of membrane filtration by generating surface shear rates that are considerably higher than those imparted by crossflow velocities. Also, with less foulants accumulating on the membrane surface, shear enhancement favorably improves membrane selectivity, and rejection efficiencies. However, it should be noted that these systems have higher costs and may have shorter life spans due to the moving mechanical parts. In addition, these systems are limited by membrane area as these are easier to build and maintain. In spite of these limitations, these dynamic systems are currently being optimized and potential applications are further explored.

2.3.5 *Vibration Shear-Enhanced Process*

One dynamic filtration system, as studied herein, is the Vibratory Shear-Enhanced Process (VSEP) by New Logic Research, Inc, shown in Figure 10. The VSEP filtration system consist of a disk membrane (laboratory-scale), or a stack of circular membranes (pilot and commercial scale) mounted on a vertical torsion shaft. The shaft spins in azimuthal oscillations from a vibrating base at resonant frequencies of up to 60 Hz [105]. These torsional oscillations impart high membrane surface shear rates (> 20,000 s^{-1}) that reduces the accumulation of the membrane foulants [106]. However, at the same pump power requirement, the energy demand of the vibratory membrane system is higher than CF membrane operation due to the added power requirement from the vibratory motor [107]. As will be presented in the succeeding sections, this added power requirement can range from 2 to 10 times the power requirement of pump in conventional non-vibratory operations. Despite the added energy requirement, the flux enhancement from higher membrane surface shear rates makes the specific energy demand, i.e. energy required per volume of permeate recovered, more economical than that of CF operation by up to 18%

[42]. Thus, the mechanism is considered energy-efficient in improving permeate fluxes and separation efficiencies [43], making operating and maintenance costs less expensive [44].

Figure 10

Vibration Shear-Enhanced Process (VSEP): (a) Schematic Diagram of Laboratory-Scale VSEP Filtration System, and (b) Shear-Enhanced Flow

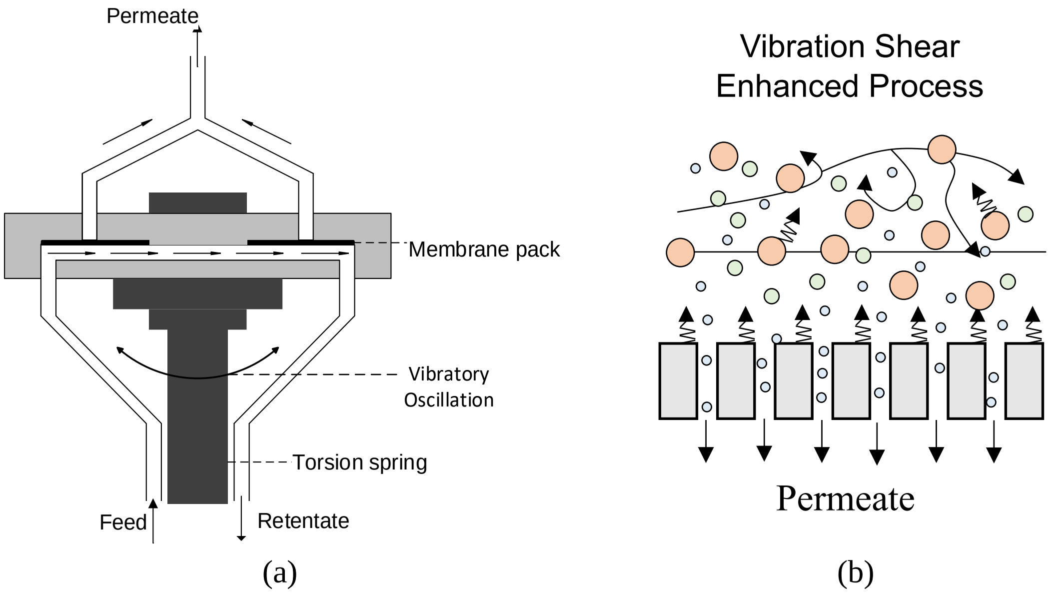

Note: Adapted From New Logic Research, Inc. [39]

In terms of design, its space-efficient vertical module design allows scale-up systems to handle larger processing volumes [39] with a smaller footprint than traditional horizontally arranged membrane modules. This vertical design makes the membrane system suitable for process integration where the limited floor space is a common challenge. Among its successes over CF filtration in food, beverages, and drinking water production include concentration of milk proteins and dairy wastewater treatment [5],

[45], clarification and yeast recovery of alcoholic beverages [2], [3], and water treatment from high salt seawater and freshwater sources [46]–[49].

2.4 Membrane Filtration Principles

Dynamic filtration systems offer an effective approach, not only in improving conventional filtration systems, but also in alleviating the negative impacts of membrane fouling. By increasing the shear rates on the membrane surface from the mechanical movement of the membrane module, dynamic systems such as the VSEP improves the potential of integrating membrane processes in wider industrial applications, especially in food and beverage production. To maximize this potential, effective fluid management becomes a critical aspect in membrane processing. Thus, it is important to understand the influence of operating factors on the hydrodynamic conditions adjacent to the membrane surface, or the extent of concentration polarization that has a direct impact on membrane fouling.

2.4.1 *Transmembrane Pressure*

Mechanical pressure drives fluids to flow across membranes. However, apart from the applied pressure, the intrinsic permeability of membranes for solvents like water, also affects the nature of separation. Most membrane separations are often dictated by membrane porosity and tortuosity, but other membranes can also be influenced by their affinity to certain fluids or solutes. For example, NF membranes are mostly negatively charged and thus, would vary in performance especially in rejecting charged and uncharged solutes.

In general, porous membranes exhibit Hagen-Poiseuille relationship, whereby the solvent is assumed to conform capillary flow through membrane pores, and the pressure drop across the membrane serves as the driving force for flow. This relation is mathematically presented in Equation 3.

$$J_v = \frac{\varepsilon\, r_p{}^2}{8\eta\tau}\frac{\Delta P}{\Delta x} \tag{3}$$

A proportionality factor in the capillary flow behavior is determined from the membrane pore radius (r_p), porosity (ε), tortuosity factor (τ), and fluid viscosity (η). On the other hand, the driving force ($\Delta P/\Delta x$) is the pressure drop along the membrane thickness. In the absence of membrane specifications, the proportionality factor in Equation 3 is analogous in form with Equation 4 and may be determined experimentally from pure water fluxes measured at various TMPs.

$$J_v = A_w \Delta P = \frac{\Delta P}{\mu R_m} \tag{4}$$

For dense membranes, like NF and RO membranes, the TMP is not only a function of the measured pressure drop, but also by the osmotic pressure difference exerted by the solution at the feed and permeate side of the membrane. Further, from Darcy's law, the membrane permeability can be interpreted as the function of the intrinsic membrane resistance (R_m) and the absolute viscosity (μ) of the fluid [108]. Using this analogy, the pressure-driven flow for dense membranes may be expressed as Equation 5.

$$J_v = A_w(\Delta P - \Delta\pi) = \frac{(\Delta P - \Delta\pi)}{\mu R_m} \tag{5}$$

For NF operations discussed herein, Equation 5 is used extensively in the succeeding sections. From the equation, the osmotic pressure serves as an important factor affecting the permeate flux and is closely related to concentration polarization. This colligative property arises from the concentration of solutes in the fluid, and serves as the threshold pressure in NF and RO systems that must be overcome for solvent (water) permeation and separation to occur [94]. As a result, NF and RO often require high-pressure operation to separate solutes from the solution, while the dense structure of the membrane allows the generation of water-rich permeate. The osmotic pressure is a function of concentration of solute (C_i), ideal gas constant (R), and absolute temperature (T). However, the parameter differs among organic solutes and inorganic salts, since the latter considers the degree of dissociation (j_i) of salts, as shown in Equation 6.

$$\pi_i = \sum j_i C_i RT \tag{6}$$

On the other hand, the osmotic pressure of organic solutes in a solution is a function of the solute concentration, ideal gas constant, absolute temperature, and molar mass of the solution (M), as shown in Equation 7.

$$\pi_i = C_i \frac{RT}{M} \tag{7}$$

2.4.2 *Mass Transfer Mechanism*

2.4.2.1 Concentration Polarization in Crossflow Filtration. At an applied pressure on the feed side of the membrane, the solute particles from the bulk phase of the fluid are transferred towards the membrane along with the solvent, commonly water. The convection of these components towards the membrane surface result in an increase in concentration and a laminar boundary layer is developed due to this difference in concentrations. This phenomenon is commonly known as concentration polarization and is schematically illustrated in Figure 11.

Figure 11

Schematic Representation of Concentration Polarization in Membrane Separation

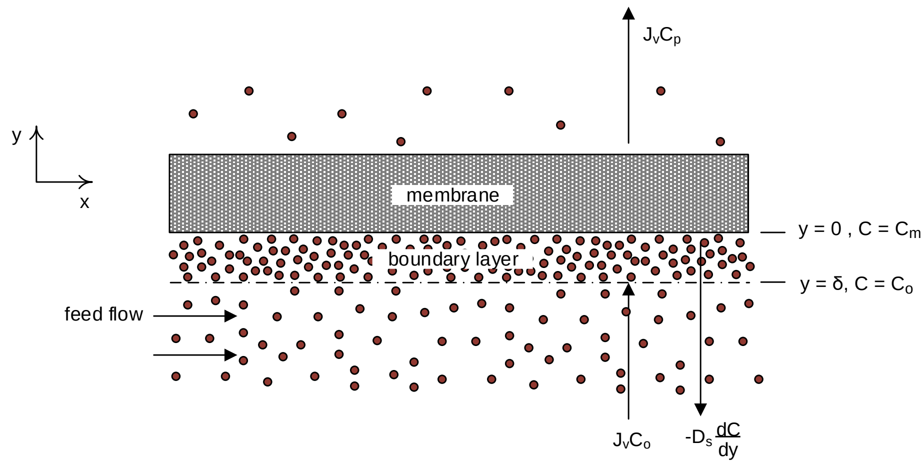

The film layer model is among the well-known concepts that demonstrate how the extent of concentration polarization is dictated by various mass transfer mechanisms occurring near the membrane surface [94], [108]. Particularly, convective flow of the solute towards membrane occurs due to the solvent flux at a given TMP. Simultaneously, the back-diffusion of solute from the membrane is also observed due to the concentration gradient between the surface and bulk phase of the fluid. The boundary layer solute mass balance is shown in Equation 8:

$$J_v C_o = -D_s \frac{dC}{dy} + J_v C_p \tag{8}$$

where C_o is the feed solute concentration, D_s is the solute diffusivity, and y is the perpendicular distance from the membrane surface. This differential form is evaluated across boundary conditions (from $y = 0$, $C = C_m$ to $y = \delta$, $C = C_p$), where δ is the thickness of the stagnant film boundary layer. Assuming that the permeate concentration is considerably negligible relative to the membrane surface and bulk concentrations, a boundary layer film model is obtained, as shown in Equation 9.

$$J_v = \frac{D_s}{\delta} \ln \frac{C_m}{C_b} \tag{9}$$

Different parameters that describe concentration polarization may be derived from the film layer model. The ratio between the concentrations on the membrane surface and bulk phase of the fluid is also known as the polarization modulus (C_m/C_b). This parameter indicates the degree of concentration polarization based on the increase in surface concentration relative to the bulk fluid. In addition, under similar processing conditions, this parameter varies depending on the type of solutes. Inorganic salts have moduli less than 2.0, organic macromolecules could have 5 or more, and proteins have moduli substantially larger than 10 [94]. Apart from the polarization modulus parameter, solutes also tend to exhibit back-diffusion due to the concentration gradient between the boundary layer region and the bulk phase of the fluid. This back transport mechanism is represented by the diffusivity coefficient and a laminar boundary layer. A ratio between these two parameters gives the mass transfer coefficient for permeate flux. Relatively low back-diffusion results in a thin boundary layer that facilitates membrane fouling

[108]. Macromolecules tend to exhibit severe localized surface concentrations that are common in MF and UF. Accordingly, these PDMPs involve small particles, colloids, and emulsions with diffusion coefficients are found to be in the order of 10^{-10} m^2 s^{-1} or less that typically contributes to considerably low mass transfer coefficients. [108]. On the other hand, for dense membranes like NF and RO, the solutes retained by the membrane tend to be considerably small and have high diffusivities in the order of 10^{-9} m^2 s^{-1} [108]. Due to the relatively higher back-diffusion index, concentration polarization for NF and RO membranes are likely to be low.

2.4.2.2 Evaluation of Concentration Polarization Parameters. The concentration polarization phenomenon is a complex mechanism and has been estimated in membrane filtration studies. Some studies verify the existence of this phenomenon by direct observation of particle deposition under a microscope [109], [110]. Some studies also employed analytical approaches to evaluate the hydrodynamic conditions at the boundary layer region. Kim [111] evaluated this phenomenon by theoretically calculating the effects of fast crossflow velocity and shear flow on the membrane surface and the resulting osmotic pressure at the membrane surface to estimate permeate flux inflection. Elimelech & Bhattacharjee [112], on the other hand, developed a theoretical model based on the hydrodynamic and thermodynamic conditions existing at equilibrium at the concentration polarization layer.

Until now, there is no conventional approach in quantifying concentration polarization in membrane systems. However, among the more straightforward approaches, uses the film layer model backed with the experimental evaluation of fluxes and rejection efficiencies of membrane operations at various operating conditions [34].

The film layer model equation can be expressed into linear form, as shown in Equation 10. From the linear expression, experimental permeate fluxes are plotted at various bulk concentrations of feed. By linear regression, the mass transfer coefficient can be evaluated from the slope of the line, while the membrane surface concentration is derived from the y-intercept of the plot.

$$J_v = -k \ln C_b + k \ln C_m \tag{10}$$

On the other hand, for membranes having partial rejection of solutes, the film layer model equation may then be modified by taking into account the concentration of the permeate, as shown in Equation 11.

$$J_v = k \ln \frac{C_m - C_p}{C_b - C_p} \tag{11}$$

In place of the concentration terms, rejection parameters can also be considered to evaluate the film layer model [34], [113]. Theoretically, a real rejection efficiency (r_{real}) can be distinguished from the apparent or observed rejection efficiency (r_o) due to the difference in membrane surface and bulk fluid concentrations. These rejection parameters can be calculated relative to the membrane surface concentration (Equation 12), and bulk fluid concentrations (Equation 13), respectively.

$$r_{real} = 1 - \frac{C_p}{C_m} \tag{12}$$

$$r_o = 1 - \frac{C_p}{C_b} \tag{13}$$

By combining Equations 11 to 13, the concentration polarization parameters may then be evaluated using experimental or observed rejection efficiencies at varying permeate fluxes. This relationship is shown linearly in Equation 14, where the mass transfer coefficient can be calculated as the reciprocal value of the slope, while the real rejection can be derived from the y-intercept.

$$\ln\frac{1-r_o}{r_o} = \frac{J_v}{k} + \ln\frac{1-r_{real}}{r_{real}} \tag{14}$$

2.4.2.3 Sherwood Number Relationship. As a rate-dependent operation, membrane processes rely on the importance of flux enhancement for an efficient design and operation of membrane filtration systems. While concentration polarization is inevitable in membrane separation, this phenomenon is minimized by controlling the hydrodynamic conditions adjacent to the membrane surface. Thus, understanding the mass transfer mechanisms in membrane separation play an important role. From the film layer model, the mass transfer coefficient is related to the design and operation of membrane systems using the Sherwood number (Sh) relationship, shown in Equation 15.

$$Sh = \frac{k \;\; d_e}{D_s} = a\ Re^b\ Sc^c \left({}^{d_h}/_{L}\right)^d \tag{15}$$

where Re is the Reynolds number, Sc the Schmidt number, and a, b, c, and d are constant parameters. The Reynolds number attributes the effective flow diameter, fluid velocity, and fluid properties such as density and viscosity. On the other hand, the Schmidt number reflects the diffusion occurring in the membrane system. From this relationship, the mass transfer coefficient is seen to be a function of the flow behavior, diffusion coefficient of the solute, and membrane module shape and dimensions.

The Sherwood number relation is well studied in fluid flow and mass transfer operations for membrane module design and operation [94], [108]. Different module geometries have been evaluated to define the Sherwood number constant parameters for laminar and turbulent flow regimes. These are summarized in Table 11.

Table 11

Sherwood Number Constants for Various Module Geometries and Flow Regimes

Module Geometry	Flow Regime	a	b	c	d	Remarks
Channel or Tube	Laminar	1.62	0.33	0.33	0.33	$100 < ReScd_h/L < 5{,}000$ Fully developed velocity profile
		0.664	0.5	0.5	0.33	Entry region
	Turbulent	0.023	0.8	0.33	-	$Sc \leq 1$
		0.023	0.875	0.25	-	$1 \leq Sc \leq 10^3$
Stirred Cell	Laminar	0.285	0.55	0.33	-	8 x 103 < Re < 32 x 103
	Turbulent	0.044	0.75	0.33	-	$Re = \rho_w r_{sc}^2/\mu$; r_{sc} = radius of cell

Note: Adapted from Schäfer [94]

For crossflow filtration having crossflow velocities following the Sherwood number relationship, the mass transfer coefficient is found to be a function of surface shear rates (Υ_w) and crossflow velocities (u) in the order shown in Equation 16.

$$k = \gamma_w u^e \tag{16}$$

From Equation 16, the exponent (e) is a parameter determined from the flow regime. For laminar conditions, the exponent is about 0.33, while for turbulent conditions, the parameter is between 0.75 to 0.91 [57]. The equation is commonly evaluated experimentally via the velocity variation method [113], in line with the alternative form of the film layer model, as shown in Equation 17.

$$\ln\frac{1-\mathrm{r_o}}{\mathrm{r_o}} = \frac{\mathrm{J_v}}{\gamma_w \mathrm{u^e}} + \ln\frac{1-\mathrm{r_{real}}}{\mathrm{r_{real}}} \tag{17}$$

By plotting experimental values of $\left[\ln\frac{1-\mathrm{r_o}}{\mathrm{r_o}}\right]$ at varying values of $\left[\frac{\mathrm{J_v}}{\mathrm{u^e}}\right]$, the surface shear generated from the crossflow velocities of the fluid can be determined from the reciprocal value of the slope. On the other hand, the real rejection parameter of the operation can be derived from the y-intercept of the plot.

Overall, the Sherwood number relation shows the dependence of the mass transfer coefficient with crossflow velocities. Under uniform module geometry and for similar fluids, the coefficient varies by an exponent of 0.33 for laminar flows, and by 0.8 for turbulent flows. This difference shows the strong influence of Reynolds number on the mass transfer. Turbulent systems favor higher permeate fluxes at the expense of larger pressure loss in the flow channel, and thus, higher energy requirement. Despite this, membrane systems dealing with high solids content often employ turbulence promoters, such as feed channel spacers, to improve the hydrodynamic conditions of the system [34], [94]. Not only do these improve the permeate flux of the membrane operation, but this approach is also one of the control strategies to reduce membrane fouling, as discussed in the succeeding section.

2.4.3 *Membrane Fouling*

The performance of membrane operations is diminished by concentration polarization, and results in the decline of permeate flux until a steady state condition is attained. The polarization phenomenon is commonly a result of surface fouling by suspended and colloidal solids or by foulants that are larger than the pore size of the membrane or that do not interact with the membrane [34]. This type of fouling is reversible via change in operating conditions, or by membrane cleaning methods such as backflushing, chemical cleaning [99], [114]. On the other hand, foulants that adhere strongly to the membrane surface by clogging the pores, deposition of a gel layer, or by adsorption result in irreversible fouling [115]. This type of fouling may manifest over the prolonged use of the membrane where a continuous flux decline is observed. Even with membrane cleaning, irreversibly fouled membranes will have a lower hydraulic permeability compared to that of a clean membrane.

2.4.3.1 Resistance-in-Series Model. Membrane fouling is a very complex phenomenon that considerably varies with several parameters. Thus, this condition has been reviewed extensively in literature [98], [116]–[119], to propose control strategies [120]–[122]. For PDMPs, the Resistance-in-Series Model theoretically quantifies fouling and how it affects the permeate flux of the membrane operation. Accordingly, membrane fouling imparts resistance to flow that results in low permeate fluxes in membrane operations. This concept expresses the permeate flux as a function of the TMP and the total resistances (R_{total}) across the membrane. This concept is shown in Equation 18.

$$J_v = \frac{\Delta P}{\mu R_{total}} = \frac{\Delta P}{\mu (R_m + R_f)} = \frac{\Delta P}{\mu \sum R_i} \tag{18}$$

For a fouled membrane, the total resistance constitutes to the sum of the fouling resistances (R_f) and the clean membrane resistance (R_m). In membrane filtration studies, the individual fouling resistances (R_i) include those influenced by concentration polarization, osmotic pressure effects, adsorption, gel formation, internal pore fouling, and cake formation [98], [119]. These fouling resistances can also be characterized as reversible and irreversible fouling resistances by comparing the membrane permeability after a series of membrane cleaning steps. A typical protocol used to experimentally assess membrane fouling is shown in Figure 12.

Initially, the membrane resistance can be evaluated using pure water filtration studies at different TMPs and by accounting for the absolute viscosity of the permeating liquid. For NF and RO operations used for recovering high-purity water, this viscosity is commonly assumed as the absolute viscosity of water. As the membrane is used for processing various solutions, permeate fluxes (J_v) are observed to be lower than that of pure water flux (J_w), owing to the contribution of solutes osmotic pressure and concentration polarization phenomenon. Under prolonged operation, permeate fluxes continually decline, leading to fluxes that are considerably lower than the initial permeate fluxes due to membrane fouling (J_f). Reversible fouling can be experimentally evaluated by measuring the permeate flux after physical cleaning by backflushing ($J_{f\ rev}$). On the other hand, irreversible fouling can be assessed from the permeate flux after chemical cleaning steps ($J_{f\ irrev}$). Some typical chemical cleaning agents include bases such as sodium hypochlorite ($NaOCl$) and sodium hydroxide ($NaOH$) or acids such as nitric acid (HNO_3) [99]. Nonetheless, despite the use of chemicals for cleaning the membrane, an irreversibly fouled membrane exhibits permeate fluxes that are lower than the pure water flux of the membrane operation.

Figure 12

Steps in Evaluating Membrane Fouling

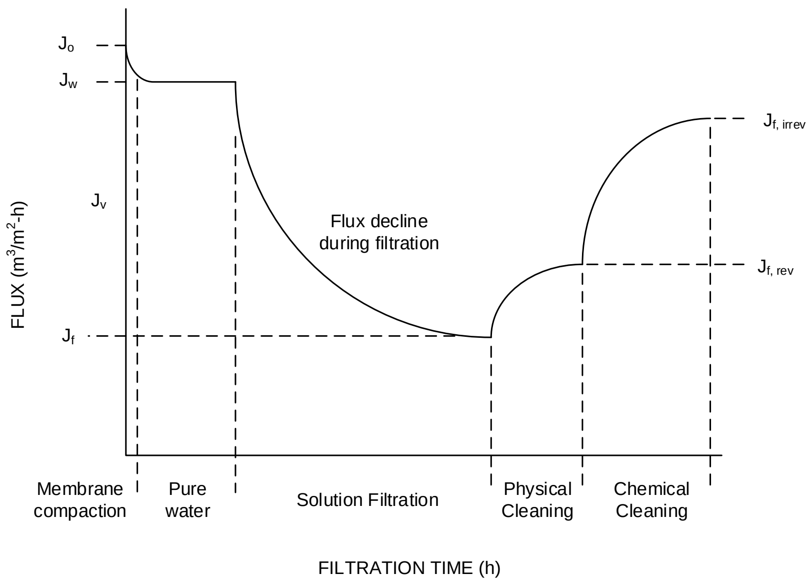

Note: Adapted from Kilduft, et al. [123]

2.4.3.2 Fouling Types, Mechanisms, and Control Strategies. Membrane fouling can be attributed to different types of foulants present in process streams that may be characterized as organic, inorganic, and biological in nature. These foulants vary in physicochemical and biological properties that influence various membrane fouling mechanisms that affect the filtration operation. Organic foulants are macromolecules that constitute natural organic matter , proteins and polysaccharides and are commonly present in freshwater sources, and in food and beverage process streams, and wastewaters [47], [124]–[127]. Organic fouling occurs in membranes throughout the filtration operation and may be attributed from the adsorption of organic solutes on the membrane surface, pore blocking, and formation of gel or cake layer [122]. These fouling mechanisms are attributed to the deposition of a thin organic cake layer or gel layer on the membrane surface, as a result of the supersaturated conditions at the boundary layer [128], [129]. On the other hand, inorganic fouling is attributed to the precipitation of salts on the membrane surface, otherwise known as scaling [98], [116], [130]. This type of fouling normally occurs towards the end of filtration operation [94] either by crystallization or particle deposition of salts and minerals, e.g. $CaSO_4$ and $CaCO_3$, on the membrane surface [98], [118]. Lastly, biological fouling, or biofouling, occur from the accumulation and growth microorganisms on the membrane surface and is commonly considered as a severe type of fouling in membrane systems [122]. For organic streams contaminated with microorganisms such as in membrane bioreactors, concentration polarization of organic solutes on membrane surface generates metabolic precursors for microbial growth [131]. This growth results in the formation of a biofilm layer that eventually leads to irreversible fouling. Overall, membrane fouling not only decreases the mass transfer rate of membrane operations, but it also leads to higher operating costs, higher energy requirement, reduced membrane lifetime, and increased cleaning frequency. Due to these adverse effects on operation and economics, several membrane fouling control strategies have been reviewed in literature and are continually being developed to optimize membrane operations [122]. These strategies include feed and membrane modification, effective design, and efficient operation, as shown in Figure 13.

Figure 13

Various Fouling Control Strategies and Operational Consequences

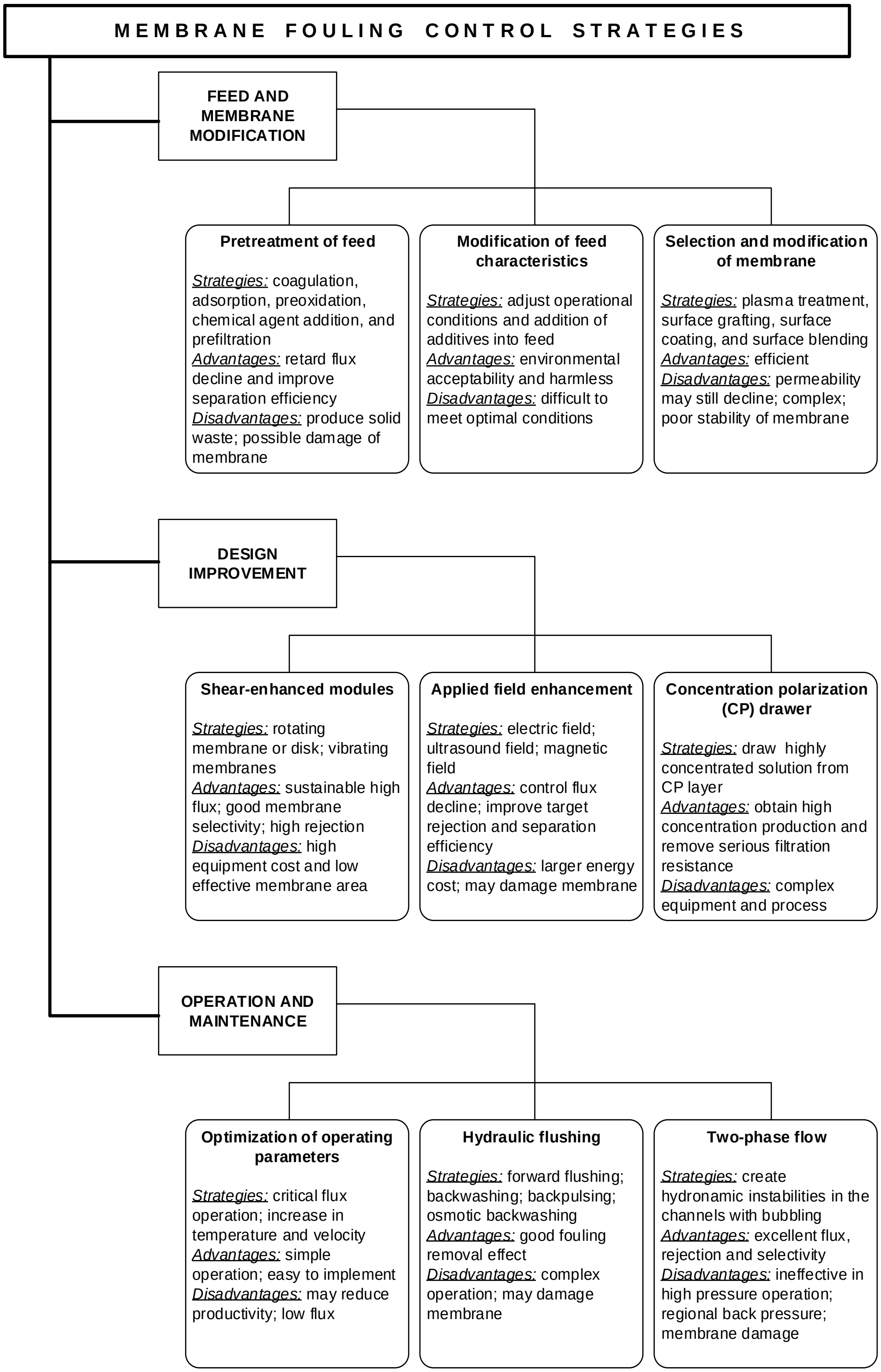

The feed may be pretreated to improve characteristics such as reduce foulant components, pH, or ionic strength and favor fewer fouling risks. On the other hand, membrane selection and surface modification can be done to improve membrane morphology, hydrophilic/hydrophobic properties, and surface charge that affect flux behavior. On the aspect of design, membrane systems may be incorporated with shear-enhanced filtration modules, applied field enhancement, or by inclusion of CP drawers to minimize concentration polarization and membrane fouling. Although effective, this aspect of fouling control is complex, expensive, and may be limited by area. Lastly, fouling can also be controlled by optimal operation, hydraulic flushing, and two-phase flow.

2.4.4 *Surface Shear Generation in Vibratory Membrane Separation*

The vibrating membrane filtration technology employed in this study uses mechanical energy to promote periodic oscillatory movements on the membrane module. These high-speed vibrations, commonly ranging between 50 Hz to 60 Hz, create shear fields that are considerably large enough to overcome local shear rates generated in conventional CF filtration. As a result, this dynamic operation allows the maintenance of permeate fluxes and solute retention without requiring large CF velocities and applied TMPs. The local membrane shear rates generated from this operation also vary sinusoidally with time and proportionally to radius [2]. The CF velocities in VSEP is a function of the transverse velocity (or azimuthal flow) of the fluid in the annular membrane channel, as shown in Figure 14.

Figure 14

Schematic Representation of L-101 VSEP membrane module: (a) Assembly, Flow and Vibration; and (b) Membrane Dimensions

(a)

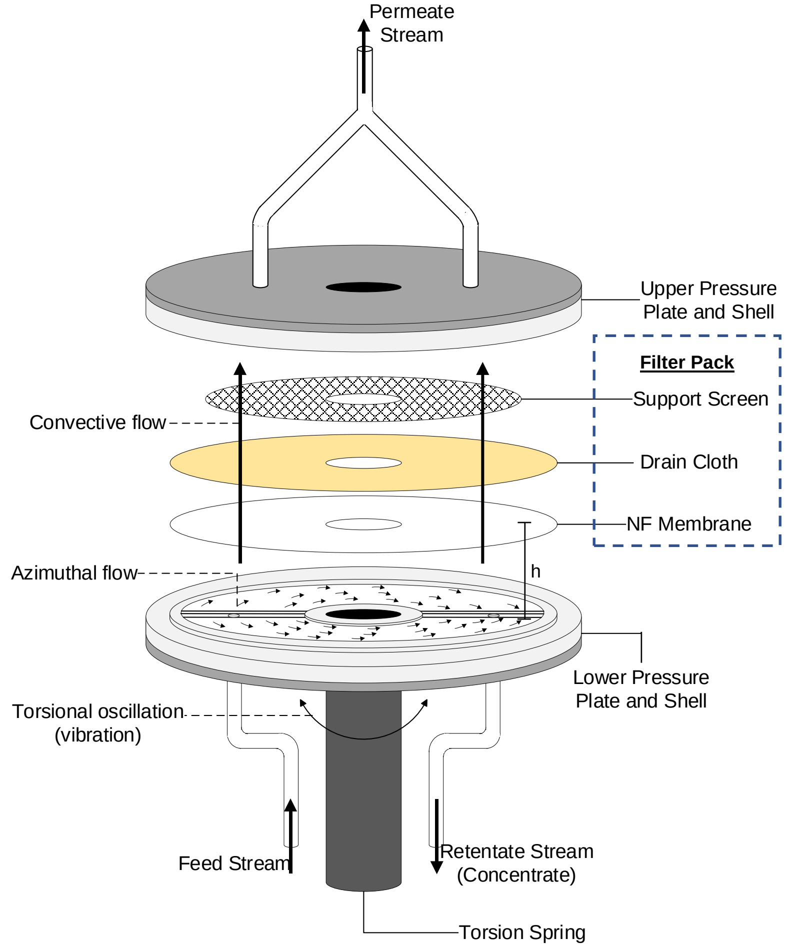

(b)

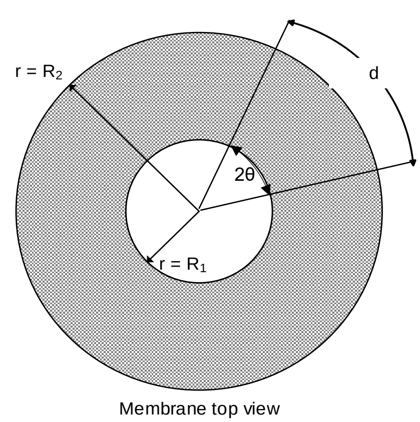

Rosenblat [132] characterized this transverse velocity (V) of fluid flowing between parallel oscillating disks as a function of radius (R_i), oscillation frequency (F), amplitude of angular velocity (Ω), along the vertical distance along the axial line of symmetry (h), as shown in Equation 19.

$$V = R_i \, \Omega e^{2\pi i F t} \qquad (19)$$

$$\text{on } z = 0, h$$

Further, the displacement resulting from the oscillation of the disks is a function of the rotational amplitude (θ) and the radial position (R_i), and the maximum displacement is measured at the disk periphery (R_2), as shown in Equation 20.

$$d = 2R_2\theta \qquad (20)$$

On the other hand, rotational amplitude is a function of the angular velocity and radius, as shown in Equation 21.

$$\theta = \frac{\Omega}{2\pi F} \qquad (21)$$

Based from Equation 20 and Equation 21, the maximum displacement attributed to the vibrations of the membrane module can be calculated from Equation 22.

$$d = \frac{R_2\Omega}{\pi F} \qquad (22)$$

For the VSEP system used in this study, the channel height was found to be approximately 3.5 mm, while the vibrational displacement at the membrane module periphery can be employed up to 3.18 cm at a corresponding frequency of 54.7 Hz. On the other hand, the flow regime (Re) in the oscillating module is a function of the fluid kinematic viscosity (υ), channel height (h), and vibrational frequency, as shown in Equation 23. Thus, for water at 25 °C processed at 54.7 Hz, the resulting flow regime is turbulent based on the Re at approximately 4,700. This flow regime will remain relatively high than those generated by high velocity that tend to considerably reduce with highly viscous fluids [2].

$$\mathrm{Re} = \frac{2\pi F h^2}{\upsilon} \tag{23}$$

Akoum, et al. [2] analyzed the hydrodynamic conditions for the VSEP membrane module, where the fluid flows azimuthally between two plates oscillating in the same phase, as opposed to the analysis made by Rosenblat [132]. Accordingly, the local transverse velocity of the fluid between the disks varies with time and relative vertical position within the channel (y = z/h), as shown in Equation 24.

$$V(y,t) = r\,\Omega\left[e^{-\sqrt{(\mathrm{Re}/2)}y}\cos\left(2\pi F t - \sqrt{(\mathrm{Re}/2)}y\right) + e^{-\sqrt{(\mathrm{Re}/2)(1-y)}}\cos\left(2\pi F t - \sqrt{(\mathrm{Re}/2)(1-y)}\right)\right] \tag{24}$$

On the other hand, the local surface shear rate (Υ_w) was found to be a function of radial position and time as shown in Equation 25.

$$\Upsilon_w(r,t) = \frac{2r\theta(\pi F)^{1.5}}{\nu^{0.5}}\left[\cos(2\pi F t) - \sin(2\pi F t)\right] \tag{25}$$

As shown in the equations, both equations are also a periodic function of time and the local shear rate is independent of the vertical distance in the flow channel, while the local transverse velocity is independent of radial position. Thus, the maximum membrane surface shear rate ($\Upsilon_{w\ max}$) can be calculated when the periodic term $[\cos(2\pi Ft) - \sin(2\pi Ft)]$ is approximately $2^{0.5}$, and at the periphery of the membrane (R_2), as shown in Equation 26.

$$\gamma_{w\ max} = \frac{R_2 \Omega Re^{0.5}}{h} = 2^{0.5} d(\pi F)^{1.5} \upsilon^{-0.5} \tag{26}$$

Lastly, the mean surface shear rate ($\Upsilon_{w\ mean}$) is calculated over a period of oscillation over the membrane annular area measured from the inner radius (R_1) and outer radius (R_2). This relationship is observed to be a function of the maximum shear rate, as shown in Equation 27.

$$\gamma_{w\ mean} = \frac{2^{1.5}\left(R_2^3 - R_1^3\right)}{3\pi R_2\left(R_2^2 - R_1^2\right)} \gamma_{w\ max} \tag{27}$$

In the case of the VSEP system, studied herein, the annular flow area corresponds to an inner radius of 4.7 cm and outer radius of 13.5 cm.

2.5 Life Cycle Assessment

The discussions, so far, stipulate how the inefficiencies in food and beverage manufacturing are commonly attributed to their water and energy use. Today, the efficient use of the limited water and energy resources, as well as the minimization of wastes are among the vital issues central to the food-water-energy nexus for sustainable industrial production. The soluble coffee production is among the food and beverage industries that could benefit from process intensification through the efficient use of water resources and by strategically integrating alternative water recovery routes. In particular, the use of membrane-based water recovery alternatives not only positively impacts the industry through wastewater reclamation [51], but may also further the potential benefits from water recovery upstream as a coffee extract preconcentration alternative to thermal evaporation. Such approach, investigated in this study, will not only promote efficiency in the use of water resources, but may also reduce the high energy consumption from thermal dewatering operations as well as the minimization of wastewater generation through water reuse. However, beyond the performance of membrane processes, aspects such as energy demand, operational limitations, design capital and operating costs, etc. may have implications that may limit the extent of process intensification. From this perspective, it is vital to balance both environmental and economic aspects from a life cycle analytical standpoint.

The International Organization for Standardization [133] defines life cycle assessment (LCA) as an environmental management tool that deals with the systematic review or evaluation of the impacts of a product's complete life cycle, i.e., from extraction of raw materials to final disposal of the product. LCA measures the transfer of these impacts from one medium to another and/or from one life cycle to another [134]. The first account of life cycle analysis was in the 1960s when Coca Cola Company conducted a study on alternative materials for their glass bottle containers, and by the 1990s, this technique has already become a global movement. As an emerging methodology, LCA provides an understanding of the environmental and economic impacts of a product or service relative to its life cycle, thus may be used as a strategic tool in process intensification, technological advancement, and for policy or decision making [135].

2.5.1 *Product Life Cycle*

LCA is also known as "cradle-to-grave" assessment. This systematic technique employs an extensive inventory-and-assessment evaluation of the product's life cycle stages that include (a) resource extraction, (b) material processing, (c) manufacturing, (d) assembly, (e) product use, and (f) end-of-life, as shown in Figure 15.

Figure 15

Stages in Product's Life Cycle

At every stage, all forms of material, energy, and labor used (inputs) and produced (outputs) are thoroughly determined. Waste streams are also accounted including reduction schemes such as recycling, reuse, recovery, and treatment. The entire life cycle is important since each stage differ in environmental impact in terms of types and relative significance. For example, it may be important to consider the higher impact of the accumulation of solid wastes produced from the disposal of packaging materials compared to the wastes from product manufacturing. In terms of resource utilization, environmental impacts may be reduced by considering reuse and recycle practices rather than extraction and disposal, e.g., processing of metals or plastics as raw materials, use of freshwater for industrial operations, wastewater discharge, etc. The impacts from the transportation of materials may also be more significant compared to those from other life cycle stages. Conducting a thorough inventory analysis on these life cycle stages can facilitate strategic planning to balance environmental protection.

2.5.2 *Steps in Life Cycle Assessment*

The International Organization for Standardization provides a general procedure in conducting life cycle assessment. A thorough discussion of this procedure is presented in ISO 14040 and 14044 [133]. In summary, LCA involves the following four distinct phases: (a) goal and scope definition, (b) inventory analysis, (c) impact assessment, and (d) interpretation, as presented in Figure 16.

Figure 16

Life Cycle Assessment Framework

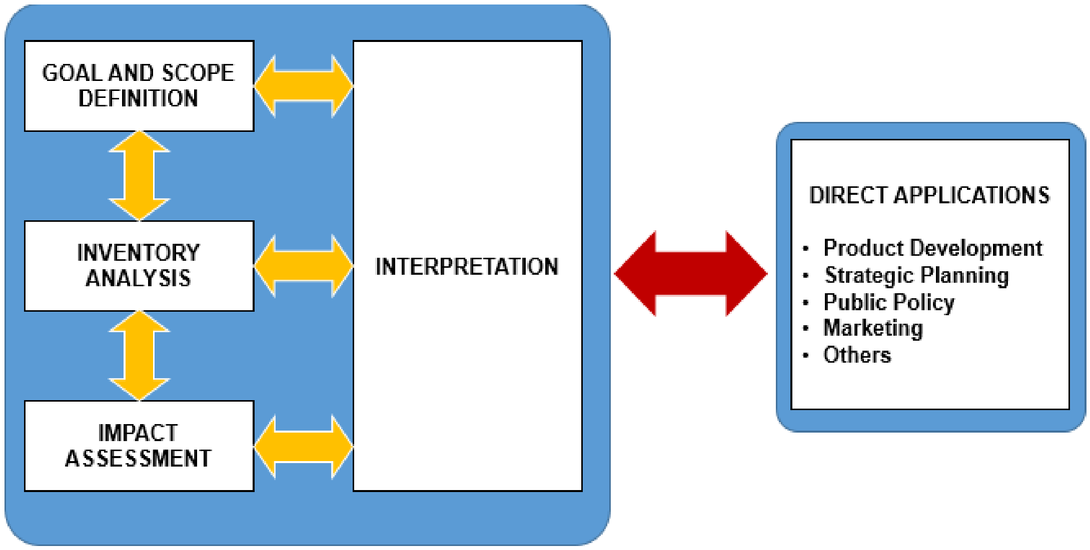

Note: Adapted from International Organization for Standardization [133]

In the first phase, the goal and scope of the LCA study is defined in terms of the intended application, the reasons for conducting the study, and its preferred audience. Scoping involves the determination of the life cycle functions and boundaries of a production system, allocation procedures, methods for impact assessment, types of data to be gathered, and the critical review of relevant working assumptions and limitations for the LCA study. These details set the guidelines on the exact approach employed in the LCA study, e.g., objectives, reference quantities, unit processes involved, flow diagrams, and impact categories, and expected outputs. As a prerequisite, the definition of goal and scope of the LCA study should be sufficient to ensure the credibility of the study.

Once the goal and scope has been defined, a life cycle inventory (LCI) analysis shall be conducted through data collection and calculation. The objective of this LCA phase is to quantify the relative impacts of the inputs and outputs within the life cycle boundaries of production system or LCA study. These LCI impacts may include a summary of the emissions or energy use associated with a material, product, or life cycle stage. Process flow charts are used to facilitate an LCI analysis. From this, material and energy balance calculation can be done with the aid of quantitative data, and valid assumptions and allocations. Mathematical models can also be employed to facilitate the iteration of material and energy flow in the different life cycle stages of the product. More importantly, apart from resource utilization and energy requirement, waste by-product generation and energy inefficiency can also be accounted from life cycle inventory analysis.

Using the results of inventory analysis, the potential environmental impacts from life cycle stages are then assessed. Impact assessment is the evaluation of the direct and indirect, secondary, cumulative, short, medium and long-term, permanent and temporary, positive and negative effects of a life cycle stage [134], [135]. Impact classification, characterization, and ranking are among the elements considered in impact assessment. Overall, the findings from LCI analysis and impact assessment are interpreted to reach conclusions and recommendations to improve the environmental aspects of a production system. More importantly, the results from a thorough LCA study can be used to facilitate product development, strategic planning, public policy, marketing strategies, and other decision-making processes in industries, government, and non-governmental organizations.

An example of LCA study can be conducted to determine the potential of an alternative process to lessen the costs and greenhouse gas emissions associated to a given product [135]. Consider, an overview of the phases of LCA study for paper production. In the first phase, one goal that may be defined is identifying which life cycle stage emits significant amounts for greenhouse gases. A possible scope for this may be defined by the type of pulping process, identifying the pulp and paper mill, and the analytical methods that shall be employed. The method of conducting comparative studies should also be specified. In the second phase, mathematical models to relate the amount and composition of gaseous emissions as a function of the amount of various raw materials used may be developed to facilitate inventory analysis. Correspondingly, in the third and fourth phases of the study, the level of significance of greenhouse gas pollution from each life cycle stage can be used to recommend possible actions to significantly address the problem on greenhouse gas emissions.

2.5.3 *Life Cycle Assessment Tools*

Despite the systematic approach, it must be emphasized that not all LCA studies may be considered as the most appropriate environmental management technique, thus may not be used in all situations. This is due to several limiting assumptions defined in the conduct of the study, especially for newly developed products or services, e.g., the use of genetically modified organisms in crop and livestock production. Some of the limiting assumptions are affected by the nature of defining the scope, models used for inventory analysis or in impact assessment, cultural differences in relevant global, regional, and local issues, and lack of spatial and temporal dimensions considered in the LCA study [133]. Moreover, LCA may not necessarily address the economic and social aspects of a product. This is the reason why other environmental management techniques, e.g., risk assessment, environmental performance evaluation, environmental auditing, and environmental impact assessment, may also be conducted and integrated in order to develop a more comprehensive decision process for a particular product or service.

Overall, while the LCA practice has evolved and extensively applied for process intensification, and policy making, it still requires a high degree of specialization among researchers conducting LCA studies. The degree of expertise and knowledgeability of LCA practitioners in addressing each stage in the life cycle framework are critical in ensure the usefulness of the results obtained from the assessment. In spite of this prerequisite, LCA has progressed to accessible for various applications and to a much wider user base through database management, transparency, and data sharing [134]. Today, LCA tools are increasingly becoming more useful in the field. LCA software applications such SimaPro by PRé Sustainability and GaBi by Sphera Solutions GmbH (then PE-international) are among the widely used databased LCA tools in evaluating product systems [136]. Both software applications have an interface for modeling the product system, life cycle unit process database, impact assessment database and various LCA methodologies, and an integrated calculator to estimate life cycle impacts based from the modeled product system [136].

Chapter 3

Materials and Methods

3.1 Coffee Extract Filtration Experiments

3.1.1 *Preparation of Simulated Coffee Extracts*

The fundamental process for soluble coffee manufacturing commonly involves the removal of water via evaporation and spray- or freeze-drying after the extraction of water-soluble components from the coffee grounds. Thus, for this study, commercial spray-dried coffee products (Nescafé® Taster's Choice®, House Blend) constituted the simulated coffee extracts. Using this procedure allowed greater consistency in the feed solutions for the various runs, and minimized the time for solution preparation. Different feed sample concentrations were prepared by increasing the coffee extract strength from a product recommended "standard" coffee cup concentration of 8.48 g L^{-1}. For this dissertation, feed coffee extract concentrations were varied based on "low-strength" concentrations (< 5% wt/wt), as opposed to commercially produced coffee extract concentrations between 10% to 15% wt/wt. This limitation was based on previous coffee extract concentration studies using conventional CF NF that also used diluted concentrations of reconstituted coffee extracts [32], [33]. However, unlike the previous coffee extract NF studies in the literature, no pretreatment of suspended and colloidal solids was performed in the reconstituted coffee extracts used in this study. All feed samples were prepared by dissolving the soluble coffee powder in water at approximately 60 °C and were cooled and stored at 4 °C. Fresh coffee extract samples were also prepared weekly to prevent the effect of biodegradation, while daily monitoring of feed characteristics ($C_{o\,i}$) was performed. On the other hand, while the characteristics of the coffee extracts may be made based on the analysis of the specific composition, e.g., caffeine, this study focused on how these components affect the membrane performance. These components were referred to as bulk characteristics that pertain to the suspended, colloidal, and dissolved organic components. Thus, in place of a compositional analysis, bulk characterization for the coffee extracts, as well as permeate samples, in this study constituted turbidity, conductivity, absorbance, pH, and chemical oxygen demand (COD).

3.1.2 *Experimental Set-Up and General Procedure*

A Series L-101 VSEP filtration system (New Logic Research, Inc., Minden, NV) was used in the study, as schematically shown in Figure 17. The system has already been used in previous vibratory membrane filtration studies at Rowan University on water recovery from bagel production [137], raw cane sugar processing, microalgae dewatering [138], and soluble coffee wastewater reclamation [51], [52]. As shown, the system consists of a feed tank, membrane filter housing, a vibratory motor with drive system, and a control panel for flow, vibration, and temperature. Pressure and flow valves control the applied TMP and retentate flowrate of the system. The membrane module makes use of a filter pack, with a circular flat membrane sheet having an area of 0.045 m^2. By default, the system conforms a crossflow configuration where the feed flows tangentially on the membrane surface. For the dynamic operation, a vibratory motor induces torsional oscillations on the membrane pack at certain vibrational frequency with corresponding displacement at the periphery of the module.

Figure 17

Schematic Flow Diagram of Series L-101 VSEP Membrane Filtration System

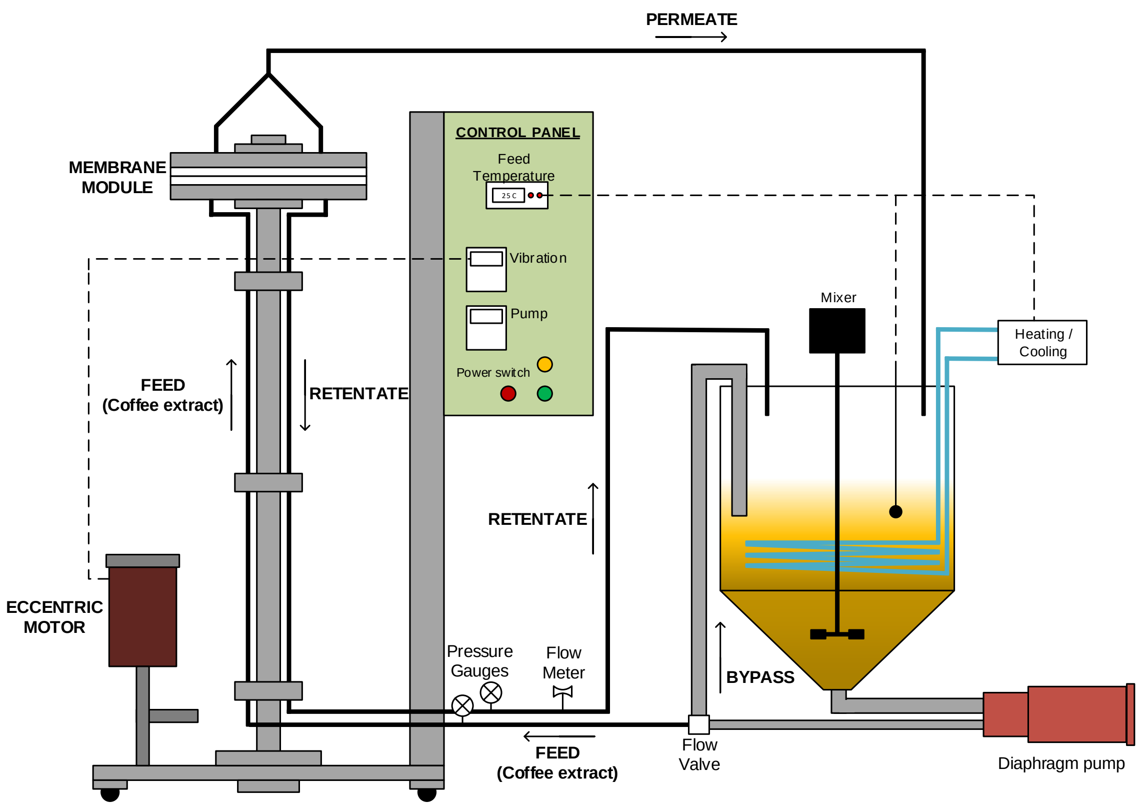

The non-vibratory crossflow filtration mode is when the system runs at 0 Hz. On the other hand, the vibratory configurations can be set up using vibrational frequencies with corresponding quarter-inch displacements relative to the periphery of the membrane module periphery. The maximum applicable vibratory displacement of 1.25 inches (3.18 cm) can be set at a vibratory frequency of 54.7 Hz, while the minimum applicable displacement was 0.25 inch (0.64 cm) at a frequency of 53.3. These conditions were the operational limitations for the module vibrations studied in the experiments, and the prolonged filtration operations beyond these settings may damage the vibratory membrane system. Also, the quarter-inch vibrational displacements were calibrated with vibrational frequencies using stroboscopic markers or visual stickers placed on the outer rim of the membrane housing. As shown in Figure 18, the markers placed at the periphery of the membrane housing create a visual effect when vibrating. The visual effect (shown as the grey part of the images) presents the back-and-forth motion of the membrane module as it vibrates at a certain frequency setting. This visual effect (or blur) indicates a measurable displacement that varies as the frequency is increased. The corresponding frequencies calibrated at quarter-inch displacements are shown in the figure below.

Figure 18

Stroboscopic Displacement Markers at the Membrane Module Periphery and Corresponding Vibrational Frequencies

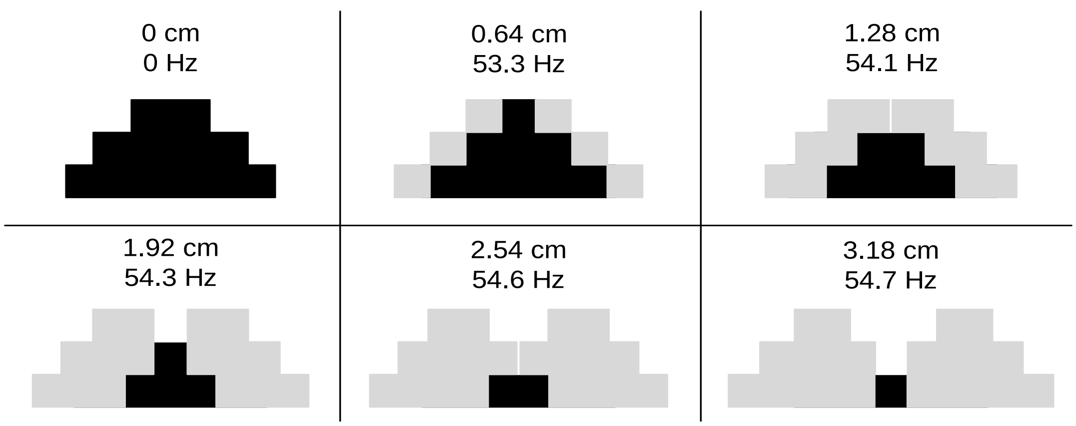

The membrane filtration experiments were conducted under full recycle mode, where the retentate (concentrate) and permeate (filtrate) streams are recirculated back to the feed tank. These experiments were conducted under different TMPs, vibration settings, feed temperature, and retentate flow rate for a working volume of 35 L. A new NF membrane was used for each operating pressure, and feed concentration employed.

The NF membrane was reused for each set of vibration settings. While no membrane cleaning was performed in between vibration settings, experiments were employed starting from the highest vibration setting (54.7 Hz, 3.18 cm) down to non-vibratory operation (0 Hz, 0 cm). In this manner, any possible concentration polarization occurring under high-vibration operations will have minimal effect on the performance of low- and non-vibratory operations. Experiments were conducted for a total filtration time of 1 hour (60 mins) to approach steady-state fluxes. Accordingly, thin film composite membranes used in this study typically approach stable fluxes within this time period, and even shorter time periods for vibratory filtration, as presented in the result. Throughout the filtration time, permeate samples were collected at 5-minute intervals to monitor permeate fluxes and characteristics. Steady-state parameters, on the other hand, were sampled at the end of the filtration time and analyzed in duplicate using standard methods of analysis enumerated in Section 3.1.4.

3.1.3 *Calculated Experimental Parameters*

3.1.3.1 Permeate Flux. Permeate samples were intermittently obtained and the measured volume (V_p) at timed intervals (t) were used to determine the permeate flux for the corresponding membrane area (A) of the membrane system, using Equation 28.

$$J_v = \frac{1}{A}\frac{dV_p}{dt} \tag{28}$$

3.1.3.2 Permeate Flux Adjustment. During filtration runs, the feed pump and eccentric motor impart mechanical friction that heat up feed and retentate streams. A cooling coil in the tank was used to regulate feed tank temperature at about 25 ± 1 °C. At this temperature range, the permeate fluxes varied slightly that needed to be normalized. The viscosity correction factor (Equation 29) was also used to normalize the permeate fluxes (J_T) to a standard temperature of 25°C ($J_{25°C}$) using the ratio between water fluxes at different temperatures ($J_{water\ T}$) with that at 25°C ($J_{water\ 25°C}$).

$$J_{25°C} = J_T \left(\frac{J_{water_{25°C}}}{J_{water_T}} \right) \tag{29}$$

3.1.3.3 Flux Decline. Experiments were conducted for a total filtration time of 60 minutes, and permeate samples were collected at 5-minute intervals to monitor permeate fluxes and characteristics. The decline in flux throughout the filtration time was measured based on time profile. The experimental fluxes were fitted according to the power law model, shown in Equation 30.

$$J_v = J_o\ t^{-b} \tag{30}$$

Using the power law model, the corresponding initial fluxes (J_o) and flux decay rates (b) at specific operating conditions were then determined. These empirical parameters served as the basis for calculating the degree of flux decline after 60 minutes of filtration using Equation 31.

$$\text{Flux decline} = \frac{J_o - J_v}{J_o} \times 100 \tag{31}$$

3.1.3.4 Observed Rejection Efficiency. Permeate samples were also characterized in terms of bulk solute characteristics ($C_{p,i}$) for turbidity, conductivity, absorbance, and chemical oxygen demand (COD). These measurements were compared with feed coffee extract characteristics to determine the observed rejection efficiencies ($\%r_{o\,i}$), calculated using Equation 32.

$$\%r_{o\,i} = \frac{C_{o_i} - C_{p_i}}{C_{o_i}} \times 100 \tag{32}$$

3.1.3.5 Surface Shear Rates. In Section 2.4.4, Akoum et al. [2] mathematically derived the maximum surface shear rates ($\gamma_{w,max}$) generated on the membrane surface. To calculate this parameter, the vibrational displacement (d) and frequency (F) of the membrane module, and the kinematic viscosity of the fluid (υ) are needed, as was shown earlier in Equations 26 (Section 2.3.5).

$$\gamma_{w\,max} = 2^{1/2} d(\pi F)^{3/2} \upsilon^{-1/2} \tag{26}$$

3.1.4 *Determination of Coffee Extract and Permeate Characteristics*

3.1.4.1 Analytical Methods. Coffee extracts are complex mixtures of mostly organic compounds that contribute to its aroma, taste, flavor, and color. Soluble, suspended, and colloidal components of varying particle sizes and charges may limit permeate fluxes and rejection efficiencies in membrane filtration operations. Due to the complex variety of compounds constituting coffee extracts, this dissertation only focused on bulk characterization of the feed and permeate samples, rather than monitoring the specific constituents present in the samples. These representative characteristics include absorbance, turbidity, conductivity, and organic concentration in terms of COD that were adapted from the membrane-based soluble wastewater reclamation studies performed by Wisniewski, et al. [50]–[52]. While these bulk characteristics are commonly employed for wastewater analyses, these metrics are considered in on-site water reuse standards observed by different industries [139]. Apart from the interest in assessing the effectiveness of membrane separation, this study shares a similar objective to assess the reusability of the permeate in various soluble coffee factory operations. From this standpoint, the investigation of a reusable permeate qualifies these bulk characteristics as proxy analyses of the variety of constituents of the feed coffee extracts and of the permeate recovered from membrane filtration experiments. Standard methods of analysis [140] were used to characterize the feed, as well as the permeate samples. These methods are generally comprised of modern analytical techniques that employ spectroscopic and electrochemical instruments for real-time measurements, rather than wet laboratory analyses that commonly require several preparation and analytical steps.

3.1.4.2 Color. The color of the feed coffee extracts at different concentrations, as well that of the permeate obtained from membrane filtration experiments, indicates the strength of colored constituents that may be present as dissolved, suspended, or colloidal solids. Coffee extracts are characterized to have a dark brown color that are commonly attributed to colored organics, such as melanoidins, produced from Maillard browning and caramelization during the roasting and thermal extraction steps [24]. The intensity of these colored compounds was determined spectrophotometrically by measuring the absorbances or the amount of light absorbed by the feed coffee extracts and permeate samples at maximum wavelength of 640 nm. This wavelength has been found to be suitable for orange-red colored compounds, generally characteristic of the dark brown color of coffee extract constituents. Solution absorbances at 640 nm wavelength were measured using Hach ® DR 1900 Spectrophotometer (Hach Company, Loveland, CO).

3.1.4.3 Total Organic Matter. The highly organic nature of the coffee extracts is also an important consideration not only when assessing membrane separation performance, but also in assessing the reusability of the permeate recovered. These organic components include proteins, polysaccharides, lipids, and organic acids that may be present in varying particle sizes, concentrations, and charges. In place of compositional analyses of the different organic constituents, this study employed bulk organic matter characterization method using chemical oxygen demand (COD) determination. COD is an indirect measurement of the amount of oxygen needed to oxidize organic matter using strong oxidizing agents such as potassium dichromate or potassium permanganate [135]. This parameter collectively characterizes all biodegradable and non-biodegradable organic components that may be present in process streams. For this study, the total organic matter concentration was measured via Hach COD analytical method 5220 D. For COD analyses, potassium dichromate solutions in standard commercially prepared vials (Hach COD reagent vials) were used as reagent. Feed coffee extracts and permeate samples were diluted, as necessary, according to the allowable COD concentration range of the reagent vials. High-range (HR) COD vials allow COD concentrations of up to 1500 mg L^{-1} from 2-mL samples, while High-range plus (HR+) COD vials allow COD concentrations of up to 15,000 mg L^{-1} from 0.2-mL samples. The samples were placed in the reagent vials and were allowed to be thermally digested or decomposed for two hours using a Hach ® DRB 200 COD Digester (Hach Company, Loveland, CO). After digestion, the vials were cooled at room temperature. During this digestion step, chemical oxidation of the organic matter from the samples takes place and the use of dissolved oxygen for these reactions have a proportional effect on the color intensity of the dichromate in the reagent vials. This change in color is measured as COD concentrations, spectrophotometrically using Hach ® DR 1900 Spectrophotometer (Hach Company, Loveland, CO). After the analysis, dilution factors were employed in determining actual COD concentrations, as necessary.

3.1.4.4 Solids. Coffee extract components can also be present as dissolved, and suspended or colloidal solids. The total dissolved solids constitute the dissociated coffee extract components like chlorogenic acids, caffeine, esters, organic acids, but may also include mineral ions or inorganic salts upon dissolution in water. These components in solution exhibit electrical charges that increase with higher coffee extract concentrations. In this study, the dissolved solids concentration in the feed and permeate samples were expressed as electrical conductivity using an Oakton CON 510 Series conductivity/TDS meter (Cole Parmer, Vernon Hills, IL). The conductivity meter works by emitting an electric charge or current through the electrodes contained in a probe. The probe is placed in the solution and the electrical charges and resistances of the constituents causes a voltage drop that can be read by the meter as electrical conductivity (in $\mu S\ cm^{-1}$). This value is representative of the total dissolved solids.

On the other hand, the suspended solids are highly dispersed constituents in the coffee extract, and may comprise of an array of organic macromolecules or colloidal particles (clusters of macromolecules) that are invisible to the naked eye due to their small particle size (> 1μm). Some of these components also carry surface charges that allow them to be highly dispersed in solutions. These surface charges arise from the ions adsorbed on the surfaces of the suspended matter that may also exhibit an electrical conductivity. Due to their relatively small size, conventional suspended solids gravimetric measurements using 2-µm filters make it difficult to distinguish colloidal suspensions from dissolved constituents. Alternatively, suspended and colloidal solids exhibit light scattering properties that can be measured in terms of turbidity. Thus, for this study, the amount of suspended and colloidal solids present in the coffee extracts were measured as turbidity (in NTU) using a Hach TL 2300 Turbidimeter (Hach Company, Loveland, CO). The nephelometric method employed in turbidity analysis compares how light is scattered by a solution sample in comparison to that of a reference or standard solution. Samples were placed in turbidity vials that are then placed in the instrument. The instrument has a light source and a detector placed perpendicularly from it measures the amount of light scattered by the solids in the sample. The amount of light detected from light scattering defines the concentration of suspended and colloidal solids in the solution.

3.1.4.5 Calculation of Fluid Properties. For fluid properties such as density and absolute viscosity, the correlations developed by Telis-Romero, et al. [141], [142] were used. The density of the coffee extract is related by the density of water at a given temperature (ρ_w) and mass fraction of water in the solution (X_w), shown in Equation 33.

$$\rho = \rho_w(1.47\text{-}0.47X_w) \tag{33}$$

On the other hand, the absolute viscosities of the coffee extracts were extrapolated from the viscosity data for coffee extracts at different concentrations and temperature, as shown in Table 12.

Table 12

Viscosities of Coffee Extracts at Different Concentrations and Temperature

X_w	Dynamic Viscosities at T(K) (10^{-3} Pa-s)					
	295	307	323	337	351	365
0.76	2.810	2.160	1.610	1.300	1.210	0.910
0.82	1.810	1.390	1.040	0.830	0.690	0.580
0.86	1.350	1.040	0.770	0.610	0.510	0.440
0.90	1.000	0.770	0.580	0.460	0.380	0.320

Note: Adapted from Telis-Romero, et al. [141]

3.1.5 *Statistical Analysis*

Experimental design, statistical analyses, and numerical optimization for this study were performed with the aid of Design Expert v12 ® (Statease, MN, USA). Model regression was performed based on various tests on model significance and statistical soundness, e.g., analyses of variance ($\alpha = 0.05$), lack-of-fit tests, coefficients of determination (R-squared), and other statistical diagnostic tools. [143]

3.2 Modified Scale-Up Study

Laboratory-scale membrane filtration experiments were conducted to derive scale-up parameters that may be used to project the operation of a commercial system to supplement thermal evaporation in preconcentrating coffee extracts and recovering 3.79×10^5 L reusable permeate per day. Typical scale-up studies involve unsteady-state filtration experiments in concentrating mode by collecting the permeate in a separate tank, while recirculating the retentate back to the feed tank [51]. Conventionally, these experiments required the monitoring of instantaneous permeate fluxes, permeate concentrations, and rejection, while continuously collecting the permeate to achieve a desired final concentration or water recovery. The pooled permeate parameters, on the other hand, are expressed in terms of average permeate flux and characteristics, that are plotted with water recovery (%R) to determine scale-up parameters.

However, the conventional concentration study requires continuous filtration runs that take several hours, or days, especially for heavily concentrated coffee extracts. Alternatively, a modified scale-up study was employed by relating different feed coffee extract concentrations (C_o) with R from a mass balance standpoint, using Equation 34.

$$\frac{C_{o,final}}{C_{o,initial}} = \frac{100}{100 - \%R} \tag{34}$$

$$C_{o\ initial} < C_{o\ final}$$

In the modified approach conducted in this study, membrane filtration was performed in recycle mode by recirculating the retentate and permeate streams to the feed tank. Steady state permeate parameters were determined in duplicate for different feed coffee extract concentrations. The experimental permeate parameters were then correlated using the film layer model, similar to those performed for the concentration of milk proteins via vibratory UF [5]. A detailed procedure of the mathematical modeling study used for scale-up is presented in Section 8.2.3. From the correlation, modeled permeate parameters (J, C_p, and $\%r_{o\ i}$) were calculated for different R or coffee extract concentrations. The modeled parameters were referred to as "instantaneous" parameters, i.e., permeate conditions at the time the permeate exits the filtrate side of the membrane. On the other hand, the pooled permeate characteristics were calculated as "average" permeate parameters at corresponding levels of %R (5%, 10%, …, 95%). The average permeate fluxes (J_{avg}) were based on cumulative average of instantaneous fluxes at different levels of %R. On the other hand, the average permeate characteristics at different levels of %R ($C_{p\ avg\ R}$) were calculated from the volume-weighted mean based on the cumulative volume of water recovered at certain %R ($V_{R,\ i}$). In place of measured cumulative volumes, the cumulative volumes from the modified concentration study were estimated at given values of R and the “scaled-up” volume of coffee extract processed (V_{coffee}) using Equation 35.

$$V_R = V_{coffee}\%R \tag{35}$$

$$(\%R = 5\%, 10\%, \ldots, 95\%)$$

From this, $C_{pavg\ R}$ were then calculated from solute mass balance relative to the cumulative volume of the pooled permeate, as shown in Equation 36. At 0% recovery, the average permeate concentration and cumulative volume are zero.

$$C_{p_{avg}\ R} = \frac{\left(C_{p_{avg}\ R-5}\right)(V_{R-5})+\left(C_{p\ R}\right)(V_R - V_{R-5})}{V_R} \tag{36}$$

The instantaneous and average permeate parameters were then plotted against C_o and R, and average permeate flux, concentrations, and rejection efficiencies were interpolated for a desired permeate flow rate of 378,500 L d^{-1} and a final coffee extract concentration of 35% (wt/wt). The projected average permeate concentrations and corresponding rejection efficiencies reflect the reusability of the permeate; while the average permeate flux was used to derive the design flux scale-up parameter.

3.3 Techno-Economic and Environmental Assessment

3.3.1 *Scale-Up Design Calculations*

3.3.1.1 i84 VSEP Filtration System. The average permeate flux at the desired final coffee extract concentration (35% wt/wt) was multiplied by a design uncertainty (U) of 0.5 to determine the design flux scale-up parameter (J_{design}), shown in Equation 37.

$$J_{design}=J_{avg}U \tag{37}$$

From here, scale-up design of the vibratory membrane system was based on commercially available VSEP i84 Filtration System from New Logic Research, Inc. [144], shown Figure 19. The filtration system is the largest among the VSEP i-series commercial membrane modules [144]. This filtration system was chosen for its suitability to process large flow rates up to 408,000 L d^{-1} and high-strength process streams [51], [144] such as the simulated coffee extract studied herein. This version of the commercial VSEP system is a commonly employed industrial system, and design information for it is readily available. Multiple module filtration systems may also be employed for larger flow capacities. However, as a licensed commercial system, no design modifications were considered for this study. As shown in the Figure, each module consists of several membranes stacked vertically, about 360 to 500 membranes with area of about 2.78ft^2 per membrane depending on the module option. Each i84 filtration module has a dimension of 1.2 m (width) x 1.2 m (length) x 4.9 m (height). The vertical stack design can be rated for indoor or non-extreme outdoor conditions due to the smaller plant footprint of the system than conventional systems. More importantly, the smaller footprint strategically allows the process to be integrated into systems commonly limited by floor space. A standard system is accompanied with a controls skid for maintaining operating pressures and temperatures, conductivity and pH measurement, vibration control [144]. A chemical metering station is also available for membrane cleaning operations. Lastly, the cost per module of the i84 filtration system is $300,000 [51], [61], and this was used as basis for calculating the capital cost.

Figure 19

Schematic Representation of Single Module i84 VSEP Filtration System

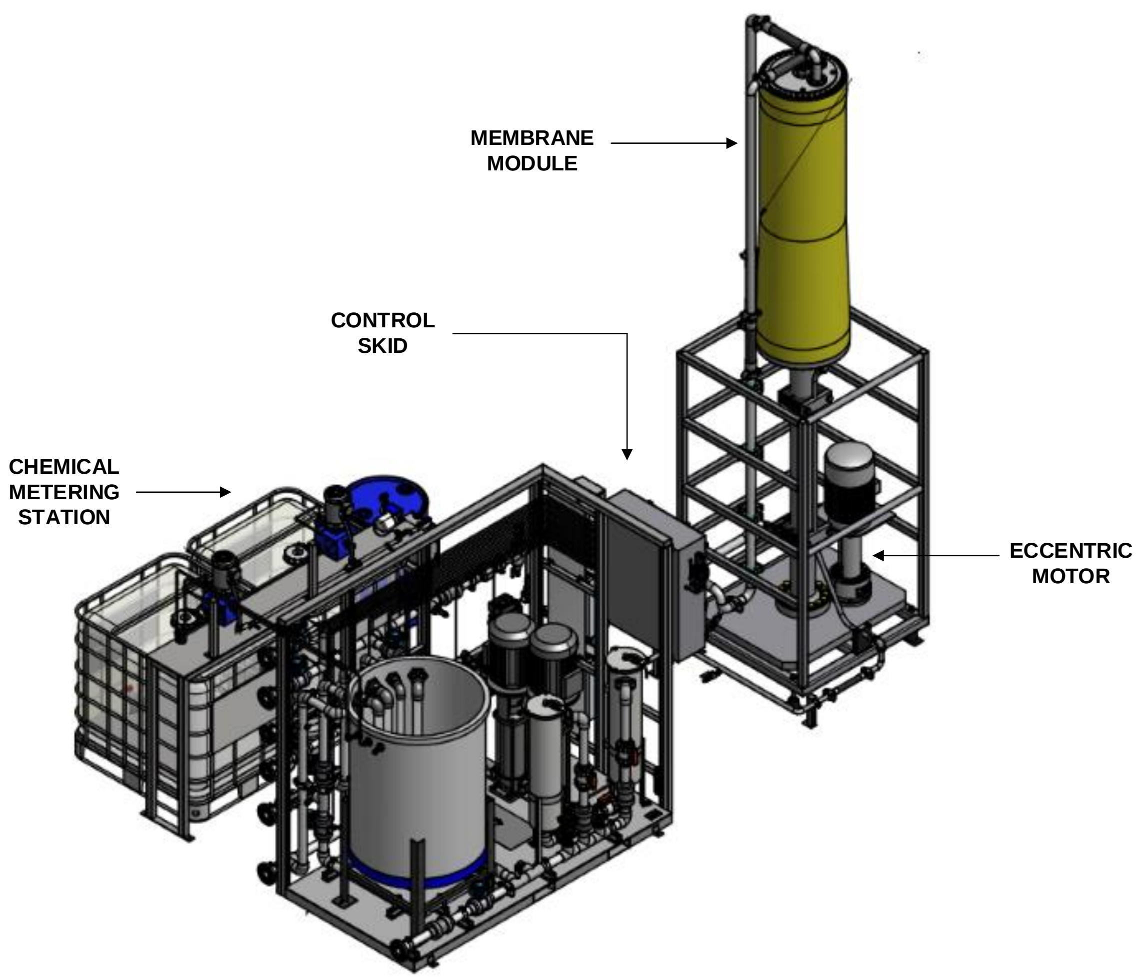

Note: Adapted from New Logic Research, Inc. [144]

The membrane system is available in membrane area options from 92.9 m^2 to 139.4 m^2 (1,000 ft^2 to 1,500 ft^2) per module. From the design flux, an optimum membrane area per module (A) corresponding to the minimum number of modules (N), hence capital cost, was selected from the commercially available membrane area options [144]. Equation 38 was used to calculate N based on the permeate flow rate, A, and J_{design} [145], with adjustments based on an overall system factor (OSF) of 1.5 accounting design uncertainty [146] and cleaning cycle time.

$$N_{module} = \frac{\text{Permeate Rate}}{(J_{design})(A_{module})}(OSF) \tag{38}$$

3.3.1.2 Operating Cost Calculation. The operating costs included the power requirement from the pump and vibratory motor of the filtration system, the cost of cleaning chemicals, and membrane replacement expense. The power requirement of the pump was calculated based on the feed flow rate (Q_F) and operating pressure (P) at a pump efficiency (η) of 0.85, while that of the vibratory motor was based on the number of modules of the system. Accordingly, each membrane module vibratory motor has a power requirement of 10 hp [144]. The power requirement of the system is determined based on Equation 39. On the other hand, the corresponding energy requirement (E) was calculated based on a daily operating time of 22 hours per day, as shown in Equation 40.

$$Power_{system}=\left(\frac{Q_F P}{\eta}\right)+(N_{module}Power_{vibration}) \tag{39}$$

$$E = Power_{system}(\text{Operating time}) \tag{40}$$

The cleaning cost was based on the amount of cleaning chemicals consumed. This operating cost parameter is a function of the volume of cleaner per module (V_c), number of cleanings (n_c), time between cleanings (t_c), concentration of the cleaner (%c), and the number of modules, as shown in Equation 41. For this system, V_c is set to 70 gal, t_c is 40,320 minutes and %c for all studies is set to 2%, or 0.02.

$$\text{Cleaner consumption} = \%c \left(\frac{V_c n_c}{t_c}\right)(N_{module}) \tag{41}$$

Lastly, the estimated membrane lifetime for the proposed vibratory NF system is 5 years that is well within the expected lifetime of polymeric membranes (3 to 5 years) used in CF filtration systems [147]. All bases for operating costs were adapted from parallel scale-up studies on vibratory nanofiltration [51].

3.3.2 *Economic Assessment*

The alternative soluble coffee process integrated with the proposed vibratory NF system was assessed and compared with the base case through a 10-year profitability study for the manufacturing plant. For this study, the estimated overall operating costs, capital cost of the proposed NF system, and projected operating cost savings were factored in a standard 10-yr cash flow. The 7-year modified accelerated cost recovery system (MACRS) depreciation method was employed along with tax and interest rates of 21% and 15%, respectively. From the cash flow, economic metrics [148] for the internal rate of return (IRR), return on investment (ROI), payback time after-tax, net present value (NPV) after 10 years were then determined.

The capital or investment cost ($Cost_{capital}$) for the economic assessment was based on the number of modules of the i84 Vibratory Filtration System and was reflected as a negative value for Year 0 in the cash flow. Depreciation cost is annually charged (D_n) from Years 1 to 10 according to the MACRS depreciation method, shown in Equation 42, where DF_n is the depreciation factor for year n.

$$D_n = \frac{Cost_{capital} DF_n}{100} \tag{42}$$

Thus, at Year n, the depreciated cost or book value of the recovery system corresponds to its net value after subtracting from the capital cost the accumulated depreciation costs from Year 1 to n (Equation 43).

$$\text{book value} = \text{investment} - \sum_{n=1}^{n=t} D_n \tag{43}$$

Income was also factored in the cash flow for Years 1 to 10 based on the difference between the pretax cash flow and D_n, shown in Equation 44.

$$\text{Income}_n = \text{pretax cash flow} - D_n \tag{44}$$

The pretax cash flow was based on the annual operating cost savings relative to the operating cost of the base case and alternative case. For this study, the operating cost (OC) comprise of those associated with the mass flows (m_i) for feedwater usage, wastewater treatment and discharge, energy consumption (E_i), and the membrane recovery system (R_i). These quantities were calculated based on mass and energy balance calculations within the life cycle boundaries, discussed in Chapter 4. In general, the operating costs of the base ($R_i = 0$) and alternative cases were calculated relative to the unit costs of the process components, as shown in Equation 45.

$$OC = \sum_{i}^{r} (OC_i \cdot R_i) + \sum_{i}^{w} (OC_i \cdot m_i) + \sum_{i}^{e} (OC_i \cdot E_i) \qquad (45)$$

On the other hand, the operating cost savings or pretax cash flow was calculated using Equation 46.

$$\text{Savings} = OC_{BC} - OC_{AC} \qquad (46)$$

Income tax was also charged for each year at a tax rate of 0.21 and was calculated using Equation 47.

$$\text{Income tax} = (\text{tax rate})(\text{Income}_{n-1}) \qquad (47)$$

Considering all the associated operating costs, savings, and taxes, the cash flow for each year was calculated using Equation 48.

$$\text{cash flow} = \text{pretax cash flow} - \text{tax} \qquad (48)$$

The cash flows from Years 1 to 10 served as the basis for calculating the different economic metrics. An average cash flow was calculated throughout the 10-year economic assessment period. This average value served as the basis for estimating the ROI and payback period after-tax of the alternative case. These metrics are calculated using Equation 49 and Equation 50, respectively.

$$\text{payback time after tax} = \frac{\text{investment}}{\text{average cash flow}} \qquad (49)$$

$$\text{ROI} = \frac{\text{average cash flow}}{\text{investment}} \tag{50}$$

Lastly, the NPV after 10 years and the IRR from the alternative case are calculated using Equation 51 and Equation 52, respectively.

$$\text{NPV}=\sum_{n=1}^{n=t}(\text{cash flow})(1+i)^{-n} \tag{51}$$

$$0=\sum_{n=1}^{n=10}(\text{cash flow})(1+i)^{-n} \tag{52}$$

3.3.3 *Environmental Assessment*

Unlike LCA studies that evaluate the impacts of extensive changes in processes, e.g., use of alternative raw materials, chemical agents, fuel sources, new reactive process, etc., process intensification in this study was only based on integrating water recovery routes in the soluble coffee process. Thus, other than the membrane-based water recovery system, all processes considered in the scope of the assessment study were based on current practices. Consequently, rather than conducting a full-scale LCA study, only the environmental impacts encompassing the water recovery aspect of the base and alternative cases were compared. Despite the partial LCA study, all necessary steps for assessment discussed in Section 2.5.2 were considered in this study.

Similar to operating cost calculations, life cycle emissions (LCEs) were estimated relative to mass and energy flow of the process components defined in the life cycle boundaries, and their corresponding LCIs. The LCIs, accounting for the corresponding emissions per unit of each process component, were estimated using SimaPro® v9 software (Pré Sustainability, Amersfoort, The Netherlands). As will be discussed in Section 4.2.1, the LCIs defined within the case studies include those of freshwater used in soluble coffee processing, treatment and disposal of wastewater, steam consumed for evaporation, and electricity used for pumps, blowers, and motors were determined [51]. LCIs based on raw environmental emissions data obtained from the LCA software were narrowed down to adequate information. This information was listed in terms air (CO_2, CO, CH_4, NO_x, non-methane volatile organic compounds, particulates, and SO_2), water (volatile organic compounds and other water pollutants), and soil emissions [149]–[151]. Using this information, the LCEs for each scenario were then calculated relative to the mass and energy flows of the process components based on Equation 53.

$$LCE=\sum_{i}^{r}(LCI_i\cdot R_i)+\sum_{i}^{w}(LCI_i\cdot m_i)+\sum_{i}^{e}(LCI_i\cdot E_i) \tag{53}$$

Once the LCEs for each scenario (base case (BC) and alternative case (AC)) have been calculated, the amount of avoided emissions were then estimated by obtaining the difference between the two cases, as shown in Equation 54.

$$LCE_{avoided} = LCE_{BC} - LCE_{AC} \tag{54}$$

Chapter 4

Base Case Assessment of the Soluble Coffee Process

4.1 Introduction

The developments in the soluble coffee industry have, so far, focused on configuring thermal dewatering operations by operating at lower boiling temperatures (vacuum evaporation and drying), or in the absence of heat (freeze dehydration) [23], [85]; integrating coffee aroma recovery routes [25]–[27]; and employing enrichment methods to improve the quality of instant coffee [24], [81]. However, while product quality is essential in soluble coffee production, the process continues to rely on energy-intensive phase-change separations for water removal. These practices, in turn, increase the water- and energy footprints of the process due to the large water and energy consumption, as well as the generation of wastewater. Consequentially, the use of water resources, energy input from steam generation, and wastewater treatment and discharge add to the overall costs and environmental emissions that further challenges the sustainability of the soluble coffee process.

To assess the benefits of process intensification, it is important to establish the benefits and disadvantages of a proposed process from an economic and environmental standpoint, relative to the current practices. In this Chapter, a base case scenario for the soluble coffee process was evaluated in terms of economic and environmental impacts. A life cycle economic and environmental assessment study was conducted based on the mass and energy flows involved within the life cycle boundaries considered for this study. Life cycle inventories, overall operating costs, and environmental emissions were calculated based on representative production practices. This case study shall serve as a basis for comparison of the benefits and limitations of the proposed membrane-integrated alternative soluble coffee process, discussed in Chapter 8.

4.2 Assessment Procedure

4.2.1 *Scope of Base Case Study*

This dissertation augments the assessment of potential water recovery routes designed for the process intensification of the soluble coffee process. As mentioned earlier, the research into sustainable production of soluble coffee products started with wastewater reclamation options for the Nestlé USA beverages production facility in Freehold, New Jersey [51], [52] conducted by Wisniewski, et al. In contrast to the downstream water recovery alternative, this study evaluated a membrane-based water recovery alternative that can be used upstream to partially replace thermal evaporation in preconcentrating coffee extracts. Thus, parallel assumptions on process flows were used in this case study to assert comparison of potential benefits and limitation of the proposed alternative with water recovery alternatives studied in the past. Subsequently, the processes involved were based on conventional approaches and no significant or multiple process modifications were considered to warrant a full-scale life cycle assessment for this study. Thus, this study only focused on assessing the process components affected by the water recovery alternative to establish life cycle inventories, projected environmental emissions, and operating costs. Particularly, representative flows were established for the case studies based on Figure 20, which are based on the prior wastewater study values.

Figure 20

Life Cycle Boundaries for Base Case and Alternative Case Operations Involved in Soluble Coffee Processing.

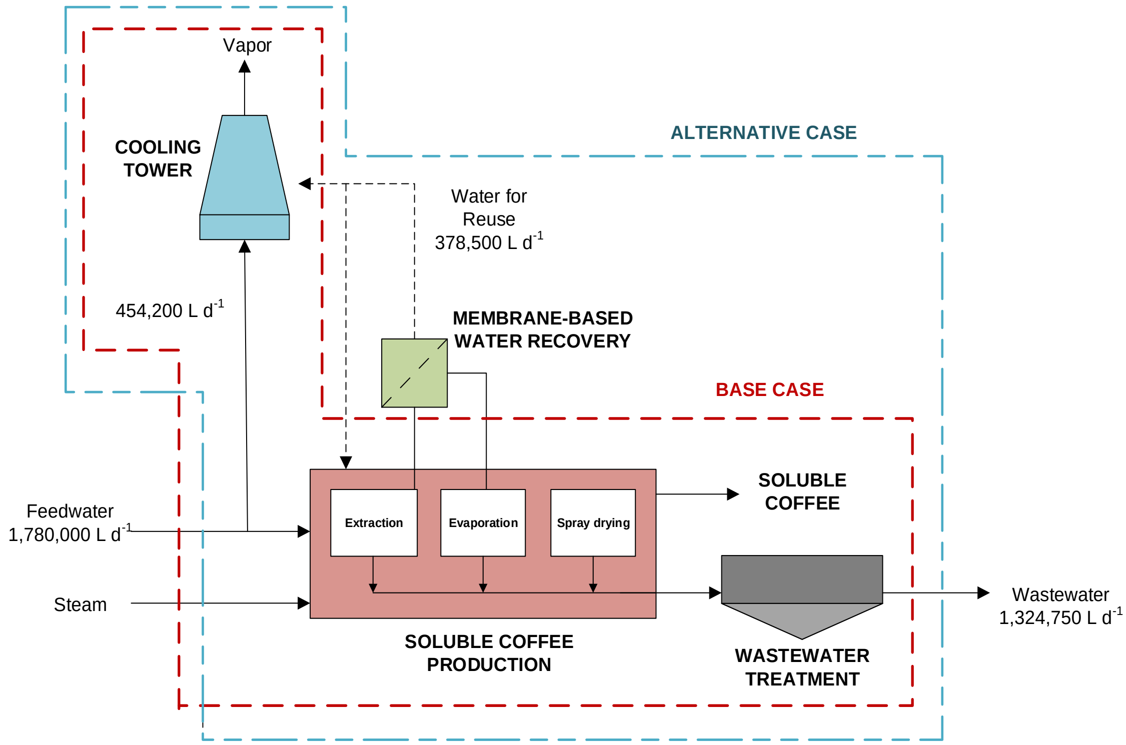

Note: Representative flows based on local soluble coffee plant operation

Process flows for freshwater use, wastewater generation, and energy consumption of the process affected by the water recovery alternative were considered. As shown in the Figure, the base case study was limited for a process having a freshwater feed of about 1.78 million L per day, 454,200 L of which is allocated for ancillary plant operations like for cooling tower operations per day. About 1.32 million L of water is directed to percolation columns per day for coffee extraction. Essentially the water fed for coffee extraction is completely evaporated to produce the dried soluble coffee powdered product. Thus, 1.32 million L ends up as process wastewater daily that undergoes on-site treatment. Similar to the soluble coffee wastewater reclamation study, the goal was to recover 378,500 L of water per day and reuse this water in ancillary plant operations, such as the factory cooling tower. For this study, the water recovery route was placed upstream to supplement thermal evaporation in preconcentrating coffee extract prior to spray drying. For this purpose, the amount of energy needed to recover 378,500 L of condensate per day from thermal evaporators was quantified based on the amount of steam needed for the operation. On the other hand, if qualified for reuse, the recovered water from this step will then reduce the factory feedwater consumption, wastewater discharge, and associated steam and energy consumption of the base case.

Mass and energy flow from process components such as feedwater, wastewater generation and discharge, electricity consumption, and steam requirement were then calculated. These served as the bases to establish the corresponding LCIs, operating costs (OCs), and life cycle emissions (LCEs) of the process components, and further, the economic and environmental metrics for the proposed alternative process. The calculated mass and energy flows of the process components, discussed herein, are summarized in Table 13.

Table 13

Estimated Annual Process Flows Relative to the Base Case Study

Process Component	Unit yr^{-1}	Estimated Flow
Freshwater	L	6.51E+08
	kg	6.50E+08
Nonhazardous wastewater	L	4.84E+08
	kg	4.82E+08
Hazardous wastewater	kg	5.18E+04
Electricity (pumps)	MJ	1.32E+06
Electricity (blowers)	MJ	8.00E+06
Steam	MJ	4.87E+07
	kg	2.84E+07

4.2.2 *Calculation of Base Case Operating Cost*

Equation 55 was used to calculate the annual operating cost by accounting for the annual feedwater (W) consumption, wastewater generation and discharge (WW), electrical consumption (E), and steam consumption (S).

$$OC_{BC} = (m_{W\ BC})OC_{W} + (m_{WW\ BC})OC_{WW} + (E_{BC})OC_{E} + (S_{BC})OC_{S} \qquad (55)$$

On the other hand, the unit costs for water use, steam generation, wastewater discharge, and electricity usage were based on the local site and are listed in Table 14.

Table 14

Unit Costs for Process Components within the Life Cycle Boundary

Process Component	Unit	Cost ($)	Remarks
Feedwater	1 kg	0.00242	Local site cost allocation
Nonhazardous Wastewater	1 kg	0.001045	Regulated cost from Ocean County Utilities Authority, New Jersey
Hazardous Wastewater	1 kg	0.88946[a] 0.84964[b]	Wastewater characterized with BOD and TSS exceeding treatment facility thresholds
Electricity	1 MJ	0.037	Estimated from energy mix of New Jersey (available in www.eia.gov/electricity/state/NewJersey)
Steam	1 MJ	0.01463	Based on boiler operations using natural gas

Note: [a] Surcharge cost per kg BOD disposed

[b] Surcharge cost per kg TSS disposed

4.2.3 *Calculation of Base Case Environmental Emissions*

Equation 56 was used to calculate the life cycle emissions of the base case operation using the LCIs and process flows determined from the process.

$$LCE_{BC} = (m_{W\,BC})LCI_W + (m_{WW\,BC})LCI_{WW} + (E_{BC})LCI_E + (S)LCI_S \quad (56)$$

On the other hand, the LCIs for water use, steam generation, wastewater discharge, and electricity usage were determined with the aid of the LCA software tool and are presented in Section 4.3.1.

4.3 Results and Discussion

4.3.1 *Process Flows and Life Cycle Inventories*

4.3.1.1 Feedwater. One of the important components of the soluble coffee process lies in its freshwater consumption, as it serves as the driving element in the extraction step. For the base case, an estimated freshwater feed of 1.78 x 10^6 L d^{-1} were considered for the analysis. Annually, this usage corresponds to about 6.5 x 10^8 L yr^{-1} of water. Notably, the water used in the manufacturing process undergoes treatment to meet the public drinking water standards.

The feedwater sourced from on-site wells and municipal water supply for the manufacturing process was assumed to have undergone pretreatment operations, such as aeration, filtration, softening, and disinfection to meet the water quality requirement [152]. Majority of the water used for the manufacturing process is drawn from on-site wells, while 2% come from municipal water supply. In a parallel study, these treatment steps were found to correspond to a unit cost of about $ 0.00242 per kg of feed water [51]. The life cycle inventory (LCI) to produce 1 kg of drinking water from groundwater sources was also determined as part of the LCE assessment. This information is presented in Table 15.

Table 15

Life Cycle Inventory for 1 kg of Drinking Water

Environmental Emission	Estimated Emissions (kg)
Air Emissions	5.60E-04
CO_2	5.55E-04
CO	9.12E-08
CH_4	6.09E-07
NO_X	-
NMVOC	1.90E-08
Particulate	1.72E-06
SO_2	6.05E-07
Water Emissions	1.23E-05
VOCs	2.08E-12
Soil Emissions	6.87E-09
Total	5.72E-04

As shown, the majority of the environmental emissions from water treatment are attributed to air emissions (~ 97.9%), primarily from CO_2 that constitutes about 97% of the total emissions. Water emissions, on the other hand contribute about 2.15% of the total emissions.

4.3.1.2 Wastewater. The water fed to the soluble coffee process ends up as process waste stream that is pretreated to specified levels of COD, BOD, and suspended solids prior to treatment in a municipal wastewater treatment facility. In doing so, the effluent undergoes a series of on-site mechanical, biological, or chemical treatment processes to meet industrial effluent standards. A typical food and beverage manufacturing plant, such as the soluble coffee industry, depend largely on aeration to degrade their highly organic waste streams. The pretreated effluent, otherwise designated as nonhazardous wastewater (NHWW), is discharged from the processing plant at the same volumetric rate as the feed, at 1.32×10^6 L d^{-1}. This is equivalent to an annual NHWW generation of about 4.84×10^8 gal yr^{-1}. For the treated process effluent discharge, a regulated unit cost of about \$ 0.001045 per kilogram of effluent is observed with the Ocean County Utilities Authority, New Jersey. In addition, a maximum regulated wastewater discharge having 300 mg L^{-1} BOD or 300 mg L^{-1} TSS is observed and treated effluents containing contaminants above these effluent limits are considered as hazardous wastewater (HWW), paid for by the facility as surcharge costs (about \$ 0.89 per kg BOD and \$ 0.85 per kg TSS) [51]. The average annual concentrations of BOD and TSS estimated from a local soluble coffee manufacturing facility were 352 mg L^{-1} and 355 mg L^{-1}, respectively [153]. Equation 57 estimates the mass flowrate of HWW discharged by the processing facility annually at about 2.51×10^5 kg yr^{-1}.

$$HWW = (BOD + TSS) \times NHWW_{volumetric} \tag{57}$$

On the other hand, the LCIs for 1 kg of NHWW and 1 kg of HWW are summarized in Table 16. In both cases, the majority of the environmental emissions from water treatment are attributed to air emissions, about 98.9% for NHWW and 97.7% for HWW. About 99% of the air emissions were also mostly attributed to CO_2 emissions. Air emissions per kilogram of wastewater were higher in NHWW than those of HWW because of the processes involved in wastewater treatment. On the other hand, due to the higher pollutant loading, HWW is observed to have higher water emissions per kilogram of the wastewater, approximately about 2.4% of the total emissions.

Table 16

Life Cycle Inventory for 1 kg of Nonhazardous and 1 kg Hazardous Wastewaters

Environmental Emissions	Estimated Emissions (kg)	
	NHWW	HWW
Total Air Emissions	2.77E-02	8.10E-02
CO_2	2.75E-02	8.05E-02
CO	2.27E-06	6.55E-06
CH_4	2.43E-05	7.05E-05
NO_X	5.74E-05	0
NMVOC	7.64E-07	2.22E-06
Particulate	7.55E-07	2.15E-06
SO_2	2.76E-05	7.93E-05
Total Water Emissions	3.59E-04	1.98E-03
VOCs	8.88E-11	2.58E-10
Total Soil Emissions	3.04E-07	8.84E-07
Total Emissions	2.80E-02	8.29E-02

4.3.1.3 Steam. An important factor considered in the base case assessment is the steam consumed for preconcentrating the coffee extracts via evaporation. In estimating this process component, a triple-effect forward feed vacuum evaporator, shown in Figure 21, was used in the calculations. The evaporator system is similar to the system evaluated by Okada, et al. [23] for a spray-dried soluble coffee production facility. The evaporator system operates at 50 °C and 7.3 kPa and the concentrations of the feed coffee extract and the concentrate are 5% and 35% solids by weight, respectively. A basis of 378,500 L d^{-1} of condensate from the water vapor was also considered for the mass and energy balance calculations, as discussed herein. This is equivalent to 373,972 kg d^{-1} of water considering the densities of liquid water and water vapor at 50 °C, which are 988.037 kg m^{-3} and 0.083 kg m^{-3}, respectively. Thus, each effect evaporates equal amounts of water vapor and produces a condensate of about 124,657 kg d^{-1} each.

Figure 21

Triple-Effect Forward Feed Vacuum Evaporator System Base Case Conditions

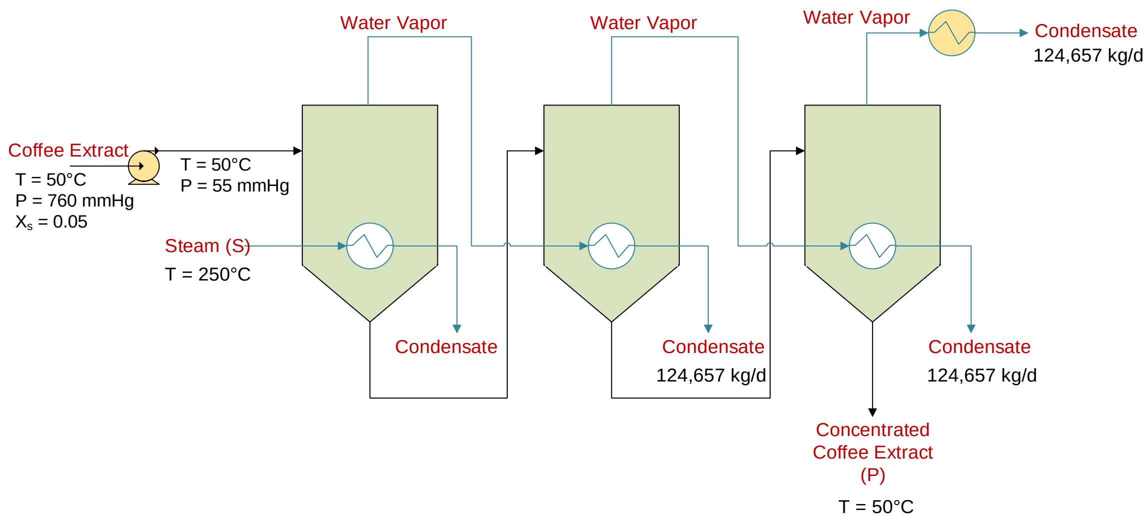

Overall and component mass balance calculations based on the initial and final concentrations of the coffee extract in the evaporator estimated a feed coffee extract at the rate of 436,300 kg d^{-1}; whereas the concentrated coffee extract after evaporation has a mass flowrate of about 62,328 kg d^{-1}. These are equivalent to volumetric flowrates of 442,845 L d^{-1} and 55,640 L d^{-1}, respectively. A reversible adiabatic pump was also considered for the calculation of shaft work (W_s) needed to reduce the pressure of the coffee extract from atmospheric pressure (1.01 x 10^5 Pa) to about 7,300 Pa. Using Equation 58 an estimated energy requirement of 50,900 kJ d^{-1} was calculated for the vacuum pump to deliver the required pressure of the feed coffee extract.

$$\dot{W}_s\left({}^{J}/_{d}\right)=\left|\frac{\dot{m}}{\rho_c}(P_{out}-P_{in})\right|=\left|\dot{V}(P_{out}-P_{in})\right| \quad (58)$$

The mass flowrates of the feed coffee extract, concentrated product, and water vapor were used to calculate the steam requirement for the evaporator system via an energy balance. In doing so, the enthalpies of the feed (H_F) and product (H_p) streams, as well as the enthalpy of evaporation (λ_V) which were used to calculate energy requirement of the triple-effect evaporator system, (Q) using Equation 59.

$$Q = \dot{m}_{Vapor}\dot{\lambda}_V + \dot{m}_{Product}\dot{H}_P - \dot{m}_{Feed}\dot{H}_F \tag{59}$$

The latent heat of evaporation at 50 °C and 55 mmHg was determined using steam table at approximately 2,587.98 kJ kg^{-1} [154]. The individual enthalpies of feed and product were calculated based on empirical correlations for specific heat of coffee extract at given water content and temperature [142], shown in Equation 60. Accordingly, the specific heats of the feed coffee extract and concentrated product are 4,041.2 J kg^{-1} $°C^{-1}$ and 3,251.1 J kg^{-1} $°C^{-1}$, respectively.

$$Cp_c\left({}^{J}/_{kg\ °C}\right) = 1439.65 + 2633.72X_W + 1.99T \tag{60}$$

Thus, the overall energy equivalent to 8.90 x 10^8 kJ d^{-1} was needed for the evaporator system. This is equivalent to 2,400 kJ of heat needed to evaporate one kilogram of water from the coffee extract that was found to be in reasonable agreement with literature [74].

The multiple effect evaporator with vapor recompression lessens the steam requirement of the operation since the steam economy (SE_n) increases by a factor (n) equivalent to the number of effects in the evaporator system. A single-effect evaporator has typical steam economy (SE_1) values between 0.75 and 0.9, while vapor recompression improves this by about 2 to 3 times [155]. The SE and steam requirement of the triple effect evaporator was calculated using Equation 61 with an assumed SE_1 and vapor recompression factor (VF) of about 0.8 and 2, respectively.

$$SE_n = n(SE_1)VF = \frac{\dot{m}_{vapor}}{\dot{m}_{steam}} \tag{61}$$

A steam requirement equivalent to 77,910 kg d^{-1} was determined from the calculations. This high-pressure steam is supplied at 250 °C and 100 kPa. Thus, the energy relative to the amount of steam supplied is approximately at 133,500 MJ d^{-1} or at 4.87×10^7 MJ yr^{-1}.

The local soluble coffee processing facility produces steam from a boiler using natural gas as fuel. The industrial cost of natural gas in New Jersey is \$ 0.0251 per MWh [156] Based on a typical boiler efficiency ranging between 80% and 90%, a boiler efficiency of about 85% was considered for the estimation of the unit cost of steam [146]. Based on this efficiency, the heating rate was calculated to be 0.475 kWh kg^{-1}. The cost of high-pressure steam was then calculated to be \$ 0.01463 kg^{-1}. On the other hand, the LCI for 1 MJ of high-pressure steam produced using natural gas is summarized in Table 17. The LCI for steam generation was among the highest environmental emissions per unit of the process component, owing to the use of natural gas as fuel to run boilers. Combustion of natural gas typically generates greenhouse gas byproducts such as CO_2 and equivalents. About 99.3% of the total emissions comprise of air emissions, approximately 99.9% of which are CO_2 emissions, and about 0.16% are CH_4 emissions. Water emissions constitute to about 0.5% while soil emissions make up about 0.002% of the total environmental emissions.

Table 17

Life Cycle Inventory for 1 MJ of Steam

Environmental Emissions	Estimated Emissions (kg)
Total Air Emissions	6.68E-02
CO_2	6.68E-02
CO	2.40E-05
CH_4	1.06E-04
NO_X	-
NMVOC	5.68E-07
Particulate	8.05E-07
SO_2	2.31E-05
Total Water Emissions	3.24E-04
VOCs	3.63E-09
Total Soil Emissions	1.26E-06
Total Emissions	6.73E-02

4.3.1.4 Electricity. The soluble coffee processing facility uses electricity to run equipment such as the pumps and blowers to deliver the process streams and pretreat the wastewater prior to discharge [153]. Within the process boundaries of the base case study, these included the electrical consumption of pump for the feed water for extraction, and the pump delivering the coffee extracts to the vacuum evaporators. Three pumps, two of which are rated at 150 hp and one rated at 75 hp power requirement, were used to determine the daily operating costs of pumping the water from on-site wells. Considering the required daily feed water flow rate, pump efficiency of 85%, and pressure drop of 2 MPa, the electrical requirement was calculated to be 1.3×10^6 MJ yr^{-1}. On the other hand, the electrical requirement of the pump delivering the coffee extract to the vacuum evaporator was estimated to be 18.6×10^3 MJ yr^{-1}. Lastly, the blowers used in wastewater pretreatment for aeration also consumes electricity. Accordingly, two blowers rated at 200 hp power requirement and motor efficiency of 0.85 were considered in this step. These blowers operate continuously, resulting to an estimated electrical consumption of about 8.00 x 10^6 MJ yr^{-1}. Overall, these base study components consume electricity of about 9.32 x 10^6 MJ yr^{-1}. Based on a unit cost of $ 0.037 per MJ electrical energy, the annual operating cost for mechanical equipment considered for the base case study was found to be $ 344,100 per year.

The LCI for the electricity used in the soluble coffee processing plant was estimated based on the type of energy used in power plants that supply electricity to the local grid. Accordingly, the local energy mix of New Jersey to produce the electricity accounts for coal, natural gas, nuclear energy, and renewable sources [157] as shown in Figure 22.

Figure 22

Energy Mix of New Jersey, USA in 2019

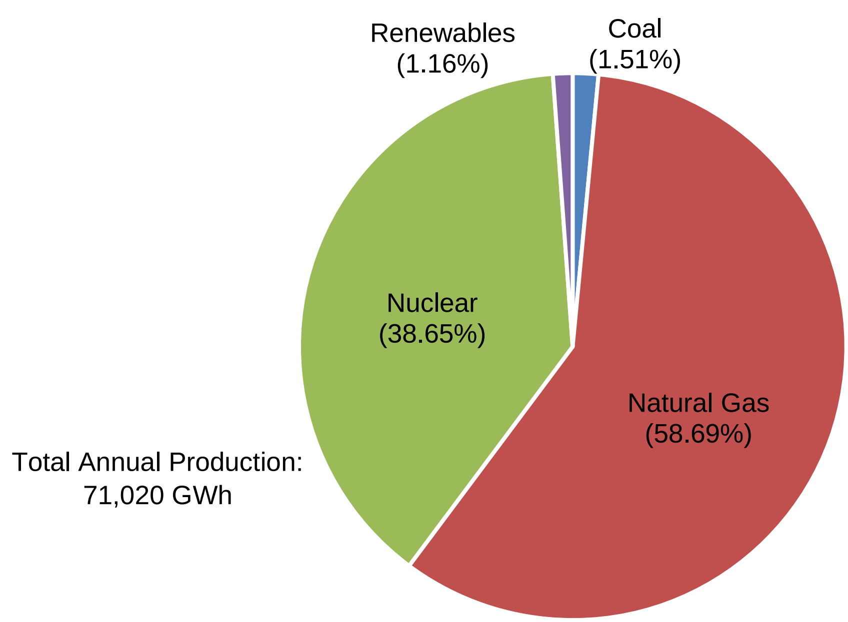

Note: Estimated from energy mix of New Jersey (available in www.eia.gov/electricity/state/NewJersey)

Using the local electrical profile, the LCA analysis software accounted for the relative generation of each fuel type to determine the LCI for 1 MJ of electricity. Specifically, 0.015 MJ from coal, 0.587 MJ from natural gas, 0.387 MJ from nuclear power, and 0.012 MJ from biomass. The LCI for 1 MJ of electricity is summarized in Table 18.

Table 18

Life Cycle Inventory for 1 MJ of Electricity

Environmental Emissions	Estimated Emissions kg
Total Air Emissions	1.13E-01
CO_2	1.12E-01
CO	8.10E-05
CH_4	5.97E-04
NO_X	8.22E-05
NMVOC	3.50E-05
Particulate	2.23E-05
SO_2	1.03E-03
Total Water Emissions	1.70E-02
VOCs	3.90E-08
Total Soil Emissions	1.21E-06
Total Emissions	1.30E-01

Like steam generation, majority of the fuel used to generate electricity is processed by the combustion of natural gas. As a result, bulk of the environmental emissions from electricity generation involved gases that are generated from the process. The LCI for electricity also had the highest impact per unit among the process components. Accordingly, 86.9% of the total emissions are air emissions and about 99.1% of which are CO_2, emissions while 0.53% are CH_4 emissions. Water emissions were also accounted the highest among process components, attributed to 13.1% of the total environmental emissions.

4.3.2 *Base Case Operating Cost*

The operating cost for the base case study was calculated relative to the process flows and unit costs involved in the life cycle boundary. These were presented earlier in Table 13 and Table 14, respectively. These process components include the feedwater usage, wastewater treatment and discharge, electricity consumption, and steam generation. An estimated overall annual operating cost of $ 1,328,000 per year was estimated for the base case operation. The allocations of the cost from each process component are presented in Figure 23.

Figure 23

Annual Operating Cost and Process Allocations for the Base Case Study

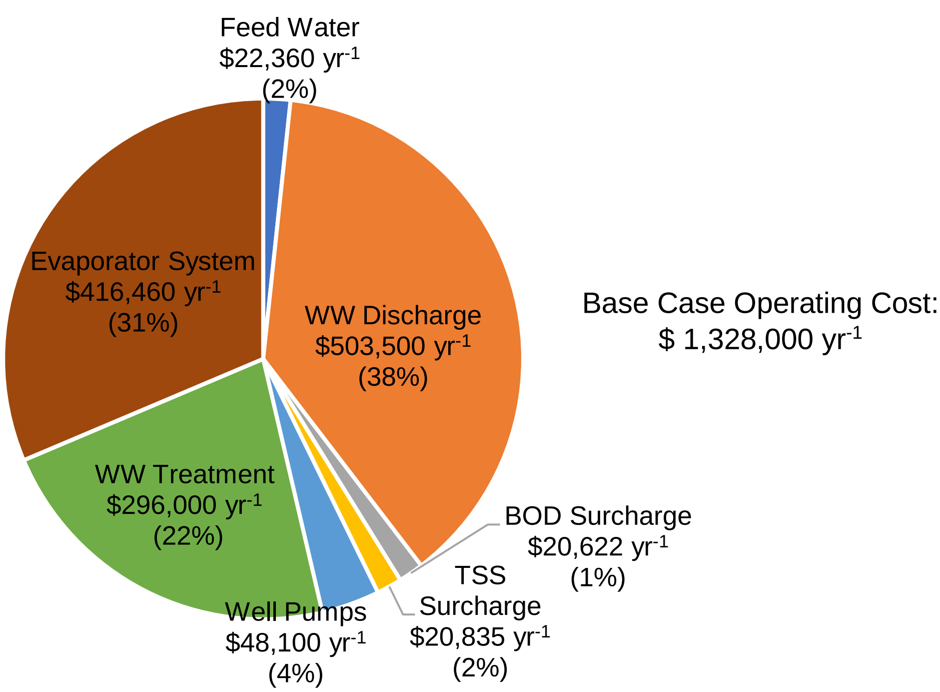

As shown in the Figure, cost allocations indicate that the primary cost of the base case study related to the combined cost for wastewater management, i.e., wastewater aeration or treatment (22%) and wastewater discharge (38%). Second highest cost among the components is that for the steam fed to thermal evaporators for the preconcentration of coffee extracts – about $416,500 per year or 31% of the overall cost of the base case study. Well pumps for feed water and wastewater consume electricity that account to 4% of the base case operating cost, while surcharges for BOD and TSS account to about 3% of the base case operating cost.

While the overall cost for the base case study does not necessarily refer to that of the whole process, but only to the cost affected by the proposed alternative, the relative costs attributed to each process component provide an insight as to where process intensification should focus. In this case, cutting down on the consumption of steam from thermal evaporation, and wastewater treatment using cost-effective water recovery measures will certainly make the process more economical. However, while the operating cost reduction positively impacts the alternative case, it is still important to consider the capital investment required. Thus, in the succeeding sections, a more thorough assessment was considered to gain an understanding of the benefits and costs of the proposed alternative process from an economic feasibility standpoint.

4.3.3 *Base Case Life Cycle Emissions*

The environmental impacts of the base case accounted to the life cycle emissions associated with the treatment of feedwater, wastewater treatment and discharge, electrical consumption, and steam consumption of the process. Relative to the mass and energy flow of the process components within the life cycle boundaries, as well as the corresponding LCIs, these emissions were calculated and presented in Table 19 and Figure 24.

Table 19

Annual Life Cycle Emissions Relative Process Flows in the Base Case Study

Emissions	Unit	Feed water	NHWW	HWW	Electricity	Steam	Total
Air Emissions	kg	3.64E+05	1.33E+07	4.20E+03	1.06E+06	3.26E+06	1.80E+07
CO_2	kg	3.61E+05	1.33E+07	4.17E+03	1.04E+06	3.26E+06	1.79E+07
CO	kg	5.93E+01	1.09E+03	3.39E-01	7.54E+02	1.17E+03	3.07E+03
CH_4	kg	3.96E+02	1.17E+04	3.65E+00	5.56E+03	5.18E+03	2.29E+04
NO_X	kg	0.00E+00	2.77E+04	0.00E+00	7.66E+02	0.00E+00	2.84E+04
NMVOC	kg	1.24E+01	3.68E+02	1.15E-01	3.26E+02	2.77E+01	7.34E+02
Particulate	kg	1.12E+03	3.64E+02	1.11E-01	2.08E+02	3.92E+01	1.73E+03
SO_2	kg	3.93E+02	1.33E+04	4.11E+00	9.58E+03	1.13E+03	2.44E+04
Water Emissions	kg	8.00E+03	1.73E+05	1.03E+02	1.58E+05	1.58E+04	3.55E+05
VOCs	kg	1.35E-03	4.28E-02	1.34E-05	3.63E-01	1.77E-01	5.84E-01
Soil Emissions	kg	4.47E+00	1.46E+02	4.58E-02	1.13E+01	6.16E+01	2.24E+02
Total Emissions	kg	3.72E+05	1.35E+07	4.30E+03	1.22E+06	3.28E+06	1.84E+07

The overall LCE of the base case corresponded to an annual emission data of about 18,400 tons per year. Based on Table 19, a bulk amount (98.3%) of these emissions is associated to air emissions, more specifically, greenhouse gas emissions. The air emissions consist of CO_2 (99.2%), CO (0.02%), CH_4 (0.13%), NO_x (0.16%), NMVOCs (0.004%), particulates (0.01%), and SO_2 (0.14%). Water emissions constitute to about 1.97% of the total environmental emissions, while soil emissions were negligible.

Figure 24

Annual Life Cycle CO_2 Emissions and Emission Sources in the Base Case Study

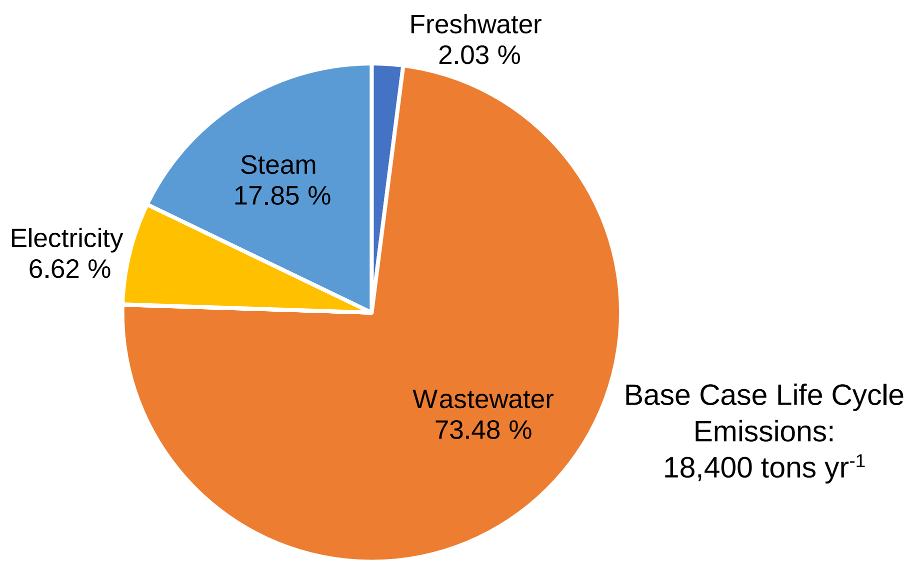

From Figure 24, it was also interesting to note that 73.48% of these emissions are associated to the management of the soluble coffee wastewater, since all the water fed to the process ends up as a waste process stream that was treated prior to discharge. The generation of steam from boilers associated to the preconcentration coffee extracts has the second highest environmental impact among the process components at 17.85%. This shows that apart from the high energy requirement of the operation, thermal evaporation contributes to greenhouse gases as it relies on natural gas as fuel for boilers. In addition, considering the amount of coffee extract evaporated (~440,000 L d^{-1}), the rated environmental emissions from steam generation (3,300 tons yr^{-1}) was still significant and comparable with those attributed to wastewater generation (13,500 tons yr^{-1} for daily process flow of 1.32 million L d^{-1}). Like the analysis on process cost, these base case LCE data indicates that reducing these process flows through process intensification can lead to a greener process. In this case, by proposing an energy-effective coffee extract preconcentration method to supplement thermal evaporation will reduce emissions from steam generation. Likewise, if the preconcentration alternative can, at the same time, directly recover water that can be reused for ancillary plant operations, and the reduction in wastewater generation will also cut down environmental emissions. Overall, addressing these two components in the process intensification alternative is important in making the process more environmentally attractive.

Chapter 5

Parametric Studies on the Vibratory Nanofiltration of Coffee Extracts

Additional graphs and tabular data of the results for this chapter are presented in Appendix B. The results presented herein are those essential to summarize the studies necessary for this dissertation's discussion.

5.1 Introduction

Membrane processes are gaining importance in shaping food and beverage industries towards sustainable production [1]. These processes operate under mild operating conditions that mitigate the effect on food product quality and minimizes operating costs. Also, when integrated as an alternative to evaporation, membrane processes offer an energy reduction of about 30% [10]. As with soluble coffee production, integrated membrane operations may not only reduce the energy consumption from dewatering operations, but also provides opportunities for reduction in feedwater consumption through water recovery and reuse. However, at this point, membrane filtration studies related to soluble coffee production are mostly on waste streams for caffeine recovery from spent coffee grounds [7], decaffeination [31], and as a water reclamation option for soluble coffee wastewater [50], [52]. On the other hand, studies involving coffee extract preconcentration have been limited only to conventional CF NF where membrane fouling has been found to limit flow through rates and cause considerable flux decline [32], [33].

The dynamic vibratory membrane system (Vibratory Shear-Enhanced Process (VSEP) (New Logic Research, Inc., Minden, NV)) introduced in this study is one of the approaches that can substantially improve the performance of conventional crossflow

(CF) filtration operations. Torsional oscillations on the membrane module at resonant frequencies of up to 60 Hz can generate substantially high surface shear rates above 20,000 s^{-1} that are sufficient to reduce the effects of concentration polarization and prevent membrane fouling [39]. These systems are especially suitable for food and beverage process streams that are prone to membrane fouling due to their complex variety of foulants – organic, biological, and colloidal solids – that, under poor operating conditions, cause flux to decline irreversibly. In fact, the vibratory filtration system has successfully improved the concentration of milk proteins and dairy wastewater treatment [5], [45], clarification and yeast recovery in alcoholic beverages [2], [3], and water treatment from high salt seawater and freshwater sources [46], [47], [49], [158].

Despite the many applications, the effective operation and maintenance of vibratory membrane systems largely rely on the characteristics of the stream being process, making direct comparison among applications difficult due to the complex nature of coffee extracts. Thus, while the technology can further the application of membrane filtration on coffee extract preconcentration, a thorough investigation of the vibratory membrane process is still necessary. This Chapter aims to establish suitable conditions and evaluate relevant membrane separation mechanisms affecting the preconcentration of coffee extracts. Membrane screening studies were initially conducted to determine a membrane with sufficient performance in terms of permeate flux, water permeability, and rejection efficiency. Parametic studies were also conducted to assess the performance of the selected membrane under CF and vibratory operations. Different feed coffee extract concentrations, applied TMPs, and vibratory settings, and their influence permeate flux, characteristics, and rejection efficiencies were assessed based on membrane separation mechanisms like shear generation, osmotic pressure effects, and concentration polarization.

5.2 Experimental Approach

A laboratory-scale VSEP filtration unit from New Logic Research, Inc., as described in Section 3.1.2, was used in this study; while simulated coffee extracts of different concentrations (8.5 g L^{-1} to 42.4 g L^{-1}) were prepared from reconstituted soluble coffee product (Nescafé® Taster's Choice®, House Blend). On a 35-L working volume, membrane filtration experiments were conducted under recycle mode for 60 mins to approach steady state conditions. Membrane screening and parametric studies in CF, and vibratory filtration modes were conducted at selected operating conditions to assess performance based on permeate flux, permeate quality, and rejection efficiencies.

5.2.1 *Membrane Screening*

Two sets of membrane screening studies were conducted to determine a suitable membrane that may be used for the succeeding coffee extract preconcentration studies. In the first membrane screening study, four membranes were evaluated to compare between microfiltration (MF, MP005), ultrafiltration (UF, PES-5/Tyvek), nanofiltration (NF, NF-4), and reverse osmosis (RO, LFC-3). The specifications of the membranes and corresponding operating pressures for this preliminary study are summarized in Table 20.

Table 20

Membrane Specifications and Operating Pressures of Various Membrane Types Used in the Initial Screening Study

Specifications	Unit	Membrane Type			
		MF	UF	NF	RO
Model		MP005	PES-5	NF-4	LFC-3
Manufacturer		Nadir	Nanostone Water	Nanostone Water	Hydranautics
Location		Goleta, CA	Waltham, MA		Oceanside, CA
Material		Polyether-sulfone	Polyether-sulfone	Polyamide	Polyamide
Nominal pore size or MWCO	µm or Da	0.05 µm	7,000 Da	225 Da	30 Da
TMP Limits	MPa	0.21 – 1.03	0.34 – 1.38	0.69 – 4.5	1.38 – 6.9
Operating pressure	MPa	1.03	1.38	2.41	2.41

Simulated coffee extract solutions were prepared for a feed concentration of 8.5 g L^{-1}. The sample was fed to the filtration system under vibratory mode (F = 54.6 Hz, d = 2.54 cm) for a retentate flowrate at 7.6 L min^{-1}. The initial membrane screening experiments were also conducted at feed temperature of 50 °C to simulate the elevated temperatures of the coffee extracts after the brewing process and before preconcentration by thermal evaporation. The four membranes were assessed at selected operating pressures applicable to each membrane type. A suitable membrane type was selected based on satisfactory performance in terms of permeate flux, permeate quality (turbidity, conductivity, and COD), and corresponding rejection efficiencies. In the first membrane screening study, these performance parameters were balanced with the operating pressure to obtain a suitable permeate flux and sufficient rejection of undesired solutes to generate water-rich permeate. This membrane type (later determined as NF membrane) was further investigated in a second membrane screening study.

Results from the initial membrane screening study determined that the NF membrane can satisfactorily fulfill membrane-based preconcentration of coffee extracts by recovering water-rich permeate intended for reuse in ancillary plant operations. A second membrane screening study was then performed to further improve the performance of the NF operation. Four thin film composite (TFC) polyamide NF membranes (TS80 , TS40, NF270, and NF500) were compared. Table 21 shows the manufacturer information of the four NF membranes. These membrane specifications were initially considered for the membrane screening study.

Table 21

Membrane Specifications for Nanofiltration Membranes Used in the Second Screening Study

Specifications	Unit	Nanofiltration Membrane			
		TS80	TS40	NF-270	NF-500
Manufacturer		Trisep Microdyn-Nadir	Trisep Microdyn-Nadir	Nanostone	Nanostone
Location		Goleta, CA	Goleta, CA	Waltham, MA	Waltham, MA
Membrane Composition		TFC polyamide	TFC polyamide	TFC polyamide	TFC polyamide
MWCO	Da	150	220	240	500
TMP Limits	MPa	0.7 – 4.5	0.7 – 4.5	1.4 – 3.4	0.7 – 4.5
NaCl Rej	%	78.3	45.3	37.0	12.4
$MgSO_4$ Rej	%	98.0	93.7	94.8	38.5
Water Flux	$L\ m^{-2}\ h^{-1}$	149	171	161	243

Note: Adapted from membrane catalogue of New Logic Research, Inc.

TFC – thin film composite; MWCO – molecular weight cut-off

TMP – transmembrane pressure

In addition to membrane characteristics, experimental parameters like membrane permeability, and NF membrane performance in separating coffee extracts such as permeate fluxes, permeate characteristics, and rejection efficiencies were also compared. The initial membrane permeabilities (A_w) of the membranes were assessed by conducting water tests under CF filtration for different applied pressures or TMPs (measured as the hydraulic pressure drop of the system, ΔP) between 1.02 to 3.79 MPa. This criterion pertains to the capacity of water to permeate through the NF membrane, as a measure of the initial membrane resistance. Plots between water fluxes (J_w) and TMPs were generated and fitted based on the linear model for flux-pressure relationship, shown in Equation 2.

$$J_w = A_w \Delta P \qquad (2)$$

Accordingly, the linear model intercepts at origin and the membrane permeability can then be determined from the slope line. In addition to water tests, the different membranes were also tested on coffee extract samples with feed coffee extract concentration of 8.48 g L^{-1} and a temperature of 25 °C. Steady-state filtration experiments were conducted at 2.41 MPa under CF mode (F = 0 Hz, d = 0 cm) and experimental parameters for flux, permeate quality, and rejection efficiencies were obtained and compared. A suitable membrane based on these criteria was selected and further investigated for parametric studies.

5.2.2 *Parametric Studies*

Using the selected NF membrane, parametric studies were then conducted to compare the performance of CF and vibratory NF operations under various operating factors. The simulated coffee extracts were processed under steady state filtration at 25 °C for five different levels of feed concentrations (8.48 g L^{-1} , < C_o < 42.4 g L^{-1}), operating pressures (1.03 MPa < ΔP < 3.79 MPa), and vibratory settings (0 Hz < F < 54.7 Hz; 0 cm < d < 3.18 cm), as listed in Table 22. Permeate samples were obtained at 5-minute intervals for the measurement of flux, permeate characteristics, and rejection efficiencies relative to feed characteristics for a total filtration time of 60 minutes. On the other hand, steady state parameters (average experimental parameters at t = 55 mins and t = 60 mins) were plotted against the different operating conditions for parametric evaluation.

Table 22

Levels of Variation Employed in Parametric Studies

Parameter	Unit	Levels				
Feed Concentration (C_o)	g L^{-1}	8.5	17.0	25.4	33.9	42.4
Operating Pressure (P) [a]	MPa	1.03	1.7	2.4	3.1	3.79
Vibratory Settings [b]						
Frequency (F)	Hz	0	53.3	54.1	54.6	54.7
Displacement (cm)	cm	0	0.64	1.28	2.54	3.18

Note: [a] also applied transmembrane pressure (TMP)

[b] paired settings based on frequency and corresponding displacement

5.3 Results and Discussion

5.3.1 *Simulated Coffee Extract Characteristics*

Due to the variety of coffee grounds and different operations involved in soluble coffee production, the composition of coffee extracts and likewise, instant coffee final products, vary considerably. Table 23 shows the composition of different coffee products including instant coffee in dry weight basis.

Table 23

Composition of Various Coffee Products in Weight Percent (% w/w)

Component	Arabica		Robusta		Instant Coffee
	Green	Roasted	Green	Roasted	
Minerals	3.9-4.2	3.5-4.5	4.0-4.5	4.6-5.0	9-10
Caffeine	0.9-1.2	~1.0	1.6-2.4	~2.0	4.5-5.1
Trigonelline	1.0-1.2	0.5-1.0	0.6-0.75	0.3-0.6	-
Lipids	12.0-18.0	14.5-20.2	9.0-13.0	11.0-16.0	1.5-1.6
Chlorogenic acids	5.5-8.0	1.2-2.3	7.0-10.0	3.9-4.6	5.2-7.4
Aliphatic acids	1.5-2.0	2.4-3.0	1.5-2.0	2.4-3.0	-
Oligosaccharides	6.0-8.0	0-3.5	5.0-7.0	0-3.5	0.7-5.2
Polysaccharides	50-55	24-39	37-47	-	~6.5
Amino Acids	2.0	0	2.0	0	0
Proteins	11-13	13-15	11-13	13-15	16-21
Others	< 7.7	10.5-39.9	< 21.3	50.3-62.8	43.2-56.6

Note: Adapted from Clifford & Wilson [96].

Coffee extract concentrations and composition vary from 15% to 60% depending on the conditions used in the extraction step [85]. However, while the composition of the soluble coffee extract from the reconstituted spray-dried coffee product is privileged information, spray-dried coffee composition has been studied in the past [85], [96], [159]. Commercial instant coffee products have been found to have mineral components like

Ca, Mg, K, Fe (9.0-10.0%); and organic components such as caffeine (4.5-5.1%), lipids (1.5-1.6%), chlorogenic acids (5.2-7.4%), saccharides (7.2-11.7%), proteins (16.0-21.0%), humic acids (15%) and other constituents (28.2-41.6%) [96], [97]. Around 800 types of volatile aromatic compounds are also identified from coffee grounds, approximately 50-70% of which are in the production of instant coffee [27], [159]. These components are responsible for the flavor, aroma, dark color, and the biodegradability of the coffee extract. However, contrary to the notion that coffee extract components completely dissolve during the extraction step, some components are water-insoluble contributing to suspended and colloidal constituents (or sediments) that are also commonly present in instant coffee powders [160]. These insoluble components constitute about 54.7% of coffee extracts, largely attributed to a polysaccharide identified as galactomannan (MW = 504 g L^{-1}) [160]. Based on the molecular weight, these suspended and colloidal components are likely to be rejected by the TS80 membrane since the NF membrane has a cut-off molecular weight of 150 Da. Overall, the soluble, suspended, and colloidal components of varying particle sizes and charges also make up the foulants that may limit the permeate fluxes of membrane filtration operations. Representative bulk characteristics in terms of suspended and colloidal solids content (turbidity), dissolved solids (conductivity), colored constituents (absorbance), and organic content (COD) were considered for this study in place of the specific components. Table 24 shows the bulk characteristics of the soluble coffee extracts at different concentrations between 8.5 g L^{-1} to 42.4 g L^{-1}.

Table 24

Characteristics of Simulated Coffee Extracts for Various Concentrations at 25 °C

Characteristics	Unit	Feed Coffee Extract Concentration (g L^{-1})				
		8.5	17.0	25.4	33.9	42.4
Bulk Characteristics [a]						
pH		5.6 ± 0.7	4.9 ± 0.2	4.7 ± 0.2	4.5 ± 0.2	4.5 ± 0.4
Turbidity	NTU	410 ± 77	1,170 ± 126	1,790 ± 158	2,250 ± 168	2,520 ± 172
Absorbance		1.2 ± 0.1	2.3 ± 0.2	2.9 ± 0.1	3.4 ± 0.1	3.9 ± 0.2
Conductivity	µS cm^{-1}	1,130 ± 68	1,750 ± 84	2,620 ± 67	3,050 ± 88	3,840 ± 91
COD	mg L^{-1}	8,450 ± 684	17,980 ± 1,412	29,180 ± 1,294	37,410 ± 1,634	47,830 ± 1,492
Fluid Properties [b]						
Density	kg m^{-3}	1,000	1,005	1,009	1,012	1,016
Dynamic viscosity	10^{-4} Pa s	8.95	9.00	9.05	9.10	9.15

The lowest concentration of 8.5 g L^{-1} from the reconstituted soluble coffee extract was found to have a turbidity of 410 NTU, conductivity of 1,130 μS cm^{-1}, and COD of 8,500 mg L^{-1}. These bulk concentrations increased linearly with the strength of the coffee extract mixture and are substantially larger than those present in soluble coffee wastewaters investigated by Wisniewski, et al. [51], [52] The density and absolute viscosity of the simulated coffee extracts also increased with concentration. The characteristics of the simulated coffee extract varied less than those observed from the soluble coffee wastewater processed by Wisniewski et al. [50]–[53], owing to the controlled preparation and storage of the simulated samples. However, it should be noted that the feed coffee extracts used in this study are reconstituted from commercial spray-dried coffee products that do not necessarily reflect the variability of coffee extracts from actual operations. It is still important to investigate actual process streams for a more realistic perspective of the membrane operation. Nonetheless, the simulated samples used in the study provide a better understanding of the membrane separation mechanisms under controlled conditions, and that the strength of the components in the simulated samples represent the various foulants that affect the process. These components make processing by conventional CF operation challenging, as they cause higher membrane fouling. Thus, higher surface shear rates may be required to improve the membrane operations.

5.3.2 *Results of Membrane Screening*

5.3.2.1 First Membrane Screening Study. In the first set of membrane screening, MF, UF, NF, and RO membranes were compared in terms of permeate flux, characteristics, and corresponding rejection, as shown in Figure 25.

Figure 25

Permeate Flux and Percent Rejections of Different Types of Membrane

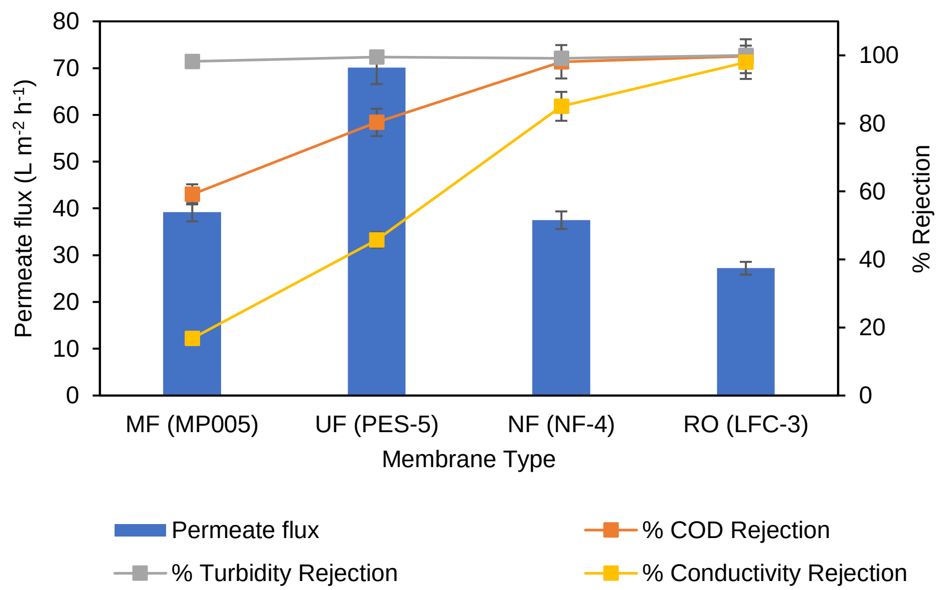

Among the four membranes tested, the highest flux obtained was that of UF at about 70.1 L m^2 h^{-1}, while the lowest was that of RO at about 27.2 L m^2 h^{-1}. A decreasing trend was also observed from the fluxes of UF, NF, and RO membranes as a result of the decreasing pore size of the membrane. On the contrary, the MF membrane, despite having the largest pore size among the four, gave the low permeate flux due to the relatively low applicable operating pressure employed compared to those of UF, NF, and

RO. UF, on the other hands, rendered higher permeate flux than NF and RO membranes as the larger pore size of the UF membrane tend to reduce the pressure drop across the feed and permeate side of the membrane. In terms of rejection efficiencies, all of the four membranes rejected above 98% of the turbidity from the feed coffee extract. Despite having the largest pore size of 0.005 µS cm^{-1}, the MF membrane was able to reject about 98.2% of the turbidity from the feed coffee extract. This high rejection indicates that a bulk fraction of the suspended and colloidal solid constituents of the coffee extract are at least larger than 0.005 µS cm^{-1}. On the other hand, the RO membrane was able to reject 100% of the turbidity owing to the dense structure of the membrane that can reject constituents with molecular weights as low as 30 g mol^{-1} (or 30 Da). In terms of conductivity rejection, the porous MF and UF membranes had the lowest rejection of dissolved solids (17% and 45%, respectively) as these constituents are relatively smaller than their pore size. NF and RO membranes had higher conductivity rejections of 85% and 98%, respectively. The lower conductivity rejection of the NF membrane was expected as its cut-off pore size only allows it to reject constituents with molecular weights of up to as small as 225 Da. In addition, NF membranes can only rejection multivalent ions unlike RO membranes that can retain even monovalent ionic constituents. The conductivity rejection of the four membranes also conformed with their level of COD rejection, indicating the some of the dissolved coffee extract components that passed through the membranes were organic compounds. Thus, MF and UF membranes rendered lower COD rejections (59.1% and 80.3%, respectively) than those of NF and RO membranes (98.1% and 99.8%, respectively).

Overall, the MF membrane was least suitable for coffee extract preconcentration since it had the lowest permeate flux and rejection of suspended, colloidal, and dissolved components. Also, despite having the highest permeate flux, the UF membrane had insufficient COD rejection that limits the membrane from water recovery operations. Nonetheless, these results leave MF and UF membranes suitable as a pretreatment option in sequential membrane filtration systems. However, as this study intended to propose a single-step water recovery operation, membrane screening was then narrowed down to NF and RO membranes. The characteristics of the permeate from the different membranes are shown in Table 25.

Table 25

Permeate Characteristics Obtained from Different Types of Membranes

Membrane Type	COD (mg L^{-1})	Turbidity (NTU)	Conductivity (µS cm^{-1})
Microfiltration (MP005)	4,262	6.75	2,680
Ultrafiltration (PES-5/Tyvek)	2,057	1.85	1,750
Nanofiltration (NF-4)	196.5	3.15	483
Reverse Osmosis (LFC-3)	26	~0	66

The RO and NF membranes employed in the study were effective in producing water-rich permeate. The RO membrane gave higher conductivity and COD rejection with permeate quality comparable to potable water as it can practically reject components as small as 30 Da compared to the cut-off molecular weight of the NF membrane at 225 Da. However, the permeate flux from this operation was lower than that of the NF membrane. Such low-flowrate operation tends to require larger membrane design areas that increases the investment cost. On the other hand, while high-pressure operations can increase the permeate flux, such conditions demand higher operating costs, making the RO membrane an impractical option for coffee extract preconcentration. On the contrary, the permeate flux from the NF membrane was relatively more acceptable and would reduce the operating cost of the operation. In addition, the NF membrane also rendered sufficient rejection of turbidity, conductivity, and COD to the level of water quality necessary for reuse in plant ancillary operations. On this basis, NF was further evaluated throughout the study.

5.3.2.2 Second Membrane Screening Study. The second membrane screening aims to identify an NF membrane that will have a more effective permeate flux and rejection efficiency in comparison to the NF-4 membrane. In the second membrane screening, four NF membranes were selected based on commercial specifications on material type, pore size in terms of MWCO, water flux, and standard salt rejection efficiencies. These NF membranes (TS80, TS40, NF270, and NF500) have MWCOs less than 500 Da with the TS80 membrane having the smallest cut-off of 150 Da. The material type of the selected NF membranes is polyamide as recommended in various food and beverage applications such as the separation of skim milk by RO [8], clarification of rough beer by MF [6], and the valorization of spent coffee grounds by NF and RO for the recovery of coffee extract components [7]. The NF membranes are also operable at applied TMPs up to 3.79 MPa and can also reject dissolved ions to a certain extent depending on the type of membrane. It should be noted that NF membranes generally have higher divalent ion rejection than monovalent ion rejection [94], as can be observed in Table 21. Among the four, the TS80 membrane has a potential to reject most of these components at about 98.0% multivalent salt rejection, and 78.3% monovalent salt rejection. However, it should be noted that the non-specific conductivity measurement used in this study is only limited on the overall dissolved solids rejection. Thus, the specific types of ions rejected in the process are not reflected.

Water tests, and coffee extract filtration experiments were also conducted to provide additional information for screening the most suitable membrane. The results of these experiments are shown in Figure 26 and Figure 27.

Figure 26

Water Fluxes under Various TMPs at 25°C for Different NF Membranes, and Corresponding Water Permeabilities

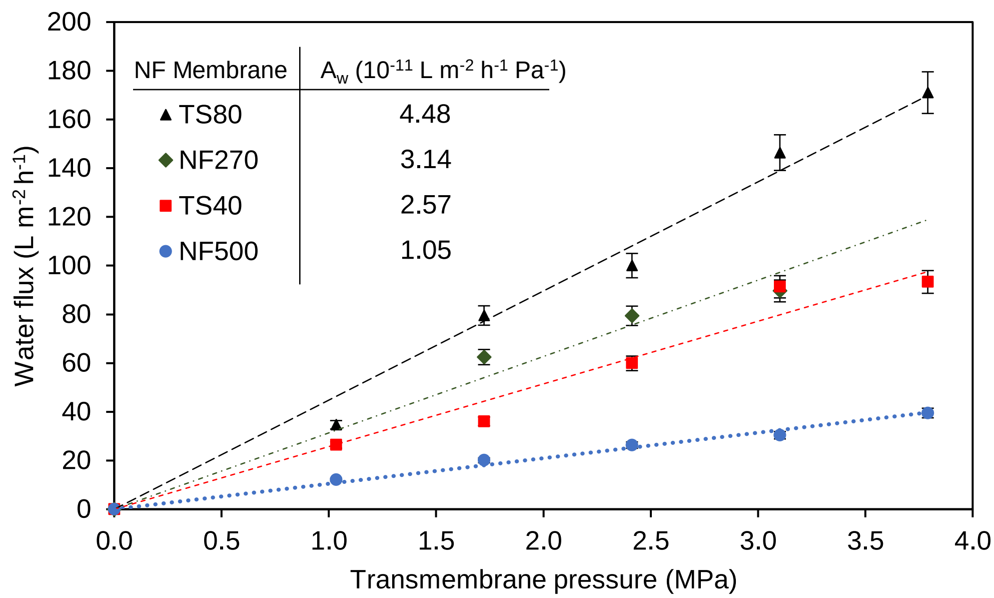

From Figure 26, the TS80 had the highest water flux among the NF membranes. It also had the highest water permeability at 4.48 x 10^{-11} L m^{-2} h^{-1} Pa^{-1}, while that of the NF270 membrane was the second highest at 3.14 x 10^{-11} L m^{-2} h^{-1} Pa^{-1}. The water permeability of the NF membrane reflects the hydraulic resistance of the membrane as affected by its pore size, effective thickness, and porosity [94]. Thus, a high membrane permeability is preferable as it directly influences high permeate generation rates for membrane filtration. As observed in Figure 27, the TS80 generated the highest steady-state permeate flux at about 20.5 L m^{-2} h^{-1} when processing coffee extracts (C_o = 8.48 g L^{-1}) under CF NF at 2.41 MPa. Next to this are those of NF270 (J = 19.9 L m^{-2} h^{-1}), TS40 (J = 17.2 L m^{-2} h^{-1}), and NF500 (J = 11.9 L m^{-2} h^{-1}) that conformed with the corresponding measured water permeabilities. A high permeate flux is desirable considering the decline in flux observed in membrane operations [51], [52]. As a rate-dependent operation, high permeate generation rates also minimize the design area requirement, and thus, the capital cost of membrane filtration systems [51].

Figure 27

Steady State Permeate Fluxes and Rejection Efficiencies of Various NF Membranes in Processing Coffee Extracts Under Crossflow Filtration

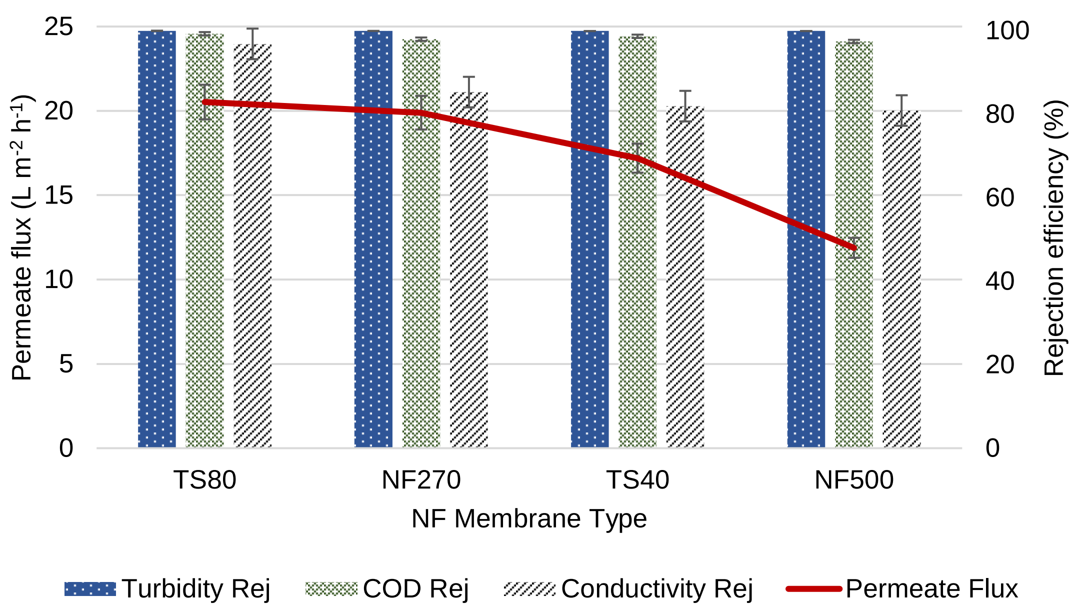

Note: Operating conditions: C_o = 8.48 g L^{-1}; F = 0 Hz, d = 0 cm; P = 2.41 MPa

The NF membranes were also screened based on their capacity to reject coffee extract components. In Figure 27, all the NF membranes rejected more than 99% of colloidal and suspended solids in terms of turbidity but differed in rejecting dissolved organic components and conductivity. The TS80 membrane had the highest conductivity and COD rejections at 96.8% and 99.3%, respectively, owing to the fact that it had the lowest MWCO (150 Da) and the highest salt rejection among the tested membranes. These metrics preferentially allow the TS80 membrane to retain important coffee extract components such as caffeine, chlorogenic acids, phenolic compounds, etc., and minimize losses or trade-offs in product quality [24], [31]. On the other hand, while all membranes tested have high organic rejection (> 97%), the residual concentrations from the permeate should meet industrial water reclamation standards set by the U.S. Environmental Protection Agency, [139] or on-site reuse specifications set by the industry. These water reuse options include urban reuse, irrigation, industrial operations, groundwater recharge, and drinking purposes. On the other hand, water reused for ancillary plant operations include reuse options for cooling towers, feed water for boilers, or as an extractant in percolation columns. Thus, while the flux of the NF270 membrane was nearly comparable to that of the TS80 membrane, its lower conductivity rejection of about 85.3% and COD rejection of about 98.0% may hinder the direct reuse of the permeate. On the other hand, the high organics rejection of the TS80 membrane allows water recovery with minimal treatment and cost required before reuse. Based on the above information, the TS80 membrane was selected for further investigation.

5.3.3 *Effect of Filtration Time*

The behavior of permeate fluxes throughout the 60-minute filtration time varied between CF and vibratory NF operations, as shown in Figure 28. The permeate fluxes under conventional CF NF at 2.41 MPa reduced to about 30% when feed coffee extract strength was five times the strength of the standard coffee cup concentration of 8.5 g L^{-1}. The flux decline after 60 minutes of filtration was also more pronounced under the non-vibratory operation that further increased with higher feed concentrations. The flux decline after 60 minutes of operation were 45% and 33% of the initial fluxes (at t = 0 min) from CF filtration involving 8.5 g L^{-1} and 42.4 g L^{-1} feed concentrations, respectively.

Figure 28

Nanofiltration Time Profiles from Coffee Extract Nanofiltration Under Crossflow and Vibratory Operation and Feed Coffee Extract Concentrations

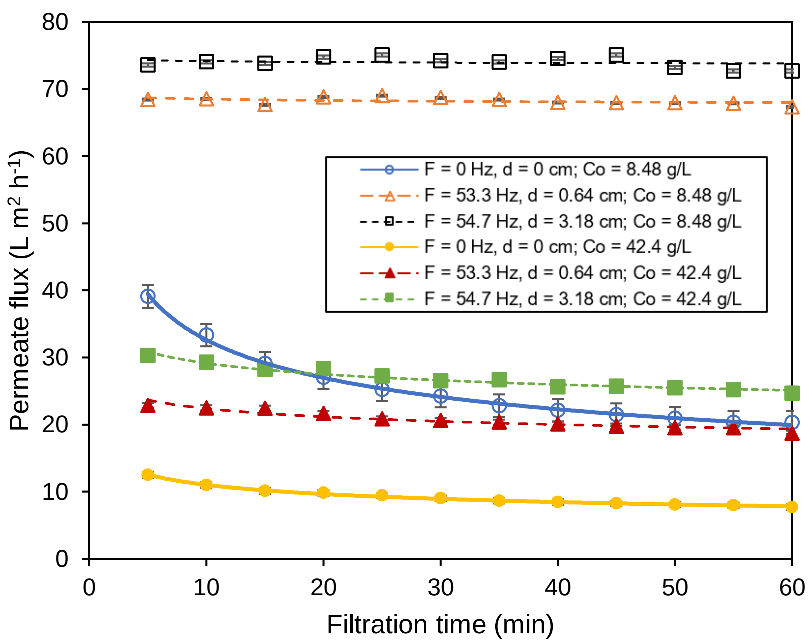

Note: TS-80 NF membrane; ΔP = 2.41 MPa; T = 25 °C

The flux decline was a result of the stronger concentration polarization arising from the higher feed and membrane surface concentrations. In addition, the surface shear generated from conventional CF velocities may not be enough to overcome viscous flows arising from high membrane surface concentrations. Thus, over time, the viscous layers build up and form a gel layer that increases the total resistance to flow, limits permeate flux, and results in poor membrane performance, and uneconomical scaled-up operation [32], [56].

On the other hand, module vibrations from 53.3 Hz to 54.7 Hz enhanced the permeate fluxes of CF NF that considerably reduced flux decline. In Figure 28, the highest permeate fluxes were observed when the vibration was at 54.7 Hz for feed concentrations at 8.5 g L^{-1} where fluxes only varied from 73.6 L m^{-2} h^{-1} to 72.7 L m^{-2} h^{-1}. After 60 minutes, the stable fluxes under this condition were 3.6 times higher than the permeate flux of the non-vibratory operation. Also, the permeate flux at 53.3 Hz for an 8.5 g L-1 feed coffee extract was 3.3 times higher than that of the non-vibratory operation. Feed concentration still affected the permeate fluxes of the vibratory NF operations that reduced the permeate fluxes by about 3 times when the feed coffee extract strength was five times higher. Despite the decrease, stable permeate fluxes under vibratory NF were still observed within the first 15 minutes of the vibratory operation.

Figure 29

Appearance of TS80 NF Membranes after Membrane Filtration of Coffee Extracts (C_o = 42.4 g L^{-1}) at 2.41 MPa at Different Vibratory Settings: (a) F = 54.7 Hz, d = 3.18 cm; (b) F = 53.3 Hz, 0.64 cm; and (c) F = 0 Hz, d = 0 cm

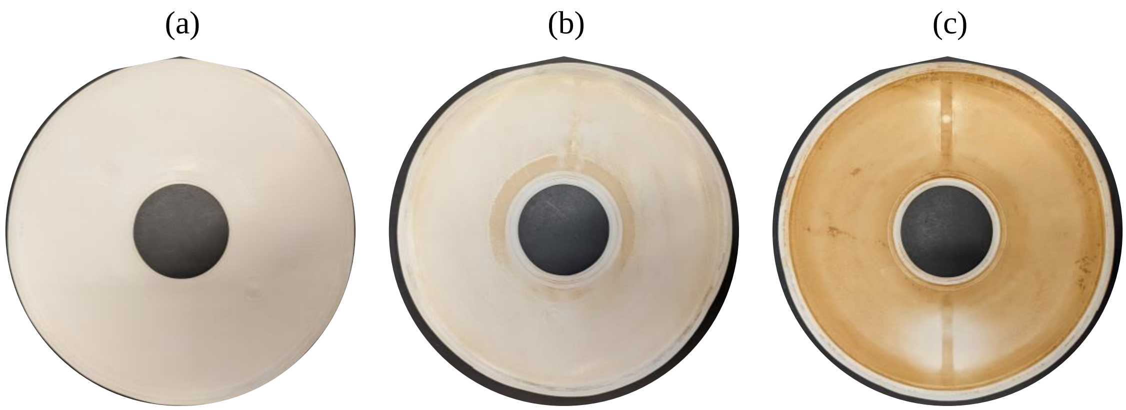

Evidence of membrane fouling was noticeable after 60 minutes of membrane filtrations under CF operation, based on the used membrane images in Figure 29. Membranes processed under non-vibratory CF configuration had visible coffee-like coloration, while those used in vibratory operations had less observable change. The variation of coloration on the membrane surface indicates the strength of concentration polarization and resulting foulant layer under various conditions. The visible coffee-like coloration in Figure 29c shows that more coffee extract solutes have either adsorbed, deposited, or formed a gel layer on the membrane surface that added to the flow resistance. Over time, this added resistance caused the observable flux decline during CF operation. On the other hand, less solutes have accumulated on the membrane surface for vibratory operations, as indicated by the lighter appearance of the TS80 NF membranes after use (Figures 29a and b).

5.3.4 *Effect of Vibration*

The steady state permeate fluxes ranged from 7.7 L m^{-2} h^{-1} to 106.3 L m^{-2} h^{-1} depending on the operating conditions. Vibratory operations (F = 53.3 Hz at d = 0.64 cm, and F = 54.7 Hz at d = 3.18 cm) enhanced the fluxes by about 2 to 3.6 times higher than those observed under CF operation, as shown in Figure 30. The highest flux enhancement was imparted by module vibration at 54.7 Hz (d = 3.18 cm), applied TMP of 3.79 MPa, and when the feed concentration was lowest at 8.5 g L^{-1}. This trend was also observed in the recovery of yeast from suspensions by MF [2], concentration of milk proteins by UF [5], brackish water purification by RO [49], and in NF studies for soluble coffee wastewater reclamation [52]. The effectiveness of flux enhancement in the dynamic vibratory filtration system is dictated by the local shear rates developed on the membrane surface during operation [2], [102], [107]. Dynamic filtration systems like that of vibratory membrane systems generate considerably larger surface shear rates than CF velocities in conventional non-vibratory filtration systems.

Figure 30

Variation of Permeate Flux with Vibratory Frequency and Displacement Under Various Applied TMP and Feed Coffee Extract Concentration at T = 25 °C

(a) C_o = 8.5 g L^{-1}

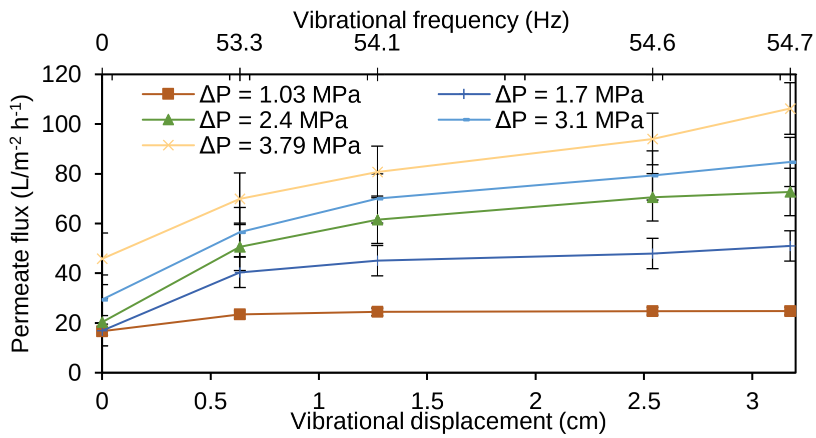

(b) C_o = 25.4 g L^{-1}

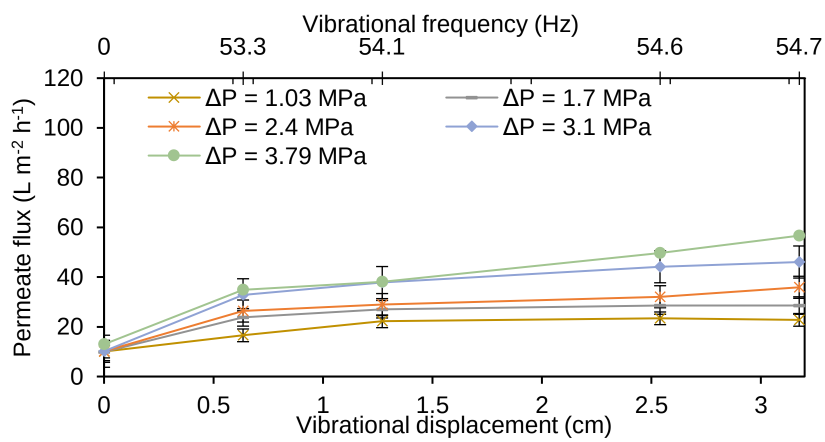

(c) C_o = 42.4 g L^{-1}

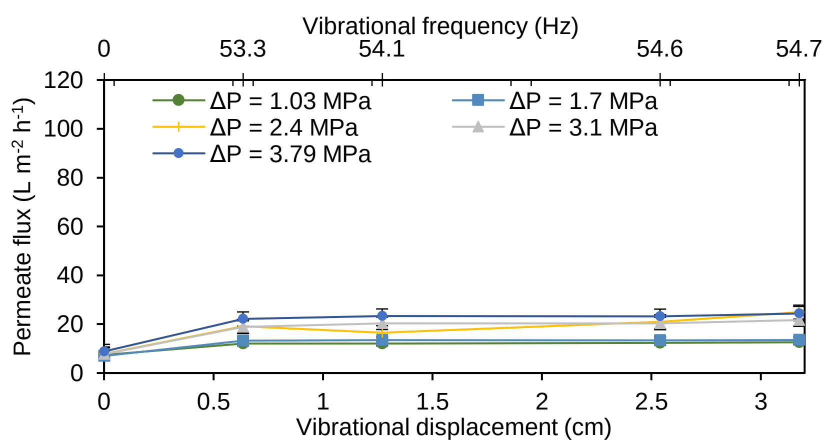

Using Equation 26, the calculated maximum surface shear rates generated between vibrational frequencies of 53.3 Hz and 54.7 Hz ranged from 20,000 s^{-1} to 106,000 s^{-1}. These shear rates are known to correlate with the permeate fluxes of vibratory filtration under a power-law model, shown in Equation 62.

$$J_v = K\,\gamma_{w\,max}{}^{n} \tag{62}$$

The power-law model assumes that vibratory membrane surface shear rates mainly govern permeate flux, and in some cases, rejection [49], [161], [162]. In the equation, the coefficient K reflects the strength of the correlation, while the exponent n measures the sensitivity of the permeate flux with the variation of surface shear rates [102]. These empirical constants were obtained from log-linear regression of the linear expression of the power-law model, shown in Equation 63.

$$\log J_v = \log K + n \log \gamma_{w_{max}} \tag{63}$$

Based on the linear expression, the calculated values of $\left[\log \gamma_{w_{max}}\right]$ were plotted against different experimental values of [$\log J_v$]. Figure 31 shows this plot in logarithmic scale for x- and y-axes. Using linear regression, the empirical parameters, K and n, were then evaluated at different feed coffee extract concentrations, and applied TMP. The exponent n was the slope of the linear plot, while the coefficient K was derived from the y-intercept. These calculated parameters are shown in Table 26.

Figure 31

Variation of Permeate Flux with Maximum Surface Shear Rate Under Various Applied Transmembrane Pressure and Feed Coffee Extract Concentration at T = 25 °C

(a) $C_o = 8.5\ g\ L^{-1}$

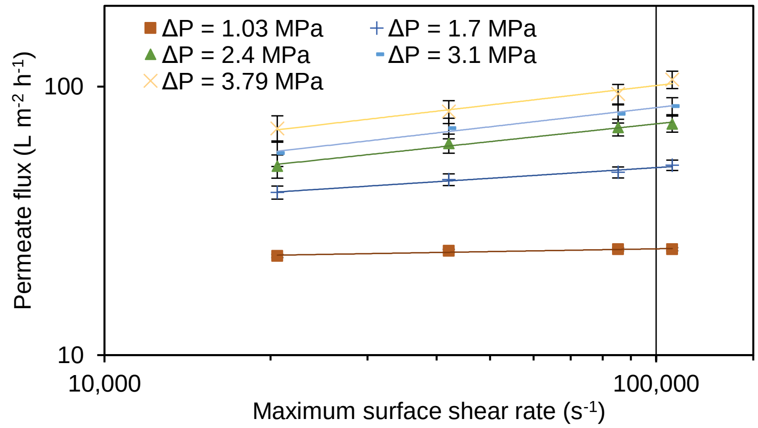

(b) $C_o = 25.4\ g\ L^{-1}$

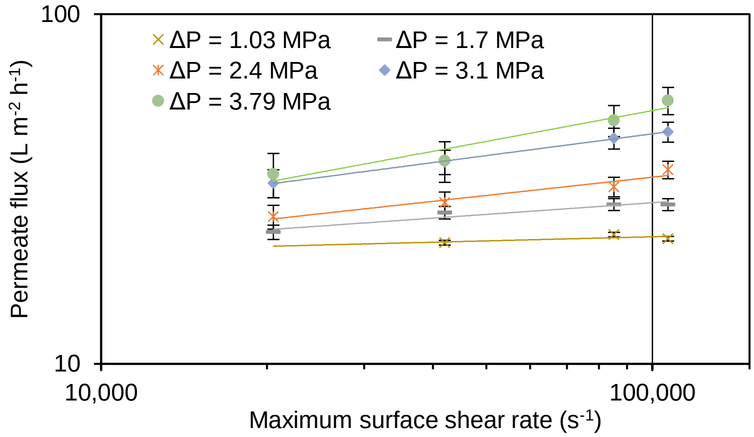

(c) $C_o = 42.4\ g\ L^{-1}$

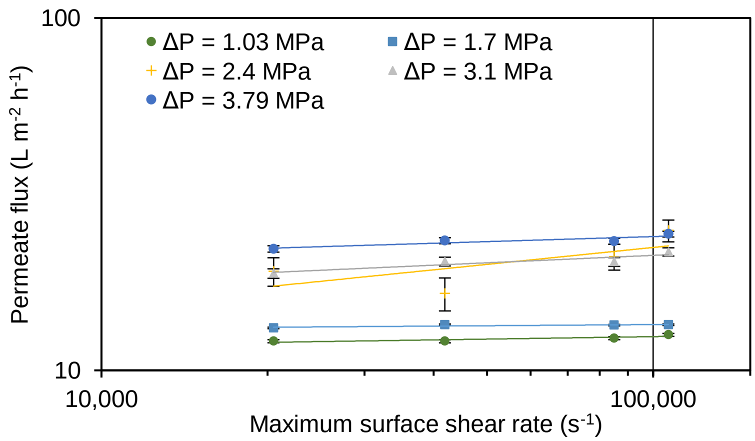

Table 26

Power Model Parameters from Shear and Permeate Flux Relation at Various Feed Coffee Extract Concentrations (C_o), and Transmembrane Pressure (TMP)

C_o (g L^{-1})	TMP (MPa)	K	n
8.5	1.03	16.75	0.034
	1.72	10.90	0.132
	2.41	5.79	0.220
	3.10	5.46	0.240
	3.79	6.34	0.240
16.7	1.03	10.85	0.151
	1.72	8.19	0.170
	2.41	9.25	0.129
	3.10	6.34	0.161
	3.79	2.22	0.194
25.4	1.03	14.68	0.039
	1.72	8.08	0.111
	2.41	4.64	0.174
	3.10	4.22	0.207
	3.79	1.82	0.293
33.9	1.03	7.51	0.025
	1.72	5.06	0.131
	2.41	0.93	0.311
	3.10	0.24	0.433
	3.79	0.15	0.518
42.4	1.03	9.54	0.023
	1.72	11.88	0.011
	2.41	3.56	0.160
	3.10	9.46	0.070
	3.79	13.85	0.048

Zsirai et al. [107] reviewed the impact of mechanically imposed surface shear on permeate flux in the power-law model based on feed characteristics, membrane pore size, and operating conditions. Accordingly, the exponent value (n) has some dependence on feed characteristics and applied TMP regardless of filtration technology used or membrane material and characteristics. The exponent values increased from 0.03 to 0.24

when TMP increased from 1.03 MPa to 3.79 MPa for feed concentration of 8.5 g L^{-1}. This behavior shows that flux increases more rapidly with surface shear rates at higher applied TMPs. This trend was also observed up to feed coffee extract concentrations of 33.9 g L^{-1}. Low exponent values under this tend to be associated with the high viscosities resulting from stronger concentration polarization [107]. On the other hand, the coefficient K inversely varied with the exponent n. The value of K relates to the macromolecular content of the feed coffee extract that affect the critical flux. These components include the suspended and colloidal solids that, as will be discussed in Section 5.3.7, largely make up the coffee extracts based on the relative rejection efficiencies of turbidity and COD. An increase in the concentration of these components lowers the limiting or critical flux of the operation, i.e., a condition wherein the permeate flux is not significantly affected by flux-enhancing conditions such as TMP and membrane surface shear [17], [163]. Consequently, conditions with high values of K and low values of n tend to be invariant with vibratory shear, as was observed when the feed coffee extract concentration was 42.4 g L^{-1}, and when the applied TMP was 1.03 MPa. As a result, the trends relating the empirical constants with system conditions also become nearly unobservable. This condition limits the power-law model since conditions other than vibratory shear, e.g., feed solute characteristics, TMP, and the resulting fouling resistances, surface concentrations, and osmotic pressure, tend to affect the performance of the vibratory NF operation. Unfortunately, no universal correlation has yet been developed relating the interactions of these operating conditions in vibratory membrane filtration.

While the correlation between TMP, Co, and surface shear rates is not clear even in literature, an attempt to relate the power law model parameters K and n with permeate was explored. A correlation between the two parameters was found to be based on the log-normal relationship of n and K [107], shown in Equation 64.

$$n = \frac{A - \log K}{B} \tag{64}$$

The correlation has been applied to rotary disk filters (RDFs), vibrating disk filters (VDFs), and vibrating hollow fiber membranes (VHFMs) as reviewed by Zsirai, et al. [107], where A and B have been found to be 5.04 and 1.98, respectively. The correlation has not been tested on oscillatory vibratory membrane systems, such as that used in this study. In the correlation, A and B are empirical parameters that can be obtained from the linear plot between [n] and [log K], as shown in Figure 32. From linear regression, A is equal to the reciprocal value of the slope, while B is the ratio between the y-intercept and the slope of the line. Based on the results of linear regression, the correlation between n and K for this study was found to be:

$$n = \frac{4.7 - \log K}{1.50} \tag{65}$$

When rounded up to the nearest whole number, the correlation obtained from the surface shear study conforms with those of RDF, VDF, VHFM. However, it should be noted that the correlation slightly differs for this system since the variation of K and n is influenced by the type of membrane technology [38].

Figure 32

Variation of Permeate Flux with Maximum Surface Shear Rate Under Various Applied Transmembrane Pressure and Feed Coffee Extract Concentration at T = 25 °C.

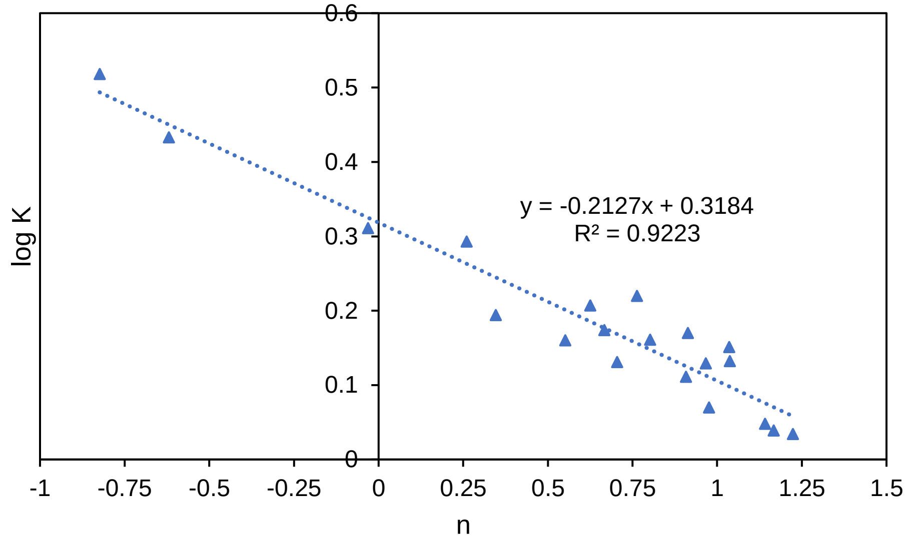

Nonetheless, the correlation may still provide an estimate on the order of permeate flux that may be obtained from vibrations. This estimate can be determined from Equation 66.

$$J \cong 10^{1.5-4.7n}\,\gamma_{w\,max}{}^{n} \tag{66}$$

Overall, the power-law model provides a good insight between surface shear rate and permeate flux relationships. However, the model has limitations especially when correlating the interaction of vibration with operating factors like feed concentrations and TMP. This prevents the model from estimating permeate quality and rejection efficiencies of the vibratory NF operation. Also, the model alone may not be simultaneously solved with other classical membrane filtration models. For example, the concentration polarization in the vibratory system may only be assessed for constant vibration settings, similar to those employed in the vibratory UF of milk proteins [5] and in parallel concentration studies of coffee extracts [164]. These limitations strongly indicate the need for alternative models that show the interplay between the important operating factors to understand, or even quantify the mechanisms involved in the vibratory NF operation.

5.3.5 *Effect of Pressure*

The enhancement of permeate fluxes with the increase in vibrational amplitude was evident especially with the increase of applied TMPs, as shown in Figure 33. Maximum values of permeate fluxes were observed when the applied TMP was at 3.79 MPa and for vibrational frequencies at 54.7 Hz (d = 3.18 cm). The TMP serves as the driving force for permeate flow through membranes, while the surface shear generated by vibration reduces the accumulation of the solute on the membrane surface. On the other hand, it can be observed that the effect of pressure on permeate flux was nearly insignificant under crossflow NF operations (F = 0 Hz, d = 0 cm), over the ranges that measurements were taken (1.03 MPa to 3.79 MPa). It is likely that the behavior is a linear relationship for CF operation at very low pressures, but this quickly transitions to a region that is dominated by the gel layer resistance. No further increase in flux was observed beyond 1.03 MPa, as the increased surface concentrations become the controlling factor for flux. The same was also observed in the vibratory NF of skim milk [165], tannery wastewaters [166], and of soluble coffee wastewater [52].

The improvement in flux presents the positive impact of the interaction between TMP and vibratory shear in the NF operation. However, the permeate flux decreased with increasing coffee extract strength and its interaction with TMP limited the extent of flux improvement. In Figure 33a, for an 8.5 g L^{-1} feed coffee extract, the permeate fluxes showed a strong linear relationship with the applied TMP for vibrational frequencies between 54.1 Hz and 54.7 Hz. The strong linear relationship between flux and TMP reflects the constant flow resistance of the membrane operation, based on Equation 18. This behavior also shows that the shear rates induced from vibrations prevented the build-up of the foulants on the membrane surface. Higher feed concentrations, however, limit the impact of surface shear rates and decreased the linear relationship between TMP and permeate fluxes. Inflections from the plots were also observable as the permeate fluxes decreased with increasing feed coffee extract concentrations. As shown in Figure 33c, despite operating at 3.79 MPa and 54.7 Hz, increasing the feed concentrations up to five times higher than the standard concentration of 8.5 g L^{-1} reduced the permeate flux by about 55.9%, or from 60.1 L m^{-2} h^{-1} to 26.5 L m^{-2} h^{-1}. These inflections reflect the increasing flow resistance due to concentration polarization that have also been observed in the NF of dairy wastewaters [17], and in the UF of soy milk [103]. At the inflection, the permeate flux slowly ceases to increase despite the increase in TMPs and vibrations, thus approaching critical flux behavior. At this point, there is also a shift from a pressure-controlled flux commonly observed at lower pressures, to a mass transfer gel layer-controlled region at higher pressures [17], [163], [167] This transition was also observed to have a quicker transition under non-vibratory CF operations, and for higher feed coffee extract concentrations. From an operational aspect, the critical flux serves as the threshold flux at which the membrane operations are economical due to the minimal impact of membrane fouling and reduced need for membrane cleaning and maintenance [122].

Figure 33

Variation of Permeate Flux with Applied Transmembrane Pressure Under Different Vibrational Frequencies and Feed Coffee Extract Concentration at T = 25 °C

(a) $C_o = 8.5$ g L^{-1}

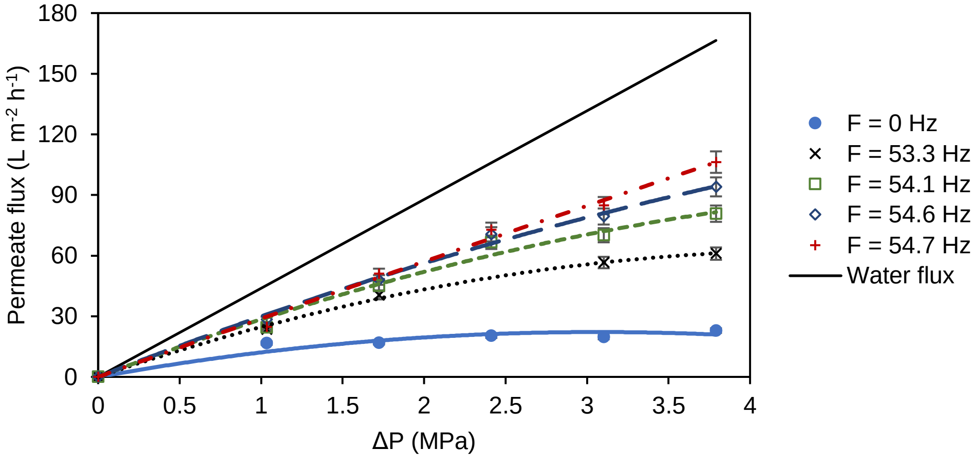

(b) $C_o = 25.4$ g L^{-1}

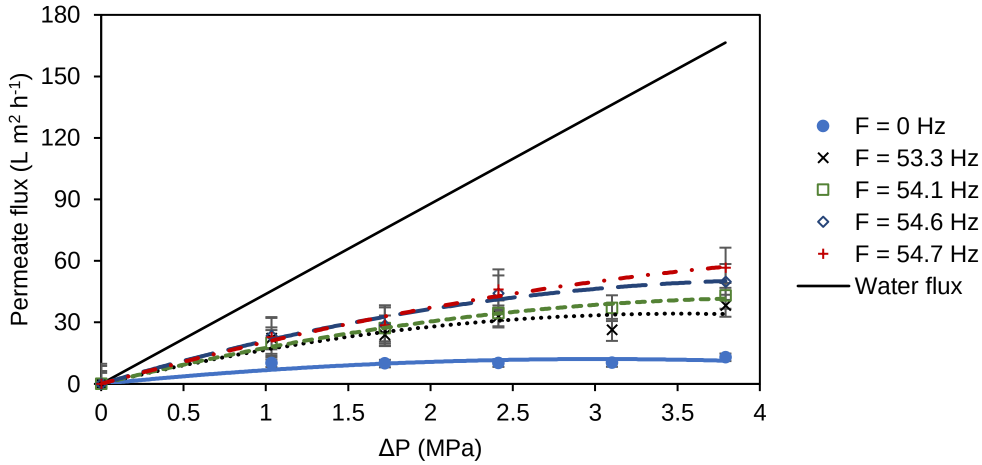

(c) $C_o = 42.4$ g L^{-1}

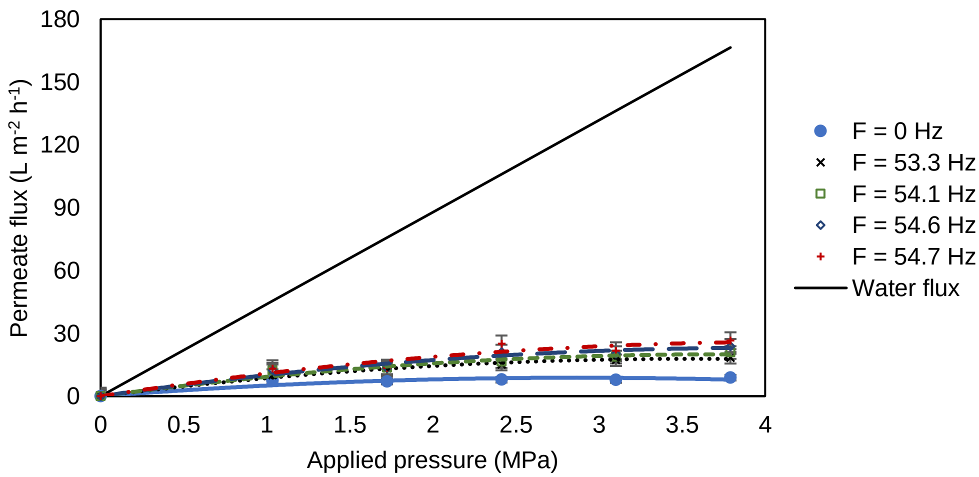

The decrease in permeate fluxes at higher feed coffee extract concentrations can also be attributed to the increase in osmotic pressure from the accumulation of solutes on the membrane surface [33]. The parameter is a function of solute concentration in the fluid that reduces the effective TMP of membrane processes especially for dense membranes such as those of NF and RO. Osmotic pressure differences were evaluated semi-empirically using the Rautenbach formula [16], [33], shown in Equation 67.

$$\pi_i = a\, C_i^{\,m} \tag{67}$$

In terms of the osmotic pressure difference ($\Delta\pi = \pi_f - \pi_p$), Equation 67 can then be expressed as a function of feed and permeate concentrations. The Rautenbach formula is highly applicable for highly rejecting membranes like those of NF and RO, where permeate concentrations are significantly low or negligible compared to feed concentrations. Using this assumption, the osmotic pressure difference can then be expressed as:

$$\Delta\pi = a\, C_o^{\,m} \tag{68}$$

The empirical parameters, a and m, are determined using the osmotic pressure model expressed for different bulk concentrations of the feed coffee extract, C_o. By taking the difference between the permeate flux and water fluxes at different pressure, the osmotic pressure model can be alternatively expressed as a logarithmic linear function of feed concentrations, as shown in Equation 69.

$$\log(J_w - J_v) = \log A_w + \log a + m \log C_o \tag{69}$$

From the osmotic pressure model, different values of $[\log C_o]$ were plotted against the values of $[\log(J_w - J_v)]$ at applied TMPs and vibratory frequencies. The empirical parameters were derived from linear regression where the exponent m was obtained from the slope of the line, and the coefficient a was derived from the y-intercept of the plot for a given membrane hydraulic permeability (A_w). Average values of the empirical parameters were plotted for various applied TMPs and vibrational frequencies, as shown in Figure 34, while the calculated osmotic pressure differences at different operating conditions are plotted in Figure 35.

Figure 34

Variation of Osmotic Pressure Parameters with (a) Applied TMP and (b) Vibrational Frequencies at T = 25 °C

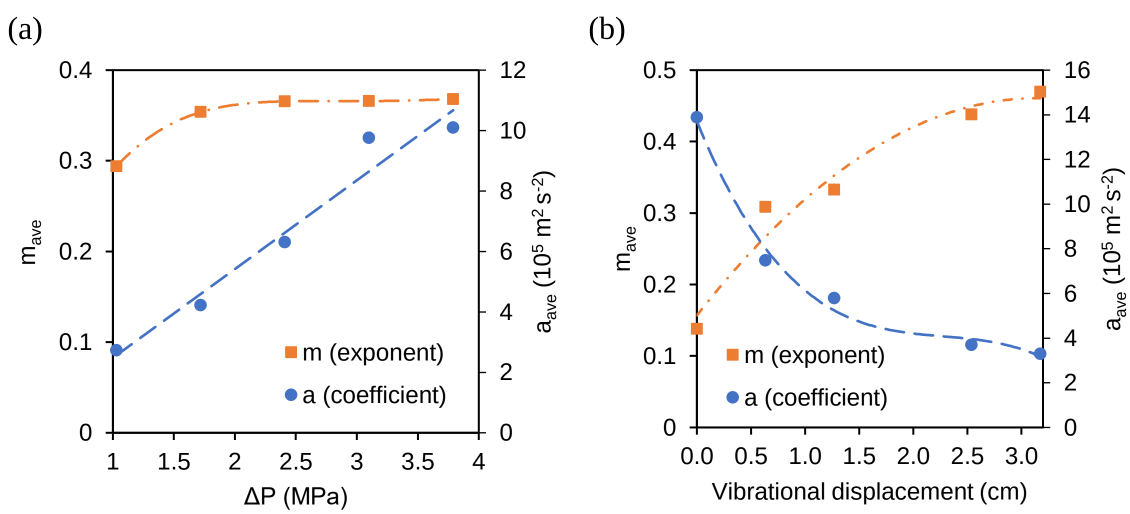

Figure 35

Osmotic Pressures as a function of Feed Coffee Extract Concentration at Various Applied TMP and Vibrational Frequencies at T = 25 °C

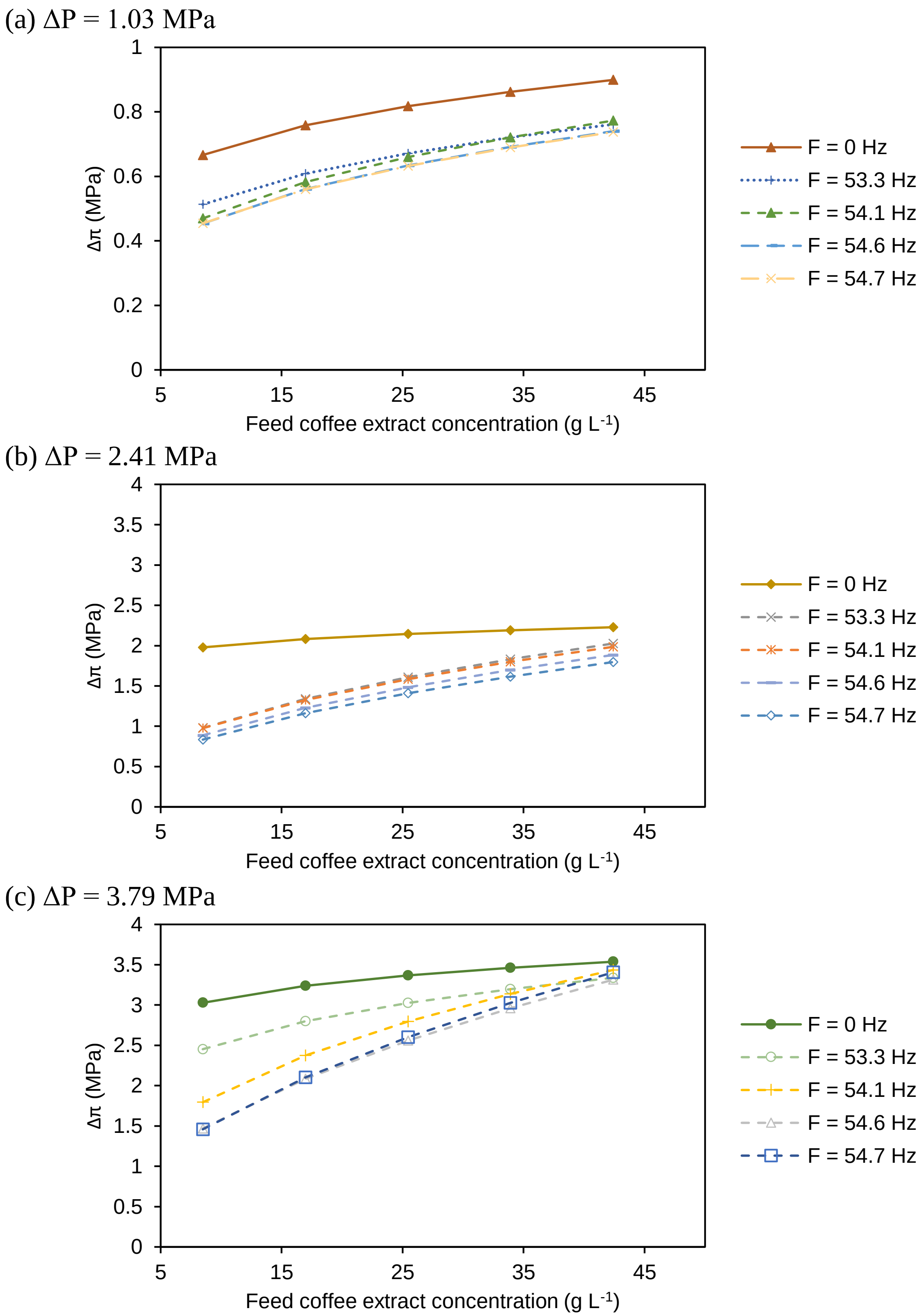

The coefficient, a, reflects the strength of the osmotic pressure effects in the NF operation. High values of a, likewise osmotic pressure differences, were measured when the applied TMP was 3.79 MPa, and for non-vibratory NF operations, as shown in Figure 34. In Figure 35 the increase in concentration increased the osmotic pressure difference from about 75.6% to 91.1% of the applied TMP under CF operation. The resulting osmotic pressure difference reduced the effective TMP and resulting permeate fluxes to about 24.4% to 8.9% relative to the measured pure water fluxes. The high osmotic pressures indicate the insufficiency of CF velocities to suppress concentration polarization in non-vibratory operations.

On the other hand, vibrations reduced the osmotic pressure effects by up to 76% of those observed for the CF operations, that resulted in enhanced permeate fluxes by up to 3 times depending on the feed concentration and applied TMP. Despite the observed positive impact of applied TMP on permeate flux, higher TMPs contributed to larger osmotic pressure effects. As shown in Figure 34, the values of the empirical coefficient, a, increased with the applied TMP and decreased with increasing vibrations. On the other hand, the values of the exponent, m, were in the order less than 0.5 that increased with increasing applied TMP and vibration. As a result, vibrations were most effective in reducing the osmotic pressure effects at low concentrations and at moderate levels of applied TMP. In Figure 35a, the vibratory conditions reduced the osmotic pressure difference between 68% to 82% of those generated by CF filtration at 1.03 MPa. At 2.41 MPa (Figure 35b), the osmotic pressure effects varied between 45% to 80% of those generated by CF filtration. However, high-pressure operations at 3.79 MPa feed concentration of 8.5 g L^{-1} were observed to have osmotic pressures between 1.46 MPa to

2.45 MPa despite the vibration. The effect of vibration also diminished as feed coffee extract concentrations increased to 42.4 g L^{-1}. At this concentration, the osmotic pressure effects were about 90% of the applied TMP, which indicated critical flux conditions. These observations indicate that while TMP serves as the driving force for permeate flux, it also draws the solute particles near the membrane surface by convection. The stronger concentration polarization and osmotic pressure effects arising from high-pressure NF operations then become the controlling factor. This condition should be prevented, as it increases the risks of membrane fouling, thus, increasing the operating cost of the operation.

5.3.6 *Effect of Concentration*

The results presented so far showed the interaction between feed coffee extract concentration, TMP, and vibration on permeate flux for CF and vibratory operations. As shown in Figure 36, the lowest permeate fluxes were observed under non-vibratory or CF operations. The improvement of flux by vibratory operation was clearly evident based on the surface shear rates generated by the torsional oscillations of the membrane module. Likewise, increasing the applied TMP also increased the permeate flux of the membrane operations. Feed concentrations decreased the permeate flux due to concentration polarization and osmotic pressure effects.

Figure 36

Permeate Flux as a function of Feed Coffee Extract Concentration at Various Applied TMP and Vibrational Frequencies at T = 25 °C

(a) ΔP = 1.03 MPa

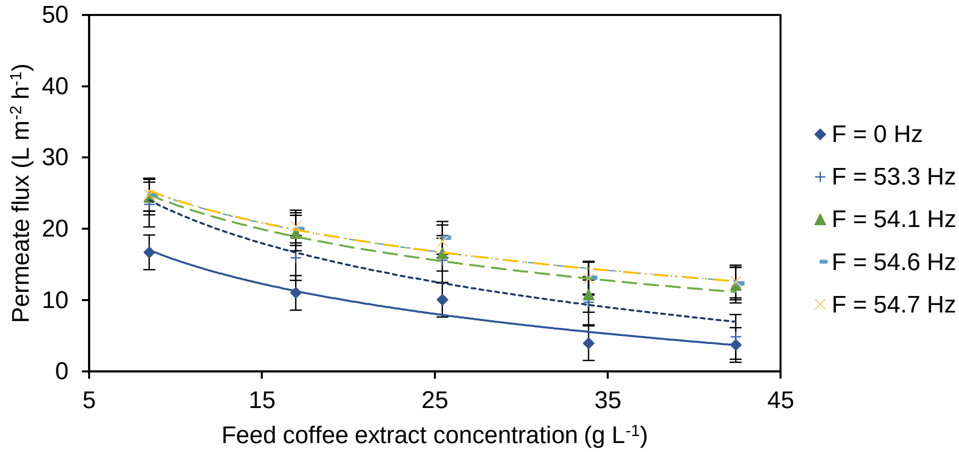

(b) ΔP = 2.41 MPa

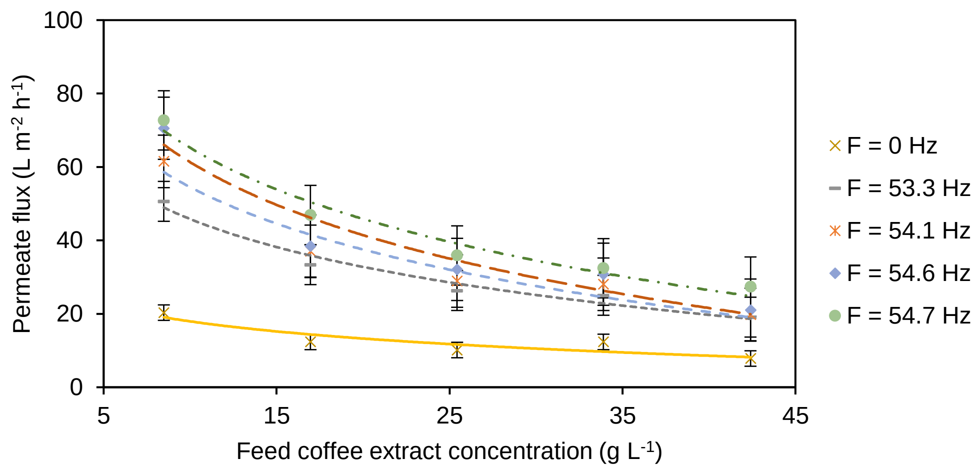

(c) ΔP = 3.79 MPa

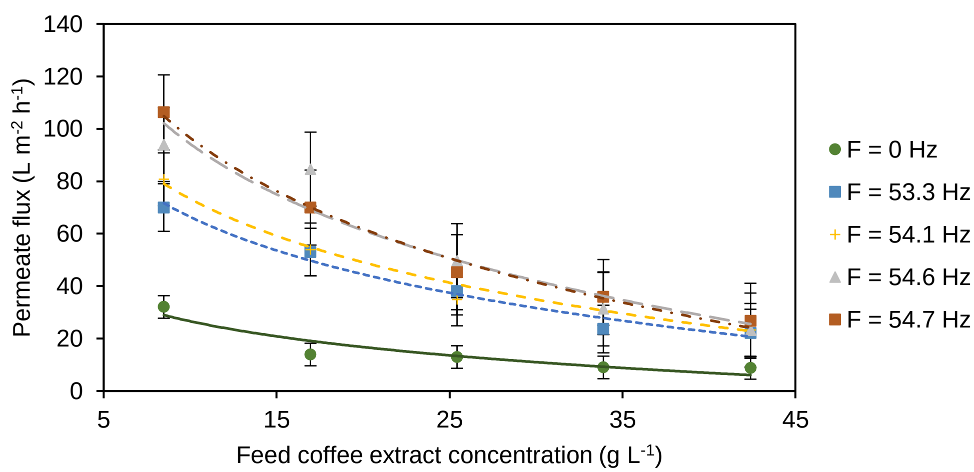

As shown in Figure 36, increasing feed coffee extract strength reduced the permeate flux, owing to the stronger concentration polarization effects that form highly viscous layers on the membrane surface that adds to the total resistance to flow. High-pressure operations further promoted concentration polarization as hydraulic pressure forced more solute particles toward the membrane surface. Apart from this, the stronger concentration polarization also contributes higher osmotic pressure effects that tend to reduce the effective TMP and permeate flux. As a result, CF and vibratory NF operations ran at excessively high applied TMPs have greater risks for membrane fouling, and thus, should be prevented. Overall, the interactions observed between the effects of feed concentration, applied TMP, and module vibration, suggest critical parameters that establish the suitable conditions of the NF operation [163].

5.3.7 *Rejection Efficiency*

The constituents rejected by the TS80 NF membrane are components that make up the simulated coffee extract from reconstituted commercial instant coffee product. As discussed earlier in Section 5.3.1, these components include mostly organic components such as proteins, polysaccharides, lipids, and organic acids; but can also include inorganic minerals and salts [96], [97]. Although soluble in water, these constituents dissociate in solution at different extents. Some constituents can homogeneously dissolve into organic and inorganic ions, but others may also disintegrate into very small particles like colloidal matter (1 nm to 1000 nm), e.g., cluster of macromolecules, that disperse in the solution as suspension. In this study, these components were characterized from feed coffee extracts and permeate samples using proxy or representative analyses for turbidity (suspended and colloidal solids), conductivity (dissolved organic and inorganic ions), and

COD (total organic matter), with analytical methods discussed in Section 3.1.4. The ability of the TS80 NF membrane to reject these components during vibratory and CF filtration operations were also investigated, as discussed herein.

The TS80 membrane effectively rejected the colloidal and suspended solids, as well as the colored constituents of the coffee extract. As shown in Figure 37, clear, water-rich permeate samples were obtained from all the NF operations regardless of the operating condition. In addition, the observed turbidity rejection and absorbance rejection efficiencies were above 99.9% and 100%, respectively. This observation indicates that most of the colored organic compounds in the feed coffee extract were also colloidal and suspended solids that were larger than the cut-off molecular weight of the TS80 NF membrane, i.e., 150 Da. In addition, an average COD rejection of about 99.1% was observed from the NF operations, that also highly suggested that most of the organic components in the coffee extracts were colloidal and suspended solids, represented by turbidity.

Figure 37

Feed Coffee Extract (a) and Permeate (b) Samples from NF Operation

(a) (b)

Despite the significant turbidity and COD rejection, permeate conductivities ranged from 13.2 µS cm^{-1} to 658.5 µS cm^{-1} that varied with the operating conditions of the NF operation. This observation indicated that dissolved organic and inorganic components smaller than 150 Da (or with molecular weights lower than 150 g mol^{-1}) were transferred through the NF membrane along with the solvent, in this case, water. Owing to the effective rejection of suspended and colloidal solids from the coffee extract, the conductivity measured from the permeate can be attributed to dissolved organic acids based on the observed permeate COD concentrations that ranged from 33 mg L^{-1} to 530 mg L^{-1} with pH between 5.01 and 6.92. This acids may include caffeine, chlorogenic acids as were also observed from previous CF NF operation of coffee extracts [33]. Relative to the feed coffee extract characteristics, this partial rejection of dissolved components resulted in conductivity rejection ranging from 44.3% to 94.8%, with COD rejection efficiencies ranging from 99.6%, to 99.9%. The permeate quality and corresponding rejection varied depending on the level of applied TMP, feed coffee extract concentration, and vibrational amplitude, as shown in Figure 38 to Figure 40 for conductivity parameters, and in Figure 41 to Figure 43 for the COD parameters.

Figure 38

Permeate Conductivity (left) and Conductivity Rejections (right) as Function of Feed Concentration at Various Applied TMPs and Vibrational Frequencies at T = 25 °C

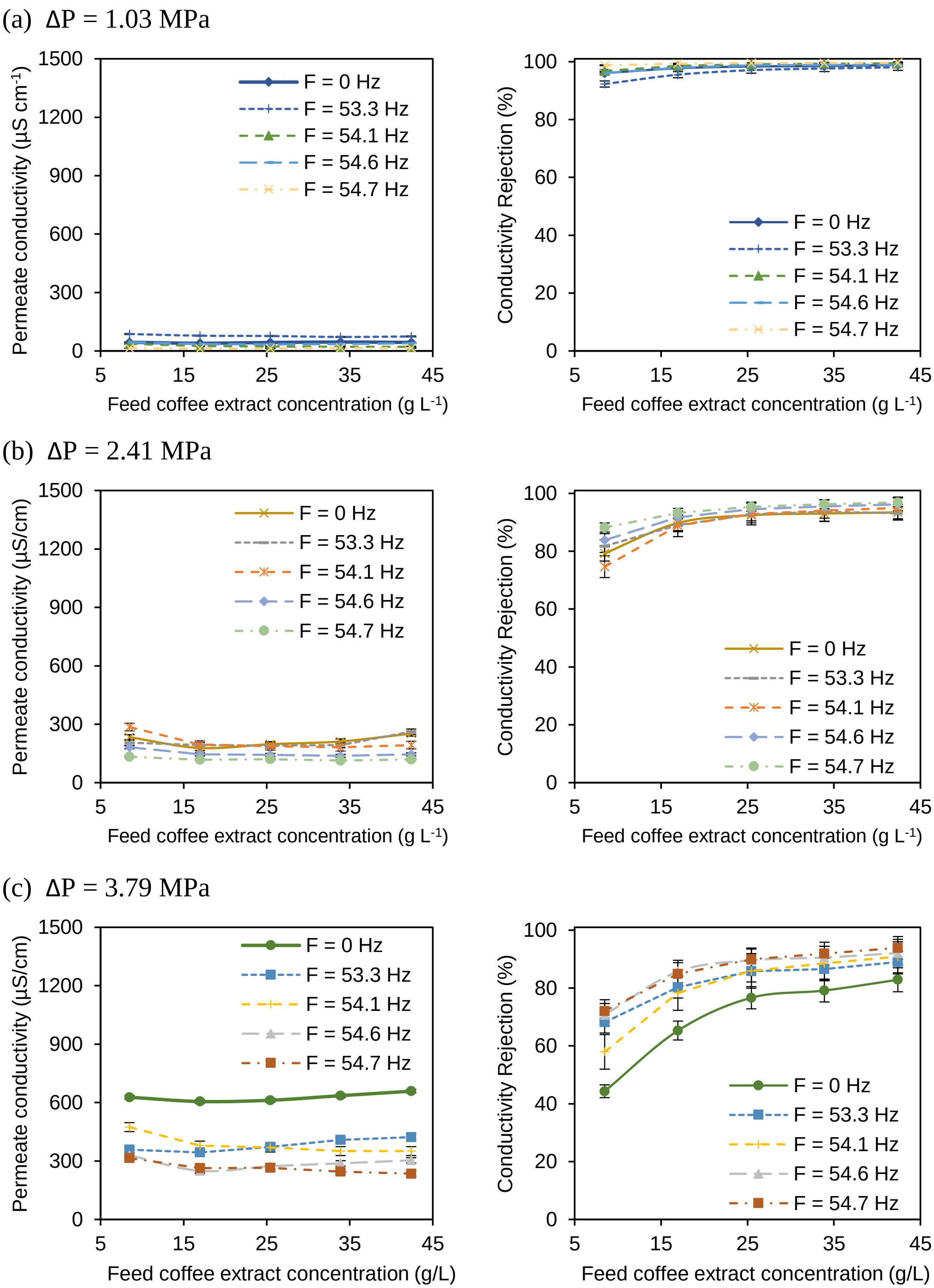

Figure 39

Permeate Conductivity (left) and Conductivity Rejection (right) as Function of Applied TMP at Various Vibrational Frequencies and Feed Concentrations at T = 25 °C

(a) F = 0 Hz, d = 0 cm (non-vibratory)

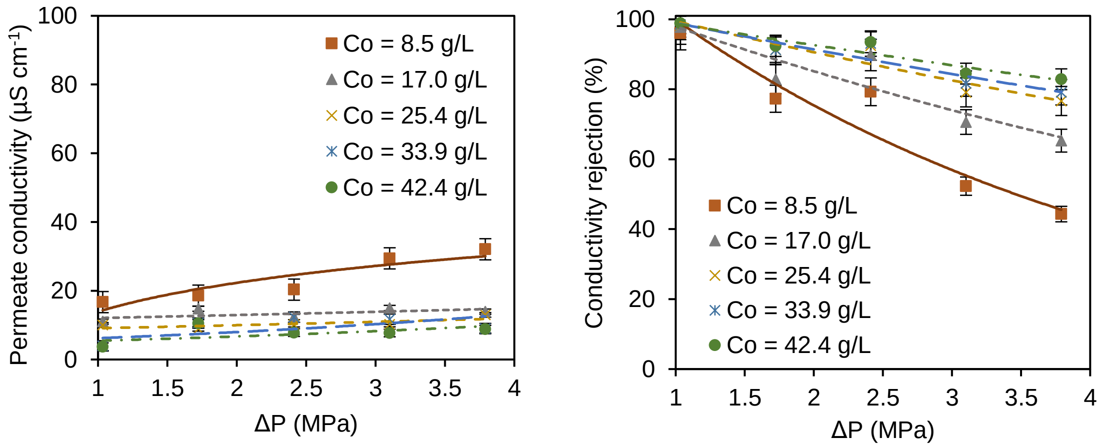

(b) F = 53.3 Hz, d = 0.64 cm

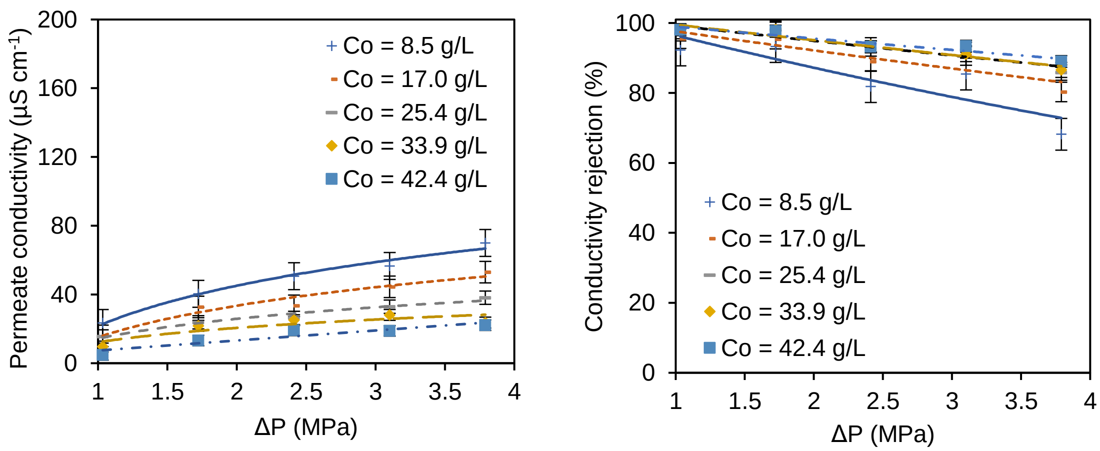

(c) F = 54.7 Hz, d = 3.18 cm

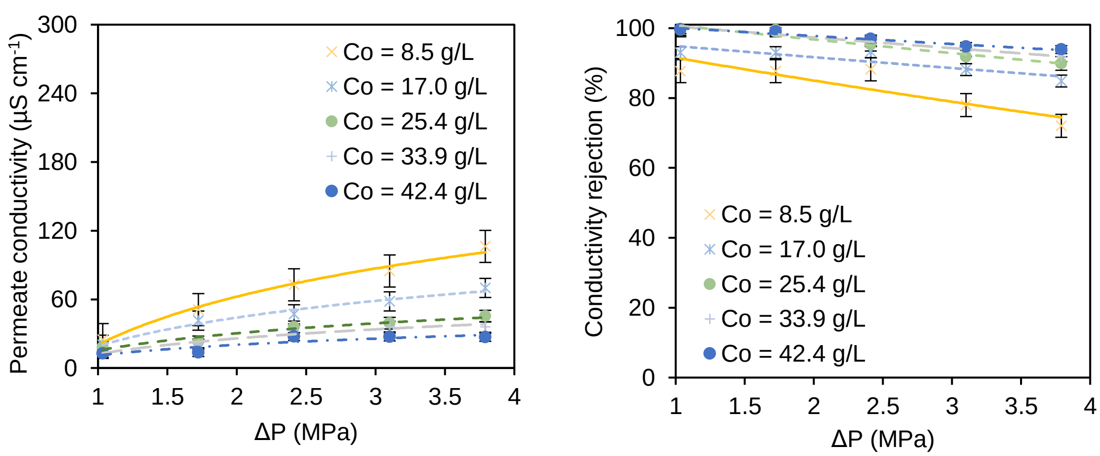

Figure 40

Permeate Conductivity (left) and Conductivity Rejection (right) as Function of Vibratory Displacement at Various Feed Concentrations and Applied TMPs at T = 25 °C

(a) C_o = 8.5 g L^{-1}

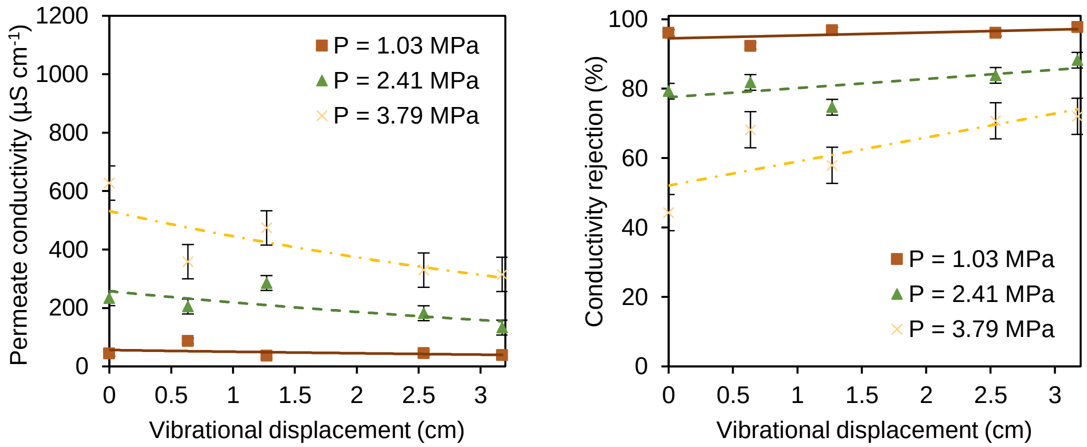

(b) C_o = 25.4 g L^{-1}

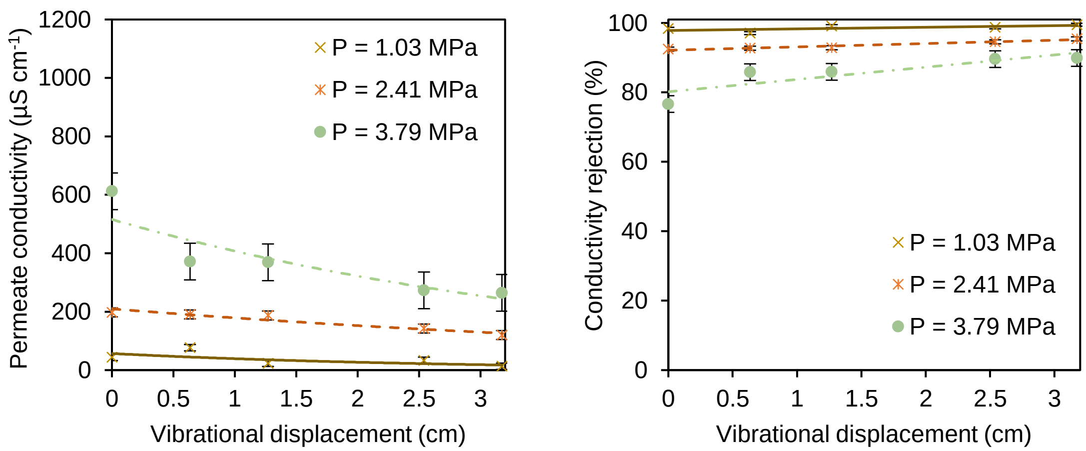

(c) C_o = 42.4 g L^{-1}

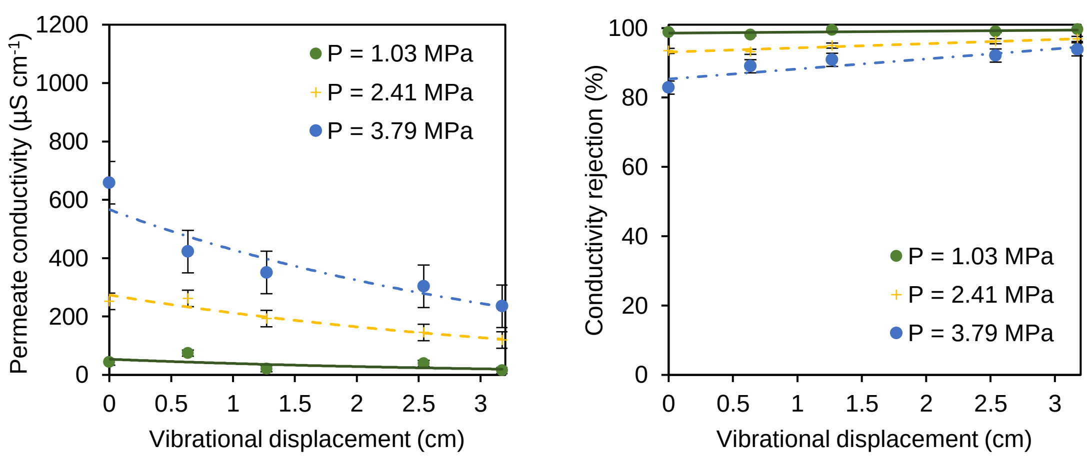

Figure 41

Permeate COD (left) and COD Rejections (right) as Function of Feed Coffee Extract Concentration at Applied TMPs and Vibrational Frequencies at T = 25 °C

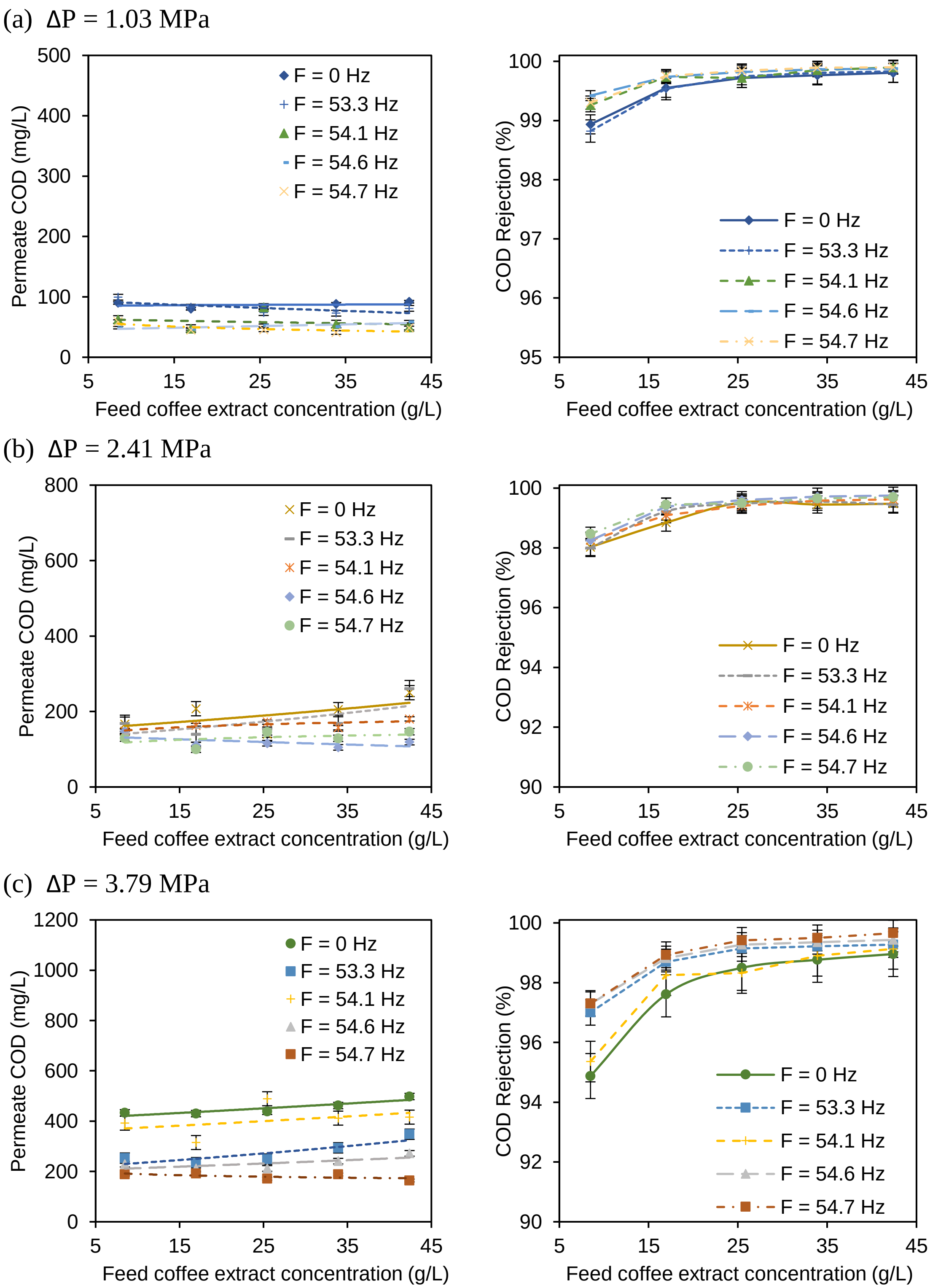

Figure 42

Permeate COD (left) and COD Rejections (right) as Function of Applied TMP at Various Vibrational Frequencies and Feed Concentration and at T = 25 °C

(a) F = 0 Hz, d = 0 cm (non-vibratory)

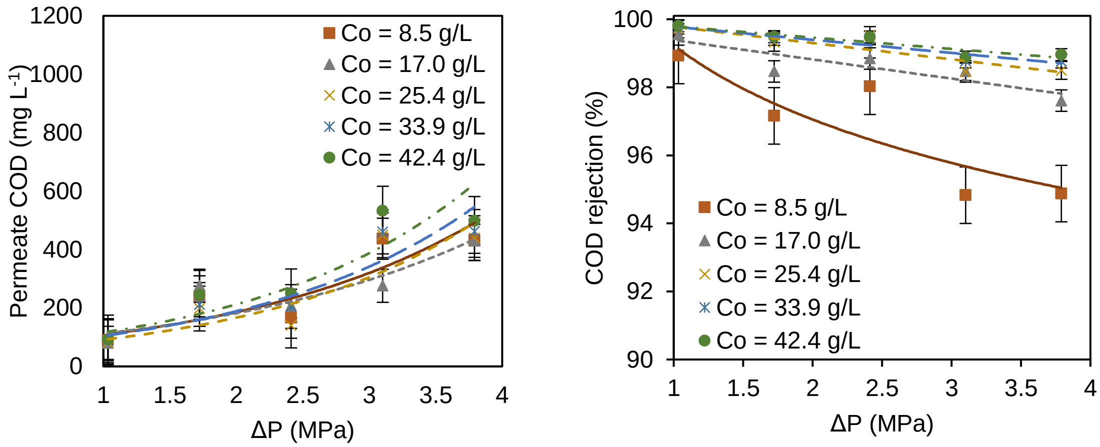

(b) F = 53.3 Hz, d = 0.64 cm

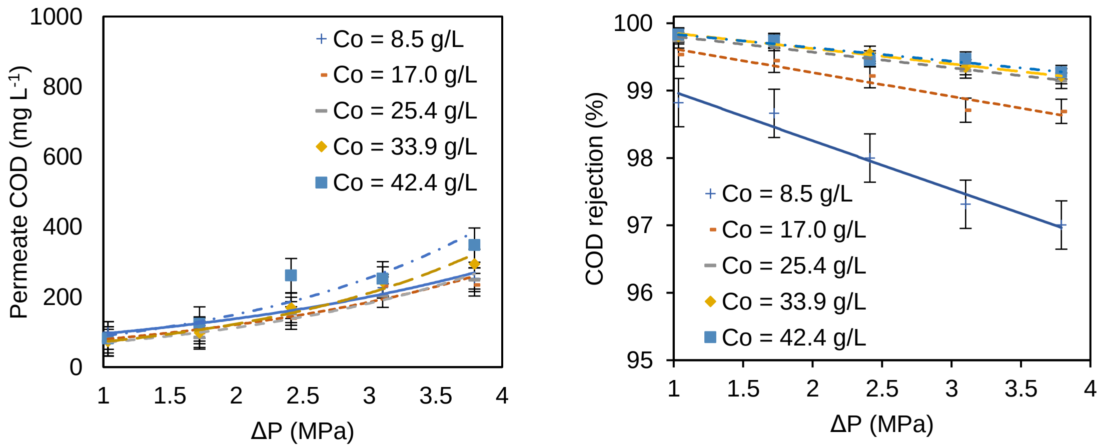

(c) F = 54.7 Hz, d = 3.18 cm

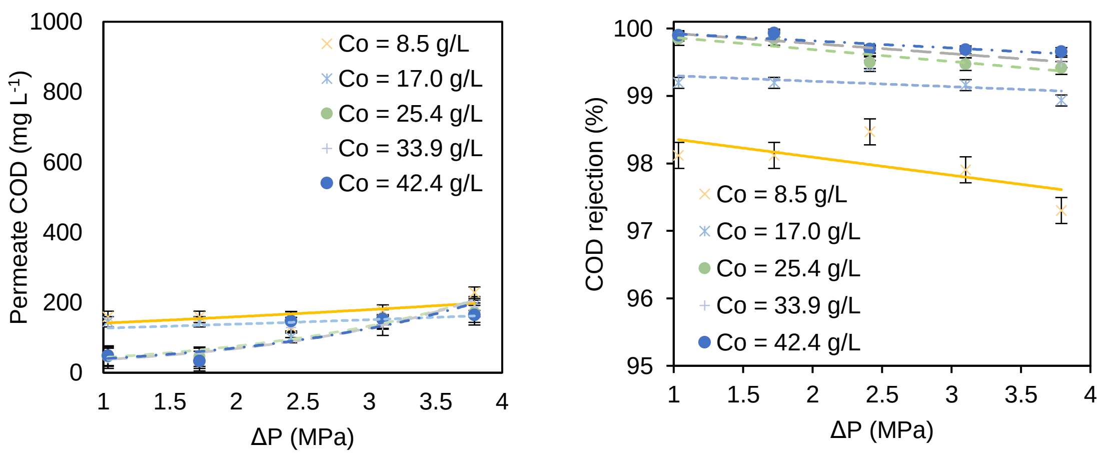

Figure 43

Conductivity and COD Rejections as Function of Vibrational Displacement at Various Feed Coffee Extract Concentration and Vibrational Frequencies at T = 25 °C

(a) $C_o = 8.5$ g L^{-1}

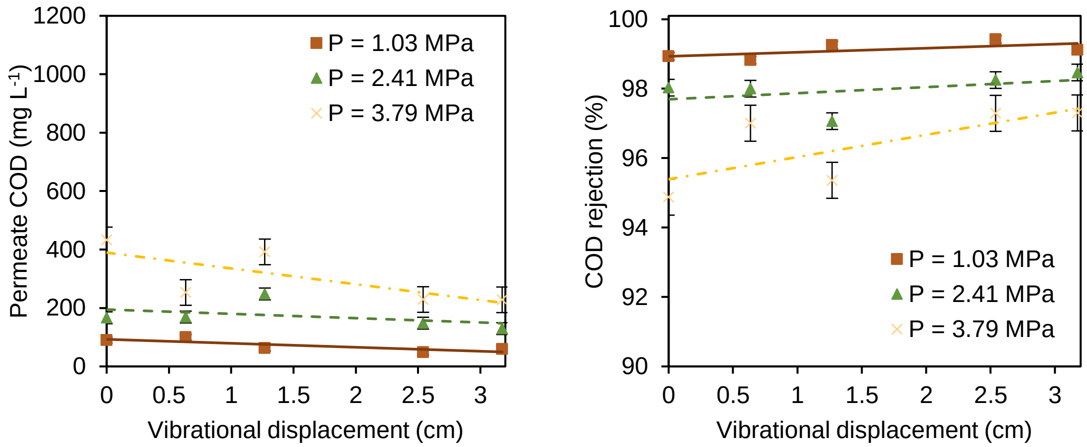

(b) $C_o = 25.4$ g L^{-1}

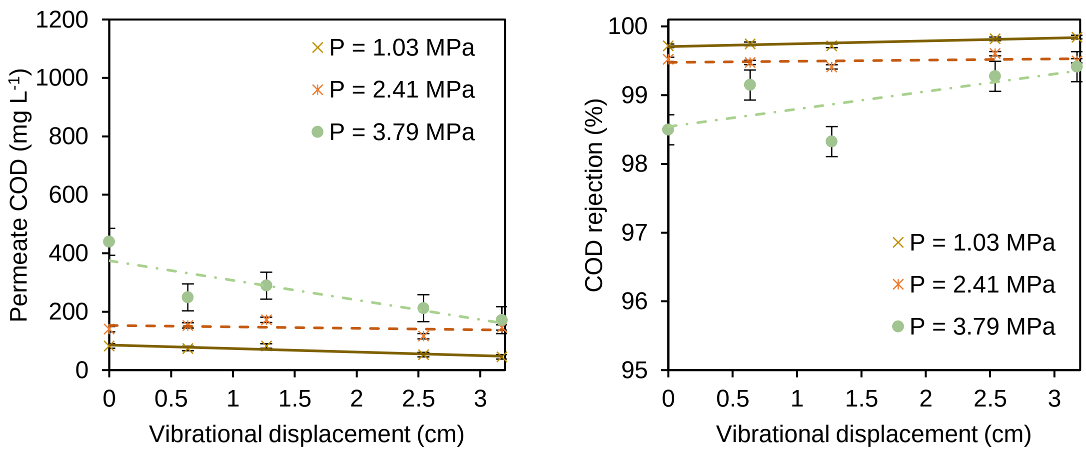

(c) $C_o = 42.4$ g L^{-1}

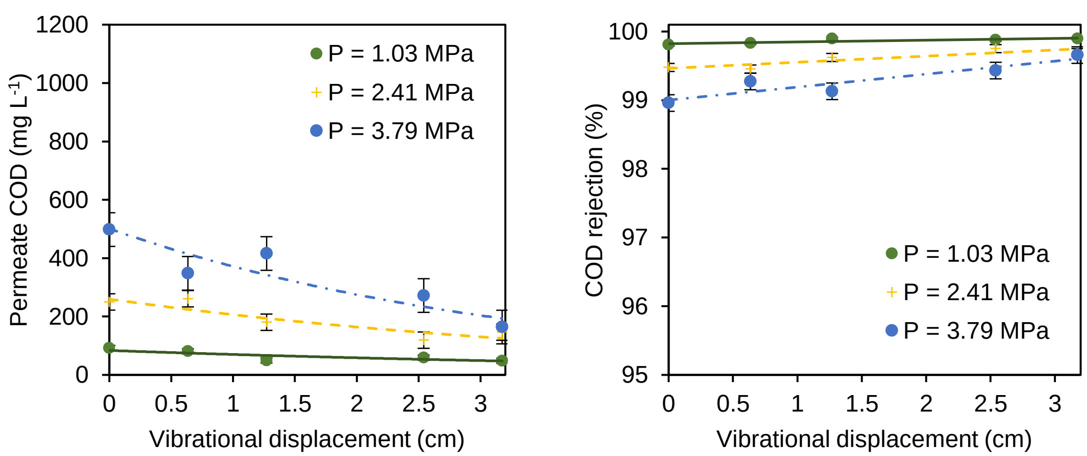

Like permeate flux, membranes exert a certain resistance to retain certain solutes that are larger than the pore size or cut-off molecular weight, or in the case of NF membranes, repel similarly charged solutes from passing through [94]. Descriptions of uncharged solute rejection in NF membranes have generally been based on steric diffusion within the membrane pores, while charged solute rejection have been modelled based on electrokinetic mechanisms relative to the membrane surface charge [168]. However, it should be noted that the permeate concentrations (turbidity, conductivity, absorbance, and COD) measured in this study were non-specific and do not provide detailed information of solute constituent sizes, and surface charges, likewise the specific mechanisms influencing rejection. Nonetheless, solute rejection of the TS80 NF membrane observed in this study were interpreted based on the relationship between the solvent flux (J_v) and the flux of the undesired solute components (J_s) passing through the membrane. This fundamental relationship is shown in Equation 70.

$$J_s = C_{p\,i}\, J_v \tag{70}$$

In terms of observed rejection, the solute flux may also be expressed as:

$$J_s = C_o(1 - r_o)\, J_v \tag{71}$$

Membrane surface concentrations further adjusts the relationship in terms of real rejection efficiencies, as shown in Equation 72.

$$J_s = C_m(1 - r_{real})\, J_v \tag{72}$$

Equations 70 to 72 only present that the transport of solute across the membrane is directly proportional to the permeate flux. Thus, conditions that increase permeate fluxes generally tend to increase the solute flux and result in lower rejection efficiencies. Likewise, conditions that increase membrane surface concentrations lead to higher solute fluxes that decrease rejection efficiencies.

Permeate conductivities and rejection efficiencies corresponded with those of COD at various operating conditions indicating the presence of dissolved organic constituents that are smaller than 150 Da that passed through the TS80 NF membrane. However, it should be noted that some of the permeate conductivity may also be attributed to inorganic ions and a more specific characterization of the dissolved components may be recommended. Nonetheless, permeate conductivities and COD concentrations were highest under non-vibratory CF operation (F = 0 Hz) and at applied pressures of 3.79 MPa. Feed coffee extract concentrations had little effect of permeate conductivities. However, it can be observed that permeate CODs slightly increased with increasing coffee extract strength. Consequently, conductivity and COD rejection efficiencies increased with the higher vibrations and feed coffee extract concentrations; and decreased with increasing applied TMPs. High membrane surface shear rates generated by torsional oscillations reduced membrane surface concentrations that, in turn, reduced the diffusive transfer of solutes through the NF membrane while enhancing the permeate flux. As shown in Figure 40 and Figure 43, compared with CF operations, module vibrations at 54.7 Hz (d = 3.18 cm) reduced permeate concentrations by about 56% for conductivity and 58% for COD at applied pressure of 3.79 MPa. On the other hand, an average reduction of 50% for permeate conductivity and 42% for permeate COD was observed at 1.03 MPa, owing to low sensitivity of permeate flux with surface shear at low TMPs (as discussed in Section 5.3.4). Nonetheless, the improvement of rejection efficiencies attributed to vibratory shear is comparable with those observed in vibratory membrane filtration of surface waters for natural organic matter (NOM) removal [47], and humic substances [40], and in the vibratory NF of skim milk [165].

On the other hand, the increase in permeate conductivities and COD concentrations, likewise, the decrease in the corresponding rejection efficiencies at increasing applied pressure can be attributed to the increase in permeate fluxes that promoted the transfer of solutes across the membrane [169]. Consequently, conductivity and COD rejections shown in Figure 39 and Figure 42 were lowest at 1.03 MPa for both CF and vibratory NF operations due to the decrease in driving force for permeate flow. The decreasing rejection efficiencies at higher applied pressure also indicates that the rejection of the solute was controlled by the convective transfer of solutes across the membrane as the membrane surface become polarized. Increasing the applied pressure promoted higher solvent fluxes that carries coffee extract components towards the membrane surface. Thus, a more concentration polarized region results from the increase in solute concentration on the membrane surface, among which are dissolved components that diffuse through membrane pores and result in higher permeate concentrations and lower rejection efficiencies [170]. This behavior were comparable with those studies conducted for the removal of arsenic by NF [169], fouling in the vibratory MF of algae cultures [171], and in the rotary disk UF of alfalfa wastewater [170]. In contrast with these results, other NF studies like those in skim milk processing [172] and in soluble wastewater reclamation [52] reported an increase in rejection efficiencies with increasing applied pressure. However, it should be noted that these studies used more diluted streams that can less likely foul membranes compared with those processed in this study. This indicates a threshold applied pressure that optimizes the vibratory NF of coffee extracts by not only meeting the critical flux, but also generates satisfactory rejection efficiencies.

The NF operation generated water-rich permeate, however, as mentioned earlier, dissolved constituents like organic and inorganic ions smaller than 150 Da are still present in the permeate, as represented by permeate conductivity and COD concentration. Despite this, most of the permeate had conductivities less than 300 μS cm^{-1}, that did not significantly vary with feed coffee extract concentrations, as shown in Figure 38. On the other hand, the organics (as COD) in the permeate were also considerably reduced relative to those observed from feed coffee extracts. Permeate COD concentrations were less than 500 mg L^{-1} that slightly increased with feed coffee extract concentrations for applied TMPs above 1.03 MPa, as shown in Figure 41. This increased concentration of organics in the permeate can be attributed to the increased solute flux as a result of the higher concentration gradient across the membrane. In the concentration of diluted milk by vibratory NF, Frappart et al. [165], reported an exponential increase in permeate conductivities and COD concentrations as a result of this diffusion. This behavior generally leads to lower rejection efficiencies, especially for low molecular weight organic solutes, and salts at dilute concentrations [108]. However, the coffee extracts used in this study were considerably higher in concentrations and were largely represented by colloidal and suspended solids. The retention of these components resulted in higher concentration polarization that, in effect, acted as an additional layer of resistance, not only for solvent flow, but also for solute transfer [94], [108]. For NF membranes this additional resistance may arise from hindered solute transport due to steric hindrance or pore blocking, and by charge exclusion [173]. According to Mulder [108], membrane rejection efficiencies can be higher for mixtures of macromolecular solutes, like in the case of coffee extracts, where suspended and colloidal components increase the retentivity especially for lower molecular weight solutes.

Chapter 6

Modeling Vibratory Nanofiltration of Coffee Extracts via Semi-Empirical Approach

Additional graphs and tabular data of the results for this chapter are presented in Appendix C. The results presented herein are those essential to summarize the studies necessary for this dissertation's discussion.

6.1. Introduction

The effectiveness of the novel dynamic vibratory filtration system is dictated not only by the local shear rates developed on the membrane surface, but also by the underlying mass transfer mechanisms affected by a variety of operating factors. In Chapter 5, the power-law model strongly related the effects of vibratory frequency and amplitude, hence surface shear rates, on permeate fluxe enhancement [2], [102], [107]. However, while the results were indicative of the significant role of vibratory shear generation in flux enhancement, other parameters still influenced the operation. Some of these indicated the effects of applied TMP and feed concentration on the resulting osmotic pressure effects, concentration polarization, and flux decline. Thus, while the information provided from the power-law model and analyses of individual effects of parameters of vibratory NF performance provide insights on understanding the mechanisms involved, the development of a predictive model relating factor interaction on the vibratory NF performance is still essential. Models not only allow us to understand the different mechanisms affecting the operation of the membrane system, but these can also aid us in managing fouling and further optimizing the process. Hence, these enable the technology to be more transferable for other extensive food and beverage process applications.

The evaluation of the filtration system from a theoretical perspective is fundamental in predicting the vibratory NF performance in processing coffee extracts. Despite the attractiveness of the method, the underlying consequences from the dynamic nature of the VSEP system, as well as that of other dynamic membrane systems, provide the challenging aspects in modeling the process [174]. Overall, this limits analytical approaches for evaluating the interplay of vibration with other operating factors to improve the prediction of filtration performance and membrane fouling. Thus, in contrast with CF filtration systems, currently, a very limited number of mathematical modeling studies for vibratory membrane systems have been reported to date [58]–[60]; and none in which coffee extract preconcentration is involved.

In the light of these limitations, this study adapted an alternative semi-empirical, resistance-in-series model that correlates vibratory NF performance with feed coffee extract concentration, applied TMP, and vibration. A combined osmotic-pressure-film-layer model was evaluated to determine model parameters for membrane surface concentrations, and real rejection at different operating conditions of the NF operation. The resistance-in-series concept was then adapted to quantify and compare the different fouling resistances generated from the nanofiltration of coffee extracts. The variation of concentration polarization, osmotic pressure effects, fouling resistances and model correlations were then compared with experimental parameters for conventional CF, and vibratory filtration operations. Overall, the model developed in this study is useful in managing membrane fouling in vibratory systems and optimizing and developing alternative approaches for its scale-up, which promotes further industrial application.

6.2 Development of the Mathematical Model

6.2.1 *Flow and Surface Shear in the L-VSEP Module*

The vibrating membrane filtration technology employed in this study uses mechanical energy to promote periodic oscillatory movements on the membrane module (Section 2.4.4). These high-speed vibrations, commonly ranging between 50 Hz to 60 Hz, create shear fields that are considerably large enough that overcome local shear rates generated from conventional CF filtration. As a result, this dynamic operation allows the maintenance of permeate fluxes and solute retention without requiring large CF velocities and applied TMPs. The local membrane shear rates generated from this operation also vary sinusoidally with time and proportionally to radius [2]. As was discussed earlier, the CF velocity of the fluid in the annular membrane is characterized by the transverse velocity (or azimuthal flow). This flow is characterized by the radius of the membrane (R_i), oscillation frequency (F) and displacement (d), angular velocity, and channel height (h). In this study, channel height has been found to be approximately 3.5 mm. On the other hand, the maximum displacement resulting from the oscillation of the membrane module is a function of the disk periphery ($r = R_2$). The flow regime of in this channel is governed by Stokes law. The kinematic viscosity (υ) and density (ρ) of the fluid dictate the Reynolds number of the fluid in the vibratory operation, as shown in Equation 23.

$$\mathrm{Re} = \frac{2\pi F h^2}{\upsilon} \tag{23}$$

The membrane surface shear rates may be expressed as maximum shear rate ($\gamma_{w\,max}$) at the disk periphery (Equation 26), while the average shear rate ($\gamma_{w\,mean}$) is determined over the membrane annular area measured from R_1 and R_2 (Equation 27).

$$\gamma_{w\,max} = \frac{R_2 \Omega Re^{0.5}}{h} = 2^{0.5} d(\pi F)^{1.5} \upsilon^{-0.5} \tag{26}$$

$$\gamma_{w\,mean} = \frac{2^{1.5}\left(R_2^3 - R_1^3\right)}{3\pi R_2\left(R_2^2 - R_1^2\right)} \gamma_{w\,max} \tag{27}$$

6.2.2 *Osmotic Pressure Model*

Like most pressure-driven membrane operations, permeate fluxes (J_v) in NF results from the effective TMP ($\Delta P - \Delta\pi$) across the membrane as proportional to the intrinsic permeability of the membrane (A_w). The osmotic pressure model can be employed by determining the osmotic pressure effects due to the accumulation of solute on the membrane surface. For this study, the osmotic pressure difference across the membrane is taken from the osmotic pressures between the feed-side surface of the membrane (π_m) and the permeating fluid (π_p). This colligative property arises from the different solute concentrations (C_m and C_p) across the membrane and can be determined from van't Hoff's law, shown in Equation 73.

$$\pi_i = aC_i = \left(\frac{RT}{M}\right) C_i \tag{73}$$

From the equation, a is the osmotic coefficient of the solution that is a function of absolute temperature (T), universal gas constant (R), and the molecular weight of the feed

(M). The average molecular weight of the coffee extract was found to be 524.5 x 10^{-3} kg mol^{-1} [175]. At 25 °C, the osmotic pressure difference is expressed as:

$$\Delta\pi = 4{,}726\left(C_m - C_p\right) \tag{74}$$

The accumulation of solute on the surface of the membrane corresponds to a real rejection parameter (r_{real}), a property of the membrane-solute system as opposed to the observed rejection that varies with the bulk concentration of the feed. This parameter is calculated relative to membrane surface and permeate solute concentrations. The osmotic pressure model is expressed in terms of the real rejection parameter and membrane surface concentration, as shown in Equation 75.

$$J_{v\ OSM} = A_w(\Delta P - 4{,}726 C_m r_{real}) \tag{75}$$

6.2.3 *Concentration Polarization*

As discussed in Section 2.4.2, concentration polarization occurs when a laminar boundary layer arises from the accumulation of solute components near the membrane surface because of the applied TMPs during filtration. Under steady-state operation, the local solute concentration on the membrane surface, similar to C_m in Equation 75, reaches a constant maximum value that influences the mass transfer across the membrane. Likewise, this concentration polarized region is also characterized by a boundary layer thickness and the diffusivity of the fluid. The film layer model (Equation 11) can be expressed in terms of real rejection and membrane surface concentrations, as shown in Equation 76.

$$J_{v\,CP} = \frac{D_s}{\delta} \ln \frac{C_m r_{real}}{C_o - C_m(1 - r_{real})} \tag{76}$$

The permeate flux through the membrane also varies proportionally with the ratio between solute diffusivity and boundary layer thickness, otherwise interpreted as the solute mass transfer coefficient ($k_s = D_s/\delta$). As discussed in Section 2.4.2.3, this parameter is a well-known function in the Sherwood relationship that relates the Reynolds number (Re) and the Schmidt number (Sc) with the convective flow in the membrane system. High values of k_s favor high throughput filtration operations, and to influence this, most conventional filtration operations operate at high CF velocities. For this system, the Harriott-Hamilton correlation, shown in Equation 77, is applicable for turbulent flows in channels of this order (Re > 4000) [35], [176].

$$Sh = 0.0096 Re^{0.91} Sc^{0.35} \tag{77}$$

The properties of the coffee extract were necessary to determine the diffusivity and Schmidt number (Sc) influencing the mass transfer of solute across the membrane. The Wilke-Chang correlation (Equation 78) was used to determine the diffusivity constant.

$$D_s = \frac{117.3 \times 10^{-18} (\varphi M_A)^{0.5} T}{\mu v^{0.6}} \tag{78}$$

The correlation accounts the molecular weight (M_A) of the solvent, in this case, that of water, and its corresponding association factor ($\varphi = 2.6$), and their ratio with the absolute viscosity of the coffee extract (μ), and solute molar volume (v). For this study, the absolute viscosities, and densities of the coffee extract at different concentrations at 25 °C were calculated from thermodynamic and rheological correlations used by Telis-Romero et al. [141], [142].

Once these parameters are calculated, C_m and r_{real} may be solved numerically by setting the difference between Equation 75 and Equation 76 equal to 0 [176], as shown in Equation 79.

$$0 = A_w(\Delta P - 4{,}726 C_m r_{real}) - \frac{D_s}{\delta} \ln \frac{C_m r_{real}}{C_o - C_m(1 - r_{real})} \tag{79}$$

Suitable numerical methods may be used to solve the equation. For this study, the General Reduced Gradient (GRG) non-linear algorithm was employed to estimate the constant parameters (C_m and r_{real}), and consequently determine the quality of the permeate, C_p. Once the empirical parameters were determined, the calculated values can then be substituted to Equation 75 may then be used to estimate the osmotic-pressure-driven permeate fluxes ($J_{v\ OSM}$).

6.2.4 *Resistance-in-Series Model*

Fouling resistances govern pressure-driven membrane processes such as the vibratory NF system. These resistances not only pertain to membrane resistance, but also account for resistances attributed to osmotic pressure, concentration polarization, membrane adsorption, gel layer formation, etc. Such resistances develop on the membrane surface as dictated by different operating conditions such as filtration time, TMP, solute concentration, and vibratory settings. On the assumption that these resistances act in series to influence NF performance. The osmotic pressure model presented so far, only account for the influence of membrane resistance (R_m) and that of osmotic pressure (R_{osm}) developed on the membrane surface at specific feed concentrations, applied TMPs, and module vibrations. Thus, the osmotic-pressure-driven flux in the model equation can be further expressed using the resistance-in-series model, shown in Equation 80.

$$J_{v\ OSM} = \frac{\Delta P - \Delta\pi}{\mu R_m} = \frac{\Delta P}{\mu(R_m + R_{osm})} \tag{80}$$

Concentration polarization additionally contributes to an additional fouling resistance. On this assumption, experimental permeate fluxes ($J_{v\ exptl}$) deviate from those obtained from the osmotic pressure model. This resistance (R_{cp}) is added, thus, correcting the model based on experimental data, as shown in Equation 81.

$$J_{v\ exptl} = \frac{\Delta P}{\mu\left(R_m + R_{osm} + R_{cp}\right)} = \frac{\Delta P - \Delta\pi}{\mu\left(R_m + R_{cp}\right)} = \frac{J_{v\ OSM}\ R_m}{\left(R_m + R_{cp}\right)} \tag{81}$$

6.3 Experimental Approach

Similar to the parametric studies in Chapter 5, the NF experiments were employed using the L-101 VSEP filtration system. Continuous NF operation in full recycle mode was conducted to approach steady-state conditions within 60 minutes of operation. Experiments were performed at 25 °C and at a retentate flowrate of 7.6 L min^{-1} for applicable ranges of TMP (1.03 MPa to 3.79 MPa), and for selected feed coffee extract concentrations (8.48 g L^{-1} to 42.4 g L^{-1}). Non-vibratory CF filtration runs were set at a vibrational frequency of 0 Hz at displacement of 0 cm; while vibratory NF experiments were employed under frequencies between 53.3 Hz and 54.7 Hz with corresponding displacements between 0.64 cm and 3.18 cm, respectively. Permeate samples were collected at 5-minute intervals to measure the permeate fluxes, and quality ($C_{p\,i}$) in terms of turbidity (suspended and colloidal solids), conductivity (dissolved organic and inorganic components), absorbance (color), and COD (total organic matter), and corresponding rejection efficiencies. However, for the permeate parameters modeled in this study, only rejection efficiencies based on COD concentrations were considered in the mathematical model since COD concentrations were expressed in mass-per-volume basis. On the other hand, the units for conductivity and turbidity characterization were not consistent with the concentration parameters used in the mathematical models. The COD is also a representative parameter for the broad range of coffee constituents present, since it measures the organic character of the solution quite well. The experimental data were simultaneously correlated with semi-empirical models for osmotic pressure effects, concentration polarization, and fouling resistances presented in Section 6.2. Parameters such as membrane surface concentrations, fouling resistances, and real rejection based on COD were observed at various operating conditions. Lastly, a model correlation for flux and permeate concentrations as a function of feed concentration, applied TMP, and vibrational frequency was determined and fitted with the experimental data to assess the applicability of the correlation in predicting vibratory NF operations.

6.4 Results and Discussion

In this study, a resistance-in-series model was developed to predict the performance of the vibratory NF operation in terms permeate flux, permeate COD, and COD rejection efficiencies. The model reflects the effects of feed coffee extract concentration, applied TMP, and vibratory settings on osmotic pressure effects, and boundary layer mass transfer to provide insight on intrinsic parameters such as membrane surface COD concentrations, real rejection efficiencies, and mass transfer coefficients. Like most traditional membrane transport process, osmotic pressure effects were modeled as a function of the membrane surface concentrations, while boundary-layer mass transfer arising from concentration polarization was modeled with the aid of the Sherwood number relationship. However, in contrast with conventional approaches of determining the mass transfer coefficient from crossflow velocities, this study employed the flow properties in the vibratory membrane module as a function of the vibratory frequency and displacement affecting the surface shear rates. The annular channel where fluid flow is assumed to split, as well as the moving walls that generate surface shear on the membrane clearly indicate the unique and complex nature of the dynamic operation. Nonetheless, hydrodynamic analyses developed by Akoum et al. [2] enable the calculation of flow regime, and surface shear rates within the vibratory membrane module with respect to the transverse velocity, vibratory frequency, displacement, and fluid viscosity. This allowed us to estimate the mass transfer coefficient, membrane surface concentrations, fouling resistances that can be used for predicting the vibratory NF performance.

6.4.1 *Membrane Surface Concentration and Permeate Flux*

The simultaneous calculation of the classical osmotic pressure and concentration polarization models serves as a useful alternative approach in modeling flux-enhanced NF systems [35], [176]. Membrane surface concentrations, and real rejection parameters in terms of COD were solved numerically using the GRG non-linear algorithm based on the calculated flow and mass transfer properties. The GRG method is one of the well-known numerical methods for nonlinear optimization where the objective function is differentiable [177], [178]. The numerical method has been applied to small-to-medium sized problems [179] just like the objective function in Equation 79. As a well-known method, the algorithm is accessible using Microsoft Excel ® Solver [180], and was also implemented in this study. The constant parameters were obtained for various feed coffee extract concentrations, TMP and vibratory settings, along with the fouling resistances that shall also be discussed herein. These are presented in Table 27. On the other hand, Figure 44 and Figure 45 show the variation of calculated membrane surface concentrations with feed coffee extract concentration, and applied TMP for non-vibratory CF, and vibratory NF operations, respectively.

Figure 44

Membrane Surface Concentration as COD at Various Feed Coffee Extract Concentrations and Applied TMP Under Conventional Crossflow at T = 25 °C

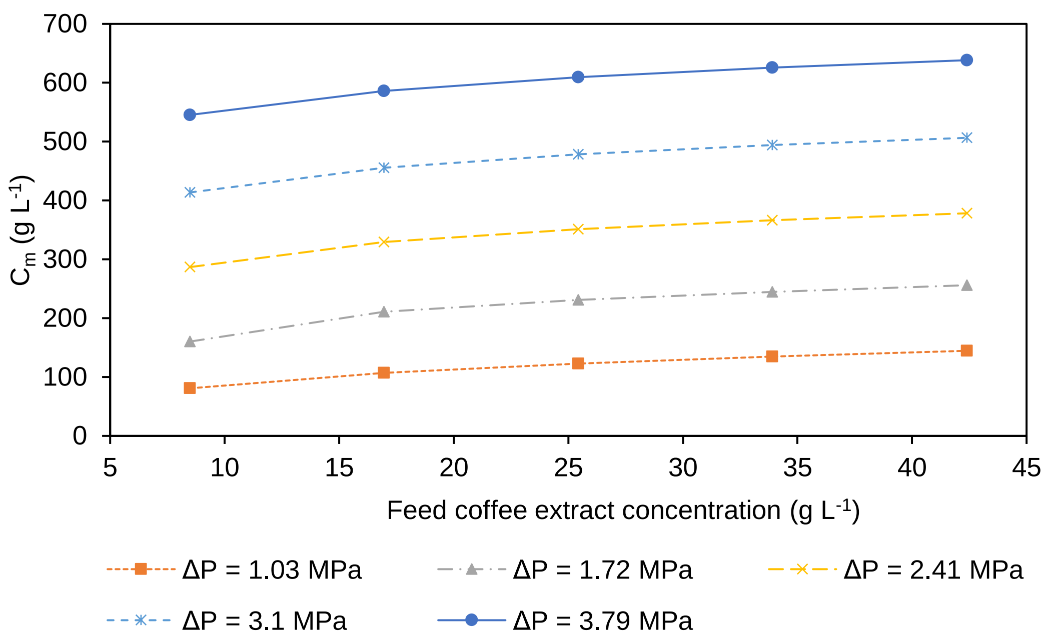

Figure 45

Membrane Surface Concentration as COD at Various Feed Coffee Extract Concentrations and Applied TMP Under Vibratory Nanofiltration at T = 25 °C

(a) $C_o = 8.5\ g\ L^{-1}$

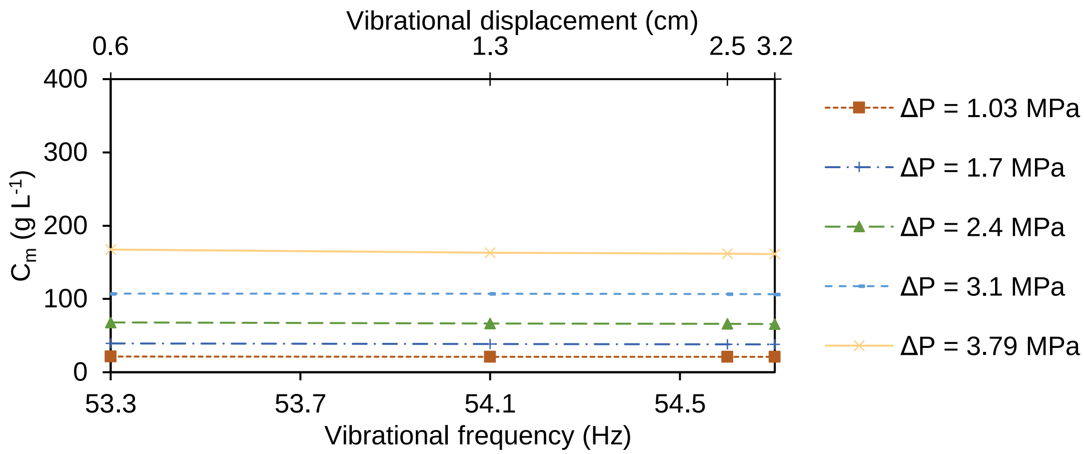

(b) $C_o = 25.4\ g\ L^{-1}$

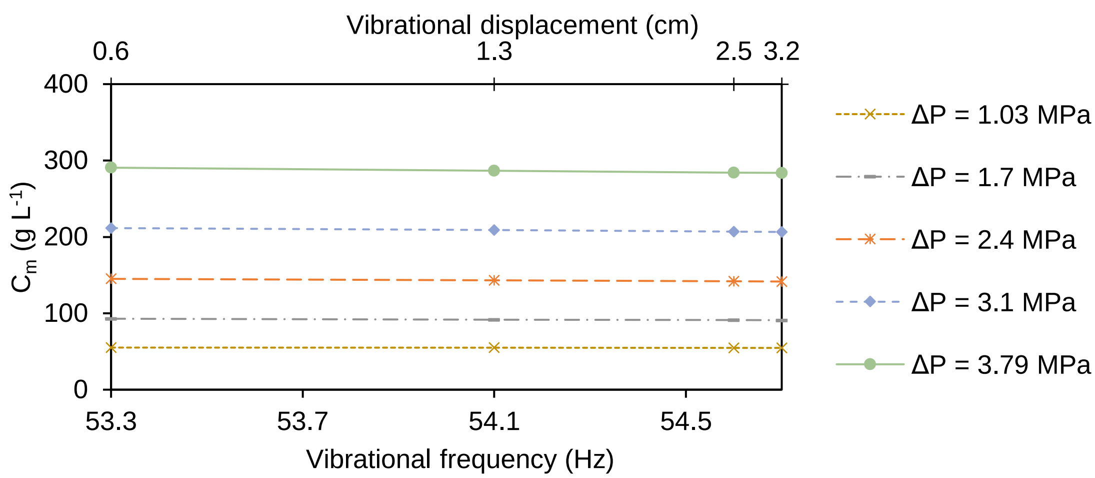

(c) $C_o = 42.4\ g\ L^{-1}$

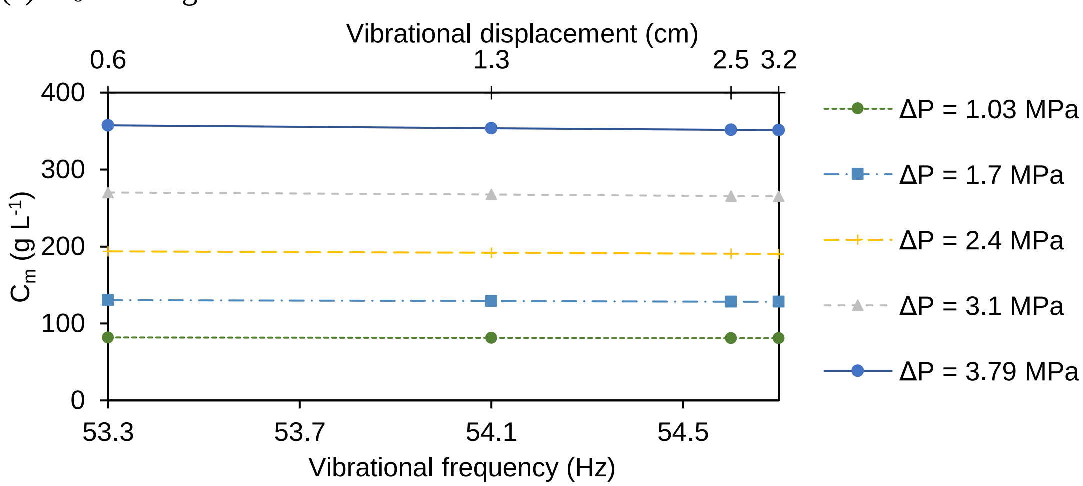

Table 27

Calculated Flow, Mass Transfer, Real Rejection Parameters, And Fouling Resistances

Operating Conditions			Model Parameters				Fouling Resistances	
TMP (Pa)	F (Hz)	d (cm)	Re	k (10^{-5} m s^{-1})	δ (10^{-5} m)	$r_{real\ COD}$	R_{OSM} (10^{14} m^{-1})	R_{CP} (10^{14} m^{-1})
C_o = 8.5 g L^{-1}								
1.03	0	0	243	0.351	11.217	0.999	1.299	0.929
	53.3	0.64	4,588	1.215	3.244	0.993	0.907	0.682
	54.1	1.27	4,657	1.231	3.201	0.994	0.906	0.615
	54.6	2.54	4,700	1.242	3.174	0.994	0.906	0.596
	54.7	3.18	4,708	1.244	3.169	0.993	0.905	0.595
2.41	0	0.0	243	0.351	11.217	0.999	1.868	1.405
	53.3	0.64	4,588	1.215	3.244	0.997	0.945	0.770
	54.1	1.27	4,657	1.231	3.201	0.997	0.941	0.470
	54.6	2.54	4,700	1.242	3.174	0.998	0.940	0.290
	54.7	3.18	4,708	1.244	3.169	0.998	0.940	0.254
3.79	0	0.0	243	0.351	11.217	0.999	2.556	2.423
	53.3	0.64	4,588	1.215	3.244	0.998	1.035	0.915
	54.1	1.27	4,657	1.231	3.201	0.998	1.028	0.661
	54.6	2.54	4,700	1.242	3.174	0.999	1.026	0.425
	54.7	3.18	4,708	1.244	3.169	0.999	1.025	0.259
C_o = 25.4 g L^{-1}								
1.03	0	0	242	0.350	11.193	0.999	1.872	1.879
	53.3	0.635	4,572	1.207	3.243	0.999	1.094	1.152
	54.1	1.27	4,640	1.224	3.200	0.999	1.094	0.582
	54.6	2.54	4,683	1.234	3.173	0.999	1.092	0.496
	54.7	3.175	4,692	1.236	3.168	0.999	1.092	0.540
2.41	0	0	242	0.350	11.193	0.999	2.624	5.943
	53.3	0.635	4,572	1.207	3.243	0.999	1.144	2.152
	54.1	1.27	4,640	1.224	3.200	0.999	1.138	1.863
	54.6	2.54	4,683	1.234	3.173	0.999	1.134	1.571
	54.7	3.175	4,692	1.236	3.168	0.999	1.133	1.286
3.79	0	0	242	0.350	11.193	0.999	3.158	7.117
	53.3	0.635	4,572	1.207	3.243	0.999	1.319	2.625
	54.1	1.27	4,640	1.224	3.200	0.999	1.312	2.306
	54.6	2.54	4,683	1.234	3.173	0.999	1.307	1.476
	54.7	3.175	4,692	1.236	3.168	0.999	1.306	1.140
C_o = 42.4 g L^{-1}								
1.03	0	0	241	0.348	11.168	0.999	2.416	5.000
	53.3	0.635	4,555	1.200	3.243	0.999	1.308	1.779
	54.1	1.27	4,623	1.216	3.199	0.999	1.304	1.774
	54.6	2.54	4,666	1.226	3.172	0.999	1.301	1.715
	54.7	3.175	4,675	1.228	3.167	0.999	1.300	1.652
2.41	0	0	241	0.348	11.168	0.999	3.403	7.938
	53.3	0.635	4,555	1.200	3.243	0.999	1.284	3.988
	54.1	1.27	4,623	1.216	3.199	0.999	1.275	3.947
	54.6	2.54	4,666	1.226	3.172	0.999	1.269	2.825
	54.7	3.175	4,675	1.228	3.167	0.999	1.268	2.178
3.79	0	0	241	0.348	11.168	0.999	4.001	11.471
	53.3	0.635	4,555	1.200	3.243	0.999	1.477	4.695
	54.1	1.27	4,623	1.216	3.199	0.999	1.464	4.585
	54.6	2.54	4,666	1.226	3.172	0.999	1.458	4.412
	54.7	3.175	4,675	1.228	3.167	0.999	1.457	4.145

The general trend shows that the membrane surface concentrations were significantly higher than the feed concentrations of the coffee extract as these concentrations represent the amount of solute accumulating at the boundary layer during the NF operation. From Figure 44, membrane surface concentrations under non-vibratory NF ranged from 80 g L^{-1} to 640 g L^{-1}, and increased with feed coffee extract concentrations and applied TMP. These concentrations were approximately 10 times higher than the feed coffee extract concentrations that consequently results in a thick boundary layer, approximately 11.2 x 10^{-5} m. Under non-vibratory CF filtration, the concentration polarization modulus (C_m/C_o) was highest (10 to 65) when feed concentrations were low at 8.5 g L^{-1}. The polarization modulus also increased with increasing applied TMP, as more organic constituents of the coffee extract were forced towards the membrane surface. On the other hand, for 42.4 g L^{-1}feed coffee extracts, the polarization modulus ranged from 3 to 13, owing to the lower boundary layer thickness calculated from the semi-empirical model. The concentration polarization region consists largely of suspended and colloidal organic solids, based on the level of turbidity and COD concentrations of the feed coffee extracts. In addition, above 99% of these suspended and colloidal solids are larger than the 150-Da cut off molecular weight of the TS80 NF membrane that are rejected effectively. However, it is also possible that the high membrane surface concentrations under non-vibratory NF can be attributed to the dissolved organics that may have precipitated out as gel layer. Collectively, the accumulation of these components on the membrane surface hinders the convection of the fluid through the membrane. On the other hand, the vibratory NF operation considerably reduced the membrane surface concentrations to magnitudes between 20 g

L^{-1} and 360 g L^{-1}, or about 60% less than those observed in CF operation, as presented in Figure 45. However, while the ideal assumption was valid when considering the relatively dilute concentrations of the coffee extracts in the bulk phase of the fluid (> 95% water), surface concentrations were considerably high that may limit the van't Hoff equation in approximating the osmotic pressure difference. Alternative calculations of this parameter to correct the potential non-ideal behavior at the membrane surface may be necessary for model improvement. On the other hand, the flow parameters under vibratory NF also improved as the Reynolds numbers were 18 times that of the non-vibratory operation, as shown in Table 27. This improvement indicates that the vibratory shear rates generated on the membrane surface overcome the viscous flow. This behavior promoted flow across the membrane as solute particles on the membrane surface are swept back to the bulk fluid region. The decrease in membrane surface concentration also thinned the boundary layer to 3.2×10^{-5} m under vibratory NF. This reduced concentration polarization region increased the mass transfer coefficient by a factor of 3.5 when compared with CF operations. Overall, based on Sherwood relationship, the vibrations promoted convection across the membrane, enhancing the permeate flux by up to 2 or 3 times that of the non-vibratory operation.

In both filtration modes, membrane surface concentrations increased with the applied TMP and feed solute concentration and decreased with module vibrations and shear. Further, feed solute concentrations showed the highest contribution to membrane surface concentration that impart osmotic pressure effects or back diffusion among the three operating factors. In addition, the viscous flow becomes more pronounced in higher strength coffee extracts, thus limiting the membrane surface shear rates in both CF and vibratory NF modes. On the other hand, while higher TMP allows the convection of solvent across the membrane, the solute components forced near the membrane surface accumulate and result in higher back-diffusion. This back-diffusion lowers the effective TMPs and permeate fluxes across the membrane. The contribution of vibration to flux enhancement was observable especially for low strength coffee extracts, as were shown earlier in Chapter 5 (Figure 30). However, while this is true when comparing between vibratory and non-vibratory NF operations, flux enhancement was only gradual within the range of vibration settings (53.3 Hz to 54.7 Hz) employed in the filtration experiments. Figure 45 also shows that membrane surface concentrations only slightly decreased with increasing vibration compared with the changes contributed by the TMP and feed solute concentration. This trend indicates that among the three operating conditions, module vibration had the least relative impact on the permeate flux of the vibratory system. As will be shown in Chapter 7, these observations agree with the statistical correlations presented by Laurio et al. [181], where the coefficients from multivariate regression analysis were used to quantify the relative impacts of feed concentration, applied TMP, and vibratory frequency. Accordingly, feed coffee extract concentrations limit the permeate fluxes from the vibratory NF operation by about 6 times the flux enhancement contributed by the module vibrations. The relative effect of vibrations on membrane surface concentrations may be due extent of vibratory frequencies considered for the study. The variation of vibratory frequencies between 53.3 Hz and 54.7 Hz only corresponded to a relative change of only 2.6%, despite the observed vibratory displacement from 0.64 cm to 3.18 cm. This small variation may have limited the changes in membrane surface concentrations. Unfortunately, these module vibrations are only limited within this range that filtration operations below or above the frequency range may damage the mechanical parts of the equipment. Thus, while higher vibratory frequencies may further reduce the membrane surface concentration, the operational constraint of the vibratory membrane system limits the process from doing so. Despite this limitation, the vibrations of the membrane module generated an appreciable amount of shear on the membrane surface that alleviated membrane fouling and flux decline. This presents favorable cost reduction in comparison to CF operation.

6.4.2 *Rejection Efficiency and Permeate Quality*

The calculated real rejection parameter was higher than the observed rejection, considering that the membrane surface concentrations in all operations were significantly above the bulk concentrations of the coffee extract, due to the extent of concentration polarization occurring. As shown in Table 27, real COD rejection efficiencies ($r_{real\ COD}$) were above 0.99, and did not varying significantly with operating conditions. This observation was due to the considerably high membrane surface concentrations obtained from CF and vibratory NF operations, relative to the permeate COD concentrations shown in Figure 46.

Figure 46

Predicted and Experimental Permeate COD Concentrations Under Different Feed Coffee Extract Concentrations, TMP, and Vibrational Settings at T = 25 °C

(a) $C_o = 8.5$ g L^{-1}

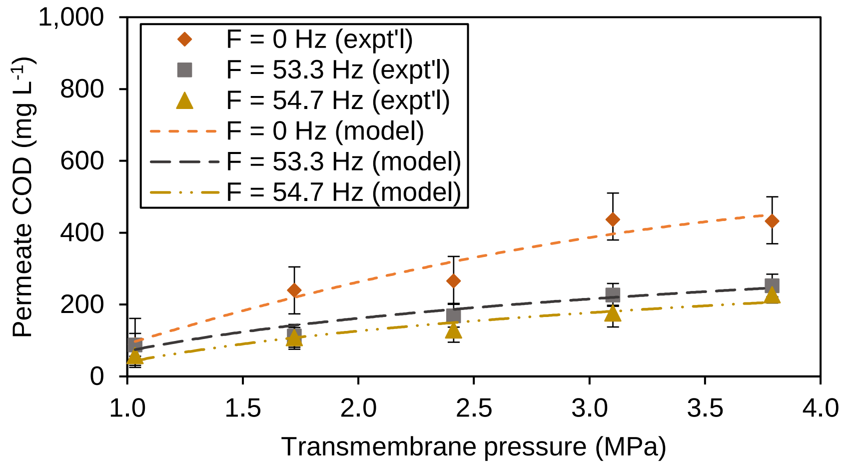

(b) $C_o = 25.4$ g L^{-1}

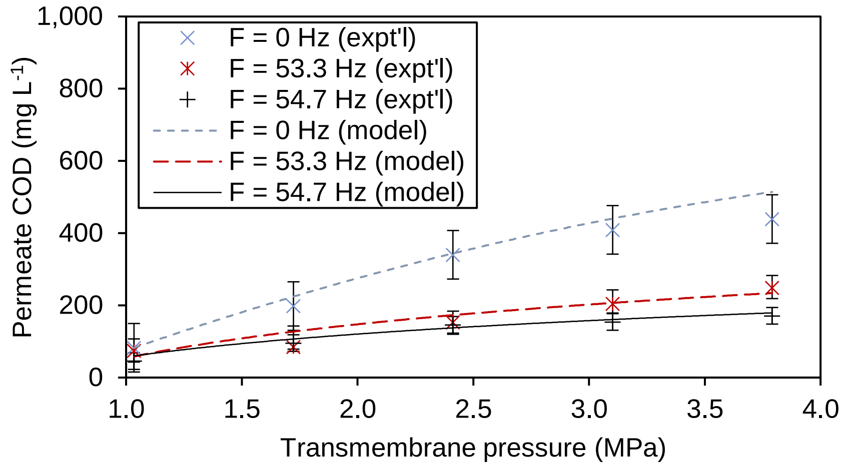

(c) $C_o = 42.4$ g L^{-1}

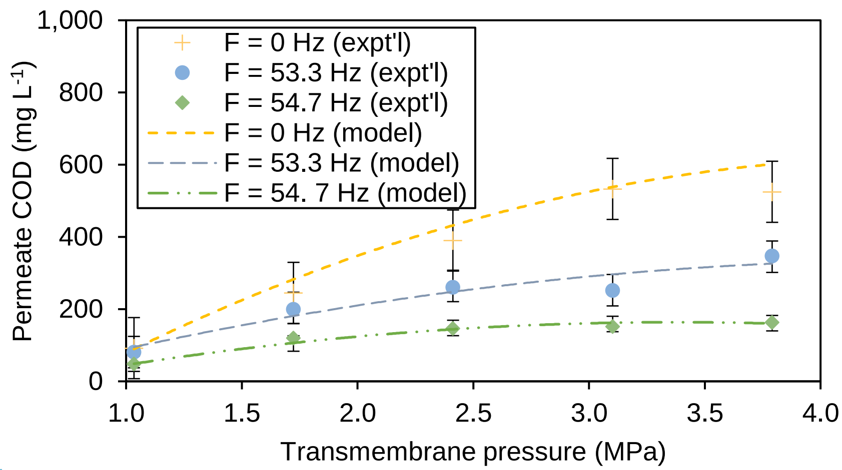

Despite the invariance of real COD rejection, the variation of permeate COD concentrations at various filtration conditions was noticeable. In addition, the permeate COD was higher under non-vibratory CF operation than those obtained from vibratory NF. At an applied TMP of 3.79 MPa, an 8.5 g L^{-1} coffee extract processed under CF filtration also rendered permeate with COD concentration that is approximately 1.7 times higher than those generated from vibratory NF operations. Higher-strength coffee extracts also rendered slightly higher COD concentrations in the permeate for vibratory NF operation. The increase in permeate COD with feed concentration was more pronounced under CF filtration mode. Fundamentally, the concentration gradient across the membrane, i.e., the difference between the amount of solute present on the membrane feed surface and that of the permeate, serves as the driving force for solute transfer [165]. Thus, low shear membrane operations like the CF operation result in lower permeate quality due to higher concentration polarization. Similarly, because of the variation of membrane surface concentrations, higher TMP and feed coffee extract concentrations tend to increase the permeate COD concentrations, while vibratory shear reduced them. However, since membrane surface concentrations provide additional resistance to the transfer of solute across the NF membrane, only minimal increase in permeate COD concentrations was observed despite increasing the concentrations. For NF membranes this additional resistance arises from hindered solute transport due to steric hindrance or pore blocking, and by charge exclusion [173]. Larger solutes also add to this resistance, in this case, those of the colloidal and suspended solids that represented a large fraction of the coffee extract components retained by the NF membrane.

The assessment of the quality of the permeate generated by the vibratory NF operation is important, especially for scale-up membrane operations where the permeate recovered is intended for reuse. Mathematical models, such as that developed in this study, serve as a useful tool in managing permeate quality by lessening membrane fouling in vibratory NF operation. For a scale-up study, the model may also be used to estimate the instantaneous permeate quality in a modified concentration study [14], [33], [56]. Average permeate concentrations may be determined as a function of water recovery from the vibratory NF of coffee extract. The projected average concentrations can then be compared with water reclamation guidelines for reuse. However, it should be noted that this study only focused on COD concentrations in mathematically modeling the impacts of the operating conditions on membrane surface and permeate concentrations. Concentrations for turbidity and conductivity may still need to be standardized against mass-per-volume basis to make them applicable in the model. While the gravimetric approach may be used to delineate the suspended and dissolved solids concentrations, more straightforward standard analytical methods such as those used in this study or useful correlation would be recommended since colloidal constituents may have overlapping definitions as both suspended and dissolved in nature. Despite this limitation, the trends with permeate COD concentrations corresponded with those observed in permeate conductivities, as presented in Table 28.

Table 28

Permeate Characteristics and Corresponding Observed Rejection Efficiencies at Various Operating Conditions

Operating Conditions			Permeate Characteristics				Observed Rejection			
TMP (MPa)	F (Hz)	d (cm)	Conductivity (μS/cm)	Turbidity (NTU)	Absorbance	COD (mg/L)	$r_{o\ cond}$	$r_{o\ turb}$	$r_{o\ abs}$	$r_{o\ COD}$
					C_o = 8.5 g/L					
1.03	0	0.00	94.4 ± 1.4	0.102 ± 0.004	0	90 ± 1.4	0.861 ± 0.0010	1.0	1.0	0.989 ± 0.0003
	53.3	0.64	86.9 ± 0.4	0.103 ± 0.028	0	88 ± 1.9	0.923 ± 0.0004	1.0	1.0	0.990 ± 0.0005
	54.7	3.18	48.7 ± 0.2	0.092 ± 0.021	0	59 ± 2.1	0.877 ± 0.0002	1.0	1.0	0.993 ± 0.0004
2.41	0	0.00	233.5 ± 0.2	0.127 ± 0.003	0	267 ± 1.8	0.793 ± 0.0002	1.0	1.0	0.968 ± 0.0002
	53.3	0.64	205.0 ± 0.6	0.193 ± 0.020	0	169 ± 3.2	0.848 ± 0.0005	1.0	1.0	0.980 ± 0.0004
	54.7	3.18	132.9 ± 2.1	0.135 ± 0.005	0	130 ± 1.1	0.882 ± 0.0020	1.0	1.0	0.985 ± 0.0001
3.79	0	0.00	627.5 ± 3.9	0.169 ± 0.044	0	433 ± 6.4	0.443 ± 0.0035	1.0	1.0	0.949 ± 0.0008
	53.3	0.64	358.5 ± 1.2	0.214 ± 0.004	0	253 ± 0.7	0.682 ± 0.0011	1.0	1.0	0.970 ± 0.0001
	54.7	3.18	315.0 ± 0.1	0.110 ± 0.012	0	228 ± 4.1	0.720 ± 0.0001	1.0	1.0	0.973 ± 0.0010
					C_o = 25.4 g/L					
1.03	0	0.00	93.6 ± 4.7	0.099 ± 0.021	0	83 ± 1.3	0.983 ± 0.0018	1.0	1.0	0.997 ± 0.0001
	53.3	0.64	76.7 ± 1.1	0.193 ± 0.006	0	74 ± 3.4	0.971 ± 0.0004	1.0	1.0	0.997 ± 0.0001
	54.7	3.18	13.2 ± 3.1	0.070 ± 0.024	0	46 ± 1.3	0.995 ± 0.0012	1.0	1.0	0.998 ± 0.0001
2.41	0	0.00	197.5 ± 4.6	0.175 ± 0.013	0	240 ± 3.5	0.925 ± 0.0017	1.0	1.0	0.992 ± 0.0001
	53.3	0.64	190.5 ± 2.7	0.157 ± 0.018	0	153 ± 2.8	0.927 ± 0.0010	1.0	1.0	0.995 ± 0.0001
	54.7	3.18	120.1 ± 3.1	0.064 ± 0.010	0	146 ± 6.0	0.954 ± 0.0012	1.0	1.0	0.995 ± 0.0002
3.79	0	0.00	612.0 ± 2.4	0.135 ± 0.008	0	439 ± 2.5	0.767 ± 0.0009	1.0	1.0	0.985 ± 0.0001
	53.3	0.64	371.5 ± 1.0	0.314 ± 0.039	0	249 ± 1.3	0.858 ± 0.0004	1.0	1.0	0.991 ± 0.0001
	54.7	3.18	264.5 ± 0.9	0.204 ± 0.010	0	171 ± 7.4	0.899 ± 0.0003	1.0	1.0	0.994 ± 0.0003
					C_o = 42.4 g/L					
1.03	0	0.00	93.8 ± 2.5	0.135 ± 0.022	0	94 ± 3.5	0.989 ± 0.0007	1.0	1.0	0.998 ± 0.0001
	53.3	0.64	74.6 ± 3.0	0.201 ± 0.051	0	81 ± 2.0	0.981 ± 0.0008	1.0	1.0	0.998 ± 0.0000
	54.7	3.18	14.8 ± 4.9	0.079 ± 0.021	0	49 ± 2.5	0.996 ± 0.0013	1.0	1.0	0.999 ± 0.0001
2.41	0	0.00	352.0 ± 3.5	0.215 ± 0.006	0	350 ± 4.9	0.908 ± 0.0009	1.0	1.0	0.993 ± 0.0001
	53.3	0.64	262.0 ± 1.5	0.179 ± 0.005	0	261 ± 6.3	0.932 ± 0.0004	1.0	1.0	0.995 ± 0.0001
	54.7	3.18	119.6 ± 3.1	0.070 ± 0.017	0	147 ± 1.3	0.969 ± 0.0008	1.0	1.0	0.997 ± 0.0000
3.79	0	0.00	658.5 ± 1.2	0.651 ± 0.012	0	498 ± 1.4	0.829 ± 0.0003	1.0	1.0	0.990 ± 0.0000
	53.3	0.64	422.5 ± 1.2	0.450 ± 0.024	0	348 ± 5.7	0.890 ± 0.0003	1.0	1.0	0.993 ± 0.0001

The observations indicated that dissolved organic and inorganic components smaller than 150 Da (or with molecular weights lower than 150 g mol^{-1}) were transferred through the NF membrane along with the solvent, in this case, water. On the other hand, the permeate turbidities were significantly low and were found to be invariant with the operating conditions, owing to the high efficiency of the NF membrane to reject colloidal and suspended solids from the simulated coffee extract. Thus, the effects of feed solute concentrations, TMP, and vibrations on permeate COD concentrations may be used in interpreting the experimental permeate conductivities from the NF operation.

Experimental and theoretical permeate organic concentrations (in terms of COD) were also found have an average deviation of 15%, as shown in Figure 47. This is satisfactory, as the fluctuations arising from the measurement of permeate concentrations, in residual amounts, cannot be ruled out. These fluctuations tend to increase as concentrations become significantly low or when there is residual COD in the permeate (< 300 mg L^{-1}). Nonetheless, the average deviation still shows that experimental and theoretical permeate COD concentrations are in reasonable agreement, and that the mathematical model may be used in estimating the permeate quality from the vibratory NF operation.

Figure 47

Comparison of Model and Experimental Permeate COD Concentrations from Vibratory and Non-vibratory Nanofiltration Operations

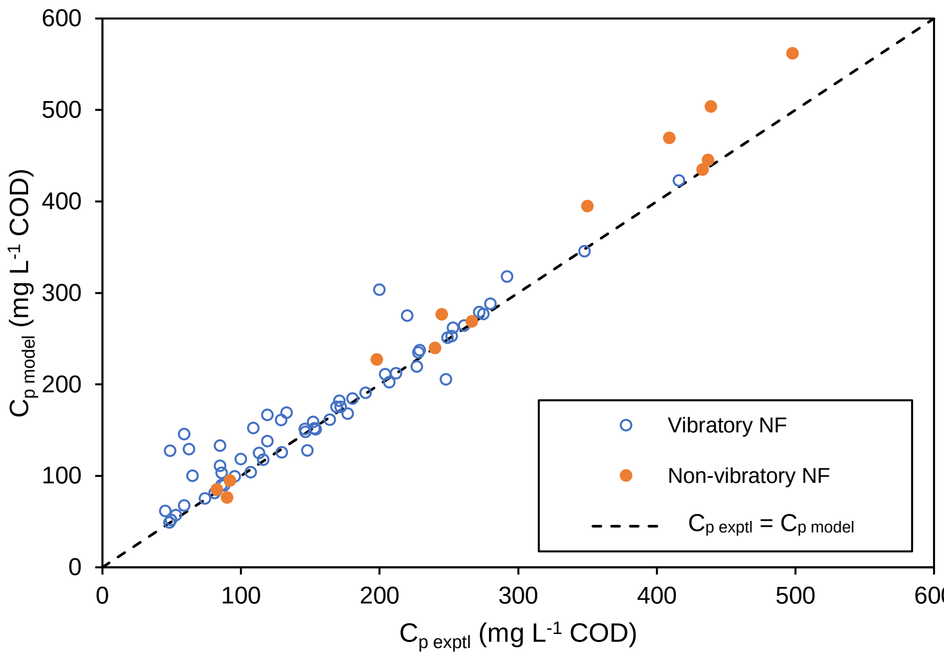

Overall, the TS80 NF membrane was highly effective in rejecting coffee extract components in both CF and vibratory NF operations, as was presented in Table 28. Moreover, the vibratory NF operation can render not only better permeate fluxes, but also permeate quality that present greater opportunities for reusability. Nearly complete rejections of turbidity and absorbance were observed, leaving a clear permeate that resembled water (shown in Chapter 5, Figure 37) with significantly low turbidity (< 1 NTU) and absorbance of 0. These observations show that the NF membrane was practically capable of rejecting the colloidal, suspended solids and colored compounds present in the coffee extract. This high rejection also corresponded to observed COD rejection efficiencies above 0.95 (or 95%) indicating that the majority of the organic components rejected during the NF operation were colloidal and suspended solids larger than the cut-off pore size of the TS80 NF membrane (~150 Da). On the other hand, the components that passed through the membrane were dissolved organics and salts that affected the conductivity of the permeate. The partial rejection of dissolved components, especially of monovalent salts, is typical in NF membranes given that their pore size is relatively larger than those of RO membranes [94]. As a result, permeate conductivities between 15 $\mu S\ cm^{-1}$ to 660 $\mu S\ cm^{-1}$ with corresponding COD concentrations ranging from 46 $mg\ L^{-1}$ to 498 $mg\ L^{-1}$ were observed depending on the operating conditions. Despite the partial rejection of dissolved components, the NF membrane is still preferred for coffee extract preconcentration since the permeate recovered from the operation is not intended for human consumption, but only for reuse in ancillary plant operation. The high organics rejection of the TS80 membrane allows water recovery with minimal treatment and cost required before reuse. When scaled-up, the permeate from the vibratory NF can be considered for reuse specifications required for cooling towers, feed water for boilers, or as an extractant in percolation columns [139].

6.4.3 *Fouling Resistances*

The fouling of the NF membrane in both vibratory and non-vibratory filtration has been identified as the primary limitation that can result in significant performance reductions over time. Foulants limit membrane filtration performance by either adhering in the internal pore structure of the membrane, or depositing directly on the membrane surface by adsorption, or gel formation. The foulants also result in pore-blocking that decreases the permeate flux of the operation, and if not properly managed, membrane fouling can be irreversible. By using the resistance-in-series model (Equation 18), various resistances were identified to characterize the effect of fouling on mass transfer across the NF membrane. Water tests were conducted to determine the membrane resistance (R_m) equivalent to 8.2 x 10^{10} m^{-1} based on the water permeability (A_w = 4.48 x 10^{-11} L m^{-2} h^{-1} Pa^{-1}) of the membrane and the absolute viscosity of water. Surface fouling resistances (R_f) were also calculated as distinct to the membrane resistance using Equation 82.

$$R_f = \frac{\Delta P}{\mu\, J_v} - R_m \tag{82}$$

The calculated fouling resistances were plotted against vibrational displacement and frequencies for various applied TMPs and feed coffee extract concentrations, as shown in Figure 48. The local shear rates on the membrane surface reflected its role in mitigating or reducing membrane fouling during the preconcentration of coffee extracts. The dynamic vibratory operation significantly reduced the fouling resistance to at least half of those observed in conventional CF filtration. Fouling resistance also increased with increasing feed solute concentration, and TMP, the highest among which was that observed at CF operation (F = 0 Hz, d = 0 cm), 3.79 MPa, and for the 42.4 g L^{-1} feed coffee extract. However, the fouling resistance remained unchanged within the vibratory mode, between 53.3 Hz and 54.7 Hz at displacements between 0.64 cm and 3.18 cm. These trends indicate the effect of operating conditions on the concentration polarization and boundary layer osmotic pressure occurring in both filtration modes that influence the permeate flux. Feed concentrations and TMPs caused high membrane surface concentrations. The highly concentration polarized region consequently added to the total resistance, reducing permeate fluxes, likewise, solute flow through the membrane.

Figure 48

Fouling Resistances Under Different Feed Coffee Extract Concentrations, Applied TMP, and Vibrational Settings at T = 25 °C

(a) $C_o = 8.5$ g L^{-1}

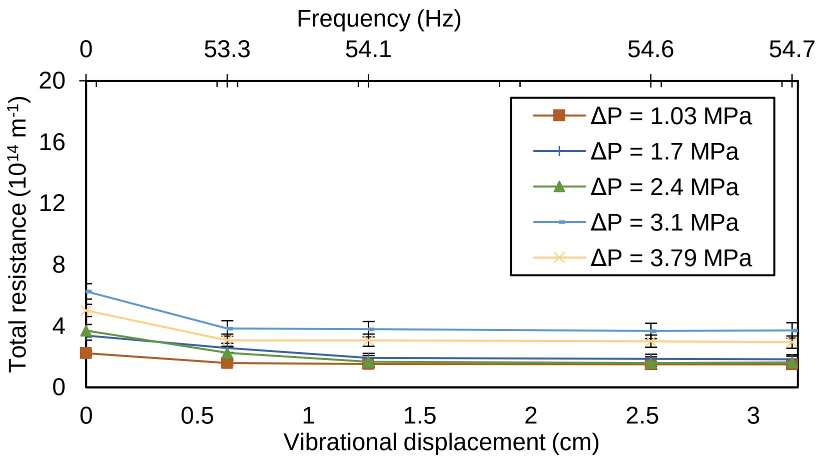

(b) $C_o = 25.4$ g L^{-1}

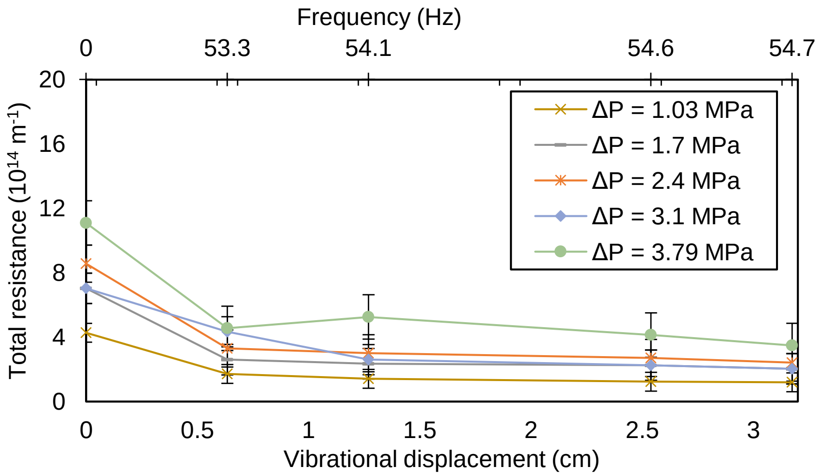

(c) $C_o = 42.4$ g L^{-1}

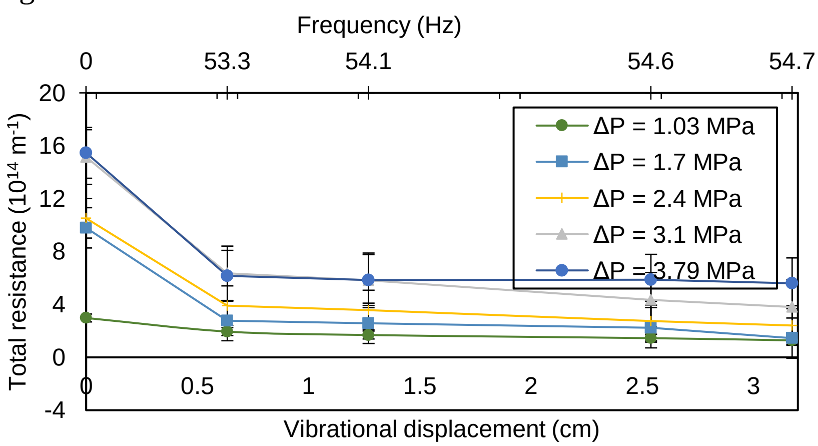

Membrane surface concentrations in the vibratory NF operation, at this point of the study, have been related as a function of TMP, feed solute concentration, and vibration. In particular, the osmotic pressure model and concentration polarization model correlated the effects of TMP and feed solute concentration, respectively, while the impact of vibratory frequency and displacement was modeled with the Sherwood relationship. However, only osmotic-pressure-driven permeate fluxes were determined, and adjustments were considered in the model equation by the inclusion of the concentration polarization resistance. Using Equation 81, the surface fouling resistances were characterized in terms of those attributed to the osmotic pressure on the membrane surface (R_{osm}), and those attributed to concentration polarization (R_{cp}). From Table 27, the fouling resistance resulting from the osmotic pressure on the membrane surface limited the permeate fluxes when the feed solute concentration was at 8.5 g L^{-1}. However, concentration polarization resistances start to overcome osmotic pressure resistances when feed solute concentrations were above 25.4 g L^{-1}. Similarly, these resistances increased with the TMP and feed solute concentrations as these conditions favored higher polarization and membrane surface concentrations. Further, vibration slightly reduced the osmotic pressure and concentration polarization resistances within the selected vibration intensities.

In Figure 49, non-vibratory CF operations rendered total flow resistance amounting from 2.2 x 10^{14} m^{-1} up to 15.5 x 10^{14} m^{-1}, while total flow resistance reduced to about half of the CF resistances under vibratory NF, from 1.2 x 10^{14} m^{-1} to 6.4 x 10^{14} m^{-1}, as shown in Figure 50. In both plots, the type of fouling resistance also varied depending on the total flow resistance affected by the operating conditions. Under CF operation, osmotic pressure resistances were less sensitive to the total resistance varying only between 1.3 x 10^{14} m^{-1} to 4.0 x 10^{14} m^{-1}, while concentration polarization resistances varied greatly from 4.2 x 10^{13} m^{-1} to as high as 11.5 x 10^{14} m^{-1}. The same behavior was observed in vibratory NF where osmotic pressure resistances only varied from 9.4 x 10^{13} m^{-1} to 4.0 x 10^{-14}, and concentration polarization resistances varied from 2.9 x 10^{13} m^{-1} to 5.0 x 10^{14} m^{-1}. The plots also show that flow resistances develop from an osmotic-pressure controlled operation to a concentration-polarization controlled operation as more solutes accumulate on or near the membrane surface. Concentration polarization starts to influence the non-vibratory NF fluxes when flow resistances exceed 4.0 x 10^{14} m^{-1}, while for vibratory NF, this behavior was observed when flow resistances exceeded 2.3 x 10^{14} m^{-1}.

Figure 49

Comparison of Fouling Resistances Under Vibratory NF Operation

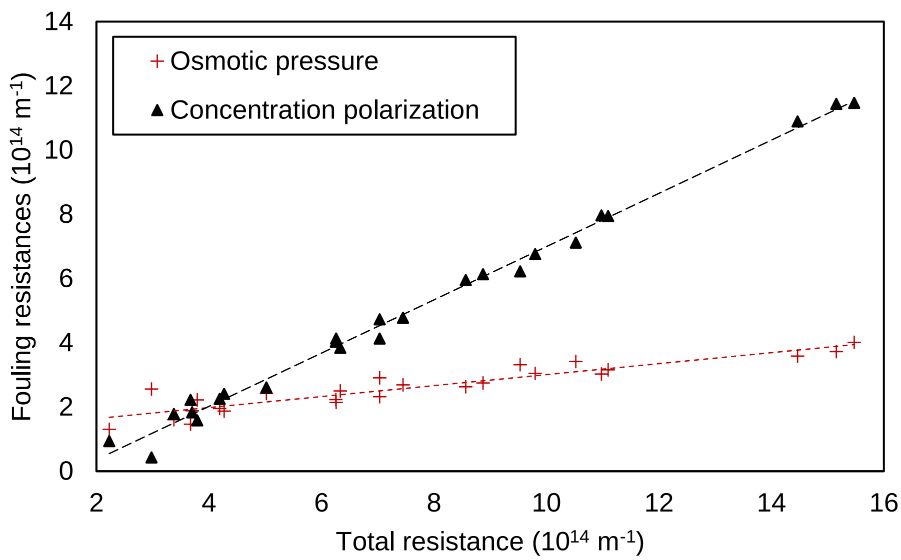

Figure 50

Comparison of Fouling Resistances Under Crossflow NF Operation

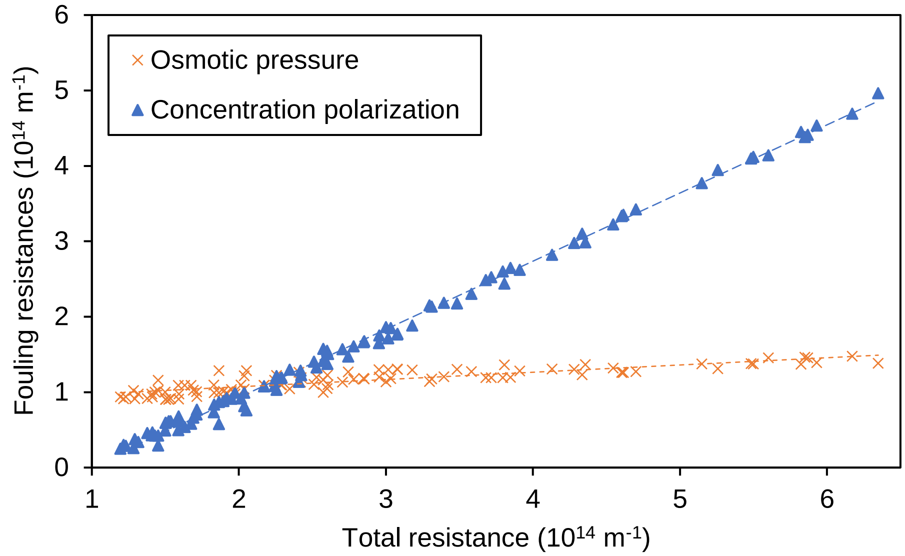

The concentration polarization resistance was also found to vary with the TMP, feed solute concentration, and vibratory shear according to Equation 83.

$$R_{CP} = 10.403\ \Delta P^{0.485} C_o^{\ 1.103} \gamma_{w\ max}^{\ \ -0.481} \tag{83}$$

The values of the parameters were obtained by multiple log-linear regression method (α = 10.403, n_1 = 0.485, n_2 = 1.103, n_3 = -0.481). The exponential parameters, n_1, n_2, and n_3, associate the relative effects of the operating conditions with the concentration polarization resistance that were also found to correspond with those observed in membrane surface concentrations. Based on the exponent parameters, feed solute concentration has the highest positive effect (n_2 = 1.103) on the concentration polarization resistance. The applied TMP also has a positive effect (n_1 = 0.485) on concentration polarization resistances at it influences the convection of the retained solutes towards the membrane surface. On the other hand, vibratory surface shear rates decreased the concentration polarization resistances as indicated by the negative sign of the exponent (n_3 = -0.481).

The correlation coefficient of the log-linear regression was 0.85, which was a satisfactory index for predicting concentration polarization resistances. Experimental and model permeate fluxes presented in Figure 51 were also found to be in reasonable agreement, indicating the reliability of the mathematical model in predicting and minimizing membrane fouling conditions. However, despite the reasonable agreement between model and experimental fluxes, further investigation of other membrane filtration models is still necessary. Developing two distinct models for vibratory and CF filtration modes may be recommended to improve the model parameters for better predictability. In addition, it is also recommended to develop a model for concentration polarization resistances from a more analytical perspective. Hydrodynamic analysis combined with a more specific retention mechanism based on analytically or numerically solving the boundary conditions of momentum and solute mass transport in the NF membrane may also be explored to circumvent the limitations of the model. However, as will be discussed in the succeeding sections, the complexities of our particular membrane module system will likely challenge further applicability of theoretical modeling methodologies. Additional parameters may be needed.

Figure 51

Comparison of Model and Experimental Permeate Fluxes from Vibratory and Non-Vibratory Nanofiltration Operation

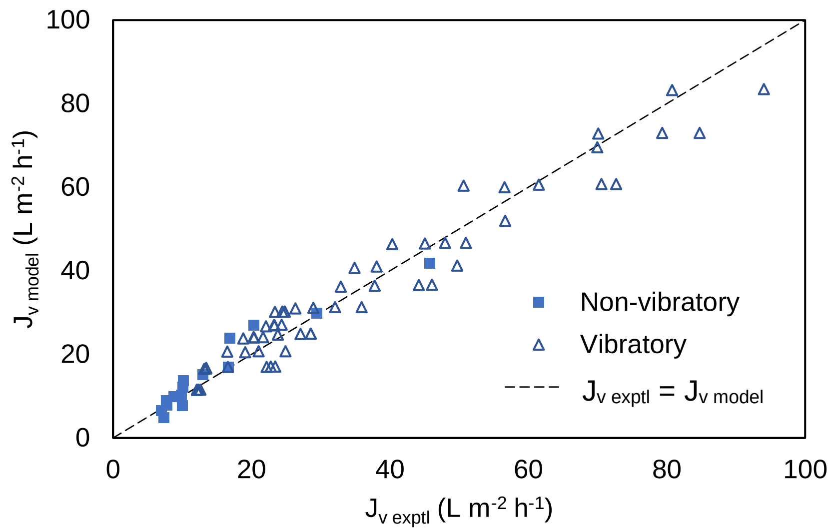

Lastly, despite its effect, vibratory shear influence in reducing concentration polarization and related fouling resistance was the least among the three operating conditions. Also, the added positive impacts of feed concentration and applied TMP on concentration polarization resistances only diminishes the extent of flux enhancement under the vibratory NF mode for frequencies between 53.3 Hz and 54.7 Hz. This observation presents a limitation of the vibratory NF operation that may be considered when optimizing the process for scale-up. In Chapter 8, in a parallel coffee extract preconcentration scale-up study, we also presented that despite the contribution of vibration, the operation may only be applied in concentrating coffee extracts to 35% wt/wt. This preconcentration limit was also observed in CF NF studies conducted by Pan et al. [32], thus, emphasizing that higher bulk solution solute concentrations increase the concentration of the membrane foulants found in coffee extracts, which in turn, limits the operation. Nonetheless, despite the small changes, the appreciable permeate flux enhancement and minimization of flux decline confirms the capability of the dynamic vibratory membrane system in managing membrane fouling, in food processing systems such as those studied herein.

Chapter 7

Optimization of Vibratory Nanofiltration of Coffee Extracts via Response Surface Methodology

Some texts and figures were reproduced and adapted with permission from M. V. O. Laurio, K. M. Yenkie, and C. S. Slater, "Optimization of vibratory nanofiltration for sustainable coffee extract concentration via response surface methodology", *Separation Science & Technology*, 2021, doi:10.1080/01496395.2021.1879858 [181]

Additional graphs and tabular data of the results for this chapter are presented in Appendix D. The results presented herein are those essential to summarize the studies necessary for this dissertation's discussion.

7.1 Introduction

Concentration polarization and membrane fouling are complex phenomena affecting almost all membrane processes to various degrees. While certain techniques such as dynamic shear generation, as with the vibratory membrane system used in this study, are available to reduce flux decline in crossflow filtration, some membrane fouling is still inevitable, as was observed in Chapter 6. Over the years, researchers have made efforts to develop models for the prediction of membrane performance. Most studies used a system of equations from semi-empirical models [35]. These models are similar to the resistance-in-series model developed in Chapter 6 from the combined osmotic pressure and film layer models. On the other hand, few attempted to analytically or numerically solve the hydrodynamic and solute mass transport analyses at the boundary conditions of the membrane [182]. However, despite the fact that these orthogonal approaches for membrane performance evaluation remain most fundamental, simplifications and assumptions make the models limited for extensive practical applications [35]. Detailed parametric studies also require extensive experimentation, making these methods time-intensive and less productive [170]. Likewise, analytical solutions could also challenge design perspectives due to inherent complexities and rigorous computational requirements. As in this study, the unique dynamic nature of the technology likely presents challenges in using these conventional approaches, and no universally accepted method is currently available to fully understand and predict the performance of dynamic membrane separation. Thus, while the resistance-in-series model in Chapter 6 provides a basis for predicting vibratory NF performance, incorporation of more process parameters, e.g., solution properties, operating conditions, etc., and further studies are still necessary for more extensive applications.

Among the alternative approaches for parametric evaluation and optimization of several processes are those employed with the aid of statistical analysis. This method involves factorial design for parametric studies; while for optimization studies, mixture design (MD) and response surface methodology (RSM) are employed [143]. Among the two optimization methods, RSM was employed in this study. Accordingly, experimental data is fitted to a polynomial equation, as presented by Equation 84.

$$Y = \beta_o + \sum \beta_i X_i + \sum \beta_{ij} X_i X_j + \sum \beta_{ii} X_i^2 + \cdots \tag{84}$$

From the equation, Y is the predicted response used as a dependent variable, β_o is the constant coefficient of the model, and β_i, β_{ij}, and β_{ii} represent coefficients for linear, interaction, and quadratic effects of the model, respectively. These coefficients are estimated by multiple regression analysis, in which the fitting quality of the polynomial model equation is mainly expressed by the regression coefficient, R^2. Other statistical tests such as analysis of variance, lack of fit tests, and other diagnostics are also used to improve the experimental models. The mathematical models can then be used to predict and optimize a wide array of process performance including yields, flow rates, energy consumption, and even economic indices [183].

Overall, the statistical methods are useful tools for a wide variety of applications involving the correlation of operating factors against process responses, primarily intended for optimization. Due to its simplicity, the optimization method has been investigated on wastewater treatment [184]–[192], membrane fabrication [193]–[195], membrane cleaning [114], and in pharmaceutical [196] and water desalination applications [197], as well. In food and beverage production, several membrane processes were optimized for the recovery of food derivatives such as phenolic compounds [198]–[200], solvent recovery from soybean isoflavone [201], astragalus extraction [202], and clarification of orange press liquor [203].

However, among dynamic filtration systems, the application of RSM has only been explored for rotary disk filtration for protein recovery from alfalfa wastewater, [170] and inulin recovery from chicory juice, [204] and none on vibratory shear-enhanced filtration systems. While both dynamic systems impart high shear rates from the movement of membrane modules, the operating conditions that induce the shear regions differ. Rotary disk systems impart high shear rates on membrane surface from a disk mounted on a shaft that rotates at a certain rotational speed. On the other hand, vibratory filtration systems such as that investigated in this study generate shear fields from the oscillatory movement of the membrane module at a given frequency. In this study, the vibratory NF was optimized for the concentration of reconstituted coffee extracts as an alternative to thermal evaporation before spray drying. Four types of NF membranes were screened in terms of their characteristics and performance in water tests and coffee extract filtration experiments. The extent of flux and rejection improvement in the vibratory NF operation was also compared with CF filtration. Mathematical models were developed to correlate the effects of TMP, feed solute concentration, vibrational frequency and their corresponding interactions influencing permeate flux and concentrations, rejection efficiencies using RSM. Lastly, these mathematical models were used to optimize vibratory NF operation.

7.2 Experimental Approach

7.2.1 *Experimental Design*

7.2.1.1. Full-Factorial Experimental Design. Initially, the performance of CF and VSEP nanofiltration runs were compared. A two-level (2^3) full-factorial experimental design was employed to screen the operating factors and responses that were further evaluated in response surface experiments. Three factors with two treatment levels were investigated. These include feed coffee extract concentration (8.48 g L^{-1} and 40.88 g L^{-1}), applied TMP (1.03 MPa and 3.79 MPa), and vibratory frequency (0 Hz and 54.7 Hz) that were evaluated in duplicate. The full-factorial experimental design is shown in Table 29.

Table 29

Two-level Full Factorial Experimental Design

Factor A	Factor B	Factor C	
Feed Concentration	Applied TMP	Vibratory Frequency	Vibratory Displacement
($g\ L^{-1}$)	(MPa)	(Hz)	(cm)
8.48	1.03	0	0
8.48	1.03	54.7	3.18
8.48	3.79	0	0
8.48	3.79	54.7	3.18
42.4	1.03	0	0
42.4	1.03	54.7	3.18
42.4	3.79	0	0
42.4	3.79	54.7	3.18

The effects of the operating factors on membrane filtration performance were compared between CF and vibratory NF operations. Among the responses assessed for this comparison include permeate flux, permeate characteristics, corresponding rejection efficiencies, and the degrees of flux decline. The experimental fluxes were also fitted according to the power law model, shown in Equation 30, to estimate the corresponding initial fluxes (J_o) and flux decay rates (b) at specific operating conditions. These empirical parameters served as the basis for calculating the degree of flux decline after 60 minutes of filtration using Equation 31.

$$J_v = J_o\ t^{-b} \tag{30}$$

$$\text{Flux decline} = \frac{J_o - J_v}{J_o} \times 100 \tag{31}$$

7.2.1.2. Response Surface Experimental Design. Response surface experiments were conducted to optimize vibratory NF operation in terms of the abovementioned factors. For this set of experiments, the Box-Behnken experimental design was used. This experimental design is commonly applied to obtain regression models of the second order. It is an independent, rotatable quadratic design with no embedded factorial or fractional factorial points [143]. The design space or variable combinations for this method include the midpoints of the edges, and a central point, as shown in Figure 52.

Figure 52

Box-Behnken Experimental Design Space

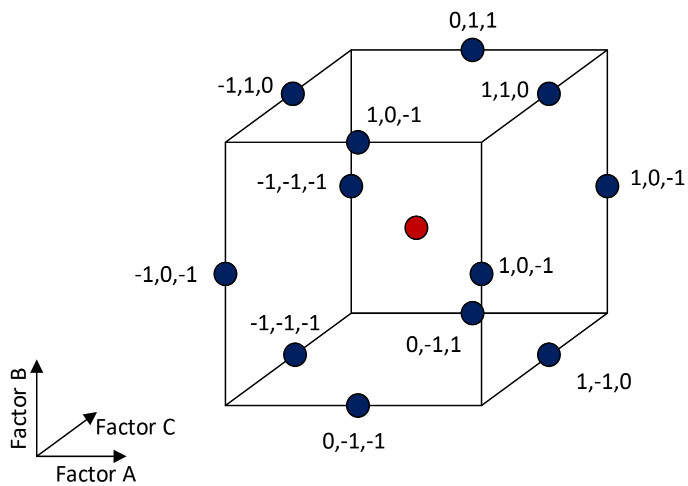

Note: Adapted from https://develve.net/Box-Behnken%20design.html

Each factor is designated to three levels high (+1), mid (0), and low (-1) treatment levels or conditions in combination with the other factors in the design space. For the vibratory NF experiments the high and low treatment levels were 8.5 g L^{-1} and 42.4 g L^{-1} for feed concentration; 1.03 MPa and 3.79 MPa for applied TMP; and 53.3 Hz (d = 0.64

cm) and 54.7 Hz (d = 3.18 cm) for vibratory frequencies. For these conditions, the experimental design consisted of 17 runs were assigned, as shown in Table 30.

Table 30

Box-Behnken Response Surface Experimental Design

Run	Factors: Factor A Feed Concentration (g L^{-1})	Factor B Applied TMP (MPa)	Factor C Vibratory Frequency (s^{-1})	Vibratory Displacement (cm)
1	42.4	2.41	53.3	0.64
2	8.5	3.79	54.1	1.27
3	25.4	2.41	54.1	1.27
4	42.4	3.79	54.1	1.27
5	25.4	3.79	54.7	3.18
6	25.4	1.03	53.3	0.64
7	25.4	2.41	54.1	1.27
8	42.4	1.03	54.1	1.27
9	8.5	2.41	54.7	3.18
10	8.5	1.03	54.1	1.27
11	25.4	2.41	54.1	1.27
12	42.4	2.41	54.7	3.18
13	25.4	3.79	53.3	0.64
14	25.4	2.41	54.1	1.27
15	8.5	2.41	53.3	0.64
16	25.4	2.41	54.1	1.27
17	25.4	1.03	54.7	3.18

The process responses for this study were permeate flux, permeate conductivity and COD, and corresponding rejection efficiencies. Multivariate regression analyses were performed for each response parameter to develop polynomial model equations according to Equation 84. ANOVA was also performed to determine the level of significance of main and interaction effects of factors on the response parameters. Model reduction was also performed by removing insignificant parameters to improve model correlations.

7.2.2 *Optimization and Experimental Verification*

Model equations obtained from multivariate regression analyses were used to optimize the vibratory NF operation for a 25.4 g L^{-1} feed coffee extract. The model equations, as well as criteria for the operating conditions and process responses were used as objective functions for optimization. The criteria for the response parameters were to maximize the permeate flux and rejection efficiencies, and minimize permeate concentrations. On the other hand, the criteria for applied TMP and vibratory frequency were set to be within the range of the experimental design space. Numerical optimization was performed to determine the optimum conditions. Lastly, the optimum solution was experimentally verified to assess the validity of the model equations in predicting the performance of the vibratory NF operation.

7.2.3 *Statistical Analytical Tool*

Experimental design, statistical analyses, and numerical optimization for this study were performed with the aid of Design Expert v12 ® (Statease, MN, USA). This statistical tool was used to aid in model regression and validate the models using various tests on model significance and statistical soundness, e.g., analyses of variance ($\alpha = 0.05$), lack-of-fit tests, coefficients of determination (R-squared), Box-Cox plots, and other statistical diagnostic tools [143].

7.3 Results and Discussion

7.3.1 *Flux Enhancement by Vibratory Nanofiltration*

The magnitude of flux enhancement attributed to the vibratory membrane operation in comparison with conventional crossflow filtration was further assessed based on a two-level full factorial experimental design. This method served to screen the operating factors and responses that were further evaluated in optimizing the NF operation. Filtration time profiles for permeate fluxes are shown in Figure 53, while the results of the factorial experiments are presented in Figure 54.

Figure 53

Coffee Extract Filtration Time Profiles for Crossflow (F = 0 Hz, d = 0 cm) and Vibratory (F = 54.7 Hz, d = 3.18 cm) Operation Using TS80 NF Membrane at Various TMPs and Feed Solute Concentrations at 25°C

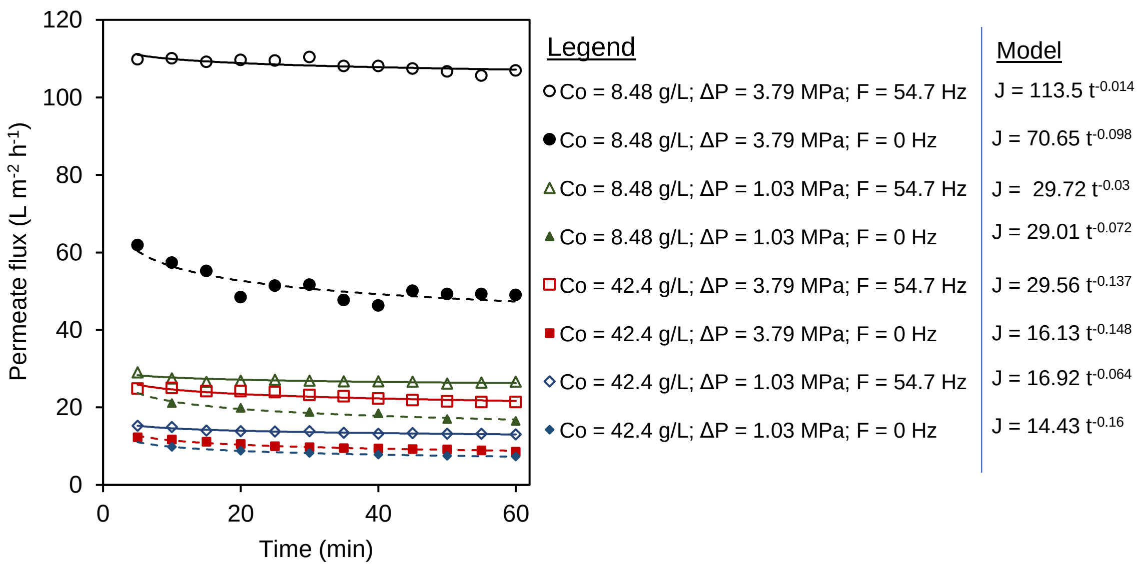

Figure 54

Performance of Crossflow (F = 0 Hz, D = 0 cm) and Vibratory (F = 54.7 Hz, d = 3.18 cm) Nanofiltration at Various TMPs and Feed Solute Concentrations at 25°C

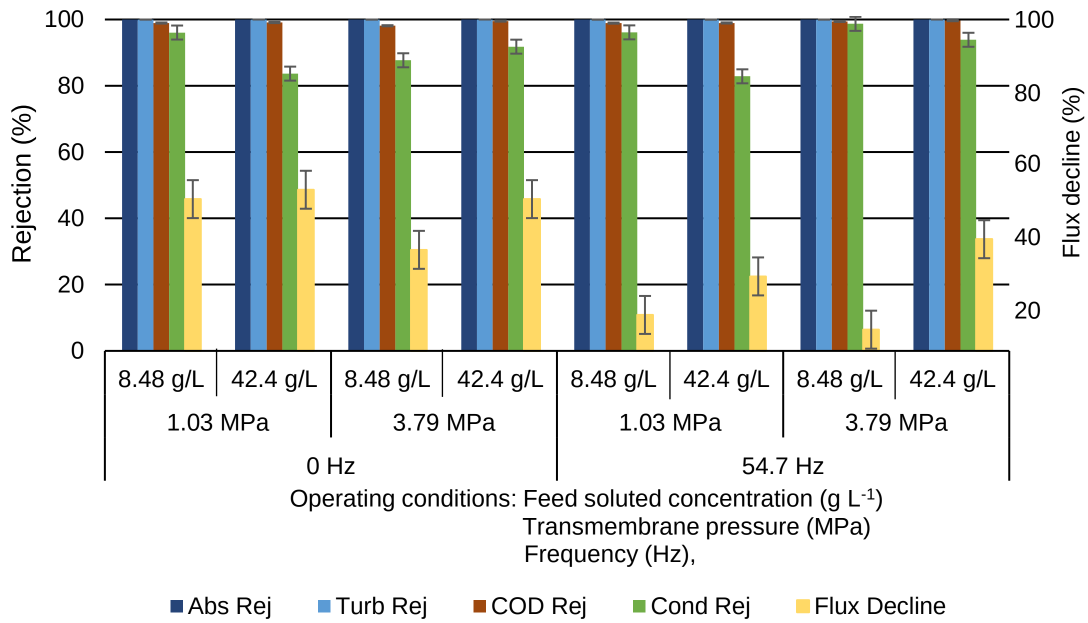

Under CF filtration mode, the TMP fundamentally served as the main driving force in membrane processes. This behavior was observed from Figure 53, where higher TMPs increased the permeate flow rates for the NF operations. However, despite the contribution of the applied TMP in permeate flux enhancement, increasing the feed coffee extract concentration from 8.48 g L^{-1} to 42.4 g L^{-1} resulted in a lower permeate flux. This behavior is commonly attributed to the osmotic pressure that the coffee extract components exert upon increasing the feed solute concentration. It is also the case that there is an associated increased amount of solute accumulating on or near the membrane surface as a result of the applied pressure drop in the system [163]. The accumulation of these components, otherwise known as concentration polarization, can lead to a viscous gel layer on the membrane surface. The high viscosities also reduce the shear rates near the membrane surface [5]. Further, this compact layer contributes to an additional resistance that, in dense membranes such as in NF and RO, promotes the back diffusion of the liquid from the membrane surface [94]. Overall, the increase in osmotic pressure difference and the additional resistance arising from the gel layer formed during CF filtration decrease the effective permeability across the membrane. This resulted in lower observed permeate fluxes for the operation.

The decline in permeate flux was also observed throughout the membrane operation based on the time profiles for the permeate fluxes throughout 60 minutes of filtration. The time profiles were also fitted with Equation 30 to evaluate the decline in flux throughout the filtration time. A pronounced decline in flux was observed in all CF filtration runs that ranged from 30% to 48% after 60 minutes of the NF operation. This decline was more prominent in runs where the feed solute concentration was 42.4 g L^{-1}, as observed from the increase in the fouling decay rate constant observed under CF filtration. On the other hand, the dynamic vibratory filtration (F = 54.7 Hz, d = 3.18 cm) resulted in significant flux enhancement by up to 3 times those observed from CF filtration with lower flux decline (< 6.5%). This type of improvement has been reported in vibratory filtration systems used for the concentration of milk proteins and dairy wastewater treatment [5], [45], clarification and yeast recovery of alcoholic beverages [2], [3], water treatment from high salt seawater and freshwater sources [46]–[49], and water recovery from soluble coffee wastewater [51], [52]. Accordingly, the torsional mechanical vibrations of the membrane assembly result in a high shear region at the surface of the membrane, thus eliminating the effect of surface fouling to a more considerable extent [35], [37], [38]. This improved performance also allows vibratory filtration systems to operate at significantly higher feed solute concentrations than those allowed in CF filtration [51]. However, it is also interesting to note that feed concentrations can increase the boundary layer osmotic pressure due to concentration polarization. Thus, increasing the feed concentrations from 8.48 g L^{-1} to 42.4 g L^{-1} resulted in lower permeate fluxes with a flux decline of about 23% to 33%. Despite the effect of feed solute concentrations, these surface shear rates generated from vibratory filtration still far exceed those generated from CF filtration. As a result, higher and more stable fluxes were observed.

The CF and vibratory NF using the TS80 membrane produced water-rich clear permeate samples that support the high rejections of absorbance, turbidity, conductivity, and COD shown in Figure 54. The permeate turbidities at the end of the filtration time were below 1 NTU, and the corresponding turbidity rejections were above 99.9% for both configurations using the TS80 membrane. This rejection efficiency shows that the bulk of the suspended and colloidal solids in the coffee extract are above the 150-Da MWCO of the TS80 membrane and that the membrane can sufficiently reject these components within the set operating conditions. The specific membrane cut-off diameter influence the steric hindrance, adsorption, and porosity of the concentration-polarized region near the membrane surface [3], [47]. The COD rejection efficiencies were also above 98% that strongly indicates that a large fraction of the organic components retained by the TS80 NF membrane was represented by suspended and colloidal solids. Despite the high COD rejection, the conductivity rejections varied between 83% and 98%, indicating the limited effectiveness of the TS80 membrane in retaining a range of dissolved organic and inorganic components. This incomplete rejection shows that while multivalent salt rejection in the NF membrane is high, monovalent salts may still pass through the membrane. Along with these salts are dissolved organics that rendered permeate CODs as high as 400 mg L^{-1}. These residual organics may have molecular weights lower than the cut-off diameter of the NF membrane, and may include phenolic and chlorogenic acids based on the acidic pH of the permeate ranging from 4.5 to 5.5. Higher feed solute concentrations significantly decreased the conductivity rejection efficiencies of the NF operation. Nonetheless, higher conductivity rejections were obtained by applying higher TMPs, and more considerably by employing vibrations on the membrane module. This improved rejection indicates that the reduced concentration polarization from the high surface shear rates generated during the vibratory operation resulted in a lower transmembrane concentration gradient [5]. The higher rejection of the vibratory membrane operation was also observed in the concentration of milk proteins under vibratory UF [5], and the removal of natural organic matter for brackish water treatment by vibratory NF [47].

7.3.2 *Effects of Operating Factors on Permeate Flux*

Based on the level of permeate flux and characteristics, and the capability to reduce the flux decline in the NF operation, the performance of the dynamic vibratory filtration operation was further investigated. Despite its positive effects on flux enhancement and rejection, increasing the applied TMP may still form a gel layer, especially under high feed coffee extract concentrations [32], [34]. On the other hand, the extent of operating at high vibrational frequencies still needs to be investigated, as it may result in shear-enhanced backflow as was observed in rotating disk membrane filtration [170]. Thus, similar to conventional membrane operations, threshold fluxes under specific operating conditions may limit the vibratory NF operation [17], [163]. In this regard, optimizing the operating conditions can minimize the limitations observed in those studies.

In this study, a Box-Behnken experimental design was used to observe the individual effects of TMP, vibration, and feed solute concentration, along with interactions in vibratory NF. Results of the experiments are shown in Table 31. Using the Design Expert v12® statistical tool, model regression was performed based on various tests on model significance and statistical soundness, e.g., analyses of variance ($\alpha = 0.05$), lack-of-fit tests, coefficients of determination (R-squared), and other statistical diagnostic tools [143]. These statistical tests are presented in Appendix E. Coded equations were developed from model regression to establish the significant main and interaction effects of TMP, vibration, and feed solute concentrations on selected responses. These equations establish the relative impacts of the coded factors for feed solute concentration (A), TMP (B), and vibratory frequency (C), along with their interactions based on factor coefficients. The numerical values of the factors in such equations are normalized on a coded scale where the low setting is set to -1 and the high set to +1. Under this coded scale, the relationship of the factors with process response is reflected without encountering the diminishing contribution of higher-order terms. The models have also been reduced in terms of the significant factors and interactions to improve their predictability with experimental results [143].

Table 31

Results of Response Surface Experiments

Run	Factors				Responses				
	Factor A	Factor B	Factor C		Response 1	Response 2	Response 3	Response 4	Response 5
	C_o (g L^{-1})	ΔP (MPa)	F (Hz)	d (cm)	J_v (L m^{-2} h^{-1})	$C_{p\ conductivity}$ (µS cm^{-1})	$C_{p\ COD}$ (mg L^{-1})	$\%r_{o\ conductivity}$	$\%r_{o\ COD}$
1	42.4	2.41	53.3	0.64	24.68	378	315	95.29	99.64
2	8.5	3.79	54.1	1.27	80.65	13.2	45.5	76.22	97.98
3	25.4	2.41	54.1	1.27	35.63	181	172	99.04	99.84
4	42.4	3.79	54.1	1.27	12.35	268	171	95.39	99.57
5	25.4	3.79	54.7	3.18	38.00	119	147	85.58	98.92
6	25.4	1.03	53.3	0.64	24.76	177	208	90.46	99.14
7	25.4	2.41	54.1	1.27	38.26	170	170	93.53	99.42
8	42.4	1.03	54.1	1.27	12.51	612	439	95.61	99.65
9	8.5	2.41	54.7	3.18	67.35	23	50	98.83	99.46
10	8.5	1.03	54.1	1.27	24.41	44	83	68.94	95.08
11	25.4	2.41	54.1	1.27	33.35	181	181	76.65	98.50
12	42.4	2.41	54.7	3.18	18.71	350	416	99.41	99.90
13	25.4	3.79	53.3	0.64	56.26	118	100	95.47	99.50
14	25.4	2.41	54.1	1.27	33.38	169	169	98.34	99.72
15	8.5	2.41	53.3	0.64	72.69	25	48	83.98	97.86
16	25.4	2.41	54.1	1.27	33.93	179	179	93.17	99.39
17	25.4	1.03	54.7	3.18	23.68	250	250	95.51	99.66

Equation 85 presents the model equations showing the effects of the operating conditions on permeate flux and surface shear rates.

$$\log_{10} J_v = 1.54 - 0.2664A + 0.1344B + 0.0429C - 0.1312AB + 0.0378BC - 0.0537A^2 - 0.1177B^2 + 0.1000C^2 \qquad (85)$$

A quadratic equation with logarithmic transform best correlated the effects of feed solute concentration, TMP, and shear rates on permeate flux within the selected boundaries of the experimental design. Among the operating conditions, feed solute concentration significantly limited the performance of the vibratory NF operation. As discussed earlier, feed solute concentrations impart osmotic pressure in NF and RO operations that reduces the effective TMP across the membrane [32], [205]. Also, the viscous flow of high-strength coffee extracts results in a gel layer resistance that inhibits the permeate flux. The applied TMP played a significant role in flux enhancement compared with that of vibrations, indicating that the pressure drop of the system is sufficient to overcome the backflow induced by the vibrations. Higher TMPs increase the driving force for mass transfer, resulting in higher throughput rates across the membrane. However, the negative quadratic effect of the applied TMP (B^2) and the interaction between feed solute concentration and TMP (AB) indicate the increase in concentration polarization on the membrane surface at high TMPs. The applied pressure drop increases the osmotic pressure difference through the membrane that decreases the permeate fluxes [49], [120], [170].

On the other hand, the vibrational frequency (C) also significantly contributed to flux improvement through surface shear enhancement. The contribution of vibrational frequency in generating high-shear regions on the surface of the membrane conforms with the theoretical equations developed by Akoum et al. [2] for vibratory membrane filtration systems. Accordingly, oscillatory vibrations promote shear-enhanced back transport that diminishes membrane fouling. These shear regions generated from vibrations are also considerably large that tends to overcome the viscous flow of concentrated coffee extracts. Calculations based on Equation 26 show that the vibratory motions generate surface shear rates as high as 106,000 s^{-1} regardless of the concentration of the feed coffee extract. On the other hand, its interaction with TMP (BC) also indicates that the back transport induced from vibratory shear can overcome the concentration polarization resulting from high TMP operations.

7.3.3 *Effects of Operating Factors on Permeate Characteristics and Rejection*

As observed in the previous section, the selected TS80 NF membrane is practically capable of rejecting all suspended and colloidal solids from the coffee extracts. However, like most NF membranes, only partial rejection of dissolved coffee extract components and salts may be attained. This performance limits COD rejection that affects the final permeate quality. The quality of the permeate recovered from the NF operation is an important parameter as it dictates its reusability in ancillary plant operations [51]. Thus, it is essential to investigate how the TMP, vibration, and feed coffee extract concentration affect the quality of permeate from the process. In the same approach, model equations were also generated to determine the effects of the abovementioned factors and their interactions on permeate quality and corresponding rejections. Equations 86 and 87 present the coded equations for permeate conductivity and conductivity rejection.

$$\log_{10} C_{p\ \text{conductivity}} = 2.25 + 0.5870A - 0.1806B - 0.0141C + 0.0707AB - 0.2790A^2 - 0.0277C^2 \quad (86)$$

$$\%r_{o\ \text{conductivity}} = 93.07 - 4.00A + 2.64B + 0.1093C + 1.79AB + 1.46BC + 1.30C^2 \quad (87)$$

The coded models for the permeate conductivity and conductivity rejections were represented by quadratic models in which feed solute concentrations profoundly limit the dissolved components from passing through the NF membrane. The larger concentration gradient arising from higher-strength coffee extracts fundamentally enhances the diffusion of solutes through the membrane [47], [206]. Feed solute concentrations can also interact with the TMP (AB), resulting in lower conductivity rejection since the higher permeate flux arising from higher system pressure drops tend to increase the driving force for mass transfer across the NF membrane [94]. However, the negative quadratic effect of feed solute concentration (A^2) indicates that higher feed solute concentrations may also result in pore-blocking that may limit the passage of the dissolved components through the membrane. High applied TMPs also led to higher conductivity rejection that may be a result of the pore blocking mechanism in membrane filtration when foulants accumulate into the membrane pores. While this mechanism enhances the rejection efficiency of the NF membrane, it is important to note that pore blocking may lead to the irreversible fouling of the membrane.

Vibration also improved the permeate conductivity and resultant conductivity rejections. The high shear rates generated from high-frequency oscillations diminish the generation of the fouling layer on the membrane surface. However, it should also be noted that the relative effect of vibrational frequency on permeate conductivity and conductivity rejection was substantially lower compared with the other factors. This observation may be due to the MWCO of the TS80 NF membrane that inherently limits its rejection of dissolved organics and salts. Unlike RO membranes that can almost completely reject solutes and produce highly pure water, the TS80 membrane can only effectively reject monovalent and multivalent salts at about 98% and 78% efficiencies, respectively. Thus, an invariance of permeate conductivity and conductivity rejection was observed despite increasing the vibrational frequency of the NF operation. Despite the limitation, compared with the CF filtration performance, the vibratory operation maximized the effectiveness of the NF operation in terms of conductivity rejection. The observations on the permeate conductivity and conductivity rejections of the vibratory NF also conformed with those observed for COD, as shown in Equations 88 and 89.

$$C_{p\,COD} = 174.83 + 158.50A - 53.00B + 24.00 - 19.75AB + 24.75AC + 32.42A^2 \qquad (88)$$

$$\%r_{o\,COD} = 99.36 + 0.2152B - 0.0564C \qquad (89)$$

Feed coffee extract concentrations had the highest impact on the final permeate of the COD, as shown in Equation 88. The pore-blocking mechanism was also reflected at higher TMPs and from its interaction with feed coffee extract concentrations. On the contrary, the vibrations slightly contributed to higher permeate CODs that indicate that, to a certain extent, high shear regions arising from vibrations may also diminish the pore-blocking mechanism. As less membrane surface is pore-blocked, more organics can diffuse, resulting in higher permeate COD. Despite the dependence of permeate COD on feed solute concentration, TMP, and vibrational frequency, the TS80 membrane effectively rejects the suspended and colloidal solids that represented a bulk fraction of coffee extracts. As a result, the total organic rejection was likely to approach 99% based on the small values of the coefficients for TMP and vibrational frequency in Equation 89.

7.3.4 *Optimum Operating Conditions for Vibratory Nanofiltration*

The operating conditions for the vibratory NF operation on coffee extract were optimized using RSM. Multivariate model regression was employed on the selected responses based on the actual values of the operating factors. In contrast to the coded equations that identify the relative impacts of the operating factors, the model equations shown in Equation 90 to Equation 94 can be used to make predictions of the response based on the actual values of factors considered in the experimental design space.

$$\begin{aligned}\log_{10} J &= 597.630 + 0.00734C_o - 1.5754\Delta P - 22.083F \\ &\quad - 0.00561C_o(\Delta P) + 0.0392(\Delta P)F - 0.000187C_o^2 \\ &\quad - 0.0620\Delta P^2 + 0.204F^2\end{aligned} \tag{90}$$

$$\begin{aligned}\log_{10} C_{p\ conductivity} &= 2.330 + 0.0767C_o - 0.2081\Delta P - 0.0202F \\ &\quad + 0.00203C_o(\Delta P) - 0.00097C_o{}^2\end{aligned} \tag{91}$$

$$\begin{aligned}C_{p\ COD} &= 1{,}063.44 - 106.93C_o - 16.96\Delta P - 18.75F \\ &\quad - 0.845C_o\Delta P + 2.08C_oF + 0.113C_o{}^2\end{aligned} \tag{92}$$

$$\begin{aligned}\%R_{conductivity} &= 8{,}007.19 - 0.421C_o - 81.91\Delta P - 289.39F \\ &\quad + 0.0768C_o(\Delta P) + 1.52(\Delta P)F + 2.65F^2\end{aligned} \tag{93}$$

$$\%R_{COD} = 103.3 + 0.16\Delta P - 0.081F \tag{94}$$

Response surface plots based on these model equations were generated with the aid of the statistical software tool. These plots are shown in Figure 55 to Figure 59.

Figure 55

Response Surface Plots for Permeate Flux as a Function of (a) TMP and Vibratory Frequency, and (b) TMP and Feed Coffee Extract Concentration

(a) $C_o = 25.44$ g L^{-1}

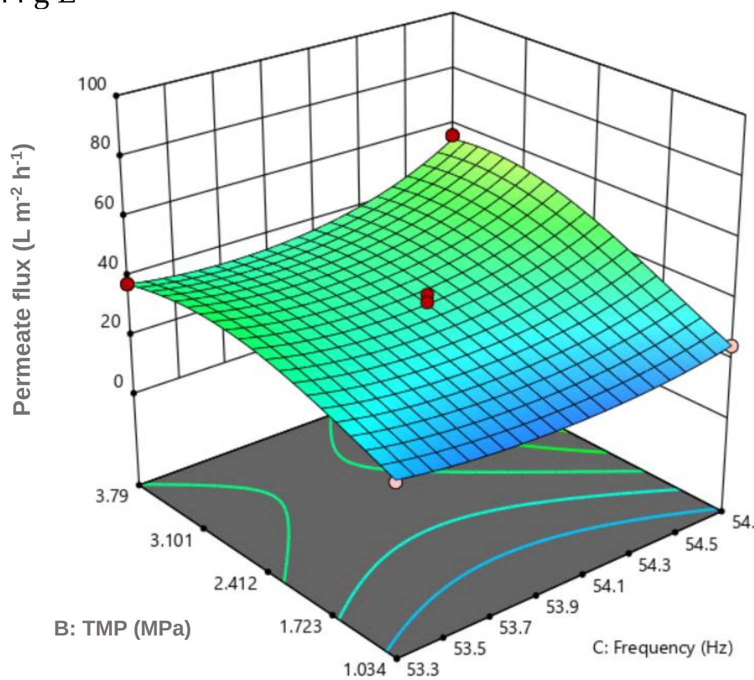

(b) F = 53.3 Hz, d = 0.64 cm

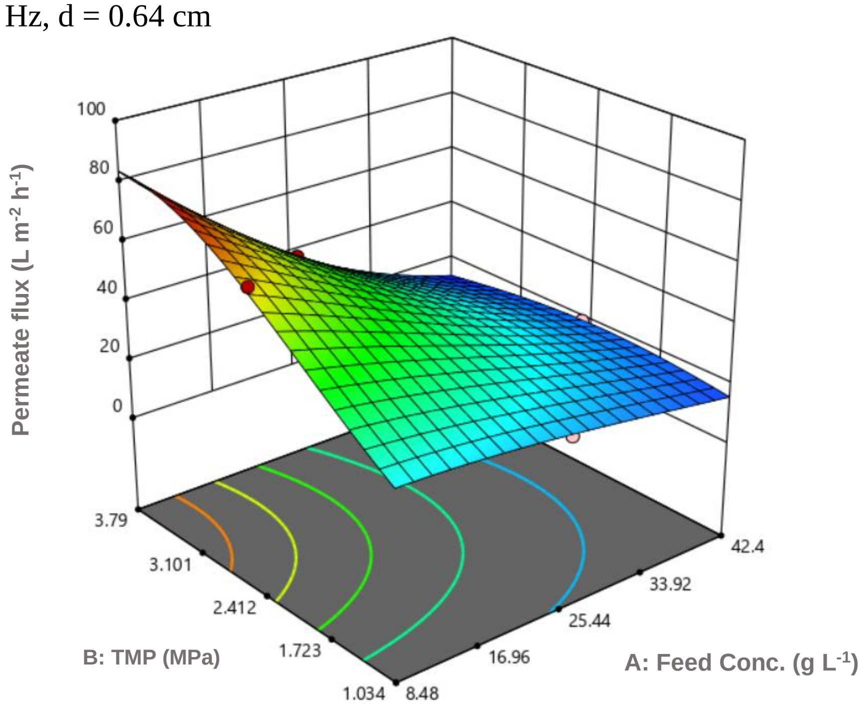

Note: TS80 membrane, T = 25°C

Figure 56

Response Surface Plots for Permeate Conductivity as a Function of (a) TMP and Vibratory Frequency, and (b) TMP and Feed Coffee Extract Concentration

(a) $C_o = 25.44$ g L^{-1}

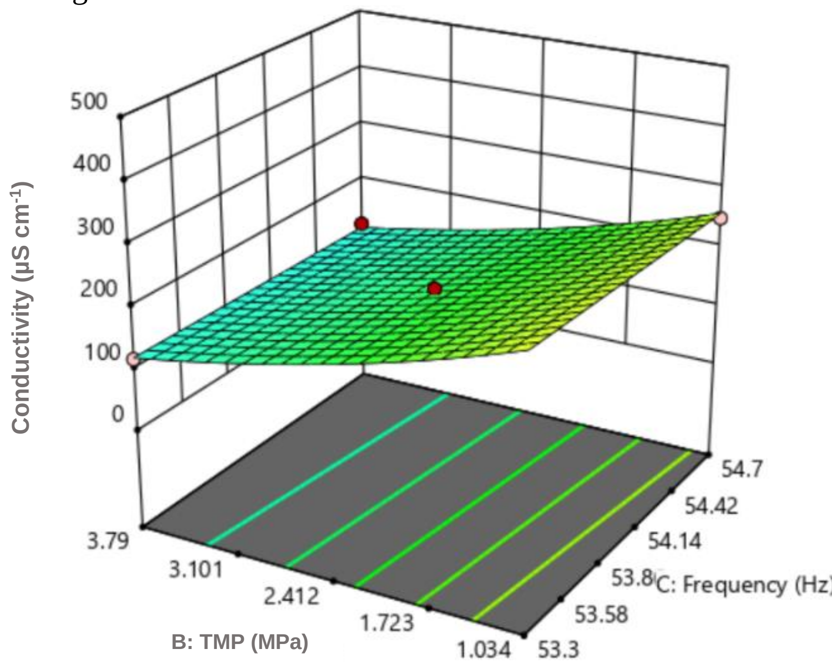

(b) F = 53.3 Hz, d = 0.64 cm

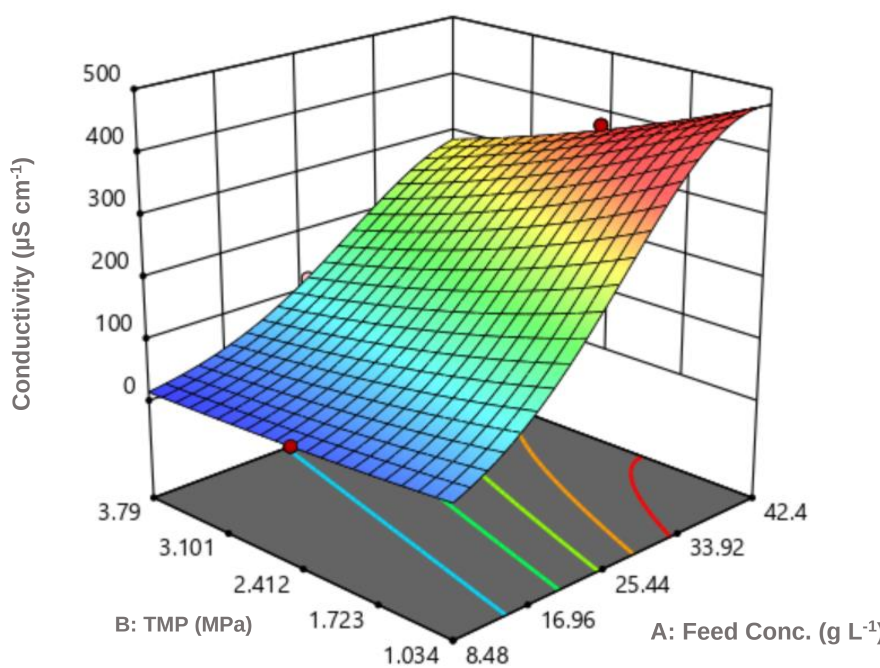

Note: TS80 membrane, T = 25°C

Figure 57

Response Surface Plots for Permeate COD as a Function of (a) TMP and Vibratory Frequency, and (b) TMP and Feed Coffee Extract Concentration

(a) C_o = 25.44 g L^{-1}

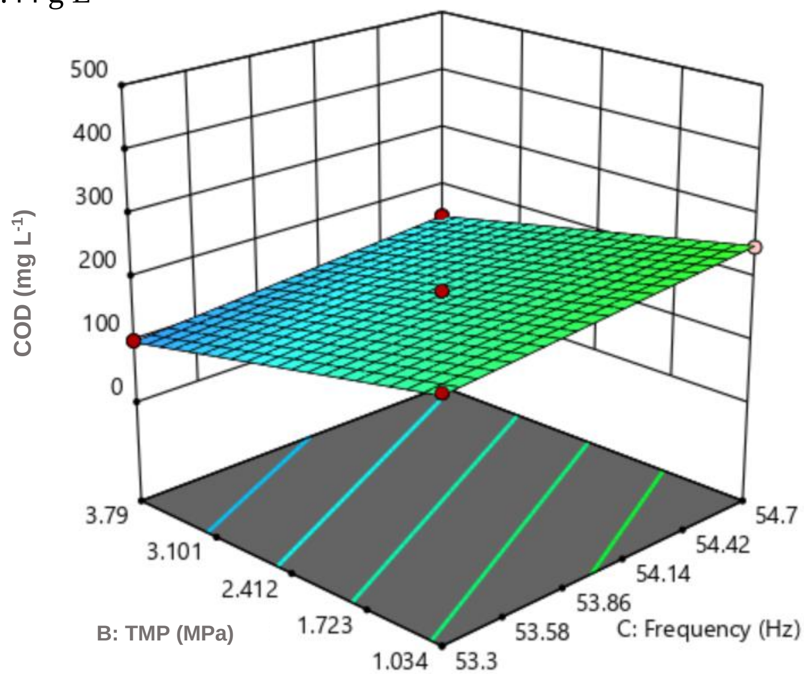

(b) F = 53.3 Hz, d = 0.64 cm

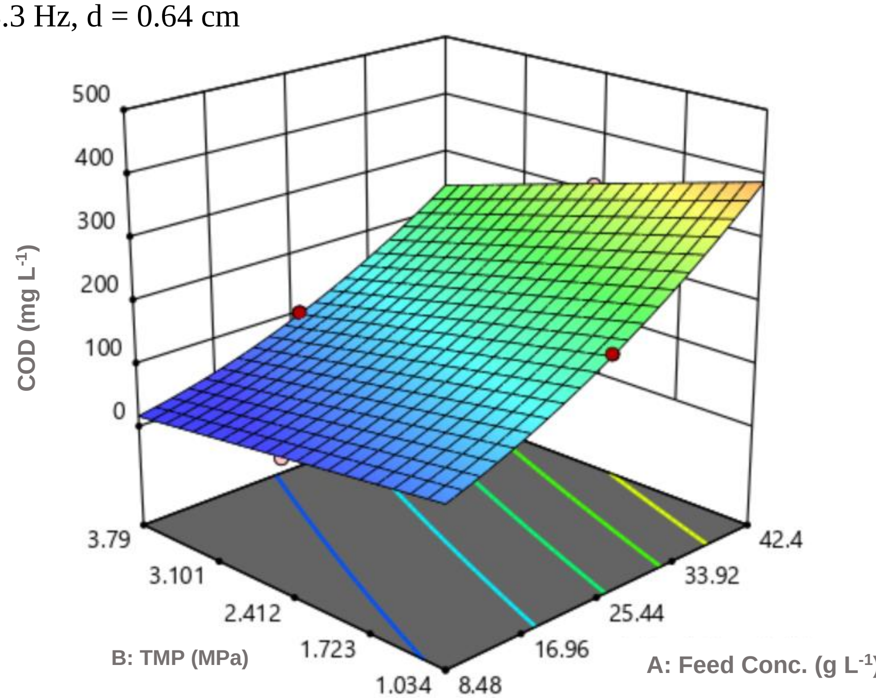

Note: TS80 membrane, T = 25°C

Figure 58

Response Surface Plots for Conductivity Rejection as a Function of (a) TMP and Vibratory Frequency, and (b) TMP and Feed Coffee Extract Concentration

(a) $C_o = 25.44$ g L^{-1}

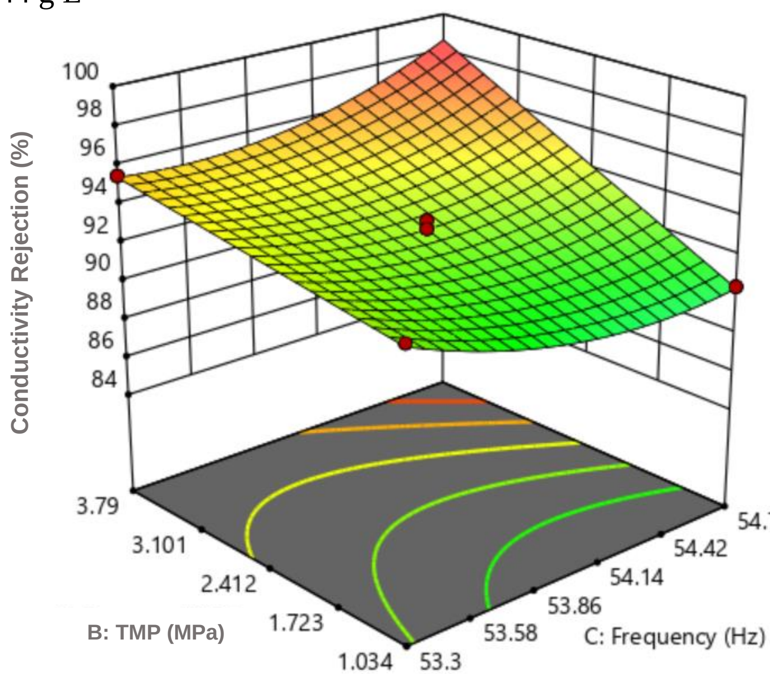

(b) F = 53.3 Hz, d = 0.64 cm

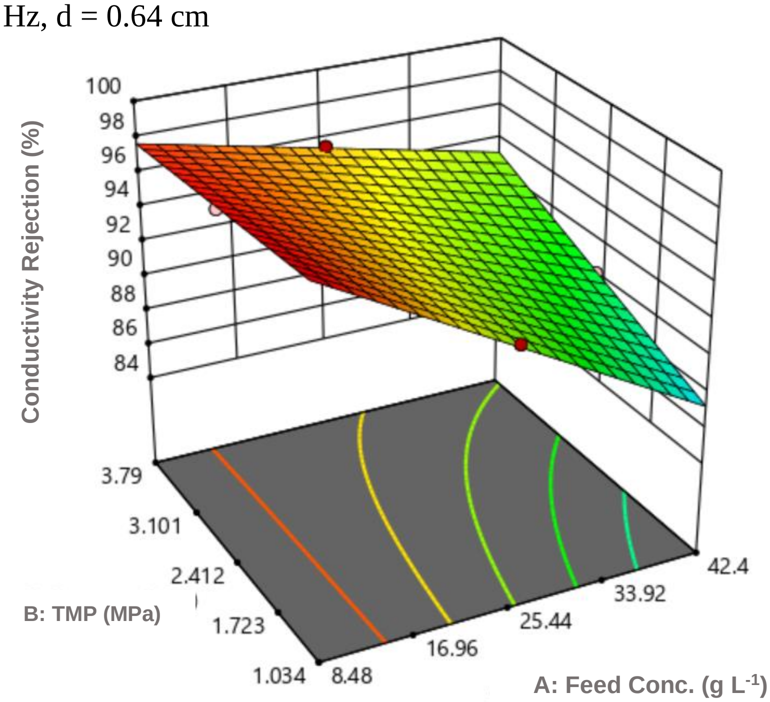

Note: TS80 membrane, T = 25°C

Figure 59

Response Surface Plots for COD Rejection as a Function of (a) TMP and Vibratory Frequency, and (b) TMP and Feed Coffee Extract Concentration

(a) $C_o = 25.44$ g L^{-1}

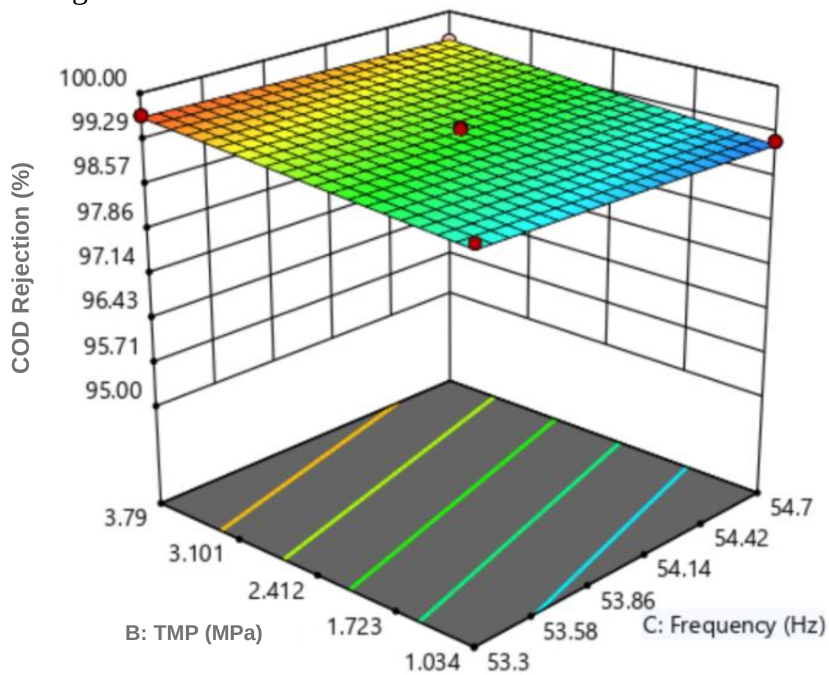

(b) F = 53.3 Hz, d = 0.64 cm

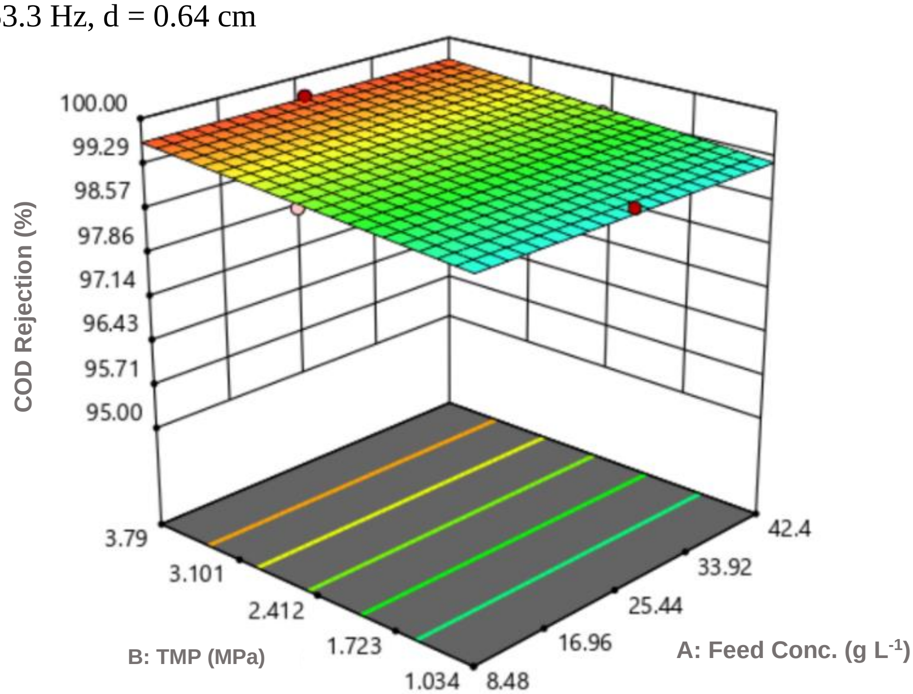

Note: TS80 membrane, T = 25°C

Numerical optimization was employed based on the model equations by establishing constraints at reasonable criteria [143]. These constraints were considered as the goals or objectives for optimizing the vibratory NF operations for a constant coffee extract concentration of 25.44 g L^{-1}. The two operating factors were set to be within the range of the experimental design, i.e., between 1.04 MPa and 3.79 MPa for the applied TMP, and between 53.3 Hz (d = 0.64 cm) and 54.7 Hz (d = 3.18 cm) for the vibrational frequency. The same objective was also set for the maximum shear rate. On the other hand, as a rate-dependent operation, the permeate flux was maximized. For an optimum permeate quality, the objectives were to minimize the permeate COD and conductivity; and maximize the corresponding rejection efficiencies. With the aid of the statistical software, four optimal solutions were found (Table 32), each with an assigned value of desirability, i.e., a function that combines all the optimization goals into a scale that can serve as an aid in screening the optimum conditions [143]. Among these optimal solutions, the one with the highest desirability was selected.

Table 32

Optimal Solutions Obtained from Numerical Optimization for C_o = 25.4 g L^{-1}

ΔP (MPa)	F (Hz)	J (L m^{-2} h^{-1})	$C_{p\ conductivity}$ (μS cm^{-1})	$C_{p\ COD}$ (mg L^{-1})	$\%r_{o\ conductivity}$	$\%r_{o\ COD}$	Desirability
3.79	54.7	54.903	112.3	145.8	98.6	99.52	0.742
3.74	54.7	55.201	114.2	148.0	98.4	99.51	0.738
3.79	54.7	52.882	112.5	144.4	98.3	99.52	0.737
3.79	54.4	44.113	113.7	136.4	97.1	99.54	0.699

Accordingly, the optimum applied TMP and vibrational frequencies were 3.79 MPa and 54.7 Hz (d = 3.18 cm), respectively. Its overall desirability was also 0.73, which is an acceptable index in meeting the optimization objective. Under these conditions, the predicted responses are 54.9 L m^{-2} h^{-1} for the permeate flux, 112.3 μS cm^{-1} for the permeate conductivity, 145.8 mg L^{-1} for the permeate COD, and the corresponding rejections are 98.6% and 99.5% for those of conductivity and COD, respectively.

7.3.5 *Experimental Verification of Optimum Operating Conditions*

Experimental verification was carried out in duplicate at the optimum conditions to validate the predicted optimum responses. The experimental values were evaluated by calculating the deviation relative to the predicted value, as shown in Table 33.

Table 33

Comparison of Predicted Responses and Experimental Results Under Optimum Conditions (C_o = 25.4 g L^{-1}, T = 25 °C)

PARAMETER	UNIT	ΔP = 3.79 MPa, F = 54.7 Hz, d = 3.18 cm		
		Predicted	Experimental	% Error
Permeate Flux	L m^{-2} d^{-1}	54.9	57.2	4.2%
Permeate conductivity	μS cm^{-1}	112.3	144.8	28.9%
Permeate COD	mg L^{-1}	145.8	160.5	9.7%
Conductivity Rej	%	98.6	94.7	3.9%
COD Rej	%	99.5	99.5	0%

The average measured results at the optimum conditions were 57.2 L m^{-2} h^{-1} for the permeate flux, 119.2 μS cm^{-1} for the permeate conductivity, 160.5 mg L^{-1} for the permeate COD, and the corresponding rejections are 94.7% and 99.5% for those of conductivity and COD, respectively. Except for permeate conductivity, all experimental values had good agreement with the corresponding predicted values at a reasonable deviation within 10%. On the other hand, the 28.9% error on experimental permeate conductivity indicates that additional studies may be conducted to provide a more specific analysis of the dissolved coffee extract components that affect the NF membrane rejection. Nonetheless, despite the error in the permeate conductivity, the corresponding conductivity rejection efficiencies only incurred about 3.9% error, and that still validates the application of the statistical models when predicting percent rejection. Overall, RSM is a promising tool to optimize the operating conditions of the vibratory NF operation for the preconcentration of coffee extract in soluble coffee production.

Chapter 8

Process Evaluation and Economic and Environmental Assessment of Vibratory Nanofiltration of Coffee Extracts for Soluble Coffee Production

Some text and figures were reproduced and adapted with permission from M. V. O. Laurio and C. S. Slater, "Process scale-up, economic, environmental assessment of vibratory nanofiltration of coffee extracts for soluble coffee production process intensification" *Clean Tech Environ Policy*, 2020 22, 1891–1908, [56]

Additional graphs and tabular data of the results for this chapter are presented in Appendix E. The results presented herein are those essential to summarize the studies necessary for this dissertation's discussion.

8.1 Introduction

Currently, the scope of studies related on the vibratory membrane filtration of coffee extracts is still limited. Particularly, the main objective of this dissertation was focused on membrane transport modeling of the vibratory NF process for coffee extract separation. Although experimental studies discussed in the previous chapters strongly suggest the process fit for this application, factors beyond parametric evaluation should be equally considered [51], [61]. For instance, despite flux and separation enhancement, the dynamic operating nature of the vibratory membrane system imposes additional maintenance and higher capital cost [43]. And although the benefits from using the system as a nonthermal dewatering alternative and as a water recovery route present environmental merits, the extent by which the operation can be integrated into the soluble coffee process should balance its economic metrics. This limited information on the environmental and economic impacts of system design prevents the translation of parallel studies on complex systems such as coffee extracts [51]. As a crucial element in sustainable food and beverage production, we evaluated the potential of integrating the process into soluble coffee production. We conducted a parallel study to gauge the potential applicability of the proposed system by deriving scale-up parameters and operating conditions from laboratory-scale experiments. The economic metrics and life cycle emissions (LCEs), in comparison with those of the current operations, were determined to gauge the advantages and limitations of the membrane-based water recovery alternative.

8.2 Materials and Methods

8.2.1 *Scope of the Alternative Case Study*

This study evaluated one of the potential water recovery routes designed for the process intensification of the soluble coffee process. Research into sustainable production of soluble coffee products started with the evaluation of membrane-based wastewater reclamation options for the Nestlé USA beverages production facility in Freehold, New Jersey [50]–[52] in 2016, and has expanded into a more wide-spread integration of water recovery in various operations. In contrast to the membrane-based soluble coffee wastewater reclamation alternatives investigated in the past by Wisniewski, et al. [50]–[52], this case study performed a techno-economic and environmental assessment of the vibratory NF system, upstream, to supplement thermal evaporation in the preconcentration of coffee extracts prior to spray- or freeze drying. As a nonthermal operation, we intend to present the benefits and costs of integrating this process, not only as a less energy-intensive method, but also as a water recovery option where the permeate can be directed for reuse in plant operations. However, no exhaustive process design optimization was performed in the scale-up of the VSEP operation. Nonetheless, the projected scale-up operation presented in this Chapter shows the potential relevance of the technology for commercial plant use.

Simplified representative flow diagrams representing the base case (discussed in Chapter 4), and an integrated membrane operation for coffee extract preconcentration (alternative case), is shown in Figure 60. As discussed in Chapter 4, representative flows from a parallel study by Wisniewski et al. [51] were adapted for this study since privileged information from actual plant operations limits the scope of analysis. Also, only the process components within the life cycle boundary or those directly affected by the alternative case were considered for the estimation of life cycle emissions and costs of the two cases. The base case represented the process flows for a typical soluble coffee production, where the feed water used for extraction is about 1.32 x 10^6 L d^{-1}. The same amount of water is essentially evaporated completely during the concentration and dehydration of the coffee extracts to produce the soluble coffee product. In turn, the water used in the production process ends up as waste stream that undergoes wastewater treatment. Mass and energy balance calculations were performed (Table 13) to determine the base case operating costs (Figure 23) and LCEs (Table 19 and Figure 24), as were discussed in Chapter 4.

Figure 60

Operations Involved in Soluble Coffee Processing for (a) Base Case, and (b) Alternative Case Studies

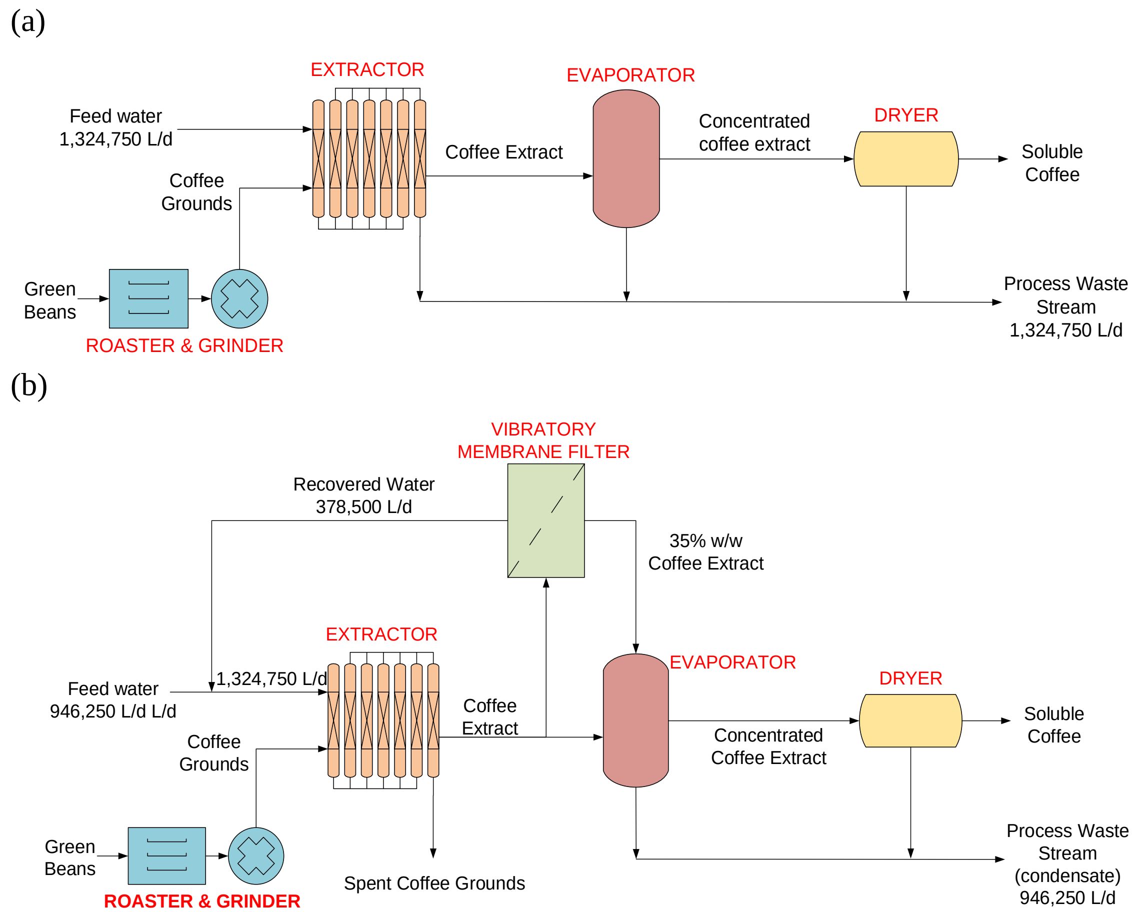

In the proposed alternative case, the membrane system intercepts a fraction of the raw coffee extract generated from percolation batteries and concentrates it to 35% (wt/wt). The proposed final concentration of coffee extract was based on the recommendation of Pan et al. [32] as a limitation resulting from the concentration polarization of coffee extract during membrane filtration at that high concentration. Despite this limitation, the concentrated coffee extract from the proposed vibratory NF operation shall be directed to evaporators for further concentration before final dehydration by spray drying. The permeate recovered will be recirculated back to the extraction process to eliminate component losses from the partial rejection of dissolved solids (expressed as conductivity) of the NF membrane [33]. These dissolved solids may contain organic constituents that may affect the quality of the coffee extracts, likewise the final soluble coffee product. The targeted water recovery from the alternative case is 378,500 L d^{-1}; to reduce freshwater use, steam consumption from thermal evaporation, and wastewater generation of the base case. Table 34 presents the scaled-up mass and energy flows associated with the proposed alternative case having the recovery operation that were compared with the base case in the succeeding discussions, in terms of life cycle emissions, flow reductions, and life cycle emissions avoided.

Table 34

Estimated Annual Process Flows of the Base and Alternative Case Studies

Process Component	Unit yr^{-1}	Estimated Flow		Flow Avoided
		Base Case [a]	Alternative Case [b]	
Freshwater	L	6.51E+08	5.11E+08	1.40E+08
	kg	6.50E+08	5.12E+08	1.38E+08
Nonhazardous wastewater	L	4.84E+08	3.45E+08	1.39E+08
	kg	4.82E+08	3.46E+08	1.36E+08
Hazardous wastewater	kg	5.18E+04	5.18E+04	-
Electricity (pumps)	MJ	1.32E+06	1.02E+06	2.94E+05
Electricity (blowers)	MJ	8.00E+06	5.71E+06	2.29E+06
Steam	MJ	4.87E+07	-	4.87E+07
	kg	2.84E+07	-	2.84E+07
Recovery system	MJ	-	1.06E+06	-1.06E+06

Note: [a] without water recovery

[b] Based on target water recovered of 3.79 x 10^5 L d^{-1}

8.2.2 *Modified Coffee Extract Concentration Study*

Typical scale-up studies involve unsteady-state filtration experiments in concentrating mode by collecting the permeate in a separate tank, while recirculating the retentate back to the feed tank [49], as shown in Figure 61. Conventionally, these experiments require the monitoring of instantaneous permeate fluxes, permeate concentrations, and rejection, while continuously collecting the permeate to achieve a desired final concentration or water recovery.

Figure 61

Conventional Flow Configuration for Concentration Study and Scale-up Design

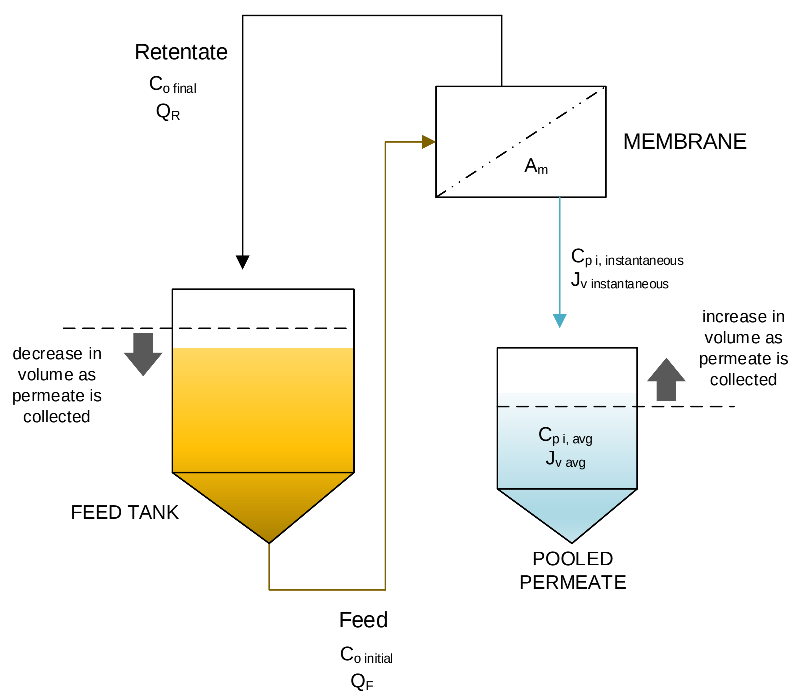

A modified concentration study was performed to estimate the scale-up parameters for the vibratory NF system. This modified approach was conducted in place of conventional concentration studies require several hours, or days, especially for the concentration of coffee extracts that are relatively stronger than previously studied soluble coffee wastewater. For the modified concentration study, various coffee extract concentrations were related with water recovery (%R) from solute mass balance calculations (Equation 34).

$$\frac{C_{o,final}}{C_{o,initial}} = \frac{1}{1 - \%R} \tag{34}$$

Membrane filtration were performed in recycle mode by recirculating the retentate and permeate streams to the feed tank. Steady state permeate parameters were determined in duplicate for different feed coffee extract concentrations. Coffee extracts (8.5 g L^{-1} to 50.8 g L^{-1}) were reconstituted from commercial spray-dried coffee powders (Nescafé® Taster's Choice®, House Blend). For a working volume of 35 L, the coffee extracts were fed to a VSEP Laboratory Membrane Filtration Unit L-101 from New Logic Research, Inc. Nanofiltration experiments were conducted using the TS80 NF membrane (Trisep®, Microdyn-Nadir, Goleta, California) that has a nominal pore size of 150 Da (~ 0.02 nm). The operating parameters for pressure (P = 2.76 MPa), vibrational frequency (F = 54.7 Hz), and retentate recirculation flowrate (Q_r = 7.6 L min^{-1}) were adapted from vibratory membrane filtration studies on soluble coffee wastewater [50]–[52]. An operating temperature of 50°C was observed to compare with feed coffee extract temperature for thermal evaporation. The experimental permeate fluxes were calculated based on a membrane flow area of 0.0045 m^2 [105]. For the characteristics, feed coffee extracts and permeate samples were analyzed in terms of bulk characteristics such as turbidity (suspended and colloidal solids), conductivity (dissolved organic and inorganic ions), and COD (total organic matter) using standard methods of analysis [52], [140]. The analytical methods are presented in Section 3.1.4.

The linearized form of the film layer model [94], [108] shown in Equation 95 was used to correlate steady-state permeate fluxes (J_v) with C_o and calculated values of %R. Model parameters for mass transfer coefficient (k) and gel layer concentration at the membrane surface (C_m) were determined from linear regression.

$$J_v = -\ k \log(C_o) + k \log(C_m) \tag{95}$$

The solute flux (J_s) through the bulk feed layer and membrane surface was used to correlates steady-state permeate concentrations (C_p) with J, as shown in Equation 96, where the model parameter B was referred to as the solute transfer coefficient.

$$J_s = J_v C_p = B(C_o - C_p) \tag{96}$$

Equations 88 and 89 were combined and linearized into Equation 97. The linear equation was then fitted with the measured values of permeate COD, turbidity, and conductivity at different coffee extract concentration.

$$\frac{C_o - C_p}{C_p} = -\frac{K}{B}\ln(C_o - C_p) + \frac{K}{B}\ln(C_g - C_p) \tag{97}$$

The model parameters were used to estimate theoretical values for J and C_p at different coffee extract concentration and percent recovery (Equation 34). The corresponding observed rejection efficiencies ($\%r_{o\,i}$) for turbidity, conductivity, and COD were also calculated using Equation 98.

$$\%r_{o\,i} = \left(1 - \frac{C_{p\,i}}{C_{o\,i}}\right) \times 100 \tag{98}$$

8.2.3 *Process Scale-Up and Design Calculations*

The permeate parameters (J_v, C_p, and $\%r_{o\,i}$) from Equation 95 to Equation 98 were referred to as "instantaneous" parameters. As discussed in Section 3.2, the instantaneous parameters pertain to the conditions of the permeate at the time it exits the filtrate side of the membrane. On the other hand, the pooled conditions of the accumulated permeate stream were referred to as "average" permeate parameters. The average permeate values are those that would be obtained for a single-pass commercial-scale operation at the recovery level desired. These average parameters were calculated from the volume-weighted mean values of the instantaneous parameters. After which, the instantaneous and average permeate parameters were plotted against coffee extract concentrations and corresponding calculated levels of R. Also, for each C_o, the corresponding feed flowrates and overall recoveries were calculated based on the desired permeate flow rate of 378,500 L d^{-1} and a final coffee extract concentration of 35% (wt/wt). The average permeate flux corresponding to the calculated overall recovery multiplied by a design uncertainty of 0.5 relates to the design flux scale-up parameter. On the other hand, the average permeate concentrations and rejection efficiencies relate to the predicted performance of the vibratory NF operation.

From the estimated design flux (J_{design}), an optimum membrane area per module (A) corresponding to the minimum number of modules (N), hence capital cost, was selected using commercially available membrane area options [144]. Equation 38 (Section 3.3.1) was used to calculate N based on the permeate flow rate, A, and J_{design}

[145], with adjustments based on an overall system factor (OSF) of 1.5 accounting for design uncertainty [146] and cleaning cycle time. For the commercial filtration system, the capital cost was determined based on an estimated investment cost per module of $300,000 [51], [61]. The operating costs included the power requirement from the pump and vibratory motor of the filtration system, the cost of cleaning chemicals, and membrane replacement expense. The estimated membrane lifetime for the proposed vibratory NF system is 5 years that is well within the expected lifetime of polymeric membranes (3 to 5 years) used in CF filtration systems [147]. The detailed discussion for the scale-up design procedure and calculations are also presented in Section 3.3.1.

8.2.4 *Economic Assessment*

The alternative soluble coffee process for the manufacturing plant, integrated with the proposed vibratory NF system, was assessed and compared with the base case through a 10-year profitability study. For this study, the estimated overall operating costs, capital cost of the proposed NF system, and projected operating cost savings were factored in a standard 10-yr cash flow. The 7-year modified accelerated cost recovery system (MACRS) depreciation method was employed, along with tax and interest rates of 21% and 15%, respectively. From the cash flow, economic metrics [148] for the internal rate of return (IRR), return on investment (ROI), payback time after-tax, net present value (NPV) after 10 years were then determined. The detailed discussion of the calculations for the economic metrics are also presented in Section 3.3.2.

8.2.5 *Environmental Assessment*

The environmental impacts of LCEs were compared between those calculated for the base case and those of the proposed alternative soluble coffee production process. These were derived from the sum of the LCIs relative to the annualized mass (m_i), energy (E_i), and recovery (R_i) flows calculated from each case, as shown in Equation 99.

$$LCE_{AC} = (m_{W\ AC})LCI_W + (m_{WW\ AC})LCI_{WW} + (E_{AC})LCI_E + (S_{AC})LCI_S + (R_{AC})LCI_R \tag{99}$$

Overall, once the life cycle emissions of the base case and water recovery alternative have been obtained, the amount of avoided emissions were then estimated by obtaining the difference between the LCEs of the two cases. The detailed discussion of the calculations for the life cycle emissions are also presented in Section 3.3.3.

8.3 Results and Discussion

8.3.1 *Results of Modified Concentration Study*

The film layer model was found to have a reasonable agreement with permeate fluxes from varying coffee extract concentrations, as shown in Figure 62. Non-vibratory CF filtration only obtained a maximum permeate flux of 51.2 L m^2 h^{-1} for a coffee extract concentration of 8.5 g L^{-1}. The increasing strength of the coffee extracts, however, decreased the permeate flux by up to a factor of 3 due to concentration polarization. This observation can also be due to the increase in the osmotic pressure exerted by the coffee extract at high concentrations, as it reduces the effective TMP across the membrane that results in lower permeate flux [94]. Like the film layer model, the osmotic pressure concept is based on concentration polarization and has been investigated for modeling membrane filtration operations [14].

Figure 62

Experimental and Projected Permeate Fluxes for Vibratory (F = 54.7 Hz) and Crossflow (no vibration) NF in Steady-State Recycle Mode for Coffee Extract Solutions at Various Initial Coffee Extract Concentrations

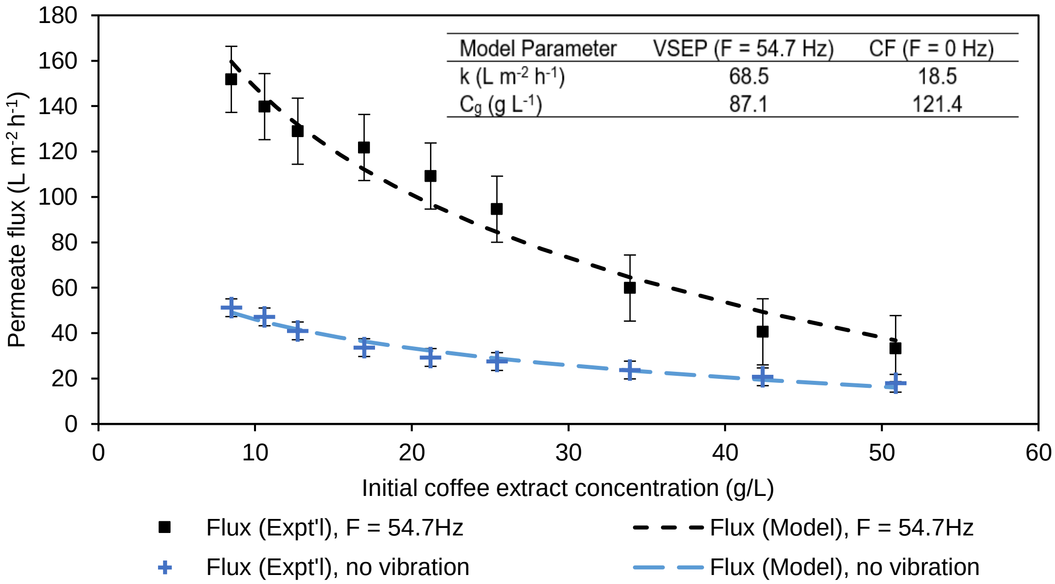

Note: TS80 NF membrane, P = 2.76 MPa, T = 50 °C

The osmotic pressure model presented in Chapter 6 showed the effect of feed concentrations and operating pressures on the osmotic pressure in the vibratory NF operation. The low permeate fluxes were in reasonable agreement with those obtained by in parallel CF NF studies [32], [33] that were found to have high risks of membrane fouling. In contrast to CF filtration, the VSEP operation (F = 54.7 Hz) enhanced the permeate fluxes by up to 3 times. The enhanced flux was also observed in parallel vibratory membrane filtration studies for concentrating milk proteins by VSEP UF [5] and brackish water purification by VSEP RO [49]. The calculated model parameters under these conditions also showed that the mass transfer coefficient of the coffee extract under vibratory NF was higher than that of CF NF by a factor of 3.7. The higher fluxes through the TS80 NF membrane were an effect of the reduced gel layer concentration of 87.1 g L^{-1} due to surface shear rates generated from vibration.

Both filtration modes produced water-rich permeate with substantial rejection of turbidity, conductivity, and COD, as shown in Figure 63 and Figure 64, respectively. The permeate turbidities were less than 1 NTU, and the corresponding average turbidity rejection efficiencies were above 99.9% in both CF and VSEP modes. On the other hand, the NF membrane partially rejected the conductivity of the coffee extract solutions (84% to 94% conductivity rejection). This rejection shows that a portion of the dissolved components is smaller than the 150 Da molecular weight cut-off of the TS80 membrane. These components may include mineral ions or hydrated salts, chlorogenic acids, caffeine, etc. [31], [33], that rendered an acidic permeate with pH between 4.95 and 6.0. Despite the low conductivity rejection, permeate COD values and corresponding COD rejection efficiencies (~98%) strongly indicate that the large fraction of organics retained by the TS80 NF membrane is represented by suspended and colloidal solids.

Figure 63

Experimental and Projected Permeate Characteristics for Vibratory NF (F = 54.7 Hz) at Various Coffee Extract Concentrations at P = 2.76 MPa, T = 50 °C

(a) Permeate COD and COD rejection

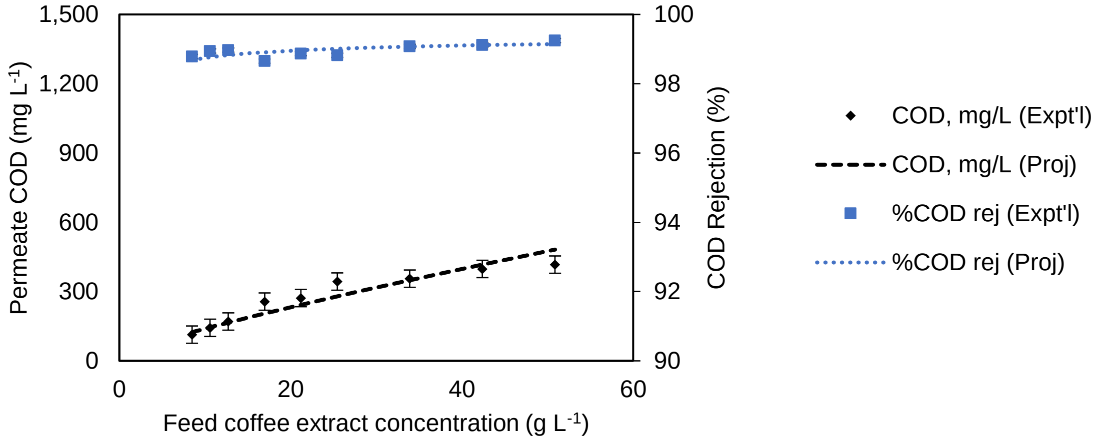

(b) Permeate conductivity and conductivity rejection

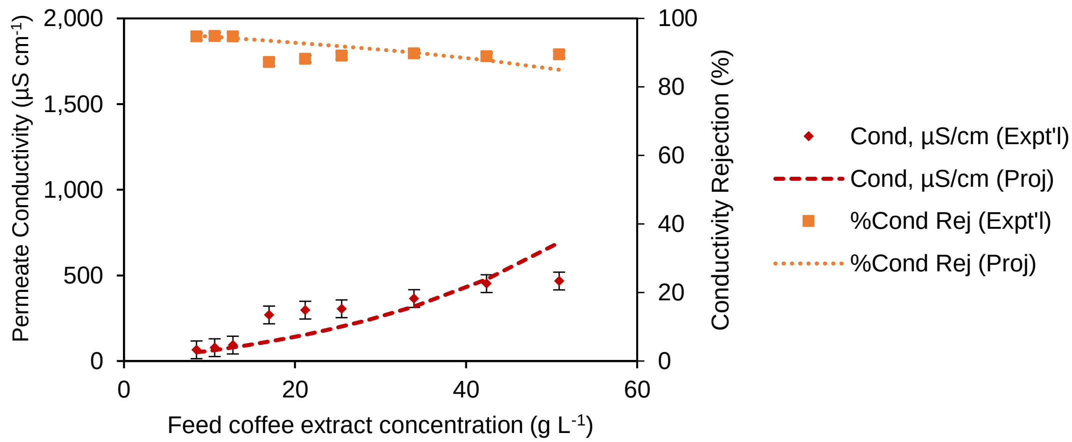

(c) Permeate turbidity and turbidity rejection

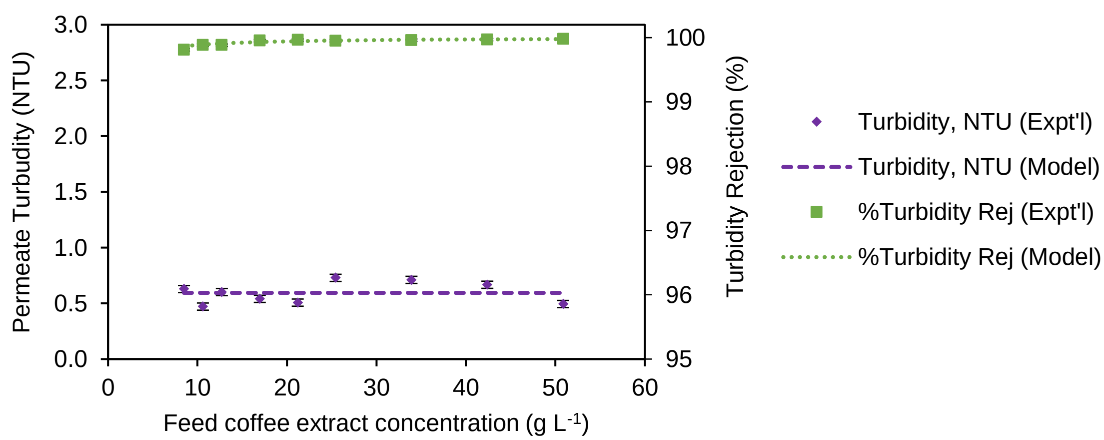

Figure 64

Experimental and Projected Permeate Characteristics for Crossflow NF (F = 0 Hz) at Various Coffee Extract Concentrations at P = 2.76 MPa, T = 50 °C

(a) Permeate COD and COD rejection

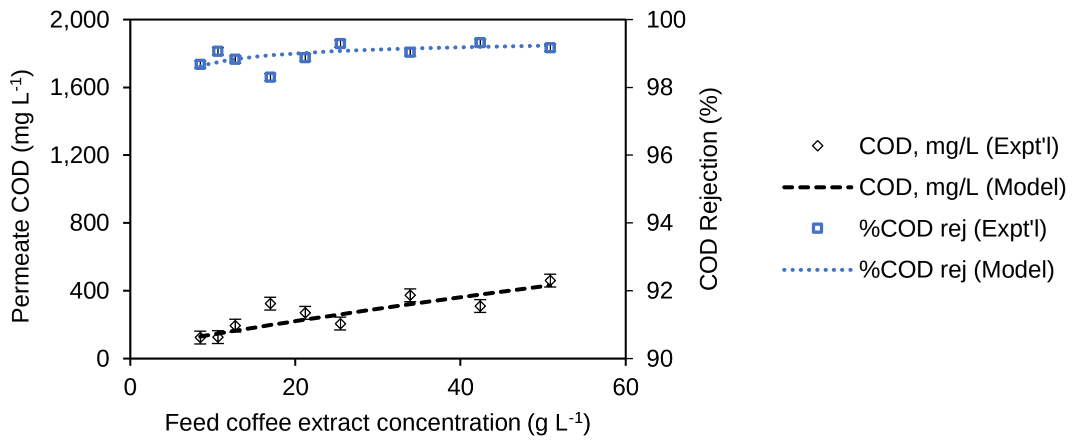

(b) Permeate conductivity and conductivity rejection

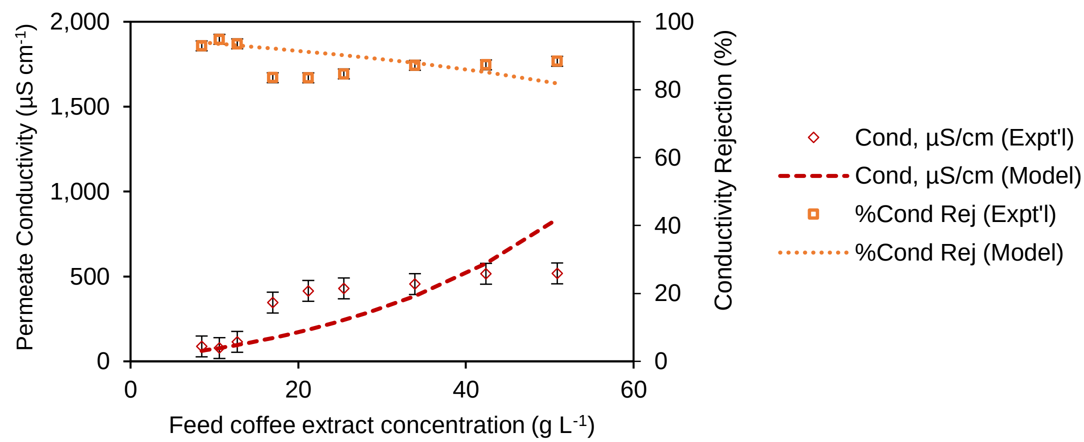

(c) Permeate turbidity and turbidity rejection

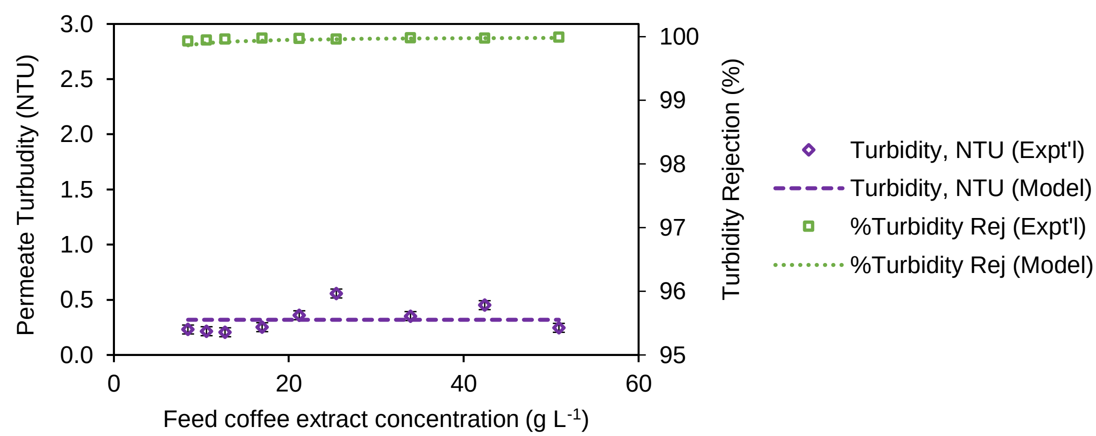

Although further analysis of the permeate is recommended, the high overall organic rejection from the vibratory NF operation indicates its effectiveness in concentrating the coffee extracts with minimal losses and trade-off in quality. Nonetheless, the quality of the coffee extract may also be further varied depending on the type of NF membrane for applications such as in decaffeination [31], or the recovery of coffee extract components from other streams such as in spent coffee grounds [207]. Unlike thermal operations that considerably degrade the flavor and aroma of soluble coffee by about 70% of that of conventionally roasted coffee due to the losses in phenolic compounds and generation of Maillard reaction byproducts [24], integrating membrane operations in the soluble coffee process considerably reduces these losses in product quality. These rejection efficiencies agree with parallel NF studies for concentrating fruits and vegetable juices, and milk and dairy products [44], [208]. In turn, the water-rich permeate recovered may be suitable for reuse when appropriate concentration studies for scale-up are conducted.

For the modified concentration study, Figure 65 and Figure 66 show the permeate parameters for the vibratory NF operation concentrating an 8.5 g L^{-1} (0.85 % wt/wt) feed coffee extract.

Figure 65

Instantaneous and Average Permeate Flux in the Simulated Concentration Study of the Proposed Vibratory NF of Coffee Extract

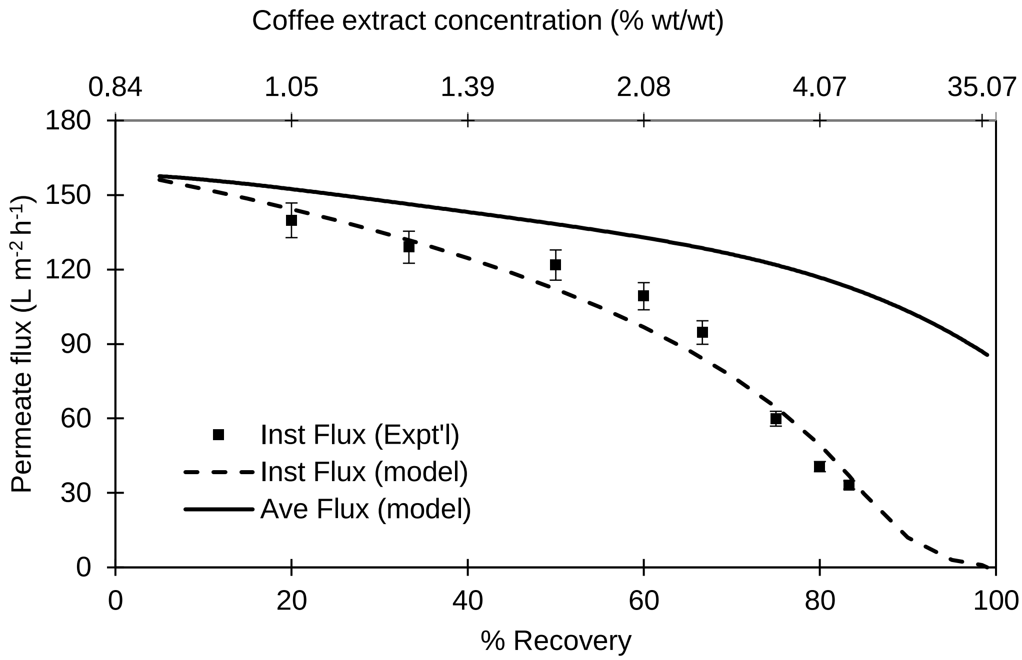

Note: Based on TS80 NF membrane at C_o = 8.48 g L^{-1} (0.84% wt/wt), P = 2.76 MPa, T = 50 °C, vibration F = 54.7 Hz

Figure 66

Instantaneous and Average Permeate Characteristics in the Simulated Concentration Study of the Proposed Vibratory NF of Coffee Extract

(a) Permeate COD

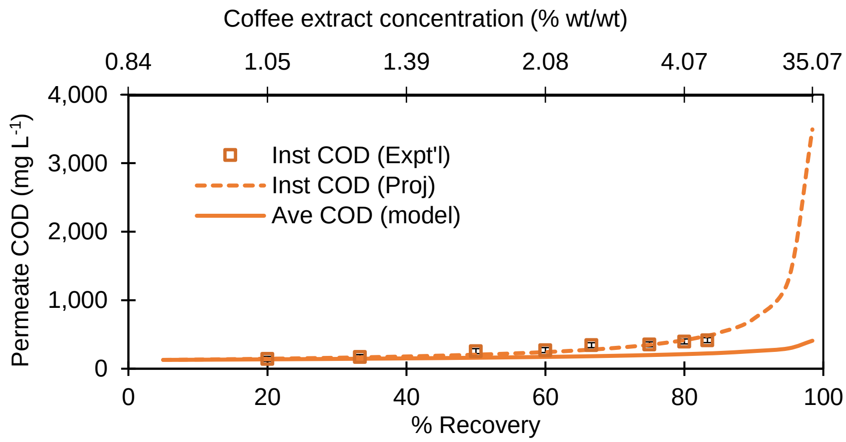

(b) Permeate conductivity

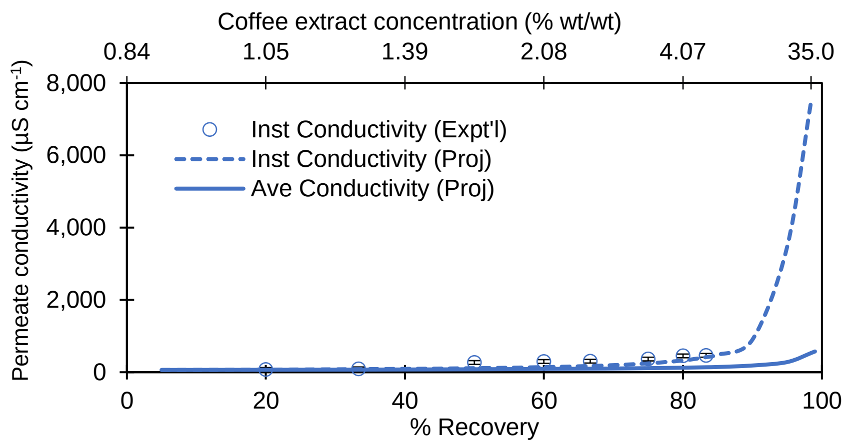

(c) Permeate turbidity

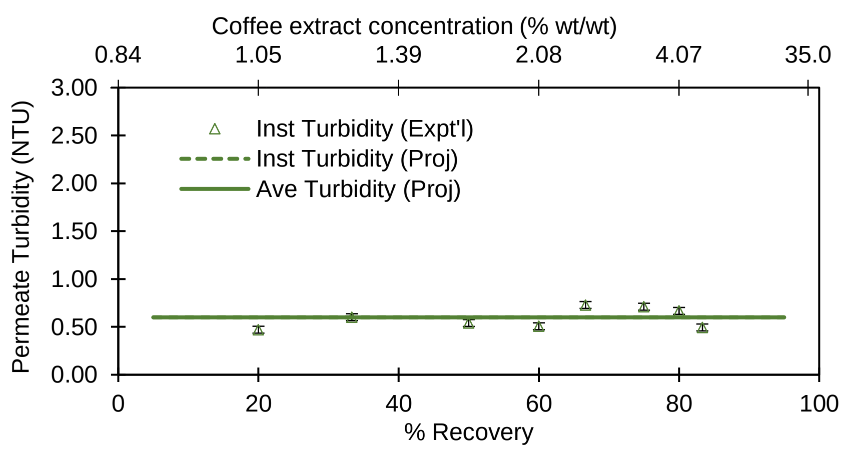

Calculations based on the film layer model show the decrease of instantaneous permeate fluxes as the coffee extract is concentrated. As the operation recovers water, a change in the slope of the instantaneous permeate flux decline was also observed at an approximate coffee extract concentration of 33 g L^{-1} (3% wt/wt), as shown in Figure 65. As a result of this decline and as coffee extract become more concentrated, an increase in the instantaneous residual organic concentration of the permeate was also project, indicating that more organics are expected to pass through the TS80 NF membrane. For a feed coffee extract concentration of 8.48 g L^{-1}, a scaled-up vibratory NF operation recovering 378,500 L d^{-1} of permeate and final coffee extract concentration of 35% corresponds a desired overall recovery of 98.4%. At this high-recovery operation, an average permeate flux of 87.4 L m^{-2} h^{-1} was estimated. In terms of permeate characteristics, the permeate will still have a negligible turbidity. However, the dissolved organics that can pass through the NF membrane was expected to affect the average COD (408 mg L^{-1}) and conductivity (464 µS cm^{-1}) of the permeate after the coffee extract preconcentration operation. The average permeate concentrations at the desired overall recovery is considered for decision making in scale-up, as it is related to the projected permeate characteristics at a specific recovery for a commercial-scale system. At this point, the level of average permeate flux is economically attractive for scale-up, and the water recovered from the permeate may be reused for ancillary plant operations. It should, however, be noted that commercial membrane filtration systems are limited to recovery operations of 40% to 50%, as osmotic pressures can drastically develop beyond theses level that may cause severe fouling [209]. As mentioned in the previous chapters, these foulants may involve colloidal solids, dissolved organics, and inorganic scaling.

Thus, it is still important to observe the fouling behavior under the high-recovery operation [210], similar to that proposed in this study, in order to optimize the scaled-up membrane operation.

8.3.2 *Scale-Up Design and Operating Cost of the Proposed Vibratory NF System*

The scale-up design of the NF-based dewatering alternative was based on the i84 VSEP membrane filtration system. The commercial filtration system has membrane area options up to 139.4 m^2 (1,500 ft^2) and is suitable for large feed rates up to 408,000 L d^{-1} [144]. The system is a vertical membrane module system atop a frame housing the drive system and control skids that allow the control of operating pressure, temperature, conductivity, pH, vibration, and chemical dosing. Each module houses a cylindrical filter pack consisting of hundreds of flat membranes, each supported by a tray. The vertical stack design can be rated for indoor or non-extreme outdoor conditions due to the smaller plant footprint of the system than conventional systems. More importantly, the smaller footprint strategically allows the process to be integrated into systems commonly limited by floor space.

Upon factoring an uncertainty of 0.5 to the average permeate flux at high-recovery, the design flux for the proposed NF system was equivalent to 43.7 L m^2 h^{-1}. This design flux is lower than those estimated in vibratory NF systems designed for soluble coffee wastewater reclamation [51]. As coffee extracts are concentrated, it is expected that process designs in this study would be larger and more expensive. Correspondingly, a 3-module system with a membrane area of 93 m^2 or 1000 ft^2 per module and a total capital cost of $900,000 was calculated. At the given operating conditions, the corresponding daily energy requirement is approximately 888 kWh d^{-1} at an estimated cost of $73 per day. Additional costs for membrane replacement at $88 per day and the cost of cleaning chemicals at $5 per day were also added as maintenance costs. Overall, the estimated annual operating cost for the VSEP NF system is $60,500 per year that is substantially smaller than that estimated for an evaporator system at approximately $416,500 per year.

However, feed coffee extract concentrations can influence the applicability of the proposed membrane alternative since the basis of the design calculations was the design flux. Thus, using the modified concentration studies, scale-up designs and operations were also estimated for more concentrated feed coffee extracts, as shown in Table 35.

Table 35

Feed Characteristics and Average Permeate Parameters at Desired Overall Recoveries from Various Feed Coffee Extract Concentrations via Vibratory Nanofiltration

Parameter	Unit	Feed Coffee Extract Concentration (% wt/wt)				
		1%	2%	3%	4%	5%
Feed Characteristics						
Flowrate	L d^{-1}	385,800	393,500	401,700	410,400	419,700
Concentration	g L^{-1}	10.1	20.4	30.9	41.7	52.6
COD	mg L^{-1}	11,180	22,580	34,220	46,100	58,240
Conductivity	µS cm^{-1}	1,540	2,330	3,140	3,960	4,800
Turbidity	NTU	520	1,040	1,580	2,140	2,700
Average Permeate Parameters						
Permeate flux	L m^{-2} h^{-1}	86.5	47.1	28.5	16.1	8.3
COD	mg L^{-1}	460	670	850	1,000	1,140
Conductivity	µS cm^{-1}	640	1,090	1,560	2,040	2,540
Turbidity	NTU	< 1	< 1	< 1	< 1	< 1
Rejection Relative to Feed Concentration						
COD	%	95.9	97.0	97.5	97.8	98.0
Conductivity	%	58.6	53.2	50.3	48.6	47.0
Turbidity	%	> 99.9	> 99.9	> 99.9	> 99.9	> 99.9

Note: Operating conditions: P = 2.76 MPa, T = 50 °C, F = 54.7 Hz, C_f = 35% wt/wt

From the table, the average permeate flux exponentially decreased with feed coffee extract concentration, and as a result, the average permeate conductivities and CODs increased. This corresponds to a substantial decrease in the average conductivity rejection of the NF membrane. However, the substantially small MWCO of the NF membrane allows above 99% rejection of turbidity. Since this parameter represents a large portion of the coffee extract, the average overall COD rejection was still above 95%, even at high recovery operations.

The higher feed coffee extract concentrations also influenced higher scaled-up operating and capital costs, as shown in Table 36. The design flux for concentrating a 5% coffee extract is 10 times lower than that estimated for a 1% coffee extract that required a larger membrane area for the targeted permeate volumetric flowrate. This large membrane area requirement increases the minimum number of modules for the dewatering operation, thus resulting in higher capital costs. The capital cost has been one of the issues not only for vibratory filtration systems but also for membrane operations, in general, compared to conventional methods such as evaporation [61], [147], [211], [212]. On the other hand, the overall operating cost of the membrane filtration operation also increased with the feed coffee extract concentration.

Table 36

Design, Operation, and Cost Specifications for the Proposed i84 VSEP Nanofiltration System for Various Feed Coffee Extract Concentrations

Scale-up Specifications	Unit	Feed Coffee Extract Concentration (% wt/wt)				
		1	2	3	4	5
Design Parameters [a]						
Design flux	$L\ m^{-2}\ h^{-1}$	43.2	23.6	14.3	8.4	4.1
Membrane area per module	ft^2	1,000	1,400	1,400	1,400	1,400
No. of modules		3	4	7	12	22
Operation and Maintenance [b]						
Feed flowrate	$L\ d^{-1}$	385,800	393,500	401,700	410,400	419,700
Overall recovery	%	98.1	96.2	94.3	92.3	90.2
Ancillary chemicals	$L\ yr^{-1}$	415	550	970	1,660	3,040
Energy requirement	$MJ\ yr^{-1}$	1,065,600	1,289,500	1,945,100	3,032,400	5,198,200
Estimated capital and annual operating costs [c]						
Capital cost	$	900,000	1,200,000	2,100,000	3,600,000	6,600,00
Operating cost	$\$\ yr^{-1}$	26,600	32,200	48,600	75,800	130,000

Note: [a] Membrane type: TS80 (Trisep®, Microdyn-Nadir, Goleta, California)

[b] Operating conditions: P = 2.76 MPa, T = 50 °C, F = 54.7 Hz

[c] Based on target water recovered of 3.79×10^5 $L\ d^{-1}$

Membrane replacement was the highest expense, followed by the electricity cost from pumps and vibratory motors, while membrane cleaning had the lowest expense, as projected in Figure 67. It should be noted that the increase in energy requirement was attributed to the electricity used by the vibratory motor. This power requirement also increases with feed coffee extract concentration, as processing higher-strength coffee extracts need more membrane modules. For a 1% coffee extract, the power requirement of the vibratory motor is twice that of the power requirement of the pump for a 3-module membrane system. On the other hand, the relatively larger membrane system required to concentrate a 5% feed coffee extract will require vibratory power that is 12 times that of the flow pump, increasing the operating cost. Even so, this energy requirement is still lower than the cost of membrane replacement. The overall operating cost of the NF operation is strongly attributed to the annualized cost of membrane replacement, considering the increasing ratio between membrane replacement cost and electricity cost for higher-strength coffee extracts. This observation limits the vibratory NF operation as the estimated overall operating cost of this alternative becomes almost equivalent to that of thermal evaporation when the feed coffee extract concentration approaches 5% wt/wt.

Figure 67

Scaled-Up Operating Costs of the Proposed Vibratory Nanofiltration Operation in Comparison with Thermal Evaporation in Preconcentrating Various Feed Coffee Extract Concentrations to 35% (wt/wt)

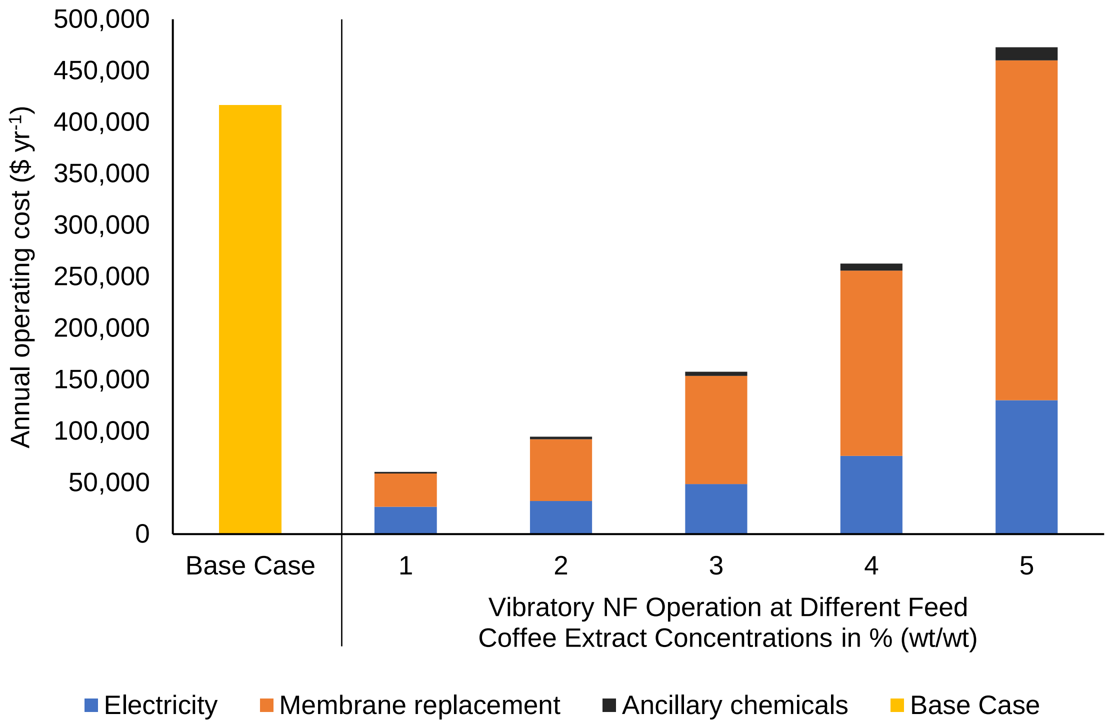

The increase in capital and overall operating costs of the membrane-based dewatering alternative was a result of the drastic decrease in design flux that required a higher membrane area, hence, number of membrane modules for the scaled-up operation for both capital acquisition and routine replacement. Overall, these estimated costs limit the feasibility of the proposed membrane operation. As a rate-dependent operation, improving the design flux of the proposed vibratory system can further make the process less expensive. Developing NF membranes with higher flux specifications may improve these estimated costs [119], [213]. However, while this may seem like a long term solution, flux-enhancing membrane modification may lead to lower component rejection efficiencies [94]. The calculated energy requirement of the membrane operation remained to be substantially lower than that required for evaporator operation. As a result, the increase in the electricity cost of the proposed vibratory NF would not be as significant as membrane replacement costs. Considering these trade-offs from the recovery system, thus, a more comprehensive economic assessment was employed.

8.3.3 *Water Reuse Options for Permeate Recovered*

Despite the high rejection efficiencies, the NF permeate may still have residual coffee extract components, present as dissolved organic and inorganic ions, based on the average permeate COD and conductivities. Higher feed coffee extract concentrations also decrease the quality of permeate recovered and may limit reusability. The U.S. Environmental Protection Agency (US EPA) sets different water reclamation guidelines for urban reuse, irrigation, industrial operations, groundwater recharge, and for drinking purposes [139]. For food and beverage industries, industrial water reuse in ancillary plant operations range from intermediate to potable water quality to minimize the risks of corrosion, scaling, accumulation of dissolved components, and contamination when reused [139], [214]. Reclaimed water of intermediate quality may be reused for heating, cooling, and in transporting products from one process to another; or in cleaning and rinsing operations; while softened water is applicable as boiler feed [215]. Specifically, water directed for cooling tower reuse requires pH between 6 to 9, biological oxygen demand (BOD) less than 30 mg L^{-1}, and total suspended solids (TSS) below 30 mg L^{-1}; while boiler feedwater has maximum limits of 15 mg L^{-1} TSS, with conductivity between 1,100 to 5,400 µS cm^{-1} [139]. Thus, based on Table 35, the permeate recovered from the proposed vibratory NF of the coffee extract may be suitable as boiler water, but may require additional treatment when directed for cooling tower reuse. When reused as a manufacturing ingredient, or as a solvent for extraction, the NF permeate would further require supplemental treatment to meet the potable water reuse specifications of the US EPA. The NF permeate would also require an extensive analysis of its alkalinity, silica content, total dissolved solids, mineral content, hardness, oily matter, microbial content, total organic content, and meet other water reuse specifications, as applicable. Additionally, it is also recommended to perform a thorough analysis of the important coffee extract components in the permeate.

Integrated membrane operations may be employed in meeting the US EPA guidelines. For example, a thickening step via MF or UF prior to NF operation, similar to those conducted for waste coffee grounds [207], may be employed to improve the quality of the NF permeate. Another option is to recover the residual coffee extract components from the NF permeate by RO, similar in high-purity water recovery from dairy processing [8], [216], [217] or by osmotic evaporation [218]. The recovered components such as phenolic compounds may then be used in the enrichment of the final soluble coffee product [24], while the water recovered may be reused for ancillary plant operations.

However, these integrated membrane operations entail additional capital and operating costs, and may only be applicable when the water recovered is obtained from wastewater treatment operations, where the waste stream is more dilute. Such is the case of a parallel study by Wisniewski et al. [51] employing vibratory NF on soluble coffee wastewater to recover water that may be reused for cooling tower operations. As in this study, since the NF permeate is recovered from upstream plant operations, water reuse should not be as stringent as those provided in US EPA guidelines that presume water reclamation from downstream waste effluents. In addition, while the NF permeate may be directed as boiler feedwater, this water reuse option would only result in coffee extract losses since the permeate may consist of essential components such as chlorogenic acids, caffeine, and other phenolic compounds. Directing the permeate from the single-step NF operation for coffee extraction would be a more attractive option for reuse to prevent losses in coffee extract components [33]. This study employed this water reuse option in the assessment of the process; however, additional study may be recommended to assess the effect of the NF permeate on coffee extraction. Nonetheless, the water recovery routes from coffee extract preconcentration and soluble coffee wastewater reclamation presents a substantial advantage in minimizing the operating costs and environmental impacts of the soluble coffee process.

8.3.4 *Economic Feasibility*

The capital and operating costs of the scaled-up vibratory NF process are among the important indices evaluated for the proposed dewatering alternative. The overall operating cost savings and its long-term economic impact of the proposed system in the soluble coffee production process should also be assessed. For the results of the economic assessment, Figure 68 shows a comparison of the overall operating costs between the base case and the proposed alternative cases, while Table 37 shows the feasibility of each case based on economic metrics.

Figure 68

Overall Operating Costs and Savings of Base Case and Each of the Alternative Case

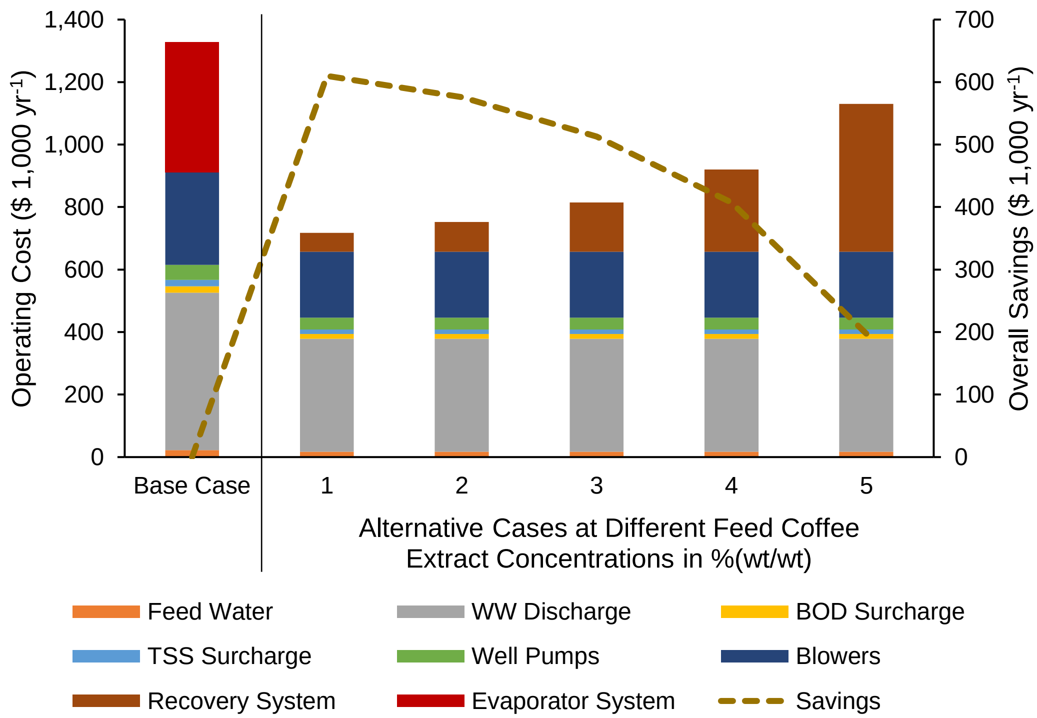

Table 37

Calculated Economic Metrics for Proposed Integrated Vibratory Nanofiltration Operations in Soluble Coffee Production at Various Feed Coffee Extract Concentrations

Economic Metric	Unit	Feed Coffee Extract Concentration (% wt/wt)				
		1	2	3	4	5
Capital Cost	$	900,000	1,200,000	2,100,000	3,600,000	6,600,000
Savings	$ yr^{-1}	579,000	545,000	481,900	376,800	166,800
IRR	%	57.3	39.5	16.8	1.2	(14.7)
ROI	%	54.3	38.9	20.7	10.7	4.2
Payback time after tax	yr	2.5	3.8	10.3	-	-
10-yr NPV	$	1,604,800	1,198,000	139,200	-	-

Note: Based on target water recovered of 3.79×10^5 L d^{-1}

For the analysis, only the process costs within the boundaries of the scope alternative process were considered since those outside the scope, such as process costs of roasting, extraction, and dehydration, were assumed constant. As shown in Figure 68, apart from the operating cost of the vibratory NF system, the combined economic benefits or gross savings from the reduction of freshwater usage from water reuse (~0.4%), electricity used by well pumps and aeration blowers for wastewater treatment (~5.3%), surcharges for wastewater disposal (~12.7%), and energy consumption from dewatering (< 47%) affect the proposed process intensification. Among these costs, substantial savings from the reduced costs of wastewater discharge, and dewatering the coffee extracts, can be observed. Recirculating the water recovered from the vibratory NF operation for reuse in coffee extraction decreases the volume of pretreated wastewater discharged to municipal wastewater treatment facilities or the environment. Additionally, steam generation for thermal evaporation is diverted to the electricity cost of the proposed vibratory NF operation, and considerably reduces the energy cost of dewatering. Dewatering a 1% feed coffee extract saves at least 47% of overall process costs. However, processing higher-strength coffee extracts tend to diminish these savings due to the increased electricity and membrane replacement costs. Above feed concentrations of 5%, only savings from wastewater discharges (~17%) are projected to be saved from the overall operation.

An economic feasibility assessment was conducted to determine the return on investment, payback period, and other economic metrics indicative of the profitability of each alternative case. As presented in Table 37, the increase in capital cost and the corresponding decrease in the estimated savings as a consequence of concentrating higher-strength coffee extracts, have a major influence on the feasibility of the proposed dewatering alternative. Smaller module systems tend to have more favorable economic metrics, which makes the dewatering alternative more attractive for feed coffee extract concentrations less than 3%. A 7-module commercial-scale i84 VSEP filtration system with a capital cost of $2,100,000 can concentrate 3% wt/wt feed coffee extract to 35%. On the other hand, the recovered 378,500 L d^{-1} of reusable water from the low-energy dewatering operation projects $481,900 of savings per year. These annualized costs and savings render an ROI of 21% for a reasonable payback period of 10 years.

8.3.5 *Environmental Emissions*

The low-energy requirement of the proposed vibratory NF, along with its capacity to generate reusable water, have substantial environmental benefits. These benefits were quantified as environmental emissions to air, soil, and water of processes within the selected life cycle boundaries of this study. The emission factors associated to each of the alternative case and in comparison with the base case are shown in Table 38. Figure

69 shows a comparison of the CO_2 emissions of the base case and alternative cases relative to the process components involved. Air emissions constitute largely both base (98.2%) and alternative cases (~97.6%) with CO_2 contributing to about 99.21% of the total air emissions. The alternative cases has a potential to reduce environmental emissions by about 37.2% to 40.1%, owing to the impact of water recovery from the membrane-based preconcentration of coffee extracts that reduced feed water usage, steam consumption, and wastewater generation, treatment, and discharge. These reductions translate to lesser greenhouse gas impacts in the environment of the soluble coffee process.

Table 38

Comparison of Life Cycle Emissions Associated with the Base Case and Each of the Alternative Case in Terms of Emission Factors

Emissions	Unit	Base Case	Alternative Cases in Terms of Feed Concentration in %				
			1	2	3	4	5
Total Air Emissions	kg	1.80E+07	1.08E+07	1.08E+07	1.08E+07	1.10E+07	1.12E+07
CO_2	kg	1.79E+07	1.07E+07	1.07E+07	1.08E+07	1.09E+07	1.11E+07
CO	kg	3.07E+03	1.46E+03	1.48E+03	1.53E+03	1.62E+03	1.80E+03
CH_4	kg	2.29E+04	1.34E+04	1.35E+04	1.39E+04	1.45E+04	1.58E+04
NO_X	kg	2.84E+04	2.05E+04	2.05E+04	2.06E+04	2.06E+04	2.08E+04
NMVOC	kg	7.34E+02	5.47E+02	5.55E+02	5.78E+02	6.16E+02	6.92E+02
Particulate	kg	1.73E+03	1.31E+03	1.32E+03	1.33E+03	1.36E+03	1.41E+03
SO_2	kg	2.44E+04	1.79E+04	1.81E+04	1.88E+04	1.99E+04	2.21E+04
Total Water Emissions	kg	3.55E+05	2.63E+05	2.67E+05	2.78E+05	2.96E+05	3.33E+05
VOCs	kg	5.84E-01	3.36E-01	3.44E-01	3.70E-01	4.12E-01	4.97E-01
Total Soil Emissions	kg	2.24E+02	1.18E+02	1.18E+02	1.19E+02	1.20E+02	1.23E+02
Total Emissions	kg	1.84E+07	1.10E+07	1.10E+07	1.11E+07	1.12E+07	1.15E+07

Figure 69

Comparison of Life Cycle CO_2 Emissions Associated with the Base Case and Each of the Alternative Case in Terms of Process Components

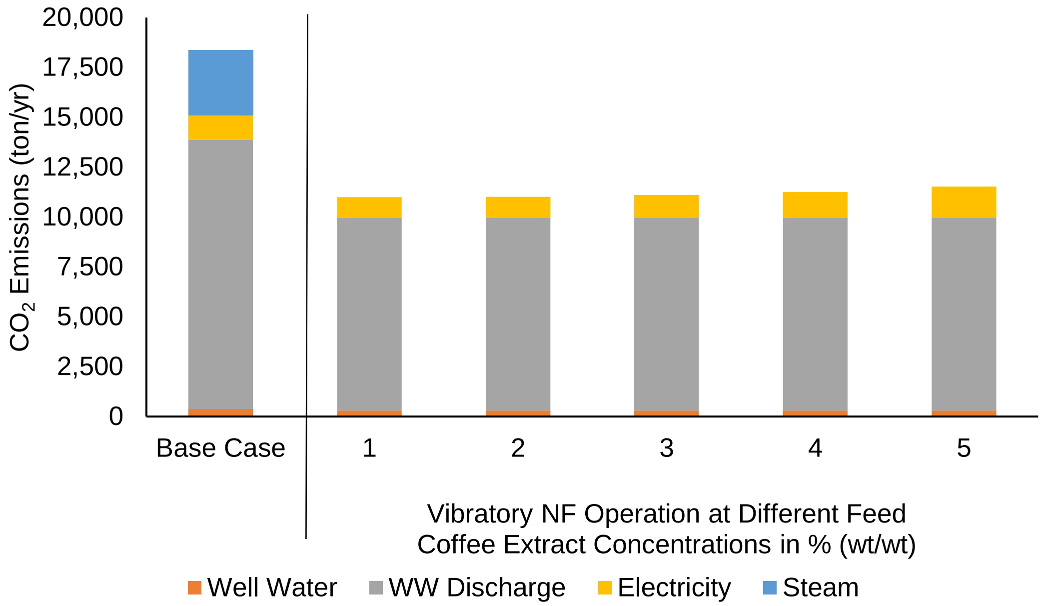

In both cases, the bulk of the life cycle emissions are still largely associated with the environmental impact of wastewater directed to the public authorities for further treatment, as shown in Figure 69. However, a membrane-based water recovery reduces the emissions from wastewater discharge by about 21% of the base case emissions, highest contributor among the process components. This reduction is due to the reuse of about 378,500 L d^{-1} of recovered water from the membrane system that minimized the generation, treatment, and discharge of wastewater from soluble coffee production. Despite the reduction of emissions from steam generation, the wastewater generation, treatment, and discharge still account for the 84% to 88% of the environmental emissions. This large allocation on emissions reflects that additional wastewater minimization approaches through water recovery and reuse may still improve the environmental impact soluble coffee process. On the other hand, about 3,300 tons yr^{-1} of CO_2 emissions can be avoided (or 18.3% of the base case emissions) by recovering 378,500 L d^{-1} of water using the proposed membrane system, and cut-down steam consumption in thermally preconcentrating coffee extracts. The increase in emissions in the alternative cases was attributed to the electrical consumption of larger vibratory NF systems designed for processing higher strength coffee extracts. However, despite these increases for the recovery system, the environmental emissions related to the combined electricity usage of pumps and blowers only constituted to about 7.5% to 11% of the total emissions of the alternative cases. This relative impact is still small compared to the significant emission reduction attributed to the reduction in steam consumption and wastewater generation. Thus, overall, the proposed water recovery alternative positively impacts the environmental emission reduction of the soluble coffee process.

Chapter 9

Conclusions

The vibration shear-enhanced filtration is a promising technology that can further membrane applications high-fouling streams such as those of the food and beverage industry. In particular, as a supplement to thermal evaporation, the integration of the membrane system can strategically present opportunities for water recovery and reuse, energy usage reduction, and wastewater minimization. In this dissertation, the potential of a vibratory membrane-based water recovery from preconcentrating coffee extracts for soluble coffee production was investigated using parametric studies, mathematical modeling, optimization, and techno-economic and environmental assessment. NF using TS80 membrane was selected from membrane screening studies, based on the levels of permeate flux, permeate quality in terms of turbidity, conductivity, absorbance, and COD, and corresponding rejection efficiencies. The performance of CF and vibratory NF was evaluated at different operating conditions for feed concentration, applied TMP, and vibratory settings.

Parametric studies in Chapter 5, showed that vibration significantly enhanced the permeate fluxes by about 2 to 3 times that of conventional CF filtration and alleviated flux decline to favor process economics. The torsional oscillations generated membrane surface shear rates from 20,000 s^{-1} to 106,000 s^{-1} within the range of vibratory frequencies of 53.3 Hz to 54.7 Hz and corresponding oscillatory displacement of 0.64 cm to 3.18 cm. The power-law model correlated the permeate fluxes with the surface shear rates generated during the vibratory operation and the relation of model parameters for the system were comparable with other high-shear dynamic systems. However, while small displacements from module vibration contributed greatly to flux enhancement, the mechanisms for membrane separation were still influenced by the other operating parameters. The applied TMP served as the driving force for convection that also increased the permeate flux of the operation. However, along with feed concentration, increasing applied TMP also promoted concentration polarization and high osmotic pressure effects that reduced the effective TMP of the CF and vibratory NF operation. These limited the high flowrate NF operation indicating critical flux conditions. While the operation effectively rejected suspended and colloidal solids (>99.9%), color (~100%), and COD (>95%), dissolved organics and ions smaller than the cut-off pore size of the TS80 membrane (150 Da) were observed to be partially rejected depending on the operating conditions, ranging from 44% to as high as 99.6%. In addition, the concentration polarized region near the membrane surface increased with feed concentrations. This increase resulted in an added a layer of resistance that caused higher rejection of coffee extract components during NF operation. Vibrations also improved the rejection efficiency of the process due to the high-shear regions on the membrane surface that reduced concentration polarization. However, the applied TMP forced the dissolved solids through the membrane by convection and resulted to lower conductivity and COD rejections. On the other hand, concentration polarization from higher feed concentrations added a layer of resistance that improved the conductivity and COD rejections of the membrane.

Different approaches for modeling the performance of the vibratory NF operation were also introduced in Chapters 6 and 7 for the preconcentration of coffee extracts. Despite the unique dynamic nature of the membrane system studied, the semi-empirical resistance-in-series mathematical model proposed in Chapter 6 can be employed not only to predict fluxes and rejection efficiencies, but it also provided additional information on mass transfer mechanisms, osmotic pressure effects, and fouling resistances by feed concentration, TMP, and module vibrations. For instance, at low feed concentrations, the resistance attributed to the osmotic pressure on the membrane surface controls the permeate flux of the operation. However, increasing feed concentrations and TMPs increased the influence of concentration polarization driven resistance that exceed those of osmotic pressure, and resulted in lower fluxes. Further, while membrane surface concentrations and fouling resistances under vibratory NF were significantly lower than those of CF filtration, the correlation showed that vibration had the least impact among the three operating conditions studied. Statistical models obtained from multivariable regression support the relative impacts of feed concentration, applied TMP, and vibratory frequency, along with their interactions on vibratory NF performance, as detailed in Chapter 7. The response surface methodology provides an alternative, and a simpler approach to model and optimize the vibratory NF operation.

In Chapter 8, the film layer model correlation was used in a modified concentration study to scale-up parameters and average permeate flux and characteristics for a high-recovery vibratory NF operation. Substantial rejection of turbidity and COD are achievable, based on calculated average permeate characteristics. However, as a result of the lower capacity of NF membranes to reject multivalent ions in comparison with RO membranes, the conductivity rejection for the scale-up operation was only projected to approach 50%. Nonetheless, the permeate that passes through the NF membrane still consist of valuable coffee components that may be recirculated back to the coffee extraction step to avoid losses. Scale-up operations based on the vertical module i84 VSEP commercial filtration systems were also determined for various feed coffee extract concentrations, to determine the applicability of the proposed membrane-based dewatering alternative in soluble coffee production. Higher feed concentrations resulted in lower design fluxes, requiring larger vibratory NF systems in terms of membrane area and number membrane modules, and thus, higher capital costs. The larger process also substantially increased the annualized operating cost of the vibratory NF system due to membrane replacement. Nonetheless, the energy consumption of the vibratory NF system from electric pumps and vibratory motors shown to be considerably lower than that consumed by thermal evaporation from steam generation. Overall, the proposed vibratory NF system promotes water reuse, producing a maximum of 47% cost savings from the reduction of freshwater usage, wastewater treatment and disposal, energy consumption relative to the base case. However, due to the effect of high feed coffee extract concentrations on operational efficiency, the proposed alternative system may only be limited to low-strength coffee extracts of less than 5% wt/wt. Economic feasibility assessment presented favorable economic metrics for small vibratory membrane module systems for feed coffee extract concentrations less than 3% wt/wt. These cases are projected to be within a reasonable payback period of 10 years.

Chapter 10

Recommendations for Future Work

10.1 Recommendations on Improving the Mathematical Models

In this dissertation, the mathematical models developed using the results from parametric experiments were based on two approaches via (a) response surface methodology, a statistical modeling approach; and (b) semi-empirical modeling using theoretical membrane filtration models – concentration polarization, osmotic pressure, and resistance-in-series. These approaches established the relationship of operating factors (feed coffee extract concentration, transmembrane pressure, and vibratory settings) with process performance (permeate flux, quality, and rejection efficiencies), as well as flow and mass transfer properties (boundary layer concentrations, real rejection, and fouling resistances). Moreover, the models developed from this study provided an alternative perspective on evaluating vibratory membrane performance, particularly VSEP, in contrast with the conventional power-law relationship between flux and vibratory surface shear rates found in literature.

Despite the contribution, it is important to note that the models are still limited and may require further improvement. For instance, the statistical models developed from multivariate regression in Chapter 7 only provide optimum conditions based on known operating parameters and may be limited when taking into account mass transfer mechanisms of membrane separation. Thus, while the models provide an insight on the effects of operating conditions and their interaction on membrane performance, sufficient theoretical background and principles are still needed to support the results. On the other hand, the osmotic pressure calculations used to establish the semi-empirical model in Chapter 6 assumes ideality where osmotic pressure linearly varies with concentration. While the ideal assumption was valid when considering the relatively dilute concentrations of the coffee extracts in the bulk phase of the fluid, membrane surface concentrations were considerably high, which may cause the van't Hoff equation to be less accurate in approximating the osmotic pressure difference. Alternative calculations of this parameter using non-ideal basis may be employed to improve the model, such as the virial osmotic pressure equation [219]–[221].

$$\pi = RT\left(\frac{C_i}{M} + BC_i^{\,2}\right) \tag{100}$$

Experimental determination of osmotic pressure of various coffee extract concentrations at different pH is recommended to determine the second osmotic pressure virial coefficient (B) [222]. Nonetheless, despite their limitations, the alternative models provide a sufficient basis on concentration polarization, osmotic pressure effects, and fouling resistance to manage membrane fouling in vibratory systems.

The investigation of additional parameters like pH, temperature, feed flowrates is also recommended for future studies to provide a more realistic approach when developing the models, likewise, screen such parameters that may have minimal effects on the vibratory membrane performance. One of our recent and ongoing attempts to improve the mathematical model was by additionally investigating the effect of varying feed flowrates on the vibratory NF performance. This study was interested in determining if feed flowrates will contribute to the vibratory NF performance along with operating pressures and module vibrations based on velocity variation experiments. CF and vibratory NF experiments, using the TS80 NF membrane, were conducted for low-strength feed coffee extract (Co = 8.5 g L^{-1}) at various feed flow rates (1.89 L min^{-1} to 15.1 L min^{-1}), applied TMP (1.03 MPa to 3.79 MPa), and vibration settings (0 Hz, 53. 3 Hz to 54.7 Hz frequency; or 0 cm, 0.64 cm to 3.18 cm displacement). In the same approach, the membrane filtration performance was evaluated based on permeate flux, characteristics (turbidity, absorbance, conductivity, and COD), and corresponding observed rejection efficiencies. At present, results of the parametric study show that higher feed flow rates increased the permeate flux and rejection efficiencies under non-vibratory CF operations. This trend indicates the contribution of increasing CF velocities to higher membrane surface shear rates during CF operations. Despite the flux enhancement, fouling resistances under CF operation were still 3 to 5 times higher than those observed under vibratory NF operation. On the other hand, the flux enhancement effect of increasing feed flow rates appeared to have diminished under vibratory NF configuration. Among the three parameters, the feed flow rate parameter had the least, or presumably negligible, effect on permeate flux. However, these results are still inconclusive, so far, and further analyses such as semi-empirical model fitting and statistical tests, are still being conducted to support the findings. Nonetheless, these research efforts and information may be helpful in guiding parallel studies on vibratory, or dynamic membrane systems.

10.1.1 *Modeling Vibratory NF by Computational Fluid Dynamics*

Another alternative approach that may be explored in predicting the vibratory membrane system performance is by employing computational fluid dynamics (CFD). The CFD method is becoming a ubiquitous tool in numerically solving different types of fluid flow problems including membrane separations [182]. The idea is to develop the partial differential equations governing the fluid flow regime of the membrane system from a transport phenomenon standpoint (continuity and Navier-Stokes equations) [174]. Given the appropriate assumptions and boundary conditions for the model, CFD uses discretized algebraic expressions to approximate the solution of the differential equation. The technique circumvents the rigorous computational requirement by using computer-aided numerical solving tools, without relying heavily on parametric experiments.

Despite the attractiveness of the method, the underlying consequences from the dynamic nature and module flow patterns of the current VSEP system, as well as of other dynamic membrane configurations, challenge this method in modeling the process. A careful description of the VSEP apparatus including annular flow geometry and dimensions of the membrane module, vibration mechanism, and flow regime must be considered [174]. An appropriate calculation mesh should also be selected. For example, an initial study to solve the structure of shear-enhanced flow on a vibrating membrane surface under VSEP operation used a rectangular parallel piped calculation domain since one portion of the circular membrane was assumed as a vibrating rectangle that served as the basis for setting up the differential continuity and Navier-Stokes equations [60]. The radial geometry for the hydrodynamic analysis of the azimuthal flow on the annular membrane channel of the VSEP [2] also appears to be a more appropriate model that may be recommended for CFD modeling. This type of investigation may be a significant undertaking on its own, and may make a worthy follow-up research activity.

In the studies conducted so far, the flow profile within the vibratory membrane is presumed to be the same for both laboratory-scale, and larger-scale (pilot and commercial) VSEP filtration system [2], [60]. In this assumption, the flow profile in the laboratory-scale VSEP system represents one of the membranes found in the pilot- and commercial-scale set-ups, and this relationship is used as the basis to set-up the pertinent hydrodynamic and mass transfer equations that may be evaluated using CFD. The oscillatory movement of the vibrating membrane module also suggests that the flow pattern is time dependent, as were shown in Equations 24 and 25, that further adds uncertainties to local velocities and shear stresses.

$$V(y,t) = r\,\Omega\left[e^{-\sqrt{(Re/2)y}}\cos\left(2\pi Ft - \sqrt{(Re/2)y}\right) + e^{-\sqrt{(Re/2)(1-y)}}\cos\left(2\pi Ft - \sqrt{(Re/2)(1-y)}\right)\right] \tag{24}$$

$$\Upsilon_w(r,t) = \frac{2r\theta(\pi F)^{1.5}}{\nu^{0.5}}\left[\cos(2\pi Ft) - \sin(2\pi Ft)\right] \tag{25}$$

Despite the availability of experimental approaches to determine local velocities and shear stresses via particle tracking, molecular tagging, laser Doppler anemometry, and electrochemical methods in some dynamic membrane systems [174], such measurements must be employed at least 1 mm from the membrane surface that makes CFD a convenient alternative to clarify the flow characteristics on the membrane surface [60]. Equations 24 and 25 are “periodic steady state” solutions where the fluid particles exhibit sinusoidal oscillations with the resonant frequency at a given amplitude [223]. In CFD calculations, local velocities and shear rates from unsteady state flow may be solved using a selected “time step” at different radial and horizontal positions. Velocity distribution simulations on the membrane surface may then be used to approximate the velocity boundary layer thickness, and average vibrating velocities that may be correlated with permeate fluxes [60].

10.1.2 *Modeling NF Rejection Mechanisms*

The results presented in this dissertation promote the use of NF for water recovery operations in food and beverage production. In the future, more effective NF membranes may be developed, and the technology can be improved to dramatically lower the costs of the operation. Thus, the potential for vibratory NF applications can be extended to different industrial applications. Furthermore, the mathematical models developed for vibratory NF operations can be improved upon by focusing on the rejection mechanisms, since the unique structural characteristics of NF membranes sets them apart from UF, MF, and RO membranes. While most membranes are characterized based on their effective pore sizes and molecular weight cut-offs, NF membranes exhibit pore-flow-like mechanisms comparable with porous UF membranes, but at the same time solution-diffusion mechanism like those of RO membranes [94]. Another important characteristic of most NF membranes is their surface charge that may be due to the dissociation of functional groups from the membrane, and adsorption of charged species from solution [173]. Thus, separation principles for NF membranes are particularly interesting as they employ steric exclusion of uncharged species, and electrostatic exclusion of charged species like ions.

The rejection efficiencies discussed in Chapter 5 only presented the influence of permeate fluxes on the transfer of coffee extract components through the NF membrane. However, rejection efficiencies at various operating conditions indicate the formation of an additional layer of resistance that affected the transfer of dissolved components across the membrane. However, the feed and permeate characterization methods were non-specific that limited the analysis of rejection efficiencies of the NF membrane. It is interesting to investigate the various mechanisms that could have affected the performance of the vibratory NF operation for the development of a water recovery strategy. Apart from membrane selection, or improvement of operating conditions, the optimization of the NF process requires a fundamental understanding of the extent of different mechanisms, chemical or physical, governing the capacity of NF membranes to reject coffee extract solutes.

The Donnan Steric Pore model (DSPM) developed by Bowen et al. has been particularly useful in modeling the retention properties of NF membranes [168]. The model is based on the extended Nernst-Planck equation that accounts for the neutral conditions inside the membrane, combined with the Donnan equilibrium to describe the partitioning of components on both solution and membrane interfaces, as shown in Equation 101 [173].

$$J_s = \left(-D_{i,p}\frac{dC_i}{dx}\right) - \left(D_{i,p}z_iC_i\frac{F_c}{RT}\frac{d\psi}{dx}\right) + \left(K_{i,c}C_iJ_v\right) \tag{101}$$

Various model parameters are accounted in the model, including hindered diffusivity ($D_{i,p}$), hindrance factor for convection ($K_{i,c}$), concentration of solute at the membrane surface (C_i), valence of solute (z_i), electric potential (ψ), permeate flux (J_v), Faraday's constant (F_c), temperature (T), and gas constant (R). From these considerations, the mechanism of solute transport across the membrane can then be described by diffusion, electromigration, and convection [94]. The model may also be simultaneously solved with concentration polarization film theory, combined with the underlying flow properties of a dynamic vibratory membrane operation. Apart from predicting solute flux and corresponding rejection, the model can possibly be applied to understand the dominant mechanism for solute transport at different conditions. Detailed characterization of coffee extract solutions using more specific conductivity measurements, and membrane properties (pore size, thickness, porosity, effective charge density) are among the important considerations to conduct for this type of study. The role of pH is also important in understanding the transport of inorganic solutes and organic acids through the NF membrane. Accordingly, surface charges on NF membranes are influenced by feed pH, and concentration of electrolytes, that altogether affect the electrokinetic transport of constituents [224]. Extensive characterization of the feed coffee extract in terms of charged and uncharged constituents will play an important role in fitting the experimental data with the DSPM correlation to improve the predictability of solute rejection. Overall, the model developed from the solute rejection standpoint of the NF membrane can additionally provide additional perspectives useful for practical membrane applications such as optimization and scale-up design of the vibratory NF system.

10.2 Characterization of Fouling Mechanism and Membrane Cleaning Approaches

10.2.1 *Characterization of Membrane Fouling Mechanism*

The vibratory membrane system effectively reduced the concentration polarization and osmotic pressure effects of the CF filtration operation. This enabled an effective enhancement of flux, with high stability that can be sustained for longer periods than those observed under non-vibratory operations. Even so, the complexity of the components in the coffee extract can still be further investigated in terms of the fouling mechanisms that may occur despite the enhancement of membrane surface shear via vibratory operation. Dissolved, colloidal, and suspended organic and inorganic constituents may still affect the membrane performance, especially as coffee extracts become more concentrated during preconcentration operation. Under poor operating conditions (high feed concentration, low effective TMP), these constituents can still result in the irreversible decline in membrane performance that can increase the need for membrane replacement. As presented in Chapter 8, the highest operating cost was attributed to membrane replacement that cost at about $75,000 for each 1400-ft^2 membrane module replaced every five years. Thus, the determination of an optimal operation, whereby irreversible fouling is avoided, can be very helpful in prolonging the usage life of the membrane and reduce membrane replacement costs.

Coffee extract constituents can affect membrane performance either by cake formation or pore blocking, organic adsorption onto membrane surface [128], gel layer formation, scaling [116], or by biofouling, as the highly organic nature of the coffee extracts can attract microorganisms that can contaminate the operation [94], [119]. Experimental investigation of membrane fouling using the protocol presented in Figure 12, may be implemented to characterize the reversibility of fouling under vibratory operation. This protocol consists of water tests, solution filtration, physical cleaning, and chemical cleaning studies quantify irreversible and reversible fouling in the vibratory membrane operation [123]. Scanning electron microscopy (SEM) may also be a useful tool in assessing the degree of fouling on a microscopic level, since some foulants, though are not readily visible can still drastically affect membrane performance. In addition, SEM can provide a better understanding of the fouling mechanism based on the morphology and structure of the fouled membrane [99]. The fouling mechanisms, such as scaling, may also be mathematically modeled based from flux time-profiles generated from filtration experiments [225]. Overall, an extensive assessment of these potential fouling mechanisms occurring in the vibratory filtration of coffee extract can be helpful in further minimizing the adverse effects of fouling on the NF membrane, and therefore, reducing membrane replacement costs.

10.2.2 *Optimization of Cleaning Operation for Vibratory Membrane Applications*

Related to the reduction of membrane replacement costs is optimizing membrane cleaning within the membrane life cycle. Physical cleaning methods like backflushing, forward flushing, and vibrations; and chemical cleaning methods with the use of alkaline solutions, acids, and active enzymes can be considered in the cleaning operations to address different fouling mechanisms and foulant types affecting the vibratory membrane operation [99]. While the cleaning protocol is usually based on a trial and error approach, the experimental methods to develop this protocol are based on the knowledge of foulants involved, degree of fouling, cleaner concentration and efficiency, and the assessment of the possible effects of various cleaners on membrane structure and properties [94]. The cleaning conditions may also be evaluated along with an optimum cleaning interval to maximize the performance of the vibratory membrane operation and usage life, while ensuring that the cost attributed to the frequency of cleaning is within a reasonable value [114]. Cleaning at the initial stage of fouling, or on a regular basis can be considered when selecting the cleaning interval. This interval may also be evaluated by determining critical limits in vibratory membrane operation, e.g., when TMP in constant flux application increases, or when flux decreases below the tolerance level in constant pressure operation [94].

10.3 Industrial Application of Vibratory Membrane Filtration in Soluble Coffee Production

This study demonstrated the benefits and limitations of the vibratory NF operation in preconcentrating coffee extracts for soluble coffee production. Indeed, the dynamic membrane system alleviates flux decline and membrane fouling and the surface shear generated from the vibration contributed to the flux enhancement in contrast with conventional CF filtration. Energy costs from the electricity used by a scaled-up membrane operation were also considerably lower than those that required for steam generation in thermal evaporation. More importantly, the reduced consumption of fresh feed water, due to water recovery and reuse, positively impacts to lower wastewater generation and lower environmental emissions. However, it is important to note that the high investment, and membrane replacement costs limit the industrial application of the vibratory membrane system to low-strength streams. A reduced water recovery flow rate for the membrane-based coffee extract preconcentration step may be recommended to render more favorable economic metrics.

The abovementioned limitation also suggests that the water recovery operation is more attractive when applied in soluble coffee wastewater reclamation, as studied by Wisniewski, et al. [50]-[52]. Compared with coffee extracts, soluble coffee process waste streams have been found to have lower COD, conductivity, and turbidity, that would only require a single module i84 VSEP commercial filtration system to recover the same amount of water for reuse in cooling tower operations [51]. Economic metrics for the wastewater study provide a favorable payback period of 3 years from cost savings due to water recovery. However, like in coffee extract preconcentration, production variability can also pose future challenges to the economics of water recovery operation from soluble coffee wastewater. In this regard, predictive models from this dissertation can be useful in optimizing the process. Results from the coffee extract filtration studies may be extended to the soluble coffee wastewater since, in principle, the components affecting the vibratory membrane operation are similar but, in more dilute concentrations than coffee extracts. Mathematical models may be developed for this purpose to project the membrane performance and determine optimum conditions for the membrane-based wastewater reclamation.

References

[1] A. Cassano and E. Drioli, *Integrated membrane operations in the food production*. Berlin, Germany: De Gruyter, 2014.

[2] O. Al Akoum, M. Y. Jaffrin, L. Ding, P. Paullier, and C. Vanhoutte, "An hydrodynamic investigation of microfiltration and ultrafiltration in a vibrating membrane module," *J. Memb. Sci.*, vol. 197, no. 1–2, pp. 37–52, 2002, doi: 10.1016/S0376-7388(01)00602-0.

[3] L. Fillaudeau *et al.*, "Investigation of rotating and vibrating filtration for clarification of rough beer," *J. Food Eng.*, vol. 80, no. 1, pp. 206–217, 2007, doi: 10.1016/j.jfoodeng.2006.05.022.

[4] A. Cassano, N. K. Rastogi, and A. Basile, "Membrane technologies for water treatment and reuse in the food and beverage industries," in *Advances in Membrane Technologies for Water Treatment: Materials, Processes and Applications*, A. Basile, A. Cassano, and N. K. Rastogi, Eds. Oxford, United Kingdom: Woodhead Publishing, 2015, pp. 551–580.

[5] O. Akoum, M. Y. Jaffrin, and L. H. Ding, "Concentration of total milk proteins by high shear ultrafiltration in a vibrating membrane module," *J. Memb. Sci.*, vol. 247, no. 1–2, pp. 211–220, 2005, doi: 10.1016/j.memsci.2004.09.021.

[6] S. P. Beier and G. Jonsson, "Separation of enzymes and yeast cells with a vibrating hollow fiber membrane module," *Sep. Purif. Technol.*, vol. 53, no. 1, pp. 111–118, 2007, doi: 10.1016/j.seppur.2006.06.019.

[7] C. Brazinha, M. Cadima, and J. G. Crespo, "Valorisation of spent coffee through membrane processing," *J. Food Eng.*, vol. 149, pp. 123–130, Mar. 2015, doi: 10.1016/j.jfoodeng.2014.07.016.

[8] M. Frappart, M. Jaffrin, and L. H. Ding, "Reverse osmosis of diluted skim milk: Comparison of results obtained from vibratory and rotating disk modules," *Sep. Purif. Technol.*, vol. 60, no. 3, pp. 321–329, 2008, doi: 10.1016/j.seppur.2007.09.007.

[9] A. Suárez, P. Fernández, J. Ramón Iglesias, E. Iglesias, and F. A. Riera, "Cost assessment of membrane processes: A practical example in the dairy wastewater reclamation by reverse osmosis," *J. Memb. Sci.*, vol. 493, pp. 389–402, 2015, doi: 10.1016/j.memsci.2015.04.065.

[10] S. S. Madaeni and S. Zereshki, "Energy consumption for sugar manufacturing. Part I: Evaporation versus reverse osmosis," *Energy Convers. Manag.*, vol. 51, no. 6, pp. 1270–1276, 2010, doi: 10.1016/j.enconman.2010.01.002.

[11] L. R. Firman, N. A. Ochoa, J. Marchese, and C. L. Pagliero, “Deacidification and solvent recovery of soybean oil by nanofiltration membranes,” *J. Memb. Sci.*, vol. 431, pp. 187–196, 2013, doi: 10.1016/j.memsci.2012.12.040.

[12] W. Cai, Y. Sun, X. Piao, J. Li, and S. Zhu, “Solvent recovery from soybean oil/hexane miscella by PDMS composite membrane,” *Chinese J. Chem. Eng.*, vol. 19, no. 4, pp. 575–580, 2011, doi: 10.1016/S1004-9541(11)60024-4.

[13] L. Firman, N. A. Ochoa, J. Marchese, and C. Pagliero, “Simultaneous improvement in solvent permeability and deacidification of soybean oil by nanofiltration,” *J. Food Sci. Technol.*, vol. 54, no. 2, pp. 398–407, 2017, doi: 10.1007/s13197-016-2476-5.

[14] I. Vincze, É. Bányai-Stefanovits, and G. Vatai, “Concentration of sea buckthorn (Hippophae rhamnoides L.) juice with membrane separation,” *Sep. Purif. Technol.*, vol. 57, no. 3, pp. 455–460, 2007, doi: 10.1016/j.seppur.2006.06.020.

[15] C. Bhattacharjee, V. K. Saxena, and S. Dutta, “Fruit juice processing using membrane technology: A review,” *Innov. Food Sci. Emerg. Technol.*, vol. 43, no. July, pp. 136–153, Oct. 2017, doi: 10.1016/j.ifset.2017.08.002.

[16] S. Banvolgyi, I. Kiss, E. Bekassy-Molnar, and G. Vatai, “Concentration of red wine by nanofiltration,” *Desalination*, vol. 198, no. 1–3, pp. 8–15, 2006, doi: 10.1016/j.desal.2006.09.003.

[17] J. Luo, L. Ding, Y. Wan, and M. Y. Jaffrin, “Threshold flux for shear-enhanced nanofiltration: Experimental observation in dairy wastewater treatment,” *J. Memb. Sci.*, vol. 409–410, pp. 276–284, 2012, doi: 10.1016/j.memsci.2012.03.065.

[18] M. Bédas *et al.*, “Nanofiltration of lactic acid whey prior to spray drying: Scaling up to a semi-industrial scale,” *LWT - Food Sci. Technol.*, vol. 79, pp. 355–360, 2017, doi: 10.1016/j.lwt.2017.01.061.

[19] S. Moulik, P. Vadthya, Y. R. Kalipatnapu, S. Chenna, and S. Sundergopal, “Production of fructose sugar from aqueous solutions: Nanofiltration performance and hydrodynamic analysis,” *J. Clean. Prod.*, vol. 92, pp. 44–53, 2015, doi: 10.1016/j.jclepro.2014.12.092.

[20] M. Malmali, S. R. Wickramasinghe, J. Tang, and H. Cong, “Sugar fractionation using surface-modified nanofiltration membranes,” *Sep. Purif. Technol.*, vol. 166, pp. 187–195, 2016, doi: 10.1016/j.seppur.2016.04.025.

[21] S. Cartier, M. A. Theoleyre, and M. Decloux, “Treatment of sugar decolorizing resin regeneration waste using nanofiltration,” *Desalination*, vol. 113, no. 1, pp. 7–17, 1997, doi: 10.1016/S0011-9164(97)00110-0.

[22] A. Giacobbo, A. Moura Bernardes, M. Filipe Rosa, and M. de Pinho, "Concentration Polarization in Ultrafiltration/Nanofiltration for the Recovery of Polyphenols from Winery Wastewaters," *Membranes (Basel).*, vol. 8, no. 3, pp. 46–56, Jul. 2018, doi: 10.3390/membranes8030046.

[23] M. Okada, M. A. Rao, J. E. Lima, and M. Torloni, "Energy consumption and the potential for conservation in a spray-dried coffee plant," *J. Food Sci.*, vol. 45, no. 3, pp. 685–688, 1980, doi: 10.1111/j.1365-2621.1980.tb04132.x.

[24] M. P. Corso, J. A. Vignoli, and M. D. T. Benassi, "Development of an instant coffee enriched with chlorogenic acids," *J. Food Sci. Technol.*, vol. 53, no. March, pp. 1380–1388, 2016, doi: 10.1007/s13197-015-2163-y.

[25] O. G. Vitzthum and K. D. Koch, "Process for the preparation of soluble coffee," 1993.

[26] T. A. Weschenfelder, P. Lantin, M. C. Viegas, F. De Castilhos, and A. D. P. Scheer, "Concentration of aroma compounds from an industrial solution of soluble coffee by pervaporation process," *J. Food Eng.*, vol. 159, pp. 57–65, 2015, doi: 10.1016/j.jfoodeng.2015.03.018.

[27] J. Zapata, V. Londoño, M. Naranjo, J. Osorio, C. Lopez, and M. Quintero, "Characterization of aroma compounds present in an industrial recovery concentrate of coffee flavor," *CYTA - J. Food*, vol. 16, no. 1, pp. 367–372, 2018, doi: 10.1080/19476337.2017.1406995.

[28] L. Wang, "Energy efficiency technologies for sustainable food processing," *Energy Effic.*, vol. 7, no. 5, pp. 791–810, Oct. 2014, doi: 10.1007/s12053-014-9256-8.

[29] J. Warczok, M. Ferrando, F. López, and C. Güell, "Concentration of apple and pear juices by nanofiltration at low pressures," *J. Food Eng.*, vol. 63, no. 1, pp. 63–70, 2004, doi: 10.1016/S0260-8774(03)00283-8.

[30] L. Xu, S. Wang, and X. Zeng, "The maltitol purification and concentration by nanofiltration," *Desalination*, vol. 184, no. 1–3, pp. 295–303, 2005, doi: 10.1016/j.desal.2005.02.064.

[31] Y. K. Ong, H. T. Ng, and T. S. Chung, "A conceptual demonstration of decaffeination via nanofiltration," *Ind. Eng. Chem. Res.*, vol. 54, no. 31, pp. 7737–7742, 2015, doi: 10.1021/acs.iecr.5b01737.

[32] B. Pan, P. Yan, L. Zhu, and X. Li, "Concentration of coffee extract using nanofiltration membranes," *Desalination*, vol. 317, pp. 127–131, 2013, doi: 10.1016/j.desal.2013.03.004.

[33] I. Vincze and G. Vatai, “Application of nanofiltration for coffee extract concentration,” *Desalination*, vol. 162, no. 1–3, pp. 287–294, 2004, doi: 10.1016/S0011-9164(04)00053-0.

[34] S. Sablani, M. Goosen, R. Al-Belushi, and M. Wilf, “Concentration polarization in ultrafiltration and reverse osmosis: A critical review,” *Desalination*, vol. 141, no. 3, pp. 269–289, 2001, doi: 10.1016/S0011-9164(01)85005-0.

[35] M. Y. Jaffrin, “Hydrodynamic Techniques to Enhance Membrane Filtration,” *Annu. Rev. Fluid Mech.*, vol. 44, no. 1, pp. 77–96, 2012, doi: 10.1146/annurev-fluid-120710-101112.

[36] O. Akoum, M. Mercier-Bonin, L. Ding, C. Fonade, P. Aptel, and M. Jaffrin, “Comparison of three different systems used for flux enhancement: Application to crossflow filtration of yeast suspensions,” *Desalination*, vol. 147, no. 1–3, pp. 31–36, 2002, doi: 10.1016/S0011-9164(02)00567-2.

[37] M. Y. Jaffrin, “Dynamic filtration with rotating disks, and rotating and vibrating membranes: An update,” *Curr. Opin. Chem. Eng.*, vol. 1, no. 2, pp. 171–177, 2012, doi: 10.1016/j.coche.2012.01.002.

[38] M. Y. Jaffrin, L. H. Ding, O. Akoum, and A. Brou, “A hydrodynamic comparison between rotating disk and vibratory dynamic filtration systems,” *J. Memb. Sci.*, vol. 242, no. 1–2, pp. 155–167, 2004, doi: 10.1016/j.memsci.2003.07.029.

[39] New Logic Research Inc., “VSEP case studies and application notes,” 2019. https://www.vsep.com/downloads/case-studies-application-notes/ (accessed Sep. 06, 2019).

[40] R. Bian, K. Yamamoto, and Y. Watanabe, “Effect of shear rate on controlling the concentration polarization and membrane fouling,” *Desalination*, vol. 131, no. 1–3, pp. 225–236, 2000, doi: 10.1016/S0011-9164(00)90021-3.

[41] L. Ding, M. Y. Jaffrin, and J. Luo, “Dynamic filtration with rotating disks, and rotating or vibrating membranes,” in *Progress in Filtration and Separation*, S. Tarleton, Ed. London, UK: Elsevier, 2015, pp. 27–59.

[42] S. Kertész, Á. Veszprémi, Z. László, J. Csanádi, G. Keszthelyi-Szabó, and C. Hodúr, “Investigation of module vibration in ultrafiltration,” *Desalin. Water Treat.*, vol. 55, no. 10, pp. 2836–2842, 2015, doi: 10.1080/19443994.2014.940226.

[43] M. Y. Jaffrin, “Dynamic shear-enhanced membrane filtration: A review of rotating disks, rotating membranes and vibrating systems,” *J. Memb. Sci.*, vol. 324, no. 1–2, pp. 7–25, 2008, doi: 10.1016/j.memsci.2008.06.050.

[44] K. Dewettinck and T. T. Le, “Membrane separations in food processing,” in *Alternatives to Conventional Food Processing*, A. Proctor, Ed. Cambridge: Royal Society of Chemistry, 2011, pp. 184–253.

[45] S. Kertész, Z. László*, E. Forgács, G. Szabó, and C. Hodúr, "Dairy wastewater purification by vibratory shear enhanced processing," *Desalin. Water Treat.*, vol. 35, no. 1–3, pp. 195–201, Nov. 2011, doi: 10.5004/dwt.2011.2485.

[46] A. Subramani, J. DeCarolis, W. Pearce, and J. G. Jacangelo, "Vibratory shear enhanced process (VSEP) for treating brackish water reverse osmosis concentrate with high silica content," *Desalination*, vol. 291, pp. 15–22, 2012, doi: 10.1016/j.desal.2012.01.020.

[47] M. D. Petala and A. I. Zouboulis, "Vibratory shear enhanced processing membrane filtration applied for the removal of natural organic matter from surface waters," *J. Memb. Sci.*, vol. 269, no. 1–2, pp. 1–14, 2006, doi: 10.1016/j.memsci.2005.06.013.

[48] X. Su, W. Li, A. Palazzolo, and S. Ahmed, "Concentration polarization and permeate flux variation in a vibration enhanced reverse osmosis membrane module," *Desalination*, vol. 433, no. December 2017, pp. 75–88, 2018, doi: 10.1016/j.desal.2018.01.001.

[49] W. Shi and M. M. Benjamin, "Fouling of RO membranes in a vibratory shear enhanced filtration process (VSEP) system," *J. Memb. Sci.*, vol. 331, no. 1–2, pp. 11–20, 2009, doi: 10.1016/j.memsci.2008.12.027.

[50] C. Wisniewski, M. Savelski, and C. S. Slater, "Eye-opening reuse: Membrane-based water recovery in coffee manufacture," *Water Environment Federation*, no. August, pp. 56–58, 2018.

[51] C. M. Wisniewski, M. V. O. Laurio, C. S. Slater, and M. J. Savelski, "Environmental and process assessment of a vibratory nanofiltration system for the recovery of water from soluble coffee manufacturing waste," *Environ. Prog. Sustain. Energy*, no. March, p. e13425, Apr. 2020, doi: 10.1002/ep.13425.

[52] C. M. Wisniewski, C. S. Slater, and M. J. Savelski, "Dynamic vibratory membrane processing for use in water recovery from soluble coffee product manufacturing wastewater," *Clean Technol. Environ. Policy*, vol. 20, no. 8, pp. 1791–1803, 2018, doi: 10.1007/s10098-018-1569-4.

[53] C. S. Slater, M. J. Savelski, and C. M. Wisniewski, "Integration of Membrane Technology into Coffee Manufacturing Operations for Water Recovery," in *7th International Congress on Sustainability Science and Engineering*, 2018, no. August, pp. 1–23.

[54] J. G. Brennan, "Evaporation and dehydration," in *Food processing handbook*, 2nd edn., J. G. Brennan and A. S. Grandison, Eds. Singapore: John Wiley & Sons, Inc., 2012, pp. 77–130.

[55] P. G. Smith, *Evaporation and drying*, 2nd edn. Boston, MA: Springer US, 2011.

[56] M. V. O. Laurio and C. S. Slater, "Process scale - up , economic , environmental assessment of vibratory nanofiltration of coffee extracts for soluble coffee production process intensification," *Clean Technol. Environ. Policy*, 2020, doi: 10.1007/s10098-020-01931-x.

[57] A. Abdelrasoul, H. Doan, A. Lohi, and C.-H. Cheng, "Mass Transfer Mechanisms and Transport Resistances in Membrane Separation Process," in *Mass Transfer - Advancement in Process Modelling*, InTech, 2015, pp. 15–40.

[58] H. G. Gomaa and S. Rao, "Analysis of flux enhancement at oscillating flat surface membranes," *J. Memb. Sci.*, vol. 374, no. 1–2, pp. 59–66, 2011, doi: 10.1016/j.memsci.2011.03.011.

[59] X. Su, W. Li, A. Palazzolo, and S. Ahmed, "Permeate flux increase by colloidal fouling control in a vibration enhanced reverse osmosis membrane desalination system," *Desalination*, vol. 453, no. December 2018, pp. 22–36, 2019, doi: 10.1016/j.desal.2018.12.003.

[60] K. Takata and K. Tanida, "Structure of shear-enhanced flow on membrane surface with horizontal vibration and its effect on filtration performance," *Chem. Eng. Res. Des.*, vol. 134, pp. 130–139, 2018, doi: 10.1016/j.cherd.2018.03.042.

[61] J. Leong, J. Tan, A. Heitz, and B. P. Ladewig, "Use of vibratory shear enhanced processing to treat magnetic ion exchange concentrate: A techno-economic analysis," *Desalination*, vol. 383, pp. 46–52, 2016, doi: 10.1016/j.desal.2016.01.002.

[62] C. Chie, "Water Chemistry and Biochemistry," in *Food Biochemistry and Food Processing*, Second Edi., B. K. Simpson, L. M. L. Nollet, F. Toldra, S. Benjakul, G. Paliyath, and Y. H. Hui, Eds. John Wiley & Sons, Inc., 2012, p. 106.

[63] P. J. Fellows, "Freeze drying and freeze concentration," in *Food processing technology - Principles and practice*, 2nd edn., P. Fellows, Ed. Cambridge, England: Woodhead Publishing, 2009, pp. 441–451.

[64] Z. Berk, *Food Process Engineering and Technology*. 2009.

[65] G. S. Tucker, *Food Preservation and Biodeterioration*. Chicester, United Kingdom: John Wiley & Sons, Incorporated, 2015.

[66] M. Mathlouthi, "Water content, water activity, water structure and the stability of foodstuffs," *Food Control*, vol. 12, no. 7, pp. 409–417, Oct. 2001, doi: 10.1016/S0956-7135(01)00032-9.

[67] G. S. Tucker, "Drying," in *Food Preservation and Biodeterioration*, 2nd edn., G. S. Tucker, Ed. West Sussex, United Kingdom: John Wiley & Sons, Inc., 2016.

[68] G. G. Santonja, P. Karlis, T. , Brinkmann, and S. Roudier, "Best Available Techniques (BAT) Reference Document on Food, Drink and Milk Industries," 2019. [Online]. Available: http://eippcb.jrc.ec.europa.eu/reference/brefdownload/download_FDM.cfm.

[69] Z. Berk, "Dehydration," in *Food Process Engineering and Technology*, 2nd edn., San Diego, USA: Elsevier Science & Technology, 2013, pp. 511–566.

[70] S. Huang *et al.*, "Spray drying of probiotics and other food-grade bacteria: A review," *Trends Food Sci. Technol.*, vol. 63, pp. 1–17, 2017, doi: 10.1016/j.tifs.2017.02.007.

[71] I. Tontul and A. Topuz, "Spray-drying of fruit and vegetable juices: Effect of drying conditions on the product yield and physical properties," *Trends Food Sci. Technol.*, vol. 63, pp. 91–102, 2017, doi: 10.1016/j.tifs.2017.03.009.

[72] J. C. Atuonwu, X. Jin, G. van Straten, H. C. van Deventer Antonius, and J. B. van Boxtel, "Reducing energy consumption in food drying: Opportunities in desiccant adsorption and other dehumidification strategies," *Procedia Food Sci.*, vol. 1, pp. 1799–1805, 2011, doi: 10.1016/j.profoo.2011.09.264.

[73] M. Compton, S. Willis, B. Rezaie, and K. Humes, "Food processing industry energy and water consumption in the Pacific northwest," *Innov. Food Sci. Emerg. Technol.*, vol. 47, no. February, pp. 371–383, 2018, doi: 10.1016/j.ifset.2018.04.001.

[74] V. A. Vaishampayan and S. I. R. Costa, *Green Technologies in Food Production and Processing*. New York, NY: Springer US, 2012.

[75] R. P. F. Guiné, "The Drying of Foods and Its Effect on the Physical-Chemical , Sensorial and Nutritional Properties," *Int. J. food Eng.*, vol. 4, no. 2, pp. 93–100, 2018, doi: 10.18178/ijfe.4.2.93-100.

[76] C. M. van 't Land, *Drying in the Process Industry*. New Jersey: John Wiley & Sons, Inc., 2012.

[77] V. Westergaard, *Milk Powder Technology Evaporation and Spray Drying*, Fifth edit. Copenhagen: GEA Process Engineering, 2010.

[78] C. Galitsky, E. Worrell, C. Galitsky, E. Masanet, and W. Graus, *Energy Efficiency Improvement and Cost Saving Opportunities for the Glass Industry. An ENERGY STAR Guide for Energy and Plant Managers*, no. July. 2008.

[79] E. Birru, "Sugar Cane Industry Overview And Energy Efficiency Considerations," *KTH Sch. Ind. Eng. Manag.*, no. 01, pp. 1–61, 2016.

[80] P. Schuck *et al.*, “Energy Consumption in the Processing of Dairy and Feed Powders by Evaporation and Drying,” *Dry. Technol.*, vol. 33, no. 2, pp. 176–184, 2015, doi: 10.1080/07373937.2014.942913.

[81] M. Benković, S. Srečec, I. Špoljarić, G. Mršić, and I. Bauman, “Fortification of instant coffee beverages - influence of functional ingredients, packaging material and storage time on physical properties of newly formulated, enriched instant coffee powders,” *J. Sci. Food Agric.*, vol. 95, no. 13, pp. 2607–2618, 2015, doi: 10.1002/jsfa.6989.

[82] T. Hatzold, “Introduction,” in *Coffee: Emerging health effects and disease prevention*, First edit., Y.-F. Chu, Ed. Blackwell Publishing Ltd., 2012, pp. 1–20.

[83] International Coffee Organization, “ICO annual review 2017/18,” 2018. http://www.ico.org/documents/cy2018-19/annual-review-2017-18-e.pdf (accessed Mar. 01, 2019).

[84] United States Department of Agriculture, “Coffee: World Markets and Trade,” 2020. [Online]. Available: http://apps.fas.usda.gov/psdonline/circulars/coffee.pdf.

[85] R. J. Clarke and R. Macrae, *Coffee*. Dordrecht, Netherlands: Springer Netherlands, 1987.

[86] M. Huang and M. Zhang, “Tea and coffee powders,” *Handb. Food Powders Process. Prop.*, pp. 513–531, 2013, doi: 10.1533/9780857098672.3.513.

[87] S. P. Ishwarya and C. Anandharamakrishnan, “Spray-Freeze-Drying approach for soluble coffee processing and its effect on quality characteristics,” *J. Food Eng.*, vol. 149, pp. 171–180, 2015, doi: 10.1016/j.jfoodeng.2014.10.011.

[88] M. Barbera and G. Gurnari, *Wastewater treatment and reuse in the food industry*. Cham: Springer International Publishing, 2018.

[89] R. W. Baker, *Membrane Technology and Applications*. John Wiley & Sons, Inc., 2012.

[90] R. Field, E. Bekassy-Molnar, F. Lipnizki, and G. Vatai, *Engineering Aspects of Membrane Separation and Application in Food Processing*. Raton, FL: CRC Press, 2017.

[91] Z. Berk, “Membrane processes,” in *Food Process Engineering and Technology*, vol. 28, no. 7, Elsevier, 2018, pp. 261–287.

[92] A. Cassano, “Integrated membrane processes in the food industry,” in *Integrated Membrane Systems and Processes*, A. Basile and C. Charcosset, Eds. John Wiley & Sons, Inc., 2016, pp. 35–60.

[93] F. Salehi, “Current and future applications for nanofiltration technology in the food processing,” *Food Bioprod. Process.*, vol. 92, no. 2, pp. 161–177, 2014, doi: 10.1016/j.fbp.2013.09.005.

[94] A. I. Schäfer, A. G. Fane, and T. D. Waite, *Nanofiltration - Principles and applications*. Oxford, United Kingdom: Elsevier Ltd, 2005.

[95] A. Cassano, C. Conidi, and R. Castro-Muñoz, “Current and Future Applications of Nanofiltration in Food Processing,” in *Separation of Functional Molecules in Food by Membrane Technology*, Elsevier, 2019, pp. 305–348.

[96] M. N. Clifford and K. C. Wilson, *Coffee: Botany, biochemistry and production of beans and beverage*. Connecticut, USA: The AVI Publishing Company, Inc., 1985.

[97] M. Oliveira *et al.*, “Intra- and interspecific mineral composition variability of commercial instant coffees and coffee substitutes: Contribution to mineral intake,” *Food Chem.*, vol. 130, no. 3, pp. 702–709, 2012, doi: 10.1016/j.foodchem.2011.07.113.

[98] S. Shirazi, C. J. Lin, and D. Chen, “Inorganic fouling of pressure-driven membrane processes - A critical review,” *Desalination*, vol. 250, no. 1, pp. 236–248, 2010, doi: 10.1016/j.desal.2009.02.056.

[99] N. Yin, Z. Zhong, and W. Xing, “Ceramic membrane fouling and cleaning in ultrafiltration of desulfurization wastewater,” *Desalination*, vol. 319, pp. 92–98, 2013, doi: 10.1016/j.desal.2013.03.028.

[100] K. Takata, K. Yamamoto, R. Bian, and Y. Watanabe, “Removal of humic substances with vibratory shear enhanced processing membrane filtration,” *Desalination*, vol. 117, no. 1–3, pp. 273–282, 1998, doi: 10.1016/S0011-9164(98)00118-0.

[101] L. M. Vane and F. R. Alvarez, “Full-scale vibrating pervaporation membrane unit: VOC removal from water and surfactant solutions,” *J. Memb. Sci.*, vol. 202, no. 1–2, pp. 177–193, 2002, doi: 10.1016/S0376-7388(01)00755-4.

[102] M. Frappart, O. Akoum, L. H. Ding, and M. Y. Jaffrin, “Treatment of dairy process waters modelled by diluted milk using dynamic nanofiltration with a rotating disk module,” *J. Memb. Sci.*, vol. 282, no. 1–2, pp. 465–472, 2006, doi: 10.1016/j.memsci.2006.06.005.

[103] O. Akoum, D. Richfield, M. Y. Jaffrin, L. H. Ding, and P. Swart, “Recovery of trypsin inhibitor and soy milk protein concentration by dynamic filtration,” *J. Memb. Sci.*, vol. 279, no. 1–2, pp. 291–300, 2006, doi: 10.1016/j.memsci.2005.12.030.

[104] Y. El Rayess *et al.*, "Wine clarification with Rotating and Vibrating Filtration (RVF): Investigation of the impact of membrane material, wine composition and operating conditions," *J. Memb. Sci.*, vol. 513, pp. 47–57, 2016, doi: 10.1016/j.memsci.2016.03.058.

[105] New Logic Research Inc., "VSEP products: Series LP," 2019. https://www.vsep.com/product/series-lp (accessed Jun. 20, 2020).

[106] L. Ding and M. Y. Jaffrin, "Benefits of High Shear Rate Dynamic Nanofiltration and Reverse Osmosis: A Review," *Sep. Sci. Technol.*, vol. 49, no. 13, pp. 1953–1967, 2014, doi: 10.1080/01496395.2014.914538.

[107] T. Zsirai, H. Qiblawey, M. J. A-Marri, and S. Judd, "The impact of mechanical shear on membrane flux and energy demand," *J. Memb. Sci.*, vol. 516, pp. 56–63, 2016, doi: 10.1016/j.memsci.2016.06.010.

[108] M. Mulder, *Basic Principles of Membrane Technology*, 2nd editio. Netherlands: Kluwer Academic Publishers, 1996.

[109] S. Zou *et al.*, "Direct microscopic observation of forward osmosis membrane fouling by microalgae: Critical flux and the role of operational conditions," *J. Memb. Sci.*, vol. 436, pp. 174–185, 2013, doi: 10.1016/j.memsci.2013.02.030.

[110] H. Li, A. G. Fane, H. G. L. Coster, and S. Vigneswaran, "Direct observation of particle deposition on the membrane surface during crossflow microfiltration," *J. Memb. Sci.*, vol. 149, no. 1, pp. 83–97, 1998, doi: 10.1016/S0376-7388(98)00181-1.

[111] A. S. Kim, "Permeate flux inflection due to concentration polarization in crossflow membrane filtration: A novel analytic approach," *Eur. Phys. J. E*, vol. 24, no. 4, pp. 331–341, 2007, doi: 10.1140/epje/i2007-10244-x.

[112] M. Elimelech and S. Bhattacharjee, "A novel approach for modeling concentration polarization in crossflow membrane filtration based on the equivalence of osmotic pressure model and filtration theory," *J. Memb. Sci.*, vol. 145, no. 2, pp. 223–241, 1998, doi: 10.1016/S0376-7388(98)00078-7.

[113] K. Akamatsu, K. Ishizaki, S. Yoshinaga, and S. I. Nakao, "Mass transfer coefficient of tubular ultrafiltration membranes under high-flux conditions," *AIChE J.*, vol. 64, no. 5, pp. 1778–1782, 2018, doi: 10.1002/aic.16052.

[114] S. S. Yoo, K. H. Chu, I. H. Choi, J. S. Mang, and K. B. Ko, "Operating cost reduction of UF membrane filtration process for drinking water treatment attributed to chemical cleaning optimization," *J. Environ. Manage.*, vol. 206, pp. 1126–1134, 2018, doi: 10.1016/j.jenvman.2017.02.072.

[115] C. Bhattacharjee, V. K. Saxena, and S. Dutta, "Analysis of fouling and juice quality in crossflow ultrafiltration of watermelon juice," *Food Sci. Technol.*, vol. 38, pp. 71–76, 2018, doi: 10.1590/1678-457x.15217.

[116] D. Vogel, A. Simon, A. Ali, B. Bilitewski, W. E. Price, and L. D. Nghiem, "Effects of fouling and scaling on the retention of trace organic contaminants by a nanofiltration membrane : The role of cake-enhanced concentration polarisation," *Sep. Purif. Technol.*, vol. 73, no. 2, pp. 256–263, 2010, doi: 10.1016/j.seppur.2010.04.010.

[117] J. Luo, L. Ding, Y. Wan, P. Paullier, and M. Y. Jaffrin, "Fouling behavior of dairy wastewater treatment by nanofiltration under shear-enhanced extreme hydraulic conditions," *Sep. Purif. Technol.*, vol. 88, pp. 79–86, 2012, doi: 10.1016/j.seppur.2011.12.008.

[118] A. Antony, J. How, S. Gray, A. E. Childress, P. Le-clech, and G. Leslie, "Scale formation and control in high pressure membrane water treatment systems : A review," *J. Memb. Sci.*, vol. 383, no. 1–2, pp. 1–16, 2011, doi: 10.1016/j.memsci.2011.08.054.

[119] W. Guo, H. H. Ngo, and J. Li, "A mini-review on membrane fouling," *Bioresour. Technol.*, vol. 122, pp. 27–34, 2012, doi: 10.1016/j.biortech.2012.04.089.

[120] W. Li, X. Su, A. Palazzolo, S. Ahmed, and E. Thomas, "Reverse osmosis membrane, seawater desalination with vibration assisted reduced inorganic fouling," *Desalination*, vol. 417, no. April, pp. 102–114, 2017, doi: 10.1016/j.desal.2017.05.016.

[121] B. Van der Bruggen, M. Mänttäri, and M. Nyström, "Drawbacks of applying nanofiltration and how to avoid them: A review," *Sep. Purif. Technol.*, vol. 63, no. 2, pp. 251–263, 2008, doi: 10.1016/j.seppur.2008.05.010.

[122] W. Zhang, J. Luo, L. Ding, and M. Y. Jaffrin, "A review on flux decline control strategies in pressure-driven membrane processes," *Ind. Eng. Chem. Res.*, vol. 54, no. 11, pp. 2843–2861, 2015, doi: 10.1021/ie504848m.

[123] J. E. Kilduft, S. Mattaraj, J. P. Pieracci, and G. Belfort, "Photochemical modification of poly(ether sulfone) and sulfonated poly(sulfone) nanofiltration membranes for control of fouling by natural organic matter," 2000. Accessed: Mar. 03, 2021. [Online]. Available: www.elsevier.com/locate/desal.

[124] T.-U. Kim, "Transport of Organic Micropollutants Through Nanofiltration (NF) and Reverse Osmosis (RO) Membranes: Mechanisms, Modeling, and Applications," Seoul National University, 2006.

[125] O. Ojajuni, D. Saroj, and G. Cavalli, "Removal of organic micropollutants using membrane-assisted processes: a review of recent progress," *Environ. Technol. Rev.*, vol. 4, no. 1, pp. 17–37, 2015, doi: 10.1080/21622515.2015.1036788.

[126] N. K. Saha, M. Balakrishnan, and M. Ulbricht, “Fouling control in sugarcane juice ultrafiltration with surface modified polysulfone and polyethersulfone membranes,” *Desalination*, vol. 249, no. 3, pp. 1124–1131, 2009, doi: 10.1016/j.desal.2009.05.013.

[127] B. Van der Bruggen and C. Vandecasteele, “Modelling of the retention of uncharged molecules with nanofiltration,” *Water Res.*, vol. 36, no. 5, pp. 1360–1368, 2002, doi: 10.1016/S0043-1354(01)00318-9.

[128] B. Van Der Bruggen, L. Braeken, and C. Vandecasteele, “Flux decline in nanofiltration due to adsorption of organic compounds,” *Sep. Purif. Technol.*, vol. 29, no. 1, pp. 23–31, 2002, doi: 10.1016/S1383-5866(01)00199-X.

[129] J. E. Kilduff, S. Mattaraj, and G. Belfort, “Flux decline during nanofiltration of naturally-occurring dissolved organic matter: Effects of osmotic pressure, membrane permeability, and cake formation,” *J. Memb. Sci.*, vol. 239, no. 1, pp. 39–53, 2004, doi: 10.1016/j.memsci.2003.12.030.

[130] G. Johnson, B. Culkin, and M. Monroe, “Kinetics of Mineral Scale Membrane Fouling: A Comparison of Conventional Crossflow Membranes and VSEP, a Vibratory Membrane System,” *Filtration*, 2003, [Online]. Available: http://scholar.google.com/scholar?hl=en&btnG=Search&q=intitle:Kinetics+of+Mineral+Scale+Membrane+Fouling+A+Comparison+of+Conventional+Crossflow+Membranes+and+V+?+SEP+,+a+Vibratory+Membrane+System+.#0%5Cnhttp://scholar.google.com/scholar?hl=en&btnG=Search&.

[131] P. Le-Clech, V. Chen, and T. A. G. Fane, “Fouling in membrane bioreactors used in wastewater treatment,” *J. Memb. Sci.*, vol. 284, no. 1–2, pp. 17–53, 2006, doi: 10.1016/j.memsci.2006.08.019.

[132] S. Rosenblat, “Flow between torsionally oscillating disks,” *J. Fluid Mech.*, vol. 8, no. 3, pp. 388–399, 1960.

[133] International Organization for Standardization, *ISO 14040 Environmental Management: Life Cycle Assessment, Principles and Framework*. Switzerland, 1997.

[134] M. A. Curran, *Life Cycle Assessment Student Handbook*. Somerset, UNITED STATES: John Wiley & Sons, Incorporated, 2015.

[135] J. R. Mihelcic and J. B. Zimmerman, *Environmental Engineering: Fundamentals, Sustainability, Design*. Singapore: John Wiley & Sons, Inc., 2010.

[136] I. T. Herrmann and A. Moltesen, “Does it matter which Life Cycle Assessment (LCA) tool you choose? - A comparative assessment of SimaPro and GaBi,” *J. Clean. Prod.*, vol. 86, pp. 163–169, 2015, doi: 10.1016/j.jclepro.2014.08.004.

[137] C. S. Slater and M. J. Savelski, "Membrane Separations for Greener Operations in the Chemical Process Industries," Maryland, 2009.

[138] C. S. Slater, M. J. Savelski, P. Kostetskyy, and M. Johnson, "Shear-enhanced microfiltration of microalgae in a vibrating membrane module," *Clean Technol. Environ. Policy*, vol. 17, no. 7, pp. 1743–1755, 2015, doi: 10.1007/s10098-015-0907-z.

[139] U.S. Environmental Protection Agency, "Guidelines for water reuse," USA, EPA/600/R-12/618, 2012. [Online]. Available: https://www.epa.gov/sites/production/files/2019-08/documents/2012-guidelines-water-reuse.pdf.

[140] E. W. Rice, R. B. Barid, A. D. Eaton, and L. S. Cleceri, *Standard methods for the examination of water and wastewater*. Washington: American Public Health Association, American Water Works Association, Water Environment Federation, 2012.

[141] J. Telis-Romero, R. A. F. Cabral, A. L. Gabas, and V. R. N. Telis, "Rheological properties and fluid dynamics of coffee extract," *J. Food Process Eng.*, vol. 24, pp. 217–230, 2001.

[142] J. Telis-Romero, A. L. Gabas, M. A. Polizelli, and V. R. N. Telis, "Temperature and water content influence on thermophysical properties of coffee extract," *Int. J. Food Prop.*, vol. 3, no. 3, pp. 375–384, 2000, doi: 10.1080/10942910009524642.

[143] Ž. R. Lazić, *Design of experiments in chemical engineering: a practical guide*. Weinheim, Germany: Wiley-VCH Verlag GmbH & Co., 2004.

[144] New Logic Research Inc., "VSEP products: Series i," 2019. https://www.vsep.com/product/series-i/ (accessed Jun. 24, 2020).

[145] P. T. Cardew and M. S. Le, "Membrane technologies," in *Membrane Processes - A Technology Guide*, Royal Society of Chemistry, 1998, pp. 2-1-2–20.

[146] G. Towler and R. K. Sinnot, *Chemical engineering design: Principles, practice and economics of plant and process design*. Elsevier Science and Technology, 2012.

[147] J. Shen, J. Huang, H. Ruan, J. Wang, and B. Van der Bruggen, "Techno-economic analysis of resource recovery of glyphosate liquor by membrane technology," *Desalination*, vol. 342, pp. 118–125, 2014, doi: 10.1016/j.desal.2013.11.041.

[148] M. Peters, K. Timmerhaus, and R. West, *Plant design and economics for chemical engineers*, 5th edn. McGraw-Hill, 2002.

[149] M. J. Raymond, C. S. Slater, and M. J. Savelski, "LCA approach to the analysis of solvent waste issues in the pharmaceutical industry," *Green Chem.*, vol. 12, no. 10, p. 1826, 2010, doi: 10.1039/c003666h.

[150] C. S. Slater, M. Savelski, G. Hounsell, D. Pilipauskas, and F. Urbanski, "Green design alternatives for isopropanol recovery in the celecoxib process," *Clean Technol. Environ. Policy*, vol. 14, no. 4, pp. 687–698, 2012, doi: 10.1007/s10098-011-0433-6.

[151] B. M. Pastore, M. J. Savelski, C. S. Slater, and F. A. Richetti, "Life cycle assessment of N-methyl-2-pyrrolidone reduction strategies in the manufacture of resin precursors," *Clean Technol. Environ. Policy*, vol. 18, no. 8, pp. 2635–2647, 2016, doi: 10.1007/s10098-016-1180-5.

[152] C. Y. Tang, Z. Yang, H. Guo, J. J. Wen, L. D. Nghiem, and E. Cornelissen, "Potable Water Reuse through Advanced Membrane Technology," *Environ. Sci. Technol.*, vol. 52, no. 18, pp. 10215–10223, 2018, doi: 10.1021/acs.est.8b00562.

[153] C. M. Wisniewski, "Process intervention for water recovery in food manufacture," Rowan University, 2018.

[154] D. W. Green and R. H. Perry, *Perry's Chemical Engineers' Handbook, Eighth Edition*, 8th ed. /. New York: McGraw-Hill Education, 2008.

[155] B. W. Hackett, "The Essentials of Continuous Evaporation | AIChE," *CEP Magazine*, no. May, pp. 24–28, 2018.

[156] U.S. Energy Information Administration, "New Jersey natural gas industrial price," 2020. https://www.eia.gov/dnav/ng/hist/n3035nj3m.htm (accessed Sep. 20, 2004).

[157] U.S. Energy Information Administration, "New Jersey electricity profile," *State Electricity Profiles*, 2020. www.eia.gov/electricity/state/NewJersey (accessed May 25, 2020).

[158] X. Su, W. Li, A. Palazzolo, and S. Ahmed, "Concentration polarization and permeate flux variation in a vibration enhanced reverse osmosis membrane module," *Desalination*, vol. 433, no. September 2017, pp. 75–88, 2018, doi: 10.1016/j.desal.2018.01.001.

[159] E. Novita, "Biodegradability Simulation of Coffee Wastewater Using Instant Coffee," *Agric. Agric. Sci. Procedia*, vol. 9, pp. 217–229, 2016, doi: 10.1016/j.aaspro.2016.02.138.

[160] P. A. Delgado, J. A. Vignoli, M. Siika-aho, and T. T. Franco, "Sediments in coffee extracts: Composition and control by enzymatic hydrolysis," *Food Chem.*, vol. 110, no. 1, pp. 168–176, 2008, doi: 10.1016/j.foodchem.2008.01.029.

[161] W. Shi and M. M. Benjamin, “Membrane interactions with NOM and an adsorbent in a vibratory shear enhanced filtration process (VSEP) system,” *J. Memb. Sci.*, vol. 312, no. 1–2, pp. 23–33, 2008, doi: 10.1016/j.memsci.2007.12.031.

[162] W. Shi and M. M. Benjamin, “Effect of shear rate on fouling in a Vibratory Shear Enhanced Processing (VSEP) RO system,” *J. Memb. Sci.*, vol. 366, no. 1–2, pp. 148–157, 2011, doi: 10.1016/j.memsci.2010.09.051.

[163] P. Bacchin, P. Aimar, and R. W. Field, “Critical and sustainable fluxes: Theory, experiments and applications,” *J. Memb. Sci.*, vol. 281, no. 1–2, pp. 42–69, 2006, doi: 10.1016/j.memsci.2006.04.014.

[164] M. Vincent, O. Laurio, · C Stewart Slater, and C. S. Slater, “Process scale-up, economic, environmental assessment of vibratory nanofiltration of coffee extracts for soluble coffee production process intensification,” *Clean Technol. Environ. Policy*, vol. 22, pp. 1891–1908, 1931, doi: 10.1007/s10098-020-01931-x.

[165] M. Frappart, M. Y. Jaffrin, L. H. Ding, and V. Espina, “Effect of vibration frequency and membrane shear rate on nanofiltration of diluted milk, using a vibratory dynamic filtration system,” *Sep. Purif. Technol.*, vol. 62, no. 1, pp. 212–221, 2008, doi: 10.1016/j.seppur.2008.01.025.

[166] A. I. Zouboulis, E. N. Peleka, and A. Ntolia, “Treatment of tannery wastewater with vibratory shear-enhanced processing membrane filtration,” *Separations*, vol. 6, no. 2, 2019, doi: 10.3390/separations6020020.

[167] C. S. Slater, M. J. Savelski, P. Kostetskyy, and M. Johnson, “Shear-enhanced microfiltration of microalgae in a vibrating membrane module,” *Clean Technol. Environ. Policy*, vol. 17, no. 7, pp. 1743–1755, 2015, doi: 10.1007/s10098-015-0907-z.

[168] W. R. Bowen and J. S. Welfoot, “Modelling the performance of membrane nanofiltration-critical assessment and model development,” *Chem. Eng. Sci.*, vol. 57, no. 7, pp. 1121–1137, 2002, doi: 10.1016/S0009-2509(01)00413-4.

[169] Y. Sato, M. Kang, T. Kamei, and Y. Magara, “Performance of nanofiltration for arsenic removal,” *Water Res.*, vol. 36, no. 13, pp. 3371–3377, Jul. 2002, doi: 10.1016/S0043-1354(02)00037-4.

[170] W. Zhang, N. Grimi, M. Y. Jaffrin, L. Ding, B. Tang, and Z. Zhang, “Optimization of RDM-UF for alfalfa wastewater treatment using RSM,” *Environ. Sci. Pollut. Res.*, vol. 25, no. 2, pp. 1439–1447, 2018, doi: 10.1007/s11356-017-0588-8.

[171] S. Jiang, Y. Zhang, F. Zhao, Z. Yu, X. Zhou, and H. Chu, “Impact of transmembrane pressure (TMP) on membrane fouling in microalgae harvesting with a uniform shearing vibration membrane system,” *Algal Res.*, vol. 35, no. October, pp. 613–623, 2018, doi: 10.1016/j.algal.2018.10.003.

[172] M. Frappart, M. Jaffrin, and L. H. Ding, “Reverse osmosis of diluted skim milk: Comparison of results obtained from vibratory and rotating disk modules,” *Sep. Purif. Technol.*, vol. 60, no. 3, pp. 321–329, 2008, doi: 10.1016/j.seppur.2007.09.007.

[173] J. Fang and B. Deng, “Rejection and modeling of arsenate by nano fi ltration : Contributions of convection , diffusion and electromigration to arsenic transport,” *J. Memb. Sci.*, vol. 453, pp. 42–51, 2014, doi: 10.1016/j.memsci.2013.10.056.

[174] C. Ming, X. Xiaomin, S. Philippe, and F. Luc, “Extensive review about industrial and laboratory dynamic filtration modules: scientific production, configurations and performances,” *Sep. Purif. Technol.*, vol. 265, no. December 2020, p. 118293, 2021, doi: 10.1016/j.seppur.2020.118293.

[175] National Center for Biotechnology Information, “PubChem Compound Summary CID 6850756, Coffee extract,” 2020. https://pubchem.ncbi.nlm.nih.gov/compound/Coffee-extract (accessed Nov. 27, 2020).

[176] T. M. Patel and K. Nath, “Modeling of permeate flux and mass transfer resistances in the reclamation of molasses wastewater by a novel gas-sparged nanofiltration,” *Korean J. Chem. Eng.*, vol. 31, no. 10, pp. 1865–1876, Oct. 2014, doi: 10.1007/s11814-014-0139-7.

[177] A. Maia, E. Ferreira, M. C. Oliveira, L. F. Menezes, and A. Andrade-Campos, *Numerical optimization strategies for springback compensation in sheet metal forming*, no. 2017. 2017.

[178] N. Andrei, *Continuous Nonlinear Optimization for Engineering Applications in GAMS Technology*, vol. 121. 2017.

[179] L. S. Lasdon, A. D. Waren, A. Jain, and M. Ratner, “Design and Testing of a Generalized Reduced Gradient Code for Nonlinear Programming,” *ACM Trans. Math. Softw.*, vol. 4, no. 1, pp. 34–50, 1978, doi: 10.1145/355769.355773.

[180] P. Markandeya Raju, A. Manasa, and G. Rohini, “Cost optimization of a rectangular singly reinforced concrete beam by Generalized Reduced Gradient method,” *IOP Conf. Ser. Mater. Sci. Eng.*, vol. 1025, p. 012005, 2021, doi: 10.1088/1757-899x/1025/1/012005.

[181] M. V. O. Laurio, K. M. Yenkie, and C. S. Slater, “Optimization of vibratory nanofiltration for sustainable coffee extract concentration via response surface methodology,” *Sep. Sci. Technol.*, 2021, doi: 10.1080/01496395.2021.1879858.

[182] G. Keir and V. Jegatheesan, “A review of computational fluid dynamics applications in pressure-driven membrane filtration,” *Rev. Environ. Sci. Biotechnol.*, vol. 13, no. 2, pp. 183–201, 2014, doi: 10.1007/s11157-013-9327-x.

[183] M. AbuKhadra, M. Shaban, and I. Saad, *Statistical modeling and optimization in separation and purification*. Lambert Academic Publishing, 2018.

[184] J. Dasgupta, D. Mondal, S. Chakraborty, J. Sikder, S. Curcio, and H. A. Arafat, "Nanofiltration based water reclamation from tannery effluent following coagulation pretreatment," *Ecotoxicol. Environ. Saf.*, vol. 121, pp. 22–30, 2015, doi: 10.1016/j.ecoenv.2015.07.006.

[185] M. Farhadian, N. Askari, and A. Razmjou, "Decolorization of ionic dyes from synthesized textile wastewater by nanofiltration using response surface methodology," *Adv. Environ. Technol.*, vol. 1, no. 2, pp. 85–92, 2015.

[186] K. C. Ho, Y. H. teow, and A. W. mohammad, "Optimization of nanocomposite conductive membrane formulation and operating parameters for electrically-enhanced palm oil mill effluent filtration using response surface methodology," *Process Saf. Environ. Prot.*, vol. 126, pp. 297–308, 2019, doi: 10.1016/j.psep.2019.03.019.

[187] N. Ghaemi *et al.*, "PES mixed matrix nanofiltration membrane embedded with polymer wrapped MWCNT: Fabrication and performance optimization in dye removal by RSM," *J. Hazard. Mater.*, vol. 298, pp. 111–121, 2015, doi: 10.1016/j.jhazmat.2015.05.018.

[188] M. Said, S. Rozaimakh Sheikh Abdullah, and A. Wahab Mohammad, "Palm Oil Mill Effluent Treatment Through Combined Process Adsorption and Membrane Filtration," *Sriwij. J. Environ.*, vol. 1, no. 2, pp. 36–41, 2016, doi: 10.22135/sje.2016.1.2.36-41.

[189] W. P. Cathie Lee, S. K. Mah, C. P. Leo, T. Y. Wu, and S. P. Chai, "Phosphorus removal by NF90 membrane: Optimisation using central composite design," *J. Taiwan Inst. Chem. Eng.*, vol. 45, no. 4, pp. 1260–1269, 2014, doi: 10.1016/j.jtice.2014.02.011.

[190] C. Akarsu *et al.*, "Electrocoagulation and nanofiltration integrated process application in purification of bilge water using response surface methodology," *Water Sci. Technol.*, vol. 74, no. 3, pp. 564–579, Aug. 2016, doi: 10.2166/wst.2016.168.

[191] E. Yuliwati, A. F. Ismail, W. J. Lau, B. C. Ng, A. Mataram, and M. A. Kassim, "Effects of process conditions in submerged ultrafiltration for refinery wastewater treatment: Optimization of operating process by response surface methodology," *Desalination*, vol. 287, pp. 350–361, 2012, doi: 10.1016/j.desal.2011.08.051.

[192] S. Gasemloo, M. Khosravi, M. Reza, S. Dastmalchi, and P. Gharbani, "Response surface methodology (RSM) modeling to improve removal of Cr (VI) ions from tannery wastewater using sulfated carboxymethyl cellulose nano fi lter," *J. Clean. Prod.*, vol. 208, pp. 736–742, 2019, doi: 10.1016/j.jclepro.2018.10.177.

[193] S. S. Madaeni, N. Arast, F. Rahimpour, and Y. Arast, "Fabrication optimization of acrylonitrile butadiene styrene (ABS)/polyvinylpyrrolidone (PVP) nanofiltration membrane using response surface methodology," *Desalination*, vol. 280, no. 1–3, pp. 305–312, 2011, doi: 10.1016/j.desal.2011.07.020.

[194] M. Khayet, M. N. A. Seman, and N. Hilal, "Response surface modeling and optimization of composite nanofiltration modified membranes," *J. Memb. Sci.*, vol. 349, no. 1–2, pp. 113–122, 2010, doi: 10.1016/j.memsci.2009.11.031.

[195] K. H. Mah, H. W. Yussof, M. N. Abu Seman, and A. W. Mohammad, "Optimisation of interfacial polymerization factors in thin-film composite (TFC) polyester nanofiltration (NF) membrane for separation of xylose from glucose," *Sep. Purif. Technol.*, vol. 209, no. July 2018, pp. 211–222, 2019, doi: 10.1016/j.seppur.2018.07.041.

[196] Y. S. Aşçı, U. Dramur, and M. Bilgin, "Investigation of the separation of carboxylic acids from aqueous solutions using a pilot scale membrane unit," *J. Mol. Liq.*, vol. 248, pp. 391–398, Dec. 2017, doi: 10.1016/j.molliq.2017.10.076.

[197] M. C. Garg and H. Joshi, "Optimization and economic analysis for a small scale nanofiltration and reverse osmosis water desalination system," *Water Sci. Technol. Water Supply*, vol. 15, no. 5, pp. 1027–1033, 2015, doi: 10.2166/ws.2015.059.

[198] A. N. Negrão Murakami *et al.*, "Concentration of phenolic compounds in aqueous mate (Ilex paraguariensis A. St. Hil) extract through nanofiltration," *LWT - Food Sci. Technol.*, vol. 44, no. 10, pp. 2211–2216, 2011, doi: 10.1016/j.lwt.2011.06.002.

[199] J. M. Ochando-Pulido, J. R. Corpas-Martínez, J. A. Vellido-Perez, and A. Martinez-Ferez, "Optimization of polymeric nanofiltration performance for olive-oil-washing wastewater phenols recovery and reclamation," *Sep. Purif. Technol.*, vol. 236, no. October 2019, p. 116261, 2020, doi: 10.1016/j.seppur.2019.116261.

[200] H. Nourbakhsh, Z. Emam-Djomeh, M. Omid, H. Mirsaeedghazi, and S. Moini, "Prediction of red plum juice permeate flux during membrane processing with ANN optimized using RSM," *Comput. Electron. Agric.*, vol. 102, pp. 1–9, 2014, doi: 10.1016/j.compag.2013.12.017.

[201] Q. Zhang and Q. Yuan, "Modeling of nanofiltration process for solvent recovery from aqueous ethanol solution of soybean isoflavones," *Sep. Sci. Technol.*, vol. 44, no. 13, pp. 3239–3257, 2009, doi: 10.1080/01496390903183105.

[202] M. Cai, S. Wang, and H. H. Liang, "Optimization of ultrasound-assisted ultrafiltration of Radix astragalus extracts with hollow fiber membrane using response surface methodology," *Sep. Purif. Technol.*, vol. 100, pp. 74–81, 2012, doi: 10.1016/j.seppur.2012.09.002.

[203] R. A. Ruby Figueroa, A. Cassano, and E. Drioli, “Ultrafiltration of orange press liquor: Optimization for permeate flux and fouling index by response surface methodology,” *Sep. Purif. Technol.*, vol. 80, no. 1, pp. 1–10, Jul. 2011, doi: 10.1016/j.seppur.2011.03.030.

[204] Z. Zhu *et al.*, “Study of rotating disk assisted dead-end filtration of chicory juice and its performance optimization,” *Ind. Crops Prod.*, vol. 53, pp. 154–162, 2014, doi: 10.1016/j.indcrop.2013.12.030.

[205] R. Ferrarini, A. Versari, and S. Galassi, “A preliminary comparison between nanofiltration and reverse osmosis membranes for grape juice treatment,” *J. Food Eng.*, vol. 50, no. 2, pp. 113–116, 2001, doi: 10.1016/S0260-8774(00)00199-0.

[206] V. Geraldes, V. Semião, and M. N. De Pinho, “Flow and mass transfer modelling of nanofiltration,” *J. Memb. Sci.*, vol. 191, no. 1–2, pp. 109–128, 2001, doi: 10.1016/S0376-7388(01)00458-6.

[207] C. Brazinha, M. Cadima, and J. G. Crespo, “Valorisation of spent coffee through membrane processing,” *J. Food Eng.*, vol. 149, pp. 123–130, 2015, doi: 10.1016/j.jfoodeng.2014.07.016.

[208] A. Cassano and E. Drioli, *Integrated Membrane Operations in the Food Production*. Berlin: De Gruyter, 2014.

[209] Y. Song, B. Su, X. Gao, and C. Gao, “Investigation on high NF permeate recovery and scaling potential prediction in NF-SWRO integrated membrane operation,” *Desalination*, vol. 330, pp. 61–69, 2013, doi: 10.1016/j.desal.2013.09.021.

[210] S. Salvador Cob *et al.*, “Silica and silicate precipitation as limiting factors in high-recovery reverse osmosis operations,” *J. Memb. Sci.*, vol. 423–424, pp. 1–10, 2012, doi: 10.1016/j.memsci.2012.07.016.

[211] P. Pal, J. Sikder, S. Roy, and L. Giorno, “Process intensification in lactic acid production: A review of membrane based processes,” *Chem. Eng. Process. Process Intensif.*, vol. 48, no. 11–12, pp. 1549–1559, 2009, doi: 10.1016/j.cep.2009.09.003.

[212] S. R. Osipi, A. R. Secchi, and C. P. Borges, “Cost assessment and retro-techno-economic analysis of desalination technologies in onshore produced water treatment,” *Desalination*, vol. 430, no. August 2017, pp. 107–119, 2018, doi: 10.1016/j.desal.2017.12.015.

[213] A. Shahmansouri and C. Bellona, “Nanofiltration technology in water treatment and reuse: Applications and costs,” *Water Sci. Technol.*, vol. 71, no. 3, pp. 309–319, 2015, doi: 10.2166/wst.2015.015.

[214] Metcalf & Eddy, T. Asano, F. Burton, and H. Leverenz, “Industrial uses of reclaimed water,” in *Water reuse: Issues, technologies, and applications*, New York, USA: McGraw-Hill Education, 2007.

[215] H. Olmez, “Water consumption, reuse and reduction strategies in food processing,” in *Sustainable Food Processing*, First edit., B. K. Tiwari, T. Norton, and N. M. Holden, Eds. John Wiley & Sons, Ltd., 2014, pp. 401–434.

[216] L. Malaeb and G. M. Ayoub, “Reverse osmosis technology for water treatment: State of the art review,” *Desalination*, vol. 267, no. 1, pp. 1–8, 2011, doi: 10.1016/j.desal.2010.09.001.

[217] V. B. Brião, A. C. Vieira Salla, T. Miorando, M. Hemkemeier, and D. P. Cadore Favaretto, “Water recovery from dairy rinse water by reverse osmosis: Giving value to water and milk solids,” *Resour. Conserv. Recycl.*, vol. 140, no. October 2018, pp. 313–323, 2019, doi: 10.1016/j.resconrec.2018.10.007.

[218] A. Paiva *et al.*, “Evaluation of the quality of coffee extracts concentrated by osmotic evaporation,” *J. Food Eng.*, vol. 222, pp. 178–184, 2018, doi: 10.1016/j.jfoodeng.2017.11.020.

[219] E. Binabaji, J. Ma, S. Rao, and A. L. Zydney, “Ultrafiltration of highly concentrated antibody solutions: Experiments and modeling for the effects of module and buffer conditions,” *Biotechnol. Prog.*, vol. 32, no. 3, pp. 692–701, 2016, doi: 10.1002/btpr.2252.

[220] E. Binabaji, S. Rao, and A. L. Zydney, “The osmotic pressure of highly concentrated monoclonal antibody solutions: Effect of solution conditions,” *Biotechnol. Bioeng.*, vol. 111, no. 3, pp. 529–536, 2014, doi: 10.1002/bit.25104.

[221] E. Binabaji, J. Ma, S. Rao, and A. L. Zydney, “Theoretical analysis of the ultrafiltration behavior of highly concentrated protein solutions,” *J. Memb. Sci.*, vol. 494, pp. 216–223, 2015, doi: 10.1016/j.memsci.2015.07.068.

[222] G. Wang, S. Wang, H. Wu, C. Yan, and Y. Liu, “Interactions of Bovine Serum Albumin Molecules in an Aqueous Sodium Sulfate Solution Determined by an Osmotic Pressure Method,” *J. Solution Chem.*, vol. 47, no. 3, pp. 586–594, 2018, doi: 10.1007/s10953-018-0738-8.

[223] R. B. Bird, W. E. Stewart, and E. N. Lightfoot, *Transport Phenomena*, 2nd editio. New York: John Wiley & Sons, Inc., 2002.

[224] S. Bandini, J. Drei, and D. Vezzani, “The role of pH and concentration on the ion rejection in polyamide nanofiltration membranes,” *J. Memb. Sci.*, vol. 264, no. 1–2, pp. 65–74, 2005, doi: 10.1016/j.memsci.2005.03.054.

[225] N. Aryanti, D. H. Wardhani, and S. Supandi, “Flux profiles and mathematical modeling of fouling mechanism for ultrafiltration of konjac glucomannan,” *Sci. Study Res. Chem. Chem. Eng. Biotechnol. Food Ind.*, vol. 17, no. 2, pp. 125–137, 2016.

Appendix A

List of Symbols and Abbreviations

List of Abbreviations

BOD	biological oxygen demand
CF	crossflow
COD	chemical oxygen demand
DE	dead end filtration
HWW	hazardous wastewater
IRR	internal rate of return
LCA	life cycle assessment
LCE	life cycle emissions
LCI	life cycle inventory
MACRS	modified accelerated cost recovery system
MF	microfiltration
NF	nanofiltration
NHWW	non-hazardous wastewater
NPV	net present value
PDMP	pressure-driven membrane process
RO	reverse osmosis
ROI	return on investment
TMP	transmembrane pressure
TSS	total suspended solids
UF	ultrafiltration
VSEP	vibration shear-enhanced process

List of Symbols

A	Membrane area (m^2)
A_{module}	Membrane area per module (m^2 $module^{-1}$)
A_w	hydraulic permeability ($L\ m^{-2}\ h^{-1}\ Pa^{-1}$)
b	Flux decay rate
C_b	bulk concentration ($g\ L^{-1}$)
C_m	membrane solute concentration ($g\ L^{-1}$)
C_o	feed concentration ($g\ L^{-1}$)
$C_{o\ i}$	feed characteristics
	turbidity (NTU)
	conductivity ($\mu S\ cm^{-1}$)
	COD ($mg\ L^{-1}$)
$C_{p\ i}$	permeate concentration / characteristics
	turbidity (NTU)
	conductivity ($\mu S\ cm^{-1}$)
	COD ($mg\ L^{-1}$)
d	Vibrational displacement (cm)
d_h	hydraulic diameter (m)

D_s	diffusivity coefficient (m^2/s)
D_n	depreciation cost ($)
DF_n	depreciation factor
dt	time interval (s)
E	energy requirement/consumption (MJ)
E_i	process energy flow (MJ)
F	vibrational frequency (Hz)
h	channel height (m)
J_{design}	design flux scale-up parameter (L m^{-2} h^{-1})
$J_{f\ rev}$	flux of reversibly fouled membrane (L m^{-2} h^{-1})
$J_{f\ irrev}$	flux from irreversible fouled membrane (L m^{-2} h^{-1})
J_i	degree of dissociation of salt
J_T	permeate flux at any measured temperature (L m^{-2} h^{-1})
$J_{25\ °C}$	permeate flux at 25 °C (L m^{-2} h^{-1})
$J_{water\ 25\ °C}$	water flux at 25 °C (L m^{-2} h^{-1})
$J_{water\ T}$	water flux at any measured temperature (L m^{-2} h^{-1})
J_o	initial flux at t = 0 min (L m^{-2} h^{-1})
J_v	permeate flux (L m^{-2} h^{-1})
J_w	water flux (L m^{-2} h^{-1})
k	mass transfer coefficient
K	power law model coefficient
L	length (m)
LCE_i	life cycle emissions of process component (kg)
LCI_i	life cycle inventory of process component (kg $unit^{-1}$)
LCE_{BC}	life cycle emissions of base case (kg)
LCE_{AC}	life cycle emissions of alternative case (kg)
$LCE_{avoided}$	avoided life cycle emissions (kg)
M	molar weight (kg mol^{-1})
m_i	process mass flow
n	power law model exponent
n_c	number of cleanings
N_{module}	number of i84 VSEP membrane module
OC	overall operating cost ($ yr^{-1})
OC_i	Operating cost of process component ($ yr^{-1})
OC_{BC}	Operating cost of base case ($ yr^{-1})
OC_{AC}	Operating cost of alternative case ($ yr^{-1})
OSF	Overall system factor (1.5)
P	Operating pressure (MPa)
Q_F	Feed flow rate (L d^{-1})
R	gas constant (8.314 J mol^{-1} K^{-1})
Re	Reynolds number
R_f	Fouling resistance (m^{-1})
R_i	Membrane radius
R_m	membrane resistance (m^{-1})
r_p	pore radius (m)
R_{total}	total flow resistance across the membrane (m^{-1})

Sc	Schmidt number
Sh	Sherwood number
SE_n	steam economy
T	absolute temperature (K)
t_c	time between cleanings
u	crossflow velocity (m s^{-1})
U	design flux uncertainty (0.5)
V	transverse velocity (m s^{-1})
V_c	volume of cleaner per module (L)
V_p	volume of permeate (L)
X_w	mass fraction of water in solution
%c	concentration of cleaner (%)
$\%r_o$	observed rejection efficiency (%)
$\%r_{real}$	real rejection efficiency (%)
%R	percent water recovery
ΔP	applied TMP (MPa)
$\Delta P/\Delta x$	pressure drop along membrane thickness (MPa)
$\Delta\pi$	osmotic pressure difference (MPa)
Υ_w	surface shear rate (s^{-1})
$\Upsilon_{w\ max}$	maximum surface shear rate (s^{-1})
$\Upsilon_{w\ mean}$	mean surface shear rate (s^{-1})
ε	porosity
η	pump efficiency (0.85)
Ω	amplitude of angular velocity
ρ	density (kg m^3)
ρ_w	density of water at given temperature (kg m^3)
τ	tortuosity
θ	
μ	Dynamic viscosity (Pa s)
υ	kinematic viscosity (m^2 s^{-1})
π_i	osmotic pressure of fluid (MPa)

Appendix B

Supporting Information for Parametric Studies

B.1 Permeate Flux Time Profiles

Figure B1

Filtration Time Profiles for Vibratory NF of Coffee Extracts (C_o = 8.5 g L^{-1}) at Various Applied TMPs and Vibrations

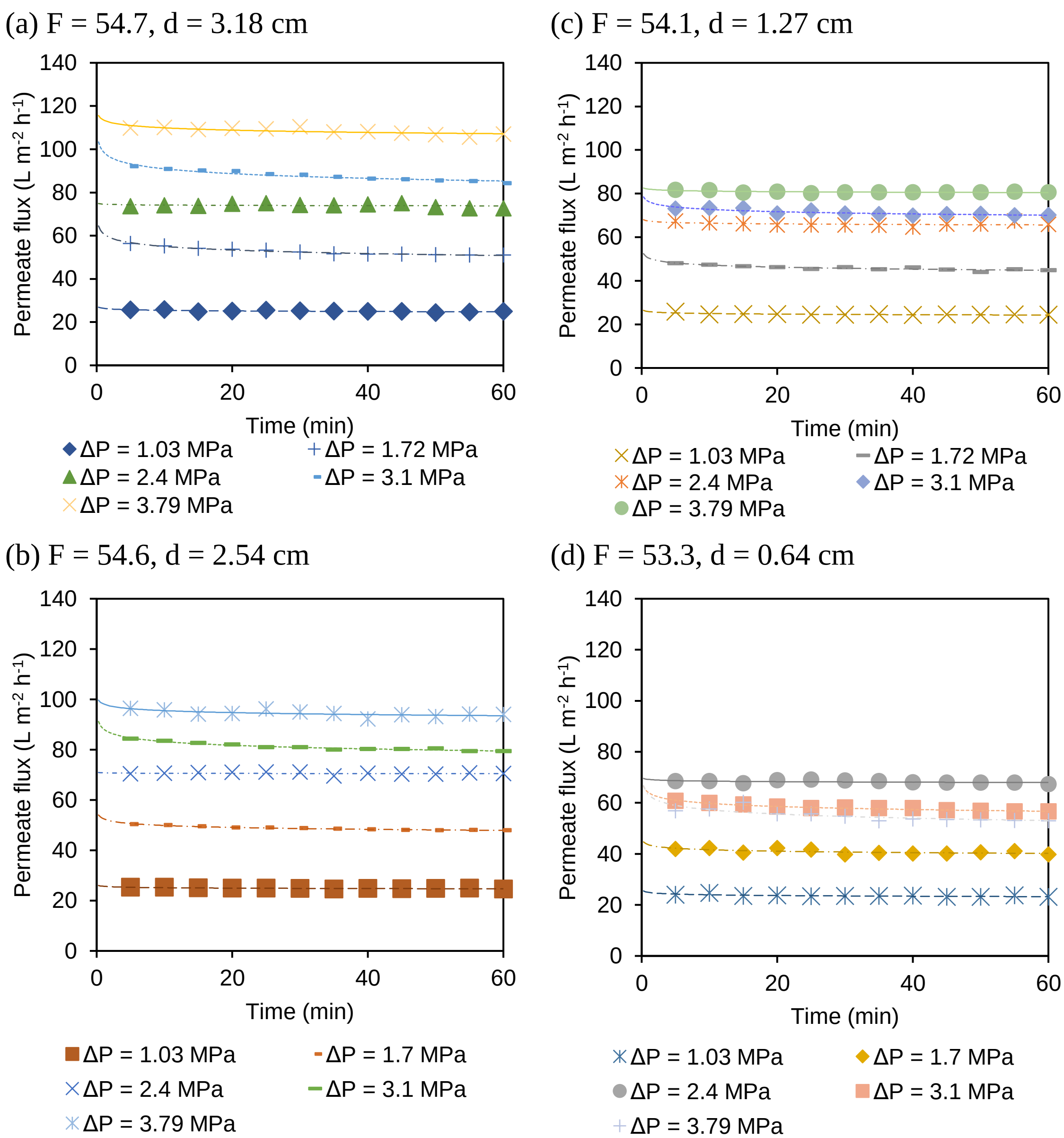

Figure B2

Filtration Time Profiles for Vibratory NF of Coffee Extracts (C_o = 17.0 g L^{-1}) at Various Applied TMPs and Vibrations

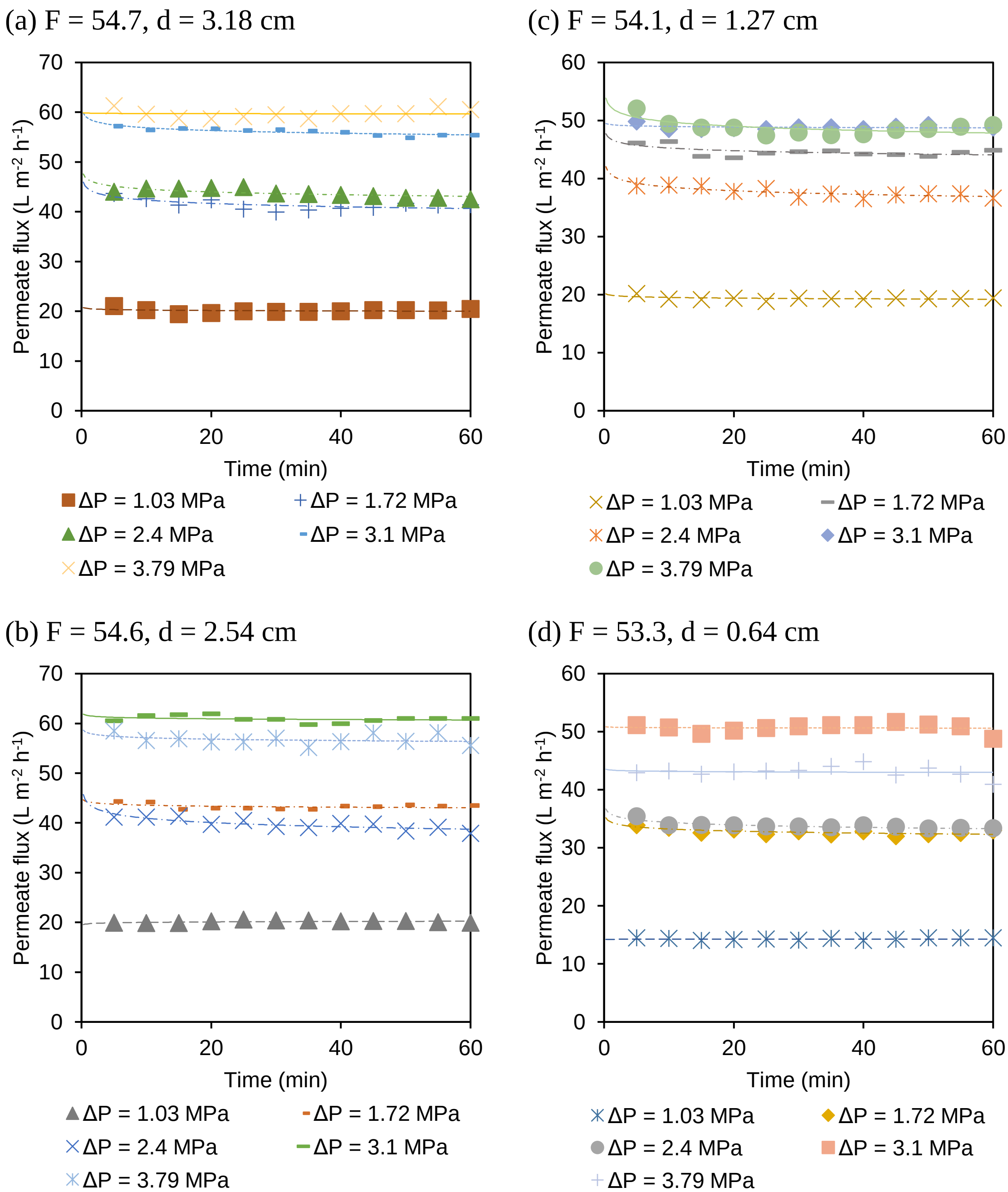

Figure B3

Filtration Time Profiles for Vibratory NF of Coffee Extracts (C_o = 25.4 g L^{-1}) at Various Applied TMPs and Vibrations

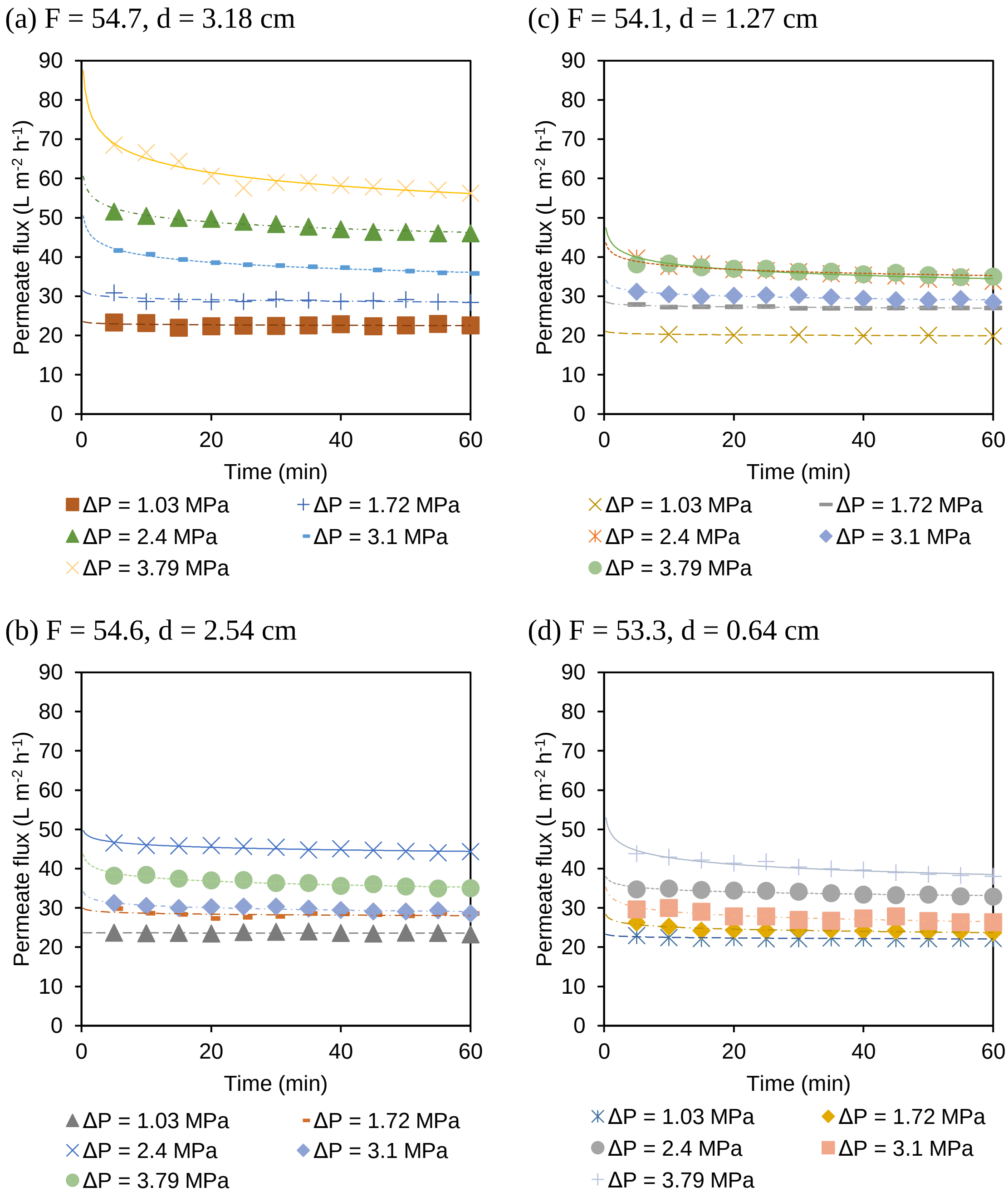

Figure B4

Filtration Time Profiles for Vibratory NF of Coffee Extracts (C_o = 33.9 g L^{-1}) at Various Applied TMPs and Vibrations

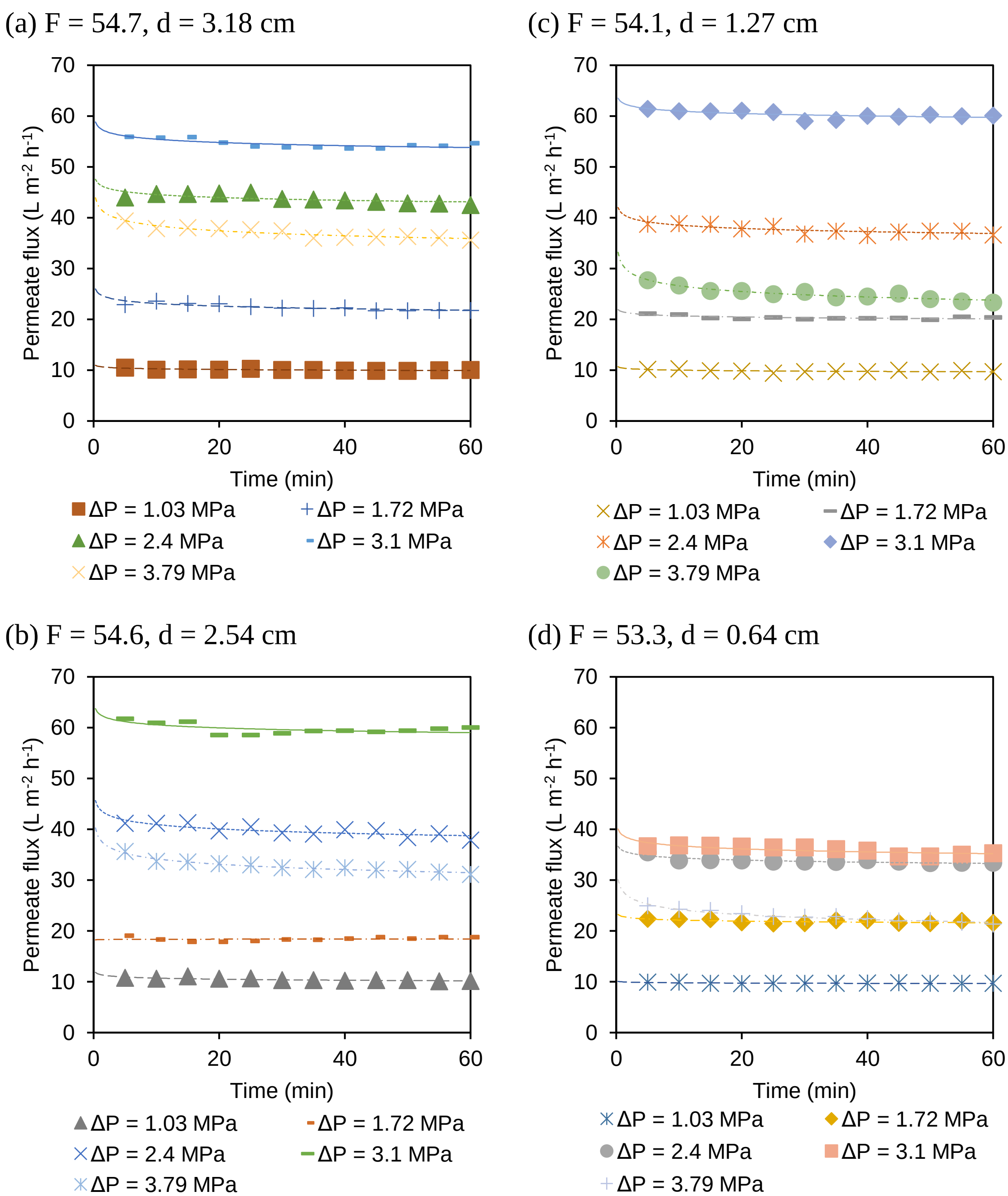

Figure B5

Filtration Time Profiles for Vibratory NF of Coffee Extracts (C_o = 42.4 g L^{-1}) at Various Applied TMPs and Vibrations

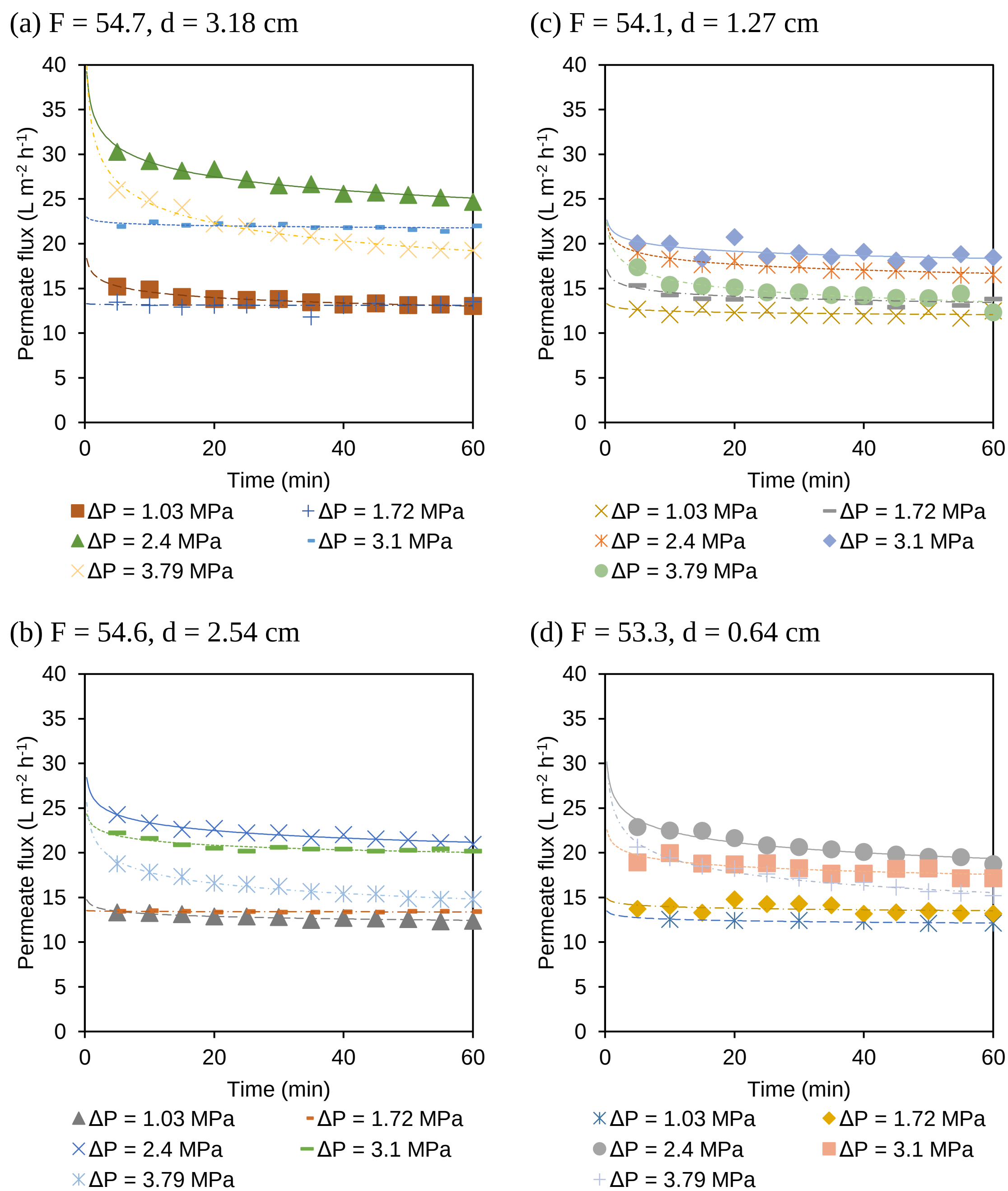

Figure B6

Filtration Time Profiles for Non-Vibratory NF (F = 0 Hz, d = 0 cm) of Coffee Extracts at Various Feed Concentrations

(a) C_o = 8.5 g L^{-1}

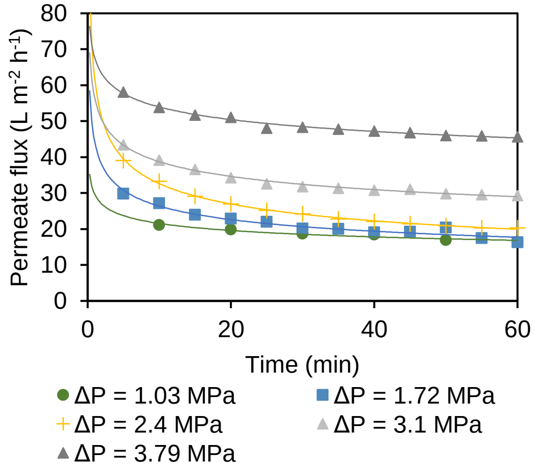

(d) C_o = 33.9 g L^{-1}

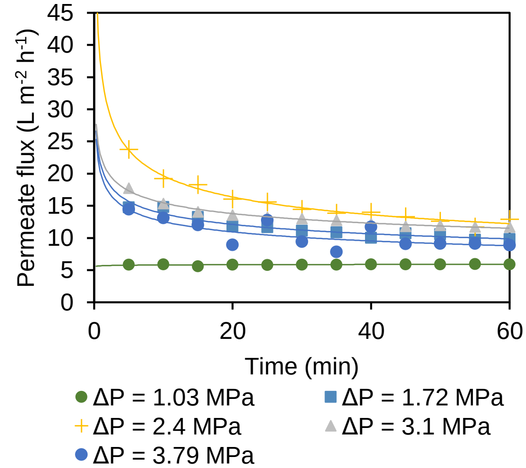

(a) C_o = 17.0 g L^{-1}

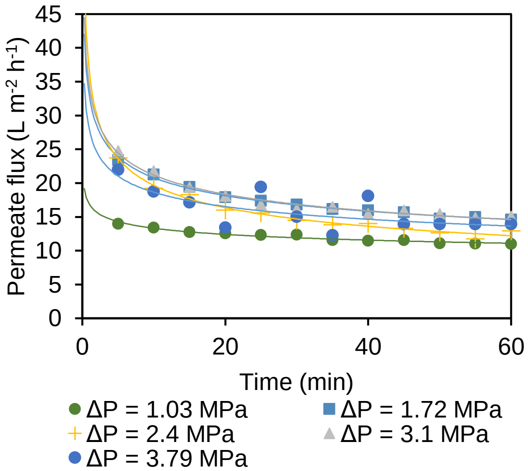

(e) C_o = 42.4 g L^{-1}

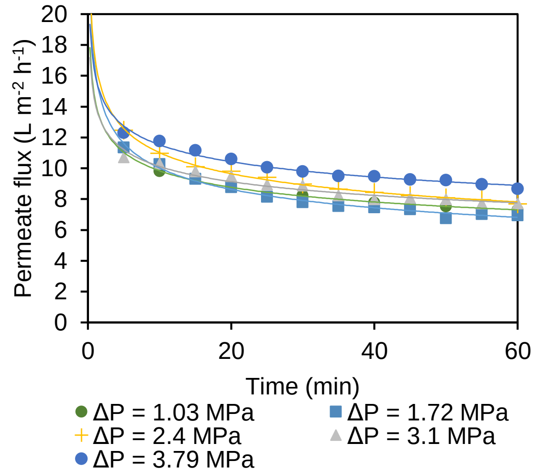

(a) C_o = 25.4 g L^{-1}

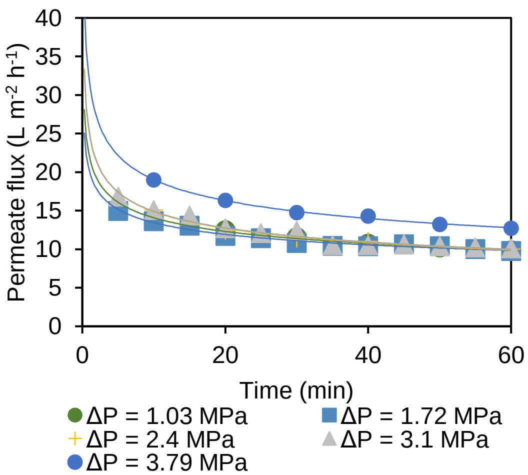

B.2 Effect of Vibration

Figure B7

Variation of Permeate Flux with Vibratory Frequency and Displacement Under Various Applied TMP and Feed Coffee Extract Concentration at T = 25 °C.

(a) $C_o = 17.0\ g\ L^{-1}$

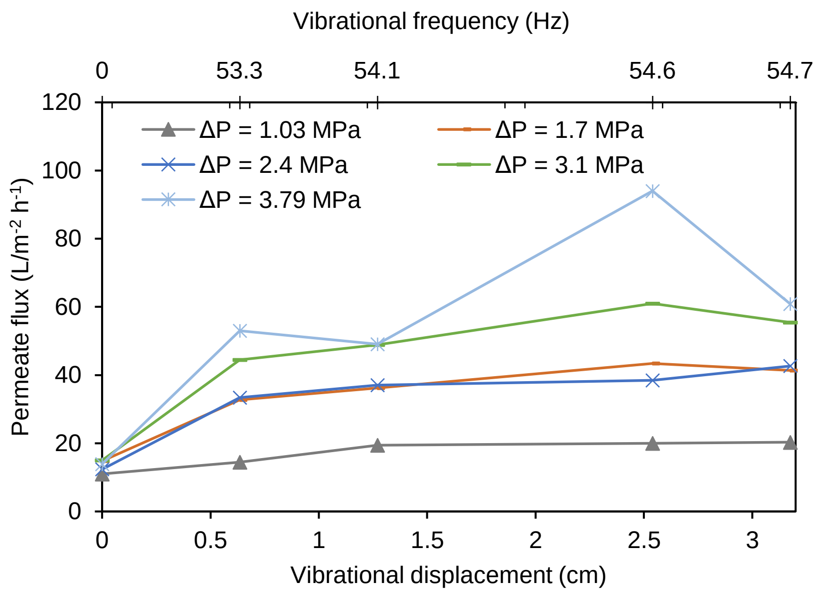

(b) $C_o = 33.9\ g\ L^{-1}$

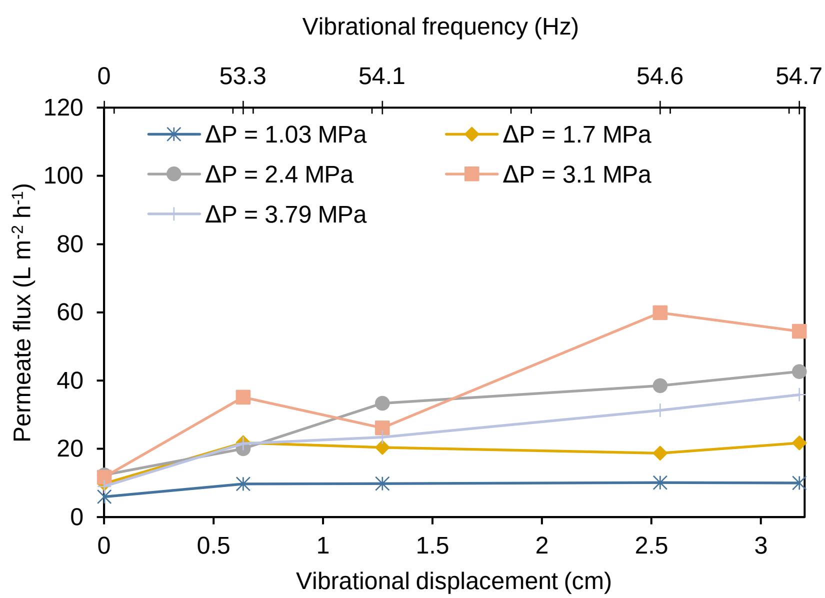

Figure B8

Variation of Permeate Flux with Maximum Surface Shear Rate Under Various Applied Transmembrane Pressure and Feed Coffee Extract Concentration at T = 25 °C

(a) $C_o = 17.0\ g\ L^{-1}$

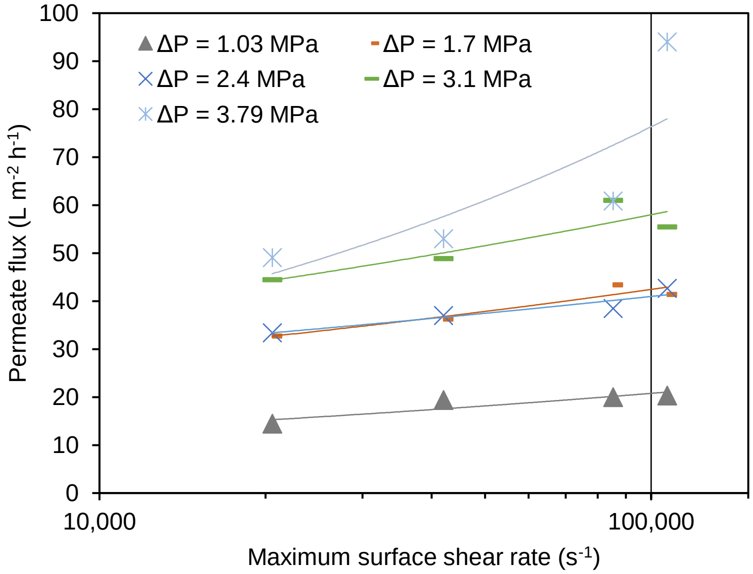

(b) $C_o = 33.9\ g\ L^{-1}$

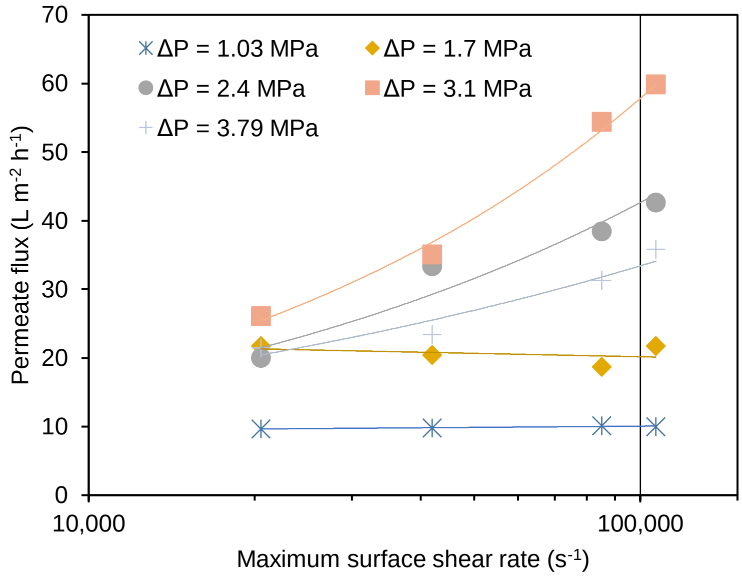

B.3 Effect of Pressure

Figure B9

Variation of Permeate Flux with Applied Transmembrane Pressure Under Different Vibrational Frequencies and Feed Coffee Extract Concentration at T = 25 °C

(a) $C_o = 17.0\ g\ L^{-1}$

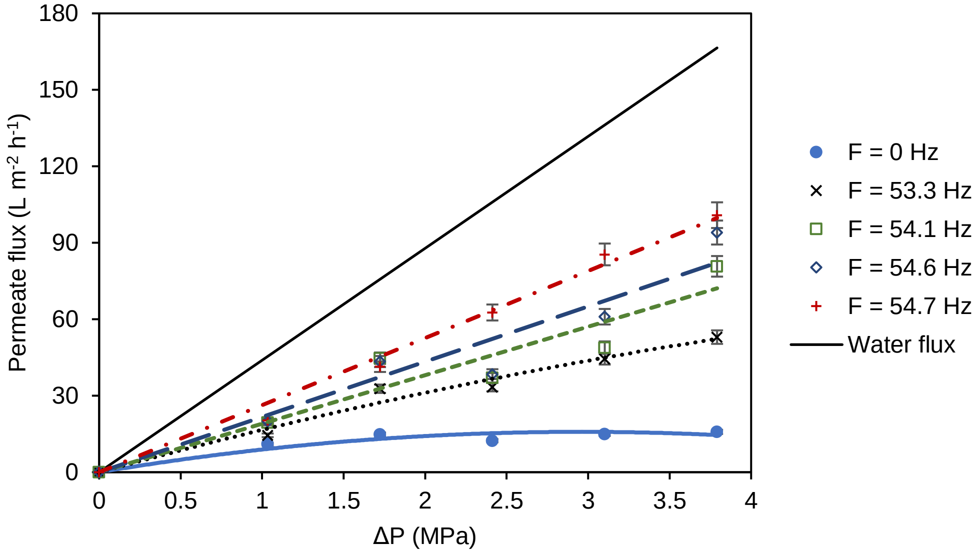

(b) $C_o = 33.9\ g\ L^{-1}$

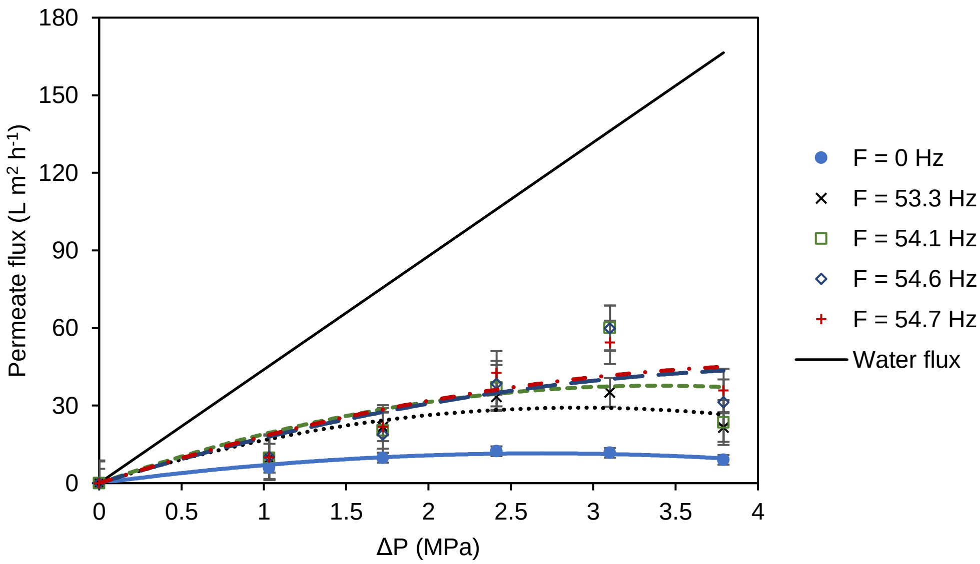

B.4 Effect of Feed Coffee Extract Concentration

Figure B10

Osmotic Pressures as a function of Feed Coffee Extract Concentration at Various Applied TMP and Vibrational Frequencies at T = 25 °C

(a) ΔP = 1.7 MPa

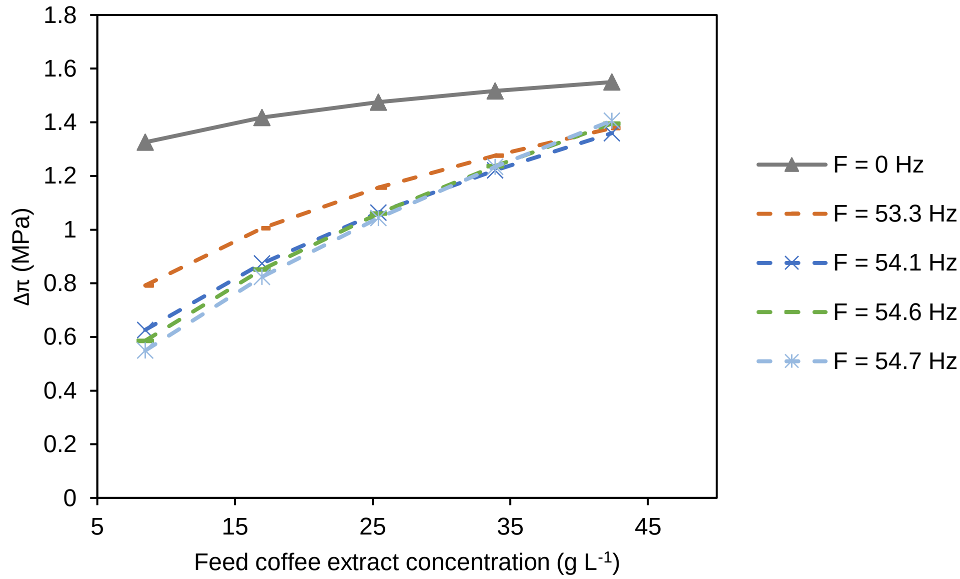

(b) ΔP = 3.1 MPa

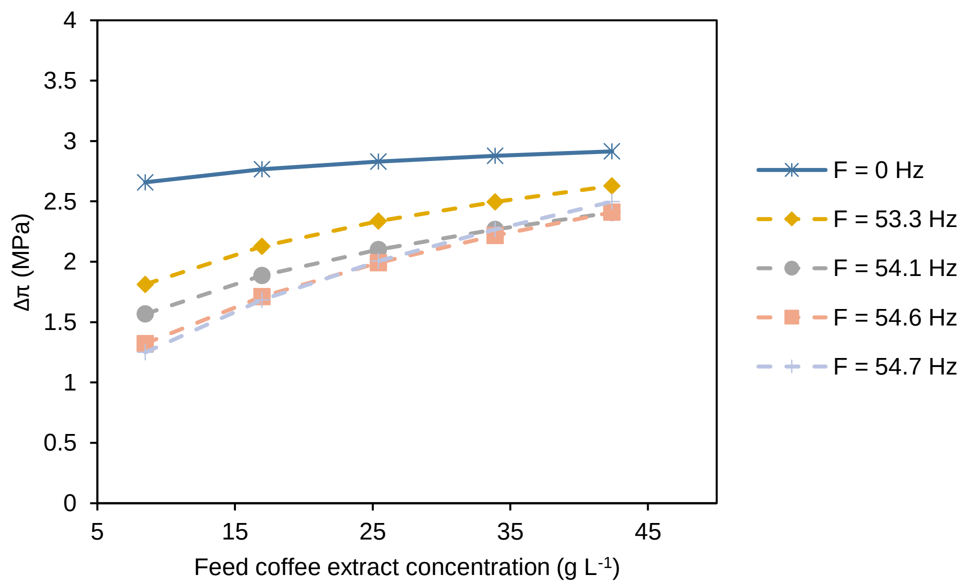

Figure B11

Permeate Flux as a function of Feed Coffee Extract Concentration at Various Applied TMP and Vibrational Frequencies at T = 25 °C

(a) ΔP = 1.7 MPa

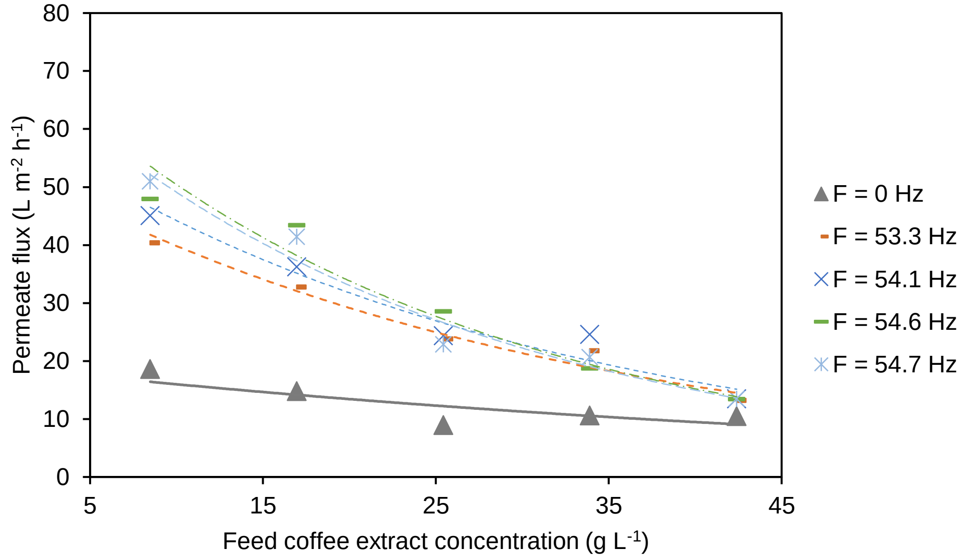

(b) ΔP = 3.1 MPa

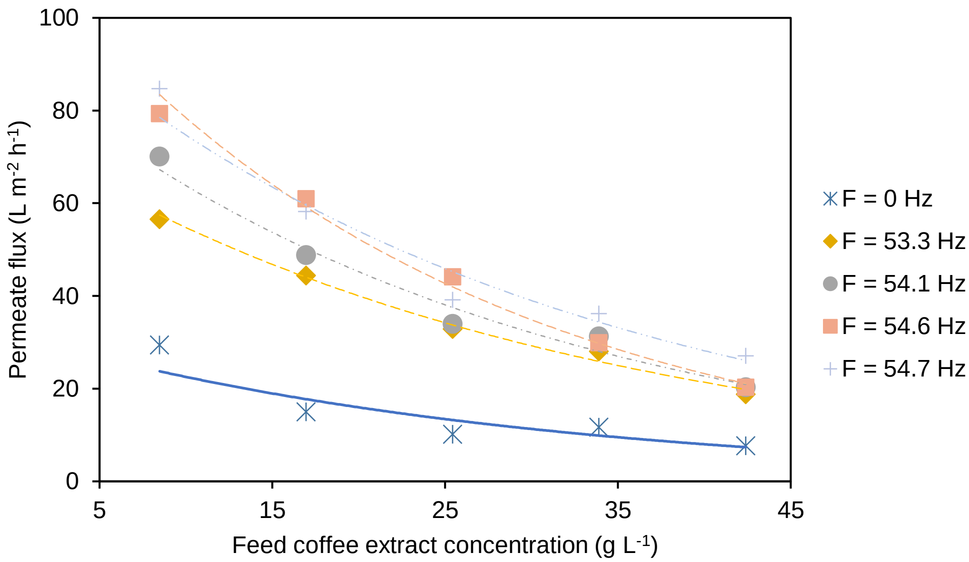

B.5 Rejection Efficiencies

Figure B12

Permeate Conductivity (left) and Conductivity Rejections (right) as Function of Feed Concentration at Various Applied TMPs and Vibrational Frequencies at T = 25 °C

(a) ΔP = 1.72 MPa

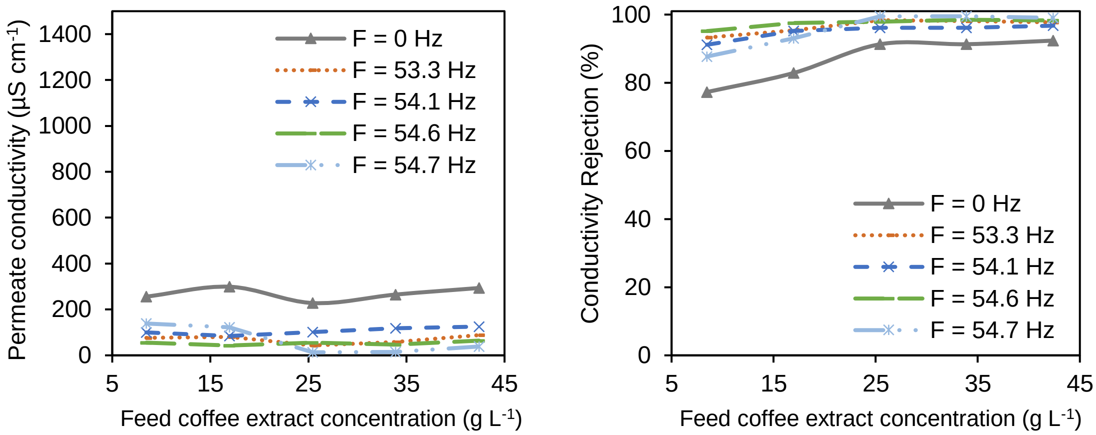

(b) ΔP = 3.1 MPa

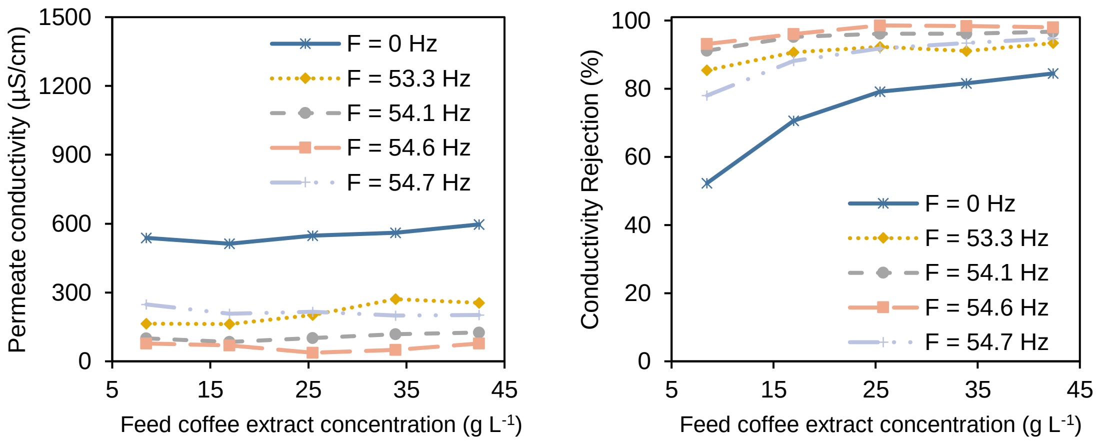

Figure B13

Permeate Conductivity (left) and Conductivity Rejection (right) as Function of Applied TMP at Various Vibrational Frequencies and Feed Concentrations at T = 25 °C

(a) F = 54.1 Hz, d = 1.27 cm

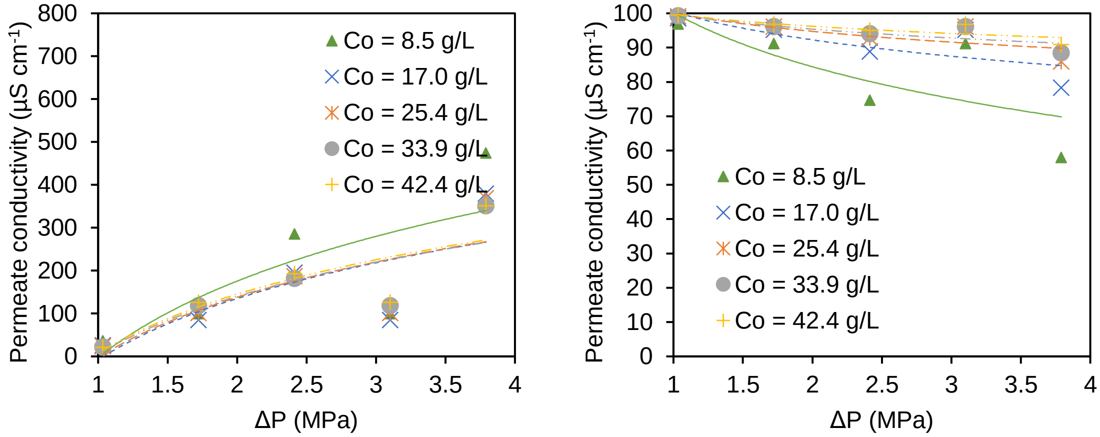

(b) F = 54.6 Hz, d = 2.54 cm

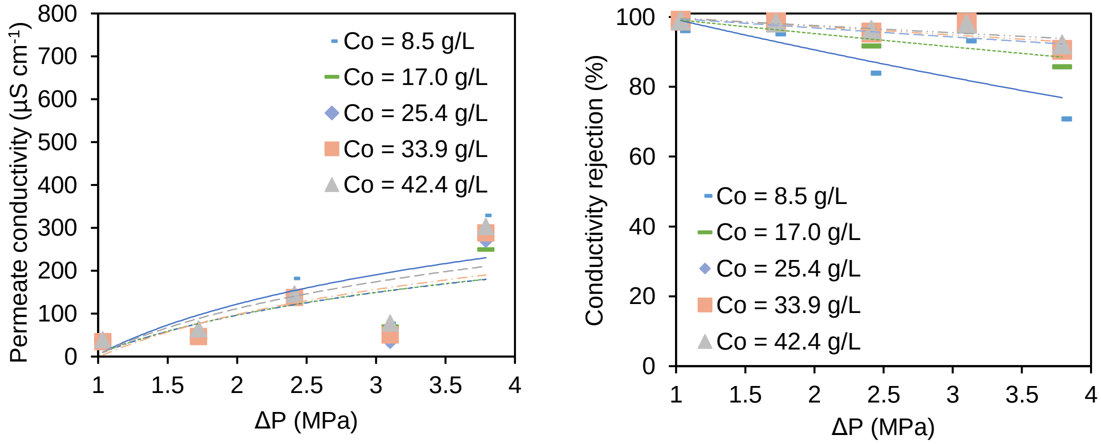

Figure B14

Permeate Conductivity (left) and Conductivity Rejection (right) as Function of Vibratory Displacement at Various Feed Concentrations and Applied TMPs at T = 25 °C

(a) $C_o = 17.0$ g L^{-1}

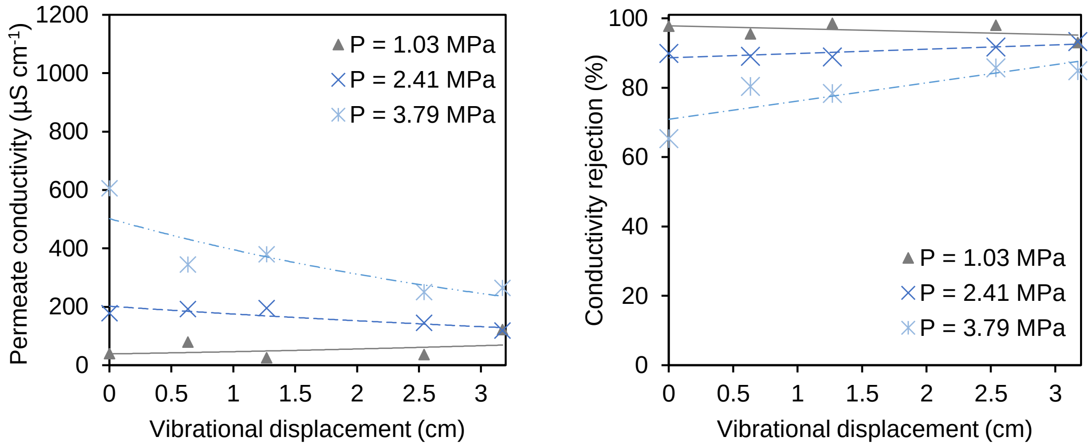

(b) $C_o = 25.4$ g L^{-1}

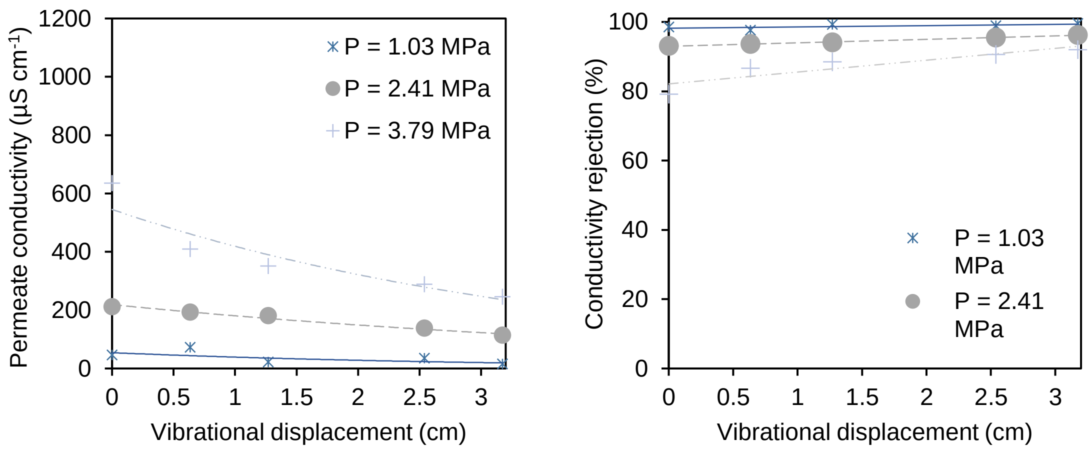

Figure B15

Permeate COD (left) and COD Rejections (right) as Function of Feed Coffee Extract Concentration at Applied TMPs and Vibrational Frequencies at T = 25 °C

(a) ΔP = 1.72 MPa

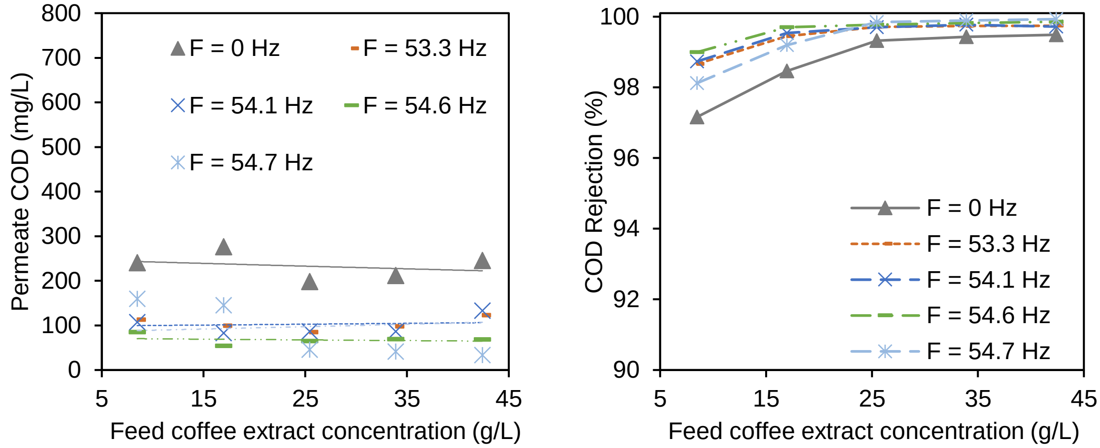

(b) ΔP = 3.1 MPa

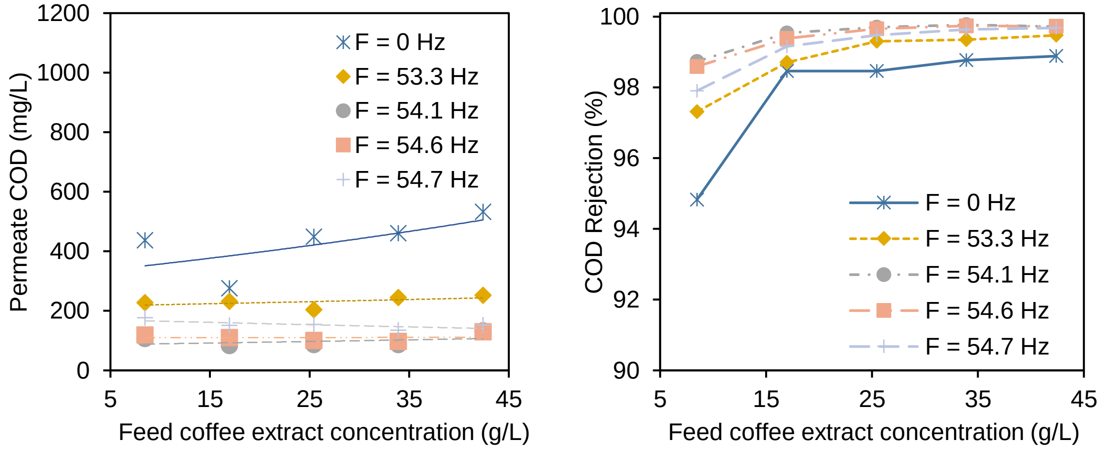

Figure B16

Permeate COD (left) and COD Rejections (right) as Function of Applied TMP at Various Vibrational Frequencies and Feed Concentration and at T = 25 °C

(a) F = 54.1 Hz, d = 1.27 cm

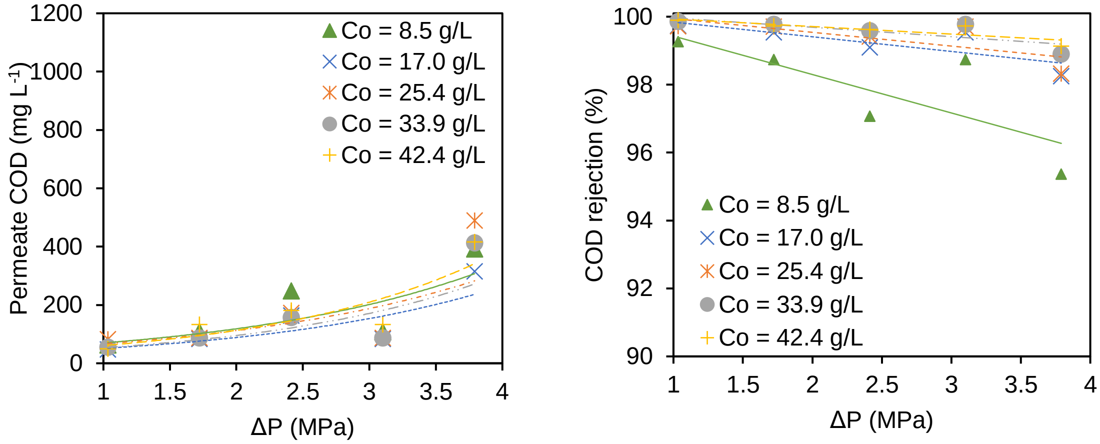

(b) F = 54.6 Hz, d = 2.54 cm

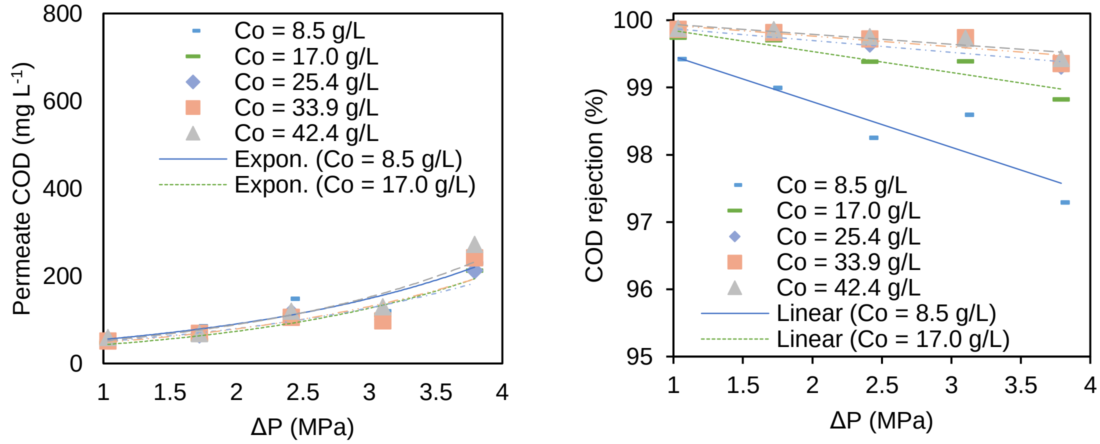

Figure B17

Permeate COD (left) and COD Rejections (right) as Function of Vibrational Displacement at Various Feed Coffee Extract Concentration and TMP at T = 25 °C

(a) $C_o = 17.0$ g L^{-1}

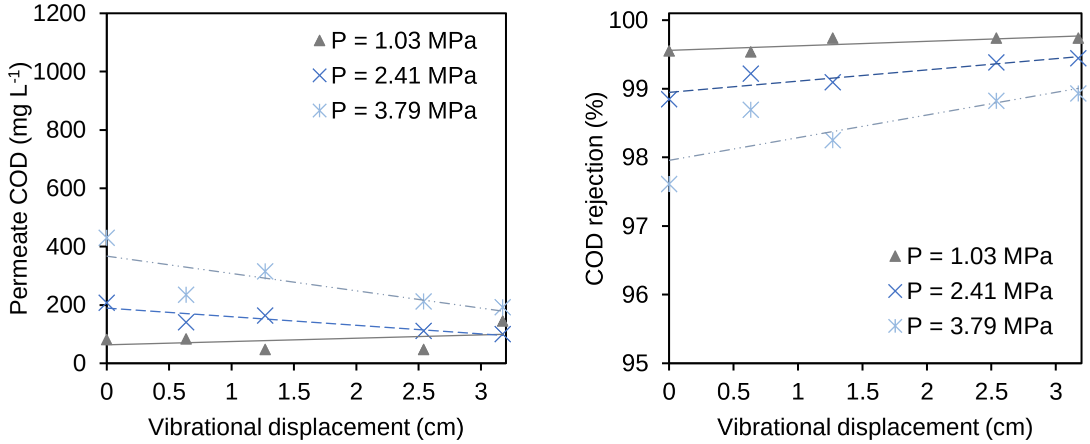

(b) $C_o = 33.9$ g L^{-1}

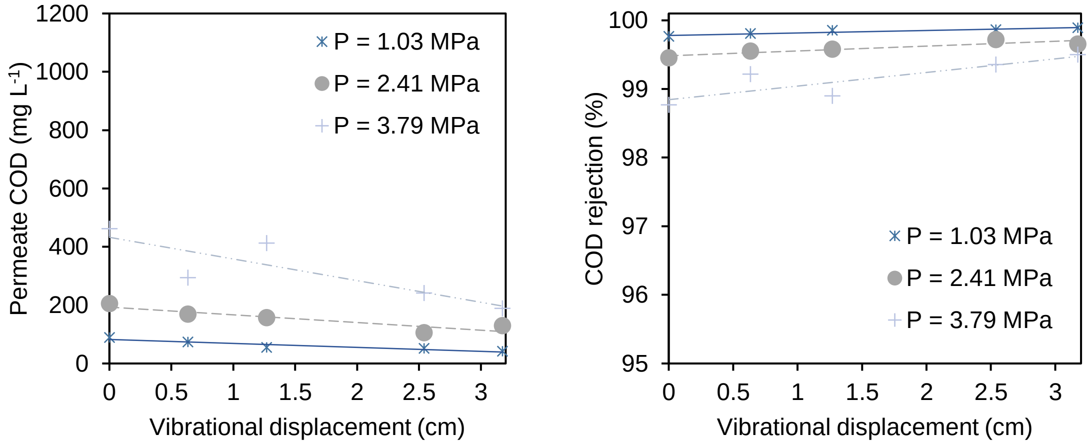

Appendix C

Supporting Information for Semi-Empirical Modeling

C.1 Membrane Surface Concentrations and Fouling Resistances

Figure C1

Membrane Surface Concentration as COD at Various Feed Coffee Extract Concentrations and Applied TMP Under Vibratory Nanofiltration at T = 25 °C

(a) C_o = 17.0 g L^{-1}

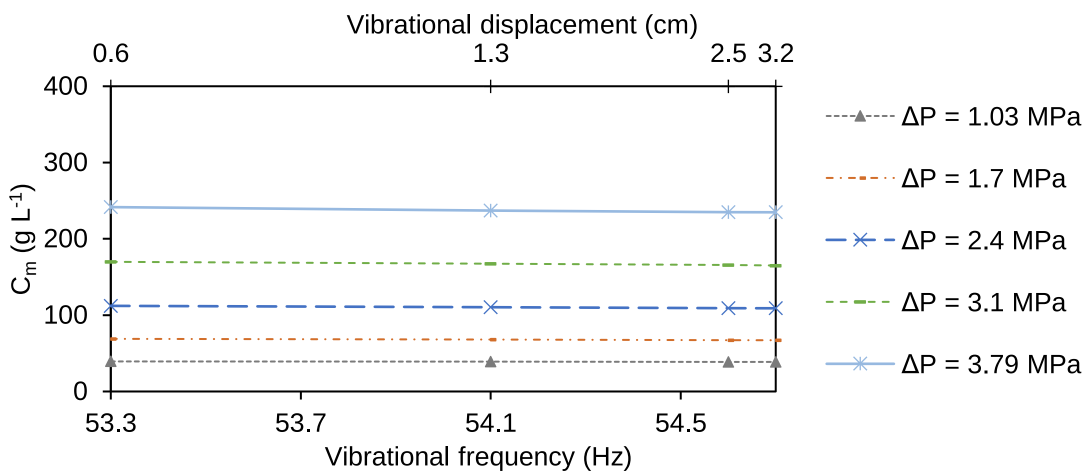

(b) C_o = 33.9 g L^{-1}

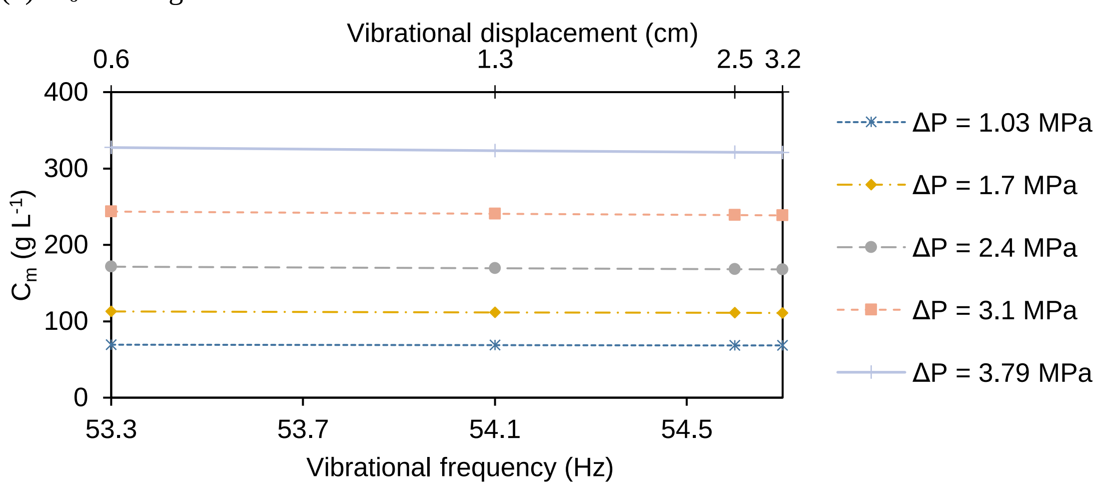

Figure C2

Fouling Resistances Under Different Feed Coffee Extract Concentrations, Applied TMP, and Vibrational Settings at T = 25 °C.

(a) $C_o = 8.5$ g L^{-1}

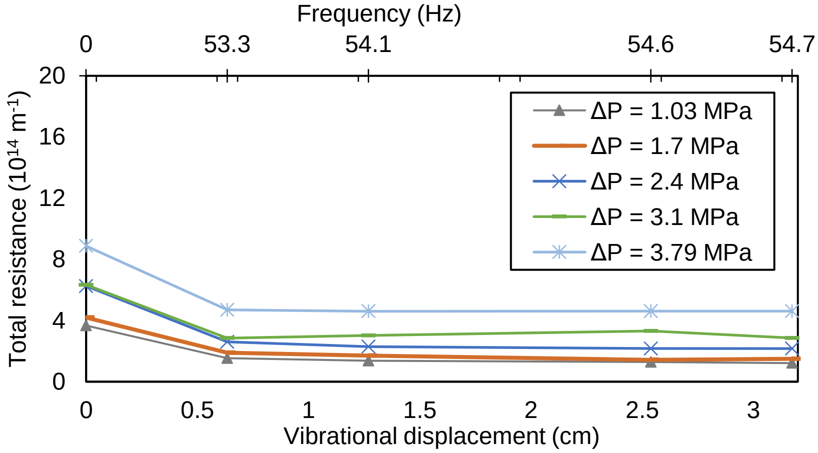

(b) $C_o = 25.4$ g L^{-1}

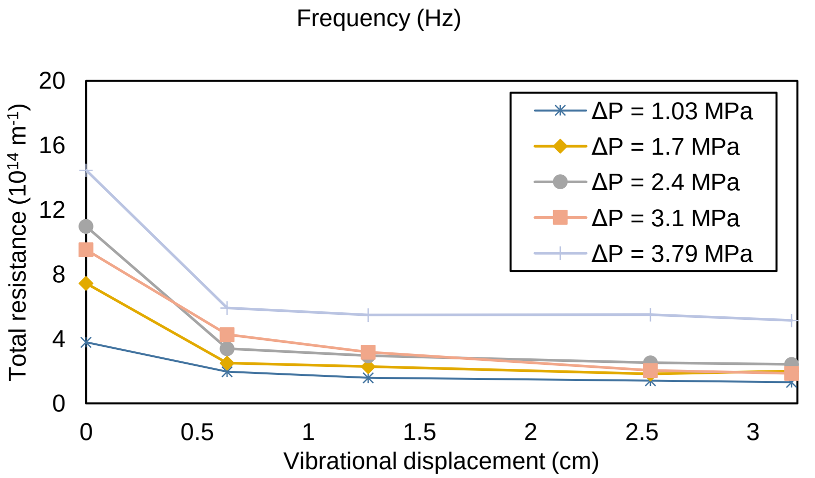

C.2 Calculated Parameters from Semi-Empirical Modeling

Table C1

Calculated Flow, Mass Transfer, Real Rejection Parameters, And Fouling Resistances for Feed Coffee Extract Concentration C_o = 8.5 g L^{-1}

Operating Conditions			Model Parameters				Fouling Resistances	
ΔP (MPa)	F (Hz)	d (cm)	Re	k (10^{-5} m/s)	δ (10^{-5} m)	$r_{real\ COD}$	R_{OSM} (10^{14} m^{-1})	R_{CP} (10^{14} m^{-1})
1.03	0	0	243	0.351	11.217	0.99906	1.299	0.929
	53.3	0.635	4,588	1.215	3.244	0.99347	0.907	0.682
	54.1	1.27	4,657	1.231	3.201	0.99389	0.906	0.615
	54.6	2.54	4,700	1.242	3.174	0.99394	0.906	0.596
	54.7	3.175	4,708	1.244	3.169	0.99305	0.905	0.595
1.72	0	0	243	0.351	11.217	0.99850	1.460	2.212
	53.3	0.635	4,588	1.215	3.244	0.99681	0.918	0.618
	54.1	1.27	4,657	1.231	3.201	0.99731	0.916	0.460
	54.6	2.54	4,700	1.242	3.174	0.99651	0.915	0.378
	54.7	3.175	4,708	1.244	3.169	0.99599	0.914	0.302
2.4	0	0	243	0.351	11.217	0.99906	1.868	2.405
	53.3	0.635	4,588	1.215	3.244	0.99741	0.945	0.770
	54.1	1.27	4,657	1.231	3.201	0.99689	0.941	0.470
	54.6	2.54	4,700	1.242	3.174	0.99806	0.940	0.290
	54.7	3.175	4,708	1.244	3.169	0.99808	0.940	0.254
3.1	0	0	243	0.351	11.217	0.99892	2.212	1.580
	53.3	0.635	4,588	1.215	3.244	0.99795	0.979	0.994
	54.1	1.27	4,657	1.231	3.201	0.99811	0.979	0.613
	54.6	2.54	4,700	1.242	3.174	0.99843	0.978	0.428
	54.7	3.175	4,708	1.244	3.169	0.99842	0.978	0.339
3.79	0	0	243	0.351	11.217	0.99920	2.556	0.423
	53.3	0.635	4,588	1.215	3.244	0.99843	1.035	0.915
	54.1	1.27	4,657	1.231	3.201	0.99804	1.028	0.661
	54.6	2.54	4,700	1.242	3.174	0.99853	1.026	0.425
	54.7	3.175	4,708	1.244	3.169	0.99854	1.025	0.259

Table C2

Calculated Flow, Mass Transfer, Real Rejection Parameters, And Fouling Resistances for Feed Coffee Extract Concentration C_o = 17.0 g L^{-1}

Operating Conditions				Model Parameters			Fouling Resistances	
ΔP (MPa)	F (Hz)	d (cm)	Re	k (10^{-5} m/s)	δ (10^{-5} m)	$r_{real\ COD}$	R_{OSM} (10^{14} m^{-1})	R_{CP} (10^{14} m^{-1})
1.03	0	0	242	0.351	11.205	0.99930	1.600	1.779
	53.3	0.635	4,580	1.211	3.244	0.99024	0.997	1.576
	54.1	1.27	4,649	1.228	3.200	0.99046	0.995	0.922
	54.6	2.54	4,692	1.238	3.173	0.99060	0.994	0.870
	54.7	3.175	4,700	1.240	3.168	0.99063	0.994	0.838
1.72	0	0	242	0.351	11.205	0.99869	1.941	2.252
	53.3	0.635	4,580	1.211	3.244	0.99864	1.010	0.884
	54.1	1.27	4,649	1.228	3.200	0.99865	1.007	0.704
	54.6	2.54	4,692	1.238	3.173	0.99754	1.004	0.424
	54.7	3.175	4,700	1.240	3.168	0.99757	1.004	0.494
2.4	0	0	242	0.351	11.205	0.99937	2.311	4.722
	53.3	0.635	4,580	1.211	3.244	0.99882	1.050	1.551
	54.1	1.27	4,649	1.228	3.200	0.99877	1.045	1.301
	54.6	2.54	4,692	1.238	3.173	0.99907	1.042	1.214
	54.7	3.175	4,700	1.240	3.168	0.99890	1.041	0.994
3.1	0	0	242	0.351	11.205	0.99939	2.678	4.773
	53.3	0.635	4,580	1.211	3.244	0.99870	1.105	1.406
	54.1	1.27	4,649	1.228	3.200	0.99953	1.100	1.184
	54.6	2.54	4,692	1.238	3.173	0.99937	1.096	0.734
	54.7	3.175	4,700	1.240	3.168	0.99905	1.094	0.919
3.79	0	0	242	0.351	11.205	0.99927	3.038	6.760
	53.3	0.635	4,580	1.211	3.244	0.99907	1.172	1.608
	54.1	1.27	4,649	1.228	3.200	0.99873	1.163	1.412
	54.6	2.54	4,692	1.238	3.173	0.99910	1.159	1.083
	54.7	3.175	4,700	1.240	3.168	0.99923	1.158	0.293

Table C3

Calculated Flow, Mass Transfer, Real Rejection Parameters, And Fouling Resistances for Feed Coffee Extract Concentration C_o = 25.4 g L^{-1}

Operating Conditions			Model Parameters				Fouling Resistances	
ΔP (MPa)	F (Hz)	d (cm)	Re	k (10^{-5} m/s)	δ (10^{-5} m)	$r_{real\ COD}$	R_{OSM} (10^{14} m^{-1})	R_{CP} (10^{14} m^{-1})
1.03	0	0	242	0.350	11.193	0.99940	1.872	1.829
	53.3	0.635	4,572	1.207	3.243	0.99881	1.094	1.152
	54.1	1.27	4,640	1.224	3.200	0.99866	1.094	0.582
	54.6	2.54	4,683	1.234	3.173	0.99909	1.092	0.496
	54.7	3.175	4,692	1.236	3.168	0.99902	1.092	0.540
1.72	0	0	242	0.350	11.193	0.99914	2.230	4.026
	53.3	0.635	4,572	1.207	3.243	0.99896	1.099	1.507
	54.1	1.27	4,640	1.224	3.200	0.99902	1.095	1.196
	54.6	2.54	4,683	1.234	3.173	0.99905	1.092	1.079
	54.7	3.175	4,692	1.236	3.168	0.99905	1.091	1.081
2.4	0	0	242	0.350	11.193	0.99960	2.624	5.943
	53.3	0.635	4,572	1.207	3.243	0.99909	1.144	2.152
	54.1	1.27	4,640	1.224	3.200	0.99893	1.138	1.863
	54.6	2.54	4,683	1.234	3.173	0.99928	1.134	1.571
	54.7	3.175	4,692	1.236	3.168	0.99907	1.133	1.286
3.1	0	0	242	0.350	11.193	0.99906	3.014	7.966
	53.3	0.635	4,572	1.207	3.243	0.99913	1.209	2.187
	54.1	1.27	4,640	1.224	3.200	0.99963	1.202	1.752
	54.6	2.54	4,683	1.234	3.173	0.99950	1.196	1.332
	54.7	3.175	4,692	1.236	3.168	0.99936	1.195	1.229
3.79	0	0	242	0.350	11.193	0.99928	3.403	7.117
	53.3	0.635	4,572	1.207	3.243	0.99925	1.284	2.625
	54.1	1.27	4,640	1.224	3.200	0.99942	1.275	2.306
	54.6	2.54	4,683	1.234	3.173	0.99935	1.269	1.476
	54.7	3.175	4,692	1.236	3.168	0.99944	1.268	1.140

Table C4

Calculated Flow, Mass Transfer, Real Rejection Parameters, And Fouling Resistances for Feed Coffee Extract Concentration C_o = 33.9 g L^{-1}

Operating Conditions			Model Parameters				Fouling Resistances	
ΔP (MPa)	F (Hz)	d (cm)	Re	k (10^{-5} m/s)	δ (10^{-5} m)	$r_{real\ COD}$	R_{OSM} (10^{14} m^{-1})	R_{CP} (10^{14} m^{-1})
1.03	0	0	241	0.349	11.180	0.99940	2.140	4.124
	53.3	0.635	4,563	1.203	3.243	0.99956	1.199	2.649
	54.1	1.27	4,632	1.220	3.199	0.99951	1.195	2.601
	54.6	2.54	4,675	1.230	3.173	0.99948	1.193	2.488
	54.7	3.175	4,683	1.232	3.167	0.99949	1.192	2.524
1.7	0	0	241	0.349	11.180	0.99913	2.491	3.843
	53.3	0.635	4,563	1.203	3.243	0.99848	1.186	1.663
	54.1	1.27	4,632	1.220	3.199	0.99851	1.180	1.852
	54.6	2.54	4,675	1.230	3.173	0.99857	1.177	2.135
	54.7	3.175	4,683	1.232	3.167	0.99842	1.176	1.676
2.4	0	0	241	0.349	11.180	0.99944	2.899	4.134
	53.3	0.635	4,563	1.203	3.243	0.99908	1.233	3.101
	54.1	1.27	4,632	1.220	3.199	0.99914	1.226	1.375
	54.6	2.54	4,675	1.230	3.173	0.99942	1.222	1.035
	54.7	3.175	4,683	1.232	3.167	0.99930	1.221	0.815
3.1	0	0	241	0.349	11.180	0.99907	3.306	6.224
	53.3	0.635	4,563	1.203	3.243	0.99909	1.302	2.979
	54.1	1.27	4,632	1.220	3.199	0.99962	1.294	1.884
	54.6	2.54	4,675	1.230	3.173	0.99960	1.289	0.762
	54.7	3.175	4,683	1.232	3.167	0.99948	1.287	0.577
3.79	0	0	241	0.349	11.180	0.99926	3.715	11.440
	53.3	0.635	4,563	1.203	3.243	0.99916	1.384	4.965
	54.1	1.27	4,632	1.220	3.199	0.99885	1.371	4.452
	54.6	2.54	4,675	1.230	3.173	0.99932	1.366	2.990
	54.7	3.175	4,683	1.232	3.167	0.99951	1.365	2.441

Table C5

Calculated Flow, Mass Transfer, Real Rejection Parameters, And Fouling Resistances for Feed Coffee Extract Concentration C_o = 42.4 g L^{-1}

Operating Conditions			Model Parameters				Fouling Resistances	
ΔP (MPa)	F (Hz)	d (cm)	Re	k (10^{-5} m/s)	δ (10^{-5} m)	$r_{real\ COD}$	R_{OSM} (10^{14} m^{-1})	R_{CP} (10^{14} m^{-1})
1.03	0	0	241	0.348	11.168	0.99942	2.416	2.605
	53.3	0.635	4,555	1.200	3.243	0.99912	1.308	1.769
	54.1	1.27	4,623	1.216	3.199	0.99944	1.304	1.774
	54.6	2.54	4,666	1.226	3.172	0.99926	1.301	1.715
	54.7	3.175	4,675	1.228	3.167	0.99946	1.300	1.652
1.7	0	0	241	0.348	11.168	0.99904	2.745	6.128
	53.3	0.635	4,555	1.200	3.243	0.99794	1.274	3.428
	54.1	1.27	4,623	1.216	3.199	0.99802	1.267	3.337
	54.6	2.54	4,666	1.226	3.172	0.99809	1.263	3.353
	54.7	3.175	4,675	1.228	3.167	0.99810	1.263	3.342
2.4	0	0	241	0.348	11.168	0.99934	3.158	7.938
	53.3	0.635	4,555	1.200	3.243	0.99879	1.319	3.228
	54.1	1.27	4,623	1.216	3.199	0.99915	1.312	3.947
	54.6	2.54	4,666	1.226	3.172	0.99936	1.307	2.825
	54.7	3.175	4,675	1.228	3.167	0.99931	1.306	2.178
3.1	0	0	241	0.348	11.168	0.99895	3.577	10.892
	53.3	0.635	4,555	1.200	3.243	0.99917	1.392	4.538
	54.1	1.27	4,623	1.216	3.199	0.99944	1.382	4.101
	54.6	2.54	4,666	1.226	3.172	0.99946	1.376	4.123
	54.7	3.175	4,675	1.228	3.167	0.99947	1.375	3.773
3.79	0	0	241	0.348	11.168	0.99922	4.001	11.471
	53.3	0.635	4,555	1.200	3.243	0.99914	1.477	4.695
	54.1	1.27	4,623	1.216	3.199	0.99894	1.464	4.385
	54.6	2.54	4,666	1.226	3.172	0.99930	1.458	4.412
	54.7	3.175	4,675	1.228	3.167	0.99959	1.457	4.145

C.3 Permeate Characteristics and Observed Rejection Efficiencies

Table C6

Permeate Characteristics and Corresponding Observed Rejection Efficiencies at Various Operating Conditions for $C_o = 8.5\ g\ L^{-1}$

Operating Conditions			Permeate Characteristics				Observed Rejection			
ΔP MPa	F Hz	d cm	Conductivity μS/cm	Turbidity NTU	Abs	COD mg/L	$r_{o\ cond}$	$r_{o\ turb}$	$r_{o\ abs}$	$r_{o\ COD}$
1.03	0	0	44	0.102	0.0	90	0.961	1.000	1.000	0.989
	53.3	0.635	87	0.103	0.0	100	0.923	1.000	1.000	0.988
	54.1	1.27	36	0.093	0.0	63	0.968	1.000	0.964	0.993
	54.6	2.54	45	0.119	0.0	49	0.960	1.000	1.000	0.994
	54.7	3.175	139	0.092	0.0	159	0.877	1.000	1.000	0.981
1.7	0	0	256	0.218	0.0	240	0.773	0.999	1.000	0.972
	53.3	0.635	76	0.150	0.0	113	0.933	1.000	1.000	0.987
	54.1	1.27	100	0.171	0.0	107	0.911	1.000	0.998	0.987
	54.6	2.54	55	0.166	0.0	85	0.952	1.000	0.996	0.990
	54.7	3.175	139	0.092	0.0	159	0.877	1.000	1.000	0.981
2.4	0	0	234	0.127	0.0	267	0.793	1.000	1.000	0.968
	53.3	0.635	205	0.193	0.0	169	0.818	1.000	1.000	0.980
	54.1	1.27	286	0.112	0.0	248	0.747	1.000	0.999	0.971
	54.6	2.54	182	0.140	0.0	148	0.838	1.000	1.000	0.982
	54.7	3.175	133	0.135	0.0	130	0.882	1.000	0.999	0.985
3.1	0	0	538	0.495	0.0	437	0.523	0.999	0.989	0.948
	53.3	0.635	165	0.277	0.0	227	0.854	0.999	0.996	0.973
	54.1	1.27	100	0.171	0.0	107	0.911	1.000	0.998	0.987
	54.6	2.54	77	0.175	0.0	119	0.931	1.000	0.998	0.986
	54.7	3.175	248	0.158	0.0	177	0.780	1.000	0.999	0.979
3.79	0	0	628	0.169	0.0	433	0.443	1.000	1.000	0.949
	53.3	0.635	359	0.214	0.0	253	0.682	0.999	1.000	0.970
	54.1	1.27	474	0.152	0.0	392	0.579	1.000	1.000	0.954
	54.6	2.54	330	0.216	0.0	229	0.708	0.999	1.000	0.973
	54.7	3.175	315	0.110	0.0	228	0.720	1.000	0.996	0.973

Table C7

Permeate Characteristics and Corresponding Observed Rejection Efficiencies at Various Operating Conditions for C_o = 17.0 g L^{-1}

Operating Conditions			Permeate Characteristics				Observed Rejection			
ΔP MPa	F Hz	d cm	Conductivity μS/cm	Turbidity NTU	Abs	COD mg/L	$r_{o\ cond}$	$r_{o\ turb}$	$r_{o\ abs}$	$r_{o\ COD}$
1.03	0	0	40	0.094	0.0	81	0.977	1.000	1.000	0.996
	53.3	0.635	78	0.209	0.0	83	0.955	1.000	1.000	0.995
	54.1	1.27	25	0.091	0.0	48	0.986	1.000	0.979	0.997
	54.6	2.54	36	0.094	0.0	47	0.979	1.000	0.997	0.997
	54.7	3.175	122	0.080	0.0	145	0.930	1.000	1.000	0.992
1.7	0	0	299	0.506	0.0	276	0.829	1.000	1.000	0.985
	53.3	0.635	81	0.134	0.0	99	0.954	1.000	0.996	0.994
	54.1	1.27	84	0.134	0.0	83	0.952	1.000	1.000	0.995
	54.6	2.54	43	0.116	0.0	54	0.975	1.000	0.998	0.997
	54.7	3.175	122	0.080	0.0	145	0.930	1.000	1.000	0.992
2.4	0	0	178	0.199	0.0	208	0.898	1.000	1.000	0.988
	53.3	0.635	192	0.109	0.0	140	0.890	1.000	1.000	0.992
	54.1	1.27	195	0.093	0.0	163	0.888	1.000	0.998	0.991
	54.6	2.54	145	0.085	0.0	111	0.917	1.000	1.000	0.994
	54.7	3.175	118	0.071	0.0	100	0.933	1.000	1.000	0.994
3.1	0	0	513	0.266	0.0	276	0.706	1.000	0.997	0.985
	53.3	0.635	162	0.134	0.0	232	0.907	1.000	1.000	0.987
	54.1	1.27	84	0.134	0.0	83	0.952	1.000	1.000	0.995
	54.6	2.54	70	0.236	0.0	110	0.960	1.000	0.999	0.994
	54.7	3.175	207	0.153	0.0	151	0.881	1.000	1.000	0.992
3.79	0	0	606	0.162	0.0	430	0.653	1.000	0.998	0.976
	53.3	0.635	344	0.242	0.0	235	0.803	1.000	1.000	0.987
	54.1	1.27	379	0.092	0.0	315	0.783	1.000	1.000	0.982
	54.6	2.54	250	0.120	0.0	212	0.857	1.000	1.000	0.988
	54.7	3.175	264	0.114	0.0	192	0.849	1.000	1.000	0.989

Table C8

Permeate Characteristics and Corresponding Observed Rejection Efficiencies at Various Operating Conditions for C_o = 25.4 g L^{-1}

Operating Conditions			Permeate Characteristics				Observed Rejection			
ΔP MPa	F Hz	d cm	Conductivity µS/cm	Turbidity NTU	Abs	COD mg/L	$r_{o\ cond}$	$r_{o\ turb}$	$r_{o\ abs}$	$r_{o\ COD}$
1.03	0	0	44	0.099	0.0	83	0.983	1.000	1.000	0.997
	53.3	0.635	77	0.193	0.0	74	0.971	1.000	1.000	0.997
	54.1	1.27	23	0.085	0.0	83	0.991	1.000	0.990	0.997
	54.6	2.54	34	0.112	0.0	53	0.987	1.000	1.000	0.998
	54.7	3.175	13	0.070	0.0	46	0.995	1.000	1.000	0.998
1.7	0	0	228	0.441	0.0	198	0.913	1.000	1.000	0.993
	53.3	0.635	43	0.158	0.0	85	0.984	1.000	0.999	0.997
	54.1	1.27	101	0.146	0.0	86	0.961	1.000	1.000	0.997
	54.6	2.54	55	0.110	0.0	65	0.979	1.000	1.000	0.998
	54.7	3.175	13	0.070	0.0	46	0.995	1.000	1.000	0.998
2.4	0	0	198	0.175	0.0	140	0.925	1.000	0.998	0.995
	53.3	0.635	191	0.157	0.0	153	0.927	1.000	1.000	0.995
	54.1	1.27	187	0.085	0.0	172	0.929	1.000	1.000	0.994
	54.6	2.54	142	0.126	0.0	116	0.946	1.000	1.000	0.996
	54.7	3.175	120	0.064	0.0	146	0.954	1.000	1.000	0.995
3.1	0	0	548	0.230	0.0	449	0.791	1.000	0.998	0.985
	53.3	0.635	202	0.234	0.0	204	0.923	1.000	0.998	0.993
	54.1	1.27	101	0.146	0.0	86	0.961	1.000	1.000	0.997
	54.6	2.54	37	0.151	0.0	100	0.986	1.000	1.000	0.997
	54.7	3.175	216	0.175	0.0	154	0.918	1.000	1.000	0.995
3.79	0	0	612	0.135	0.0	439	0.767	1.000	1.000	0.985
	53.3	0.635	372	0.314	0.0	249	0.858	1.000	1.000	0.991
	54.1	1.27	369	0.147	0.0	489	0.859	1.000	1.000	0.983
	54.6	2.54	273	0.158	0.0	212	0.896	1.000	1.000	0.993
	54.7	3.175	265	0.204	0.0	171	0.899	1.000	1.000	0.994

Table C9

Permeate Characteristics and Corresponding Observed Rejection Efficiencies at Various Operating Conditions for C_o = 33.9 g L^{-1}

Operating Conditions			Permeate Characteristics				Observed Rejection			
ΔP MPa	F Hz	d cm	Conductivity μS/cm	Turbidity NTU	Abs	COD mg/L	$r_{o\ cond}$	$r_{o\ turb}$	$r_{o\ abs}$	$r_{o\ COD}$
1.03	0	0	46	0.120	0.0	89	0.985	1.000	1.000	0.998
	53.3	0.635	72	0.134	0.0	73	0.976	1.000	0.997	0.998
	54.1	1.27	22	0.136	0.0	55	0.993	1.000	0.991	0.999
	54.6	2.54	35	0.109	0.0	51	0.989	1.000	0.999	0.999
	54.7	3.175	16	0.084	0.0	41	0.995	1.000	1.000	0.999
1.7	0	0	265	0.219	0.0	212	0.913	1.000	0.999	0.994
	53.3	0.635	58	0.216	0.0	98	0.981	1.000	0.999	0.997
	54.1	1.27	118	0.132	0.0	86	0.961	1.000	0.991	0.998
	54.6	2.54	46	0.123	0.0	69	0.985	1.000	1.000	0.998
	54.7	3.175	16	0.084	0.0	41	0.995	1.000	1.000	0.999
2.4	0	0	212	0.167	0.0	205	0.931	1.000	1.000	0.995
	53.3	0.635	193	0.139	0.0	169	0.937	1.000	1.000	0.995
	54.1	1.27	181	0.079	0.0	157	0.940	1.000	1.000	0.996
	54.6	2.54	138	0.131	0.0	105	0.955	1.000	1.000	0.997
	54.7	3.175	114	0.075	0.0	129	0.963	1.000	0.998	0.997
3.1	0	0	560	0.393	0.0	460	0.816	1.000	1.000	0.988
	53.3	0.635	271	0.443	0.0	244	0.911	1.000	0.999	0.993
	54.1	1.27	118	0.132	0.0	86	0.961	1.000	0.991	0.998
	54.6	2.54	50	0.197	0.0	97	0.983	1.000	1.000	0.997
	54.7	3.175	200	0.155	0.0	135	0.935	1.000	0.999	0.996
3.79	0	0	636	0.225	0.0	462	0.791	1.000	1.000	0.988
	53.3	0.635	409	0.256	0.0	294	0.866	1.000	1.000	0.992
	54.1	1.27	351	0.101	0.0	412	0.885	1.000	1.000	0.989
	54.6	2.54	288	0.179	0.0	241	0.905	1.000	1.000	0.994
	54.7	3.175	246	0.104	0.0	188	0.919	1.000	0.999	0.995

Table C10

Permeate Characteristics and Corresponding Observed Rejection Efficiencies at Various Operating Conditions for C_o = 42.4 g L^{-1}

Operating Conditions			Permeate Characteristics				Observed Rejection			
ΔP MPa	F Hz	d cm	Conductivity µS cm^{-1}	Turbidity NTU	Abs	COD mg L^{-1}	$r_{o\ cond}$	$r_{o\ turb}$	$r_{o\ abs}$	$r_{o\ COD}$
1.03	0	0	44	0.135	0.0	92	0.989	1.000	1.000	0.998
	53.3	0.635	75	0.201	0.0	81	0.981	1.000	1.000	0.998
	54.1	1.27	21	0.091	0.0	50	0.994	1.000	1.000	0.999
	54.6	2.54	39	0.155	0.0	59	0.990	1.000	0.998	0.999
	54.7	3.175	15	0.079	0.0	49	0.996	1.000	1.000	0.999
1.7	0	0	294	0.324	0.0	245	0.924	1.000	1.000	0.995
	53.3	0.635	88	0.205	0.0	123	0.977	1.000	0.999	0.997
	54.1	1.27	125	0.229	0.0	133	0.967	1.000	1.000	0.997
	54.6	2.54	64	0.129	0.0	68	0.983	1.000	1.000	0.999
	54.7	3.175	38	0.174	0.0	33	0.990	1.000	1.000	0.999
2.4	0	0	252	0.215	0.0	250	0.934	1.000	1.000	0.995
	53.3	0.635	262	0.179	0.0	261	0.932	1.000	1.000	0.995
	54.1	1.27	193	0.108	0.0	181	0.950	1.000	0.998	0.996
	54.6	2.54	145	0.104	0.0	119	0.962	1.000	1.000	0.998
	54.7	3.175	120	0.070	0.0	147	0.969	1.000	1.000	0.997
3.1	0	0	597	0.703	0.0	533	0.845	1.000	0.998	0.989
	53.3	0.635	255	0.454	0.0	252	0.934	1.000	0.997	0.995
	54.1	1.27	125	0.229	0.0	133	0.967	1.000	1.000	0.997
	54.6	2.54	78	0.240	0.0	129	0.980	1.000	1.000	0.997
	54.7	3.175	202	0.237	0.0	152	0.948	1.000	0.999	0.997
3.79	0	0	659	0.651	0.0	498	0.829	1.000	1.000	0.990
	53.3	0.635	423	0.450	0.0	348	0.890	1.000	1.000	0.993
	54.1	1.27	351	0.134	0.0	416	0.909	1.000	1.000	0.991
	54.6	2.54	304	0.300	0.0	272	0.921	1.000	1.000	0.994
	54.7	3.175	235	0.113	0.0	164	0.939	1.000	1.000	0.997

C.3 R_{CP} Correlation

Table C11

Fit Statistics for R_{CP} Correlation

Regression Statistics	
Multiple R	0.909
R Square	0.857
Adjusted R Square	0.849
Standard Error	0.148
Observations	75

Table C12

Analysis of Variance for R_{CP} Correlation

	df	*SS*	*MS*	*F*	*Significance F*
Regression	3	10.787	3.596	112.95	5.801E-27
Residual	71	2.260	0.032		
Total	74	13.047			

Table C13

Regression Analysis for R_{CP} Correlation

	Coefficients	*Standard Error*	*t Stat*	*P-value*
Intercept	10.403	0.668	15.567	0.000
Log ΔP	0.485	0.103	4.692	0.000
Log C_o	1.103	0.071	15.612	0.000
Log $\Upsilon_{w\ max}$	-0.481	0.056	-8.549	0.000

Appendix D

Supporting Information for Statistical Analyses

D.1 Statistical Analysis for Multivariate Regression

Table D1

Analysis of Variance (ANOVA) for Reduced Quadratic Model for Permeate Flux with Logarithmic Transform

Source	Sum of Squares	df	Mean Square	F-value	p-value	Remarks
Model	0.9096	8	0.1137	158.49	< 0.0001	significant
A-Feed Conc	0.5676	1	0.5676	791.14	< 0.0001	
B-Pressure	0.1445	1	0.1445	201.47	< 0.0001	
C-Frequency	0.0147	1	0.0147	20.52	0.0019	
AB	0.0688	1	0.0688	95.95	< 0.0001	
BC	0.0057	1	0.0057	7.95	0.0225	
A^2	0.0122	1	0.0122	16.98	0.0033	
B^2	0.0584	1	0.0584	81.45	< 0.0001	
C^2	0.0421	1	0.0421	58.66	< 0.0001	
Residual	0.0057	8	0.0007			
Lack of Fit	0.0032	4	0.0008	1.22	0.4260	not significant
Pure Error	0.0026	4	0.0006			
Cor Total	0.9153	16				

Table D2

Fit Statistics for Permeate Flux Correlation

Parameter	Value
Std. Dev.	0.0268
Mean	1.51
C.V. %	1.78
R^2	0.9937
Adjusted R^2	0.9875
Predicted R^2	0.9716

Table D3

Analysis of Variance (ANOVA) for Reduced Quadratic Model for Permeate Conductivity with Logarithmic Transform

Source	Sum of Squares	df	Mean Square	F-value	p-value	Remarks
Model	2.91	5	0.5820	2223.43	< 0.0001	significant
A-Feed Conc	2.03	1	2.03	7763.54	< 0.0001	
B-Pressure	0.1531	1	0.1531	584.82	< 0.0001	
C-Frequency	0.0013	1	0.0013	5.05	0.0512	
AB	0.0117	1	0.0117	44.63	< 0.0001	
A^2	0.2722	1	0.2722	1040.00	< 0.0001	
Residual	0.0024	9	0.0003			
Lack of Fit	0.0014	5	0.0003	1.20	0.4423	not significant
Pure Error	0.0009	4	0.0002			
Cor Total	2.91	14				

Table D4

Fit Statistics for Permeate Flux Correlation

Parameter	Value
Std. Dev	0.0162
Mean	2.06
C.V. %	0.7871
R^2	0.9992
Adjusted R^2	0.9987
Predicted R^2	0.9969
Adequate Precision	140.6875

Table D5

Analysis of Variance (ANOVA) for Reduced Quadratic Model for Permeate COD

Source	Sum of Squares	df	Mean Square	F-value	p-value	Remarks
Model	1.951E+05	6	32517.46	1615.77	< 0.0001	significant
A-Feed Conc	1.005E+05	1	1.005E+05	4993.24	< 0.0001	
B-Pressure	14981.33	1	14981.33	744.41	< 0.0001	
C-Frequency	4608.00	1	4608.00	228.97	< 0.0001	
AB	520.08	1	520.08	25.84	0.0009	
AC	2450.25	1	2450.25	121.75	< 0.0001	
A^2	3519.09	1	3519.09	174.86	< 0.0001	
Residual	161.00	8	20.12			
Lack of Fit	39.30	4	9.82	0.3229	0.8503	not significant
Pure Error	121.70	4	30.42			

Table D6

Fit Statistics for Permeate Flux Correlation

Parameter	Value
Std. Dev	4.49
Mean	194.87
C.V. %	2.30
R^2	0.9992
Adjusted R^2	0.9986
Predicted R^2	0.9970
Adequate Precision	127.4236

Table D7

Analysis of Variance (ANOVA) for Reduced Quadratic Model for Conductivity Rejection

Source	Sum of Squares	df	Mean Square	F-value	p-value	Remarks
Model	164.97	6	27.49	144.13	< 0.0001	significant
A-Feed Conc	94.17	1	94.17	493.64	< 0.0001	
B-Pressure	28.24	1	28.24	148.02	< 0.0001	
C-Frequency	0.0696	1	0.0696	0.3646	0.5627	
AB	7.49	1	7.49	39.27	0.0002	
BC	4.90	1	4.90	25.68	0.0010	
C^2	5.77	1	5.77	30.24	0.0006	
Residual	1.53	8	0.1908			
Lack of Fit	1.30	4	0.3261	5.88	0.0572	not significant
Pure Error	0.2217	4	0.0554			

Table D8

Fit Statistics for Permeate Flux Correlation

Parameter	Value
Std. Dev	0.4368
Mean	93.07
C.V. %	0.4693
R^2	0.9908
Adjusted R^2	0.9840
Predicted R^2	0.9428
Adequate Precision	46.3940

Table D9

Analysis of Variance (ANOVA) for Reduced Linear Model for COD Rejection

Source	Sum of Squares	df	Mean Square	F-value	p-value	Remarks
Model	0.3958	2	0.1979	24.92	< 0.0001	significant
B-Pressure	0.3703	1	0.3703	46.65	< 0.0001	
C-Frequency	0.0254	1	0.0254	3.20	0.0951	
Residual	0.1111	14	0.0079			
Lack of Fit	0.1097	10	0.0110	30.71	0.0024	significant
Pure Error	0.0014	4	0.0004			
Cor Total	0.5069	16				
Model	0.3958	2	0.1979	24.92	< 0.0001	significant

Table D10

Fit Statistics for Permeate Flux Correlation

Parameter	Value
Std. Dev	0.0891
Mean	99.36
C.V. %	0.0897
R^2	0.7807
Adjusted R^2	0.7494
Predicted R^2	0.6652
Adequate Precision	14.5090

D.2 Diagnostic Tools

Figure D1

Normal Plot of Residuals for Reduced Quadratic Model Correlation of Permeate Flux with Logarithmic Transform

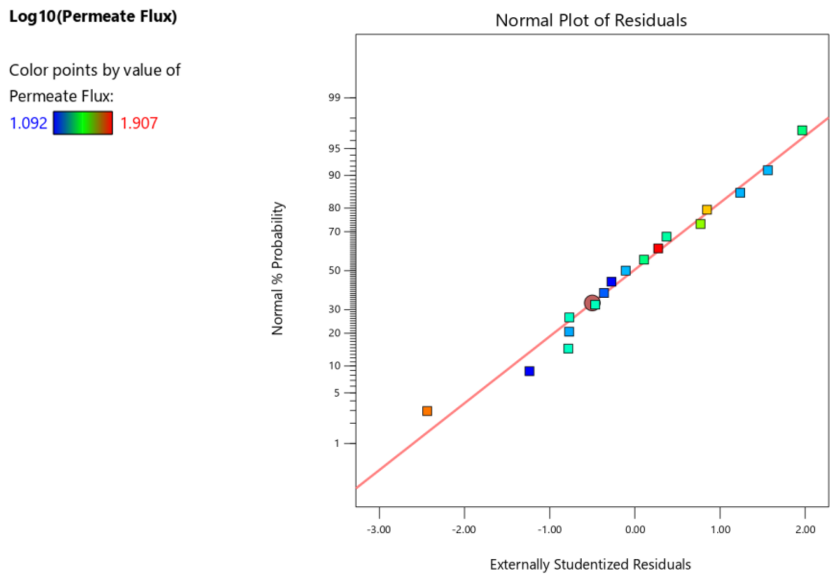

Figure D2

Residuals vs Predicted Diagnostic Plot for Reduced Quadratic Model Correlation of Permeate Flux with Logarithmic Transform

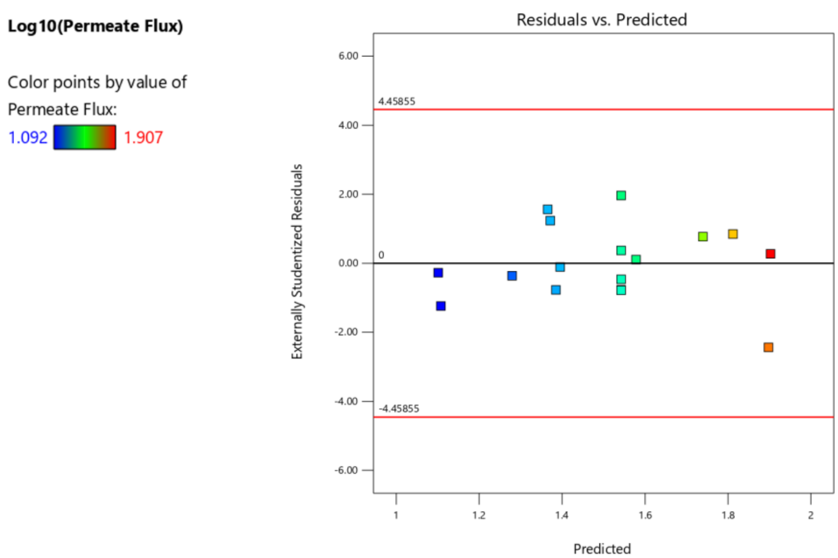

Figure D3

Box-Cox Plot for Reduced Quadratic Model Correlation of Permeate Flux with Logarithmic Transform

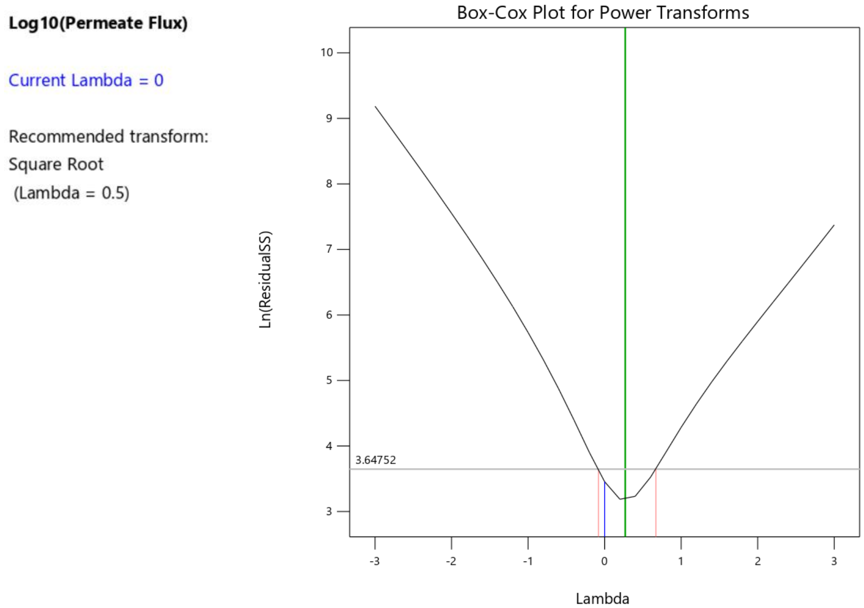

Figure D4

Predicted vs Actual Diagnostic Plot for Reduced Quadratic Model Correlation of Permeate Flux with Logarithmic Transform

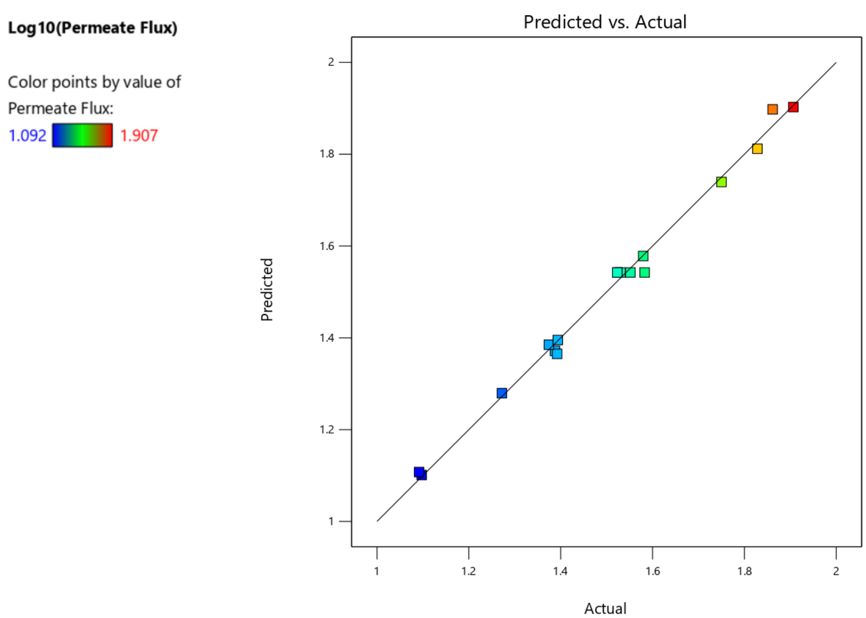

Figure D5

Normal Plot of Residuals for Reduced Quadratic Model Correlation of Permeate Conductivity with Logarithmic Transform

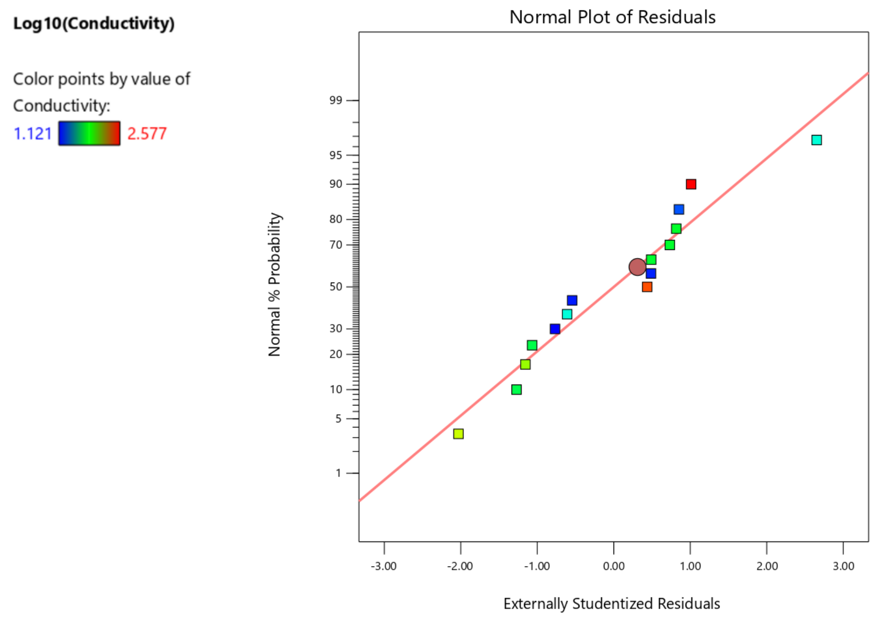

Figure D6

Residuals vs Predicted Diagnostic Plot for Reduced Quadratic Model Correlation of Permeate Conductivity with Logarithmic Transform

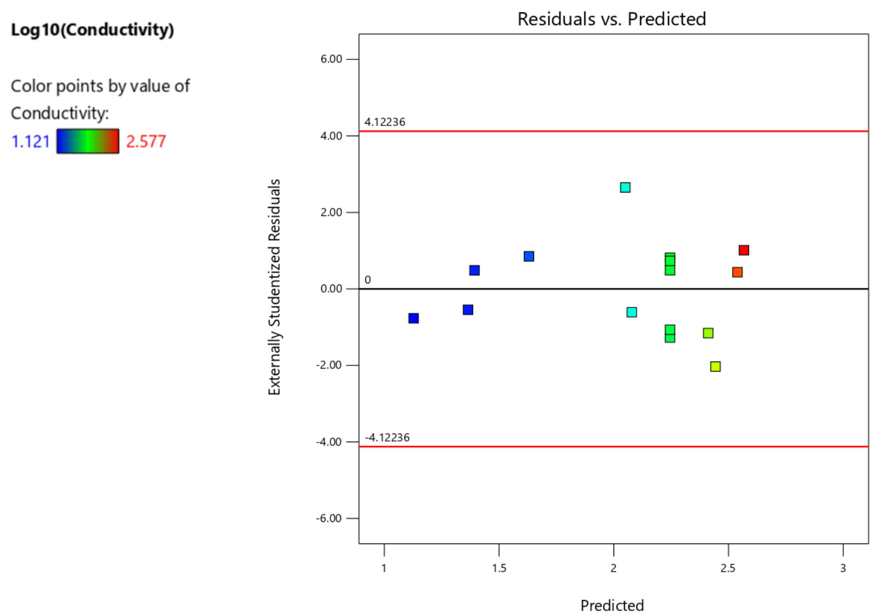

Figure D7

Box-Cox Plot for Reduced Quadratic Model Correlation of Permeate Conductivity with Logarithmic Transform

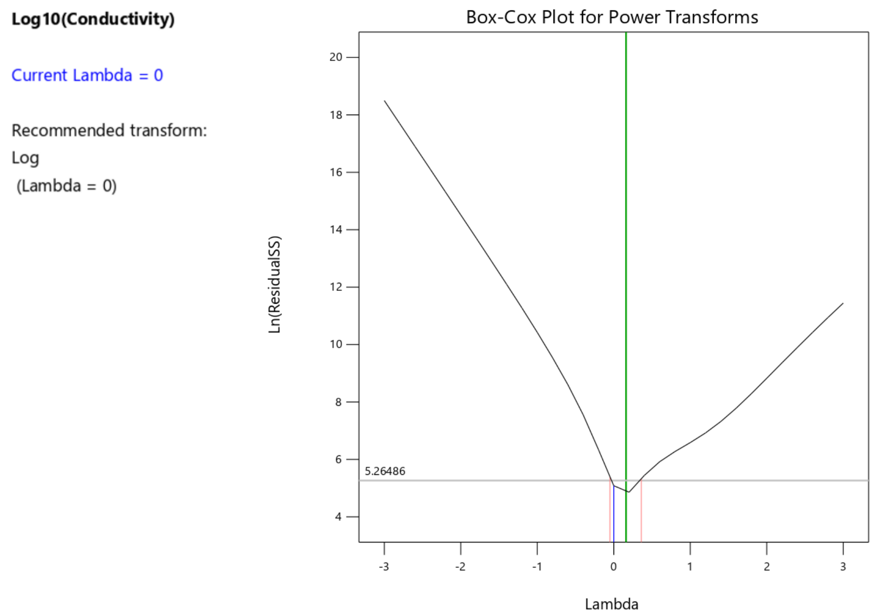

Figure D8

Predicted vs Actual Diagnostic Plot for Reduced Quadratic Model Correlation of Permeate Conductivity with Logarithmic Transform

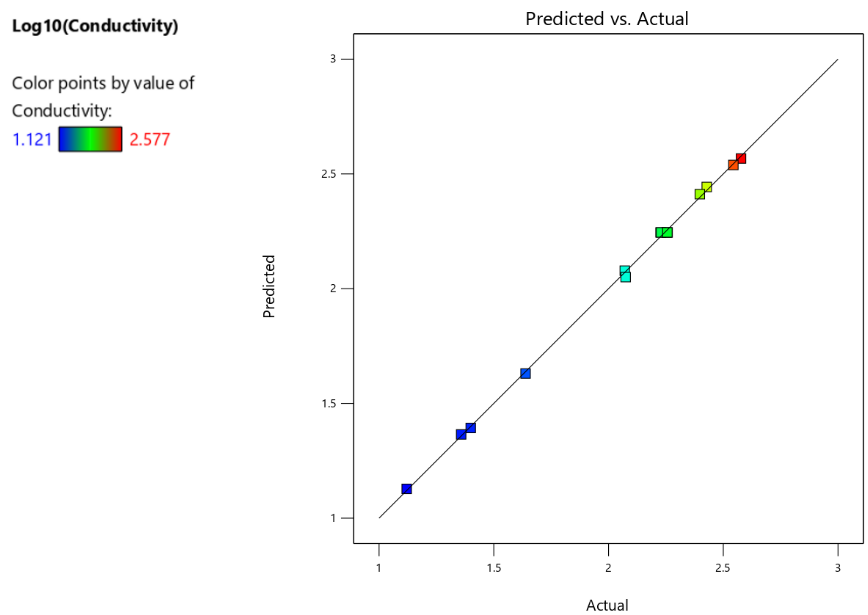

Figure D9

Normal Plot of Residuals for Reduced Quadratic Model Correlation of Permeate COD

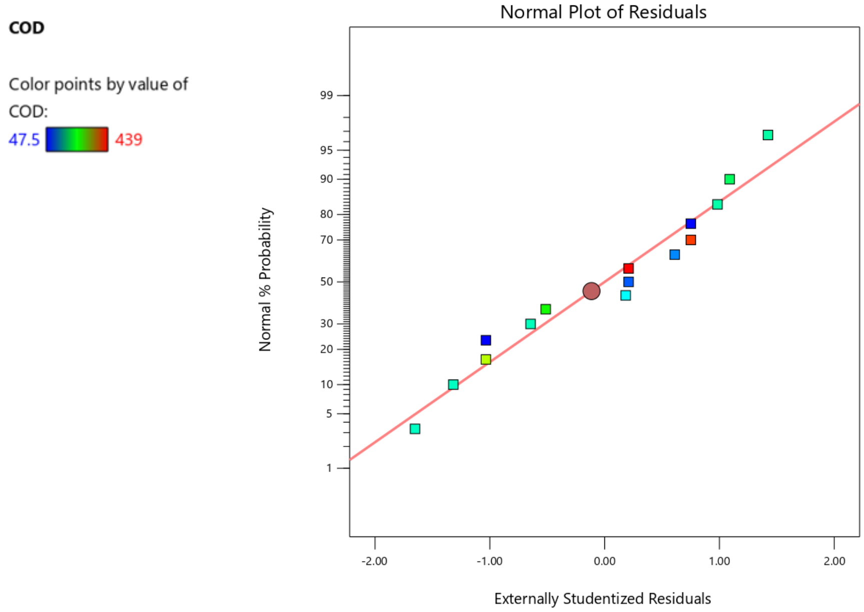

Figure D10

Residuals vs Predicted Diagnostic Plot for Reduced Quadratic Model Correlation of Permeate COD

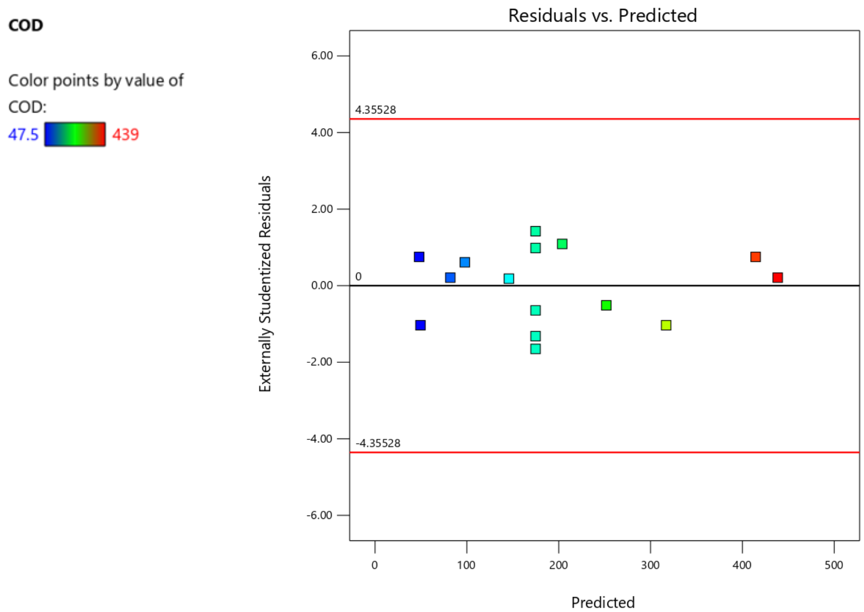

Figure D11

Box-Cox Plot for Reduced Quadratic Model Correlation of Permeate COD

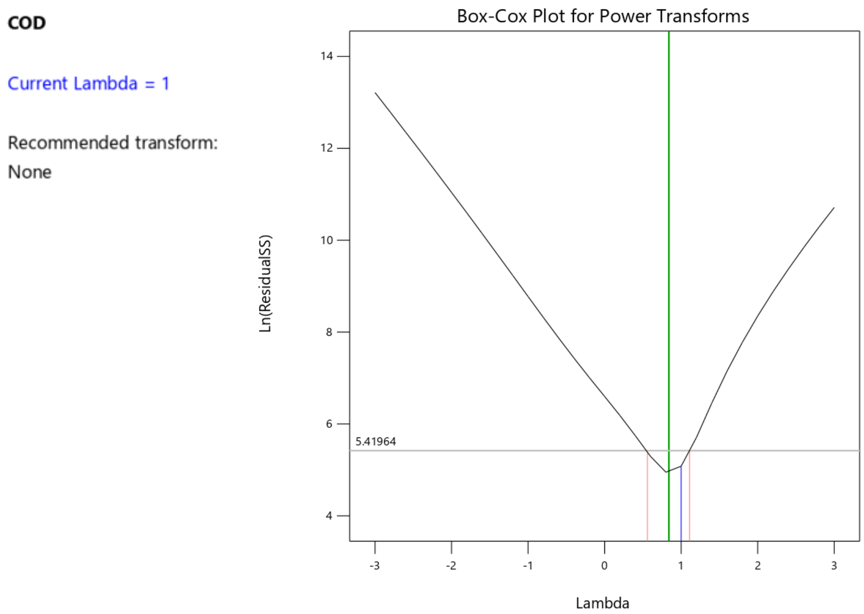

Figure D12

Predicted vs Actual Diagnostic Plot for Reduced Quadratic Model Correlation of Permeate COD

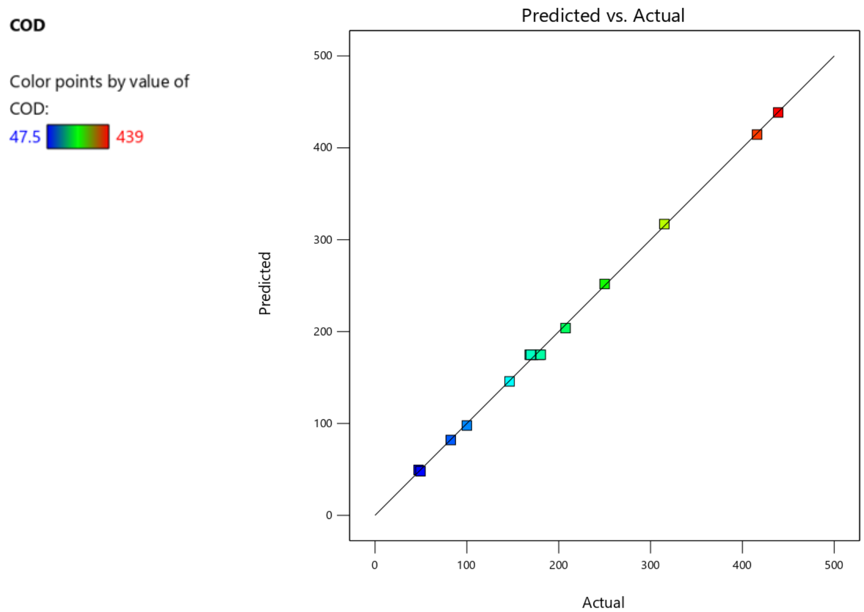

Figure D13

Normal Plot of Residuals for Reduced Quadratic Model Correlation of Conductivity Rejection

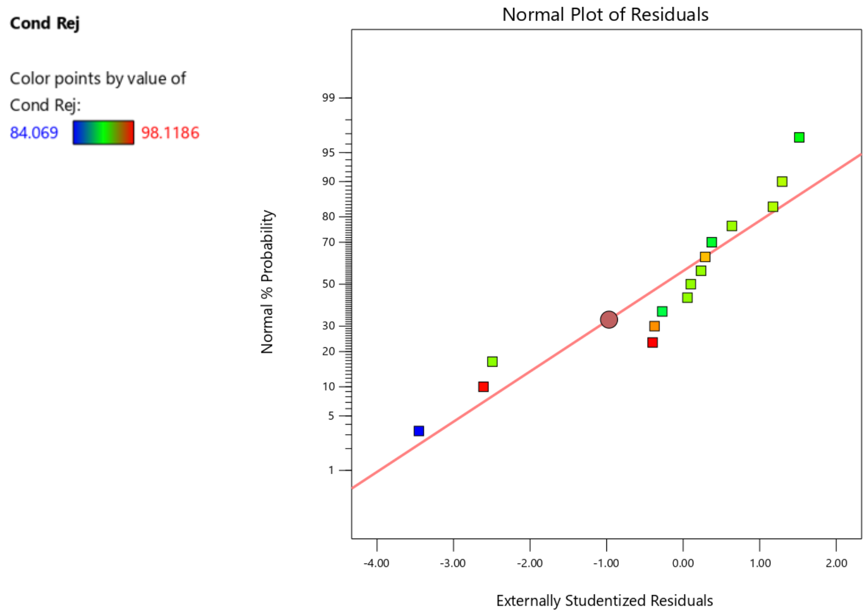

Figure D14

Residuals vs Predicted Diagnostic Plot for Reduced Quadratic Model Correlation of Conductivity Rejection

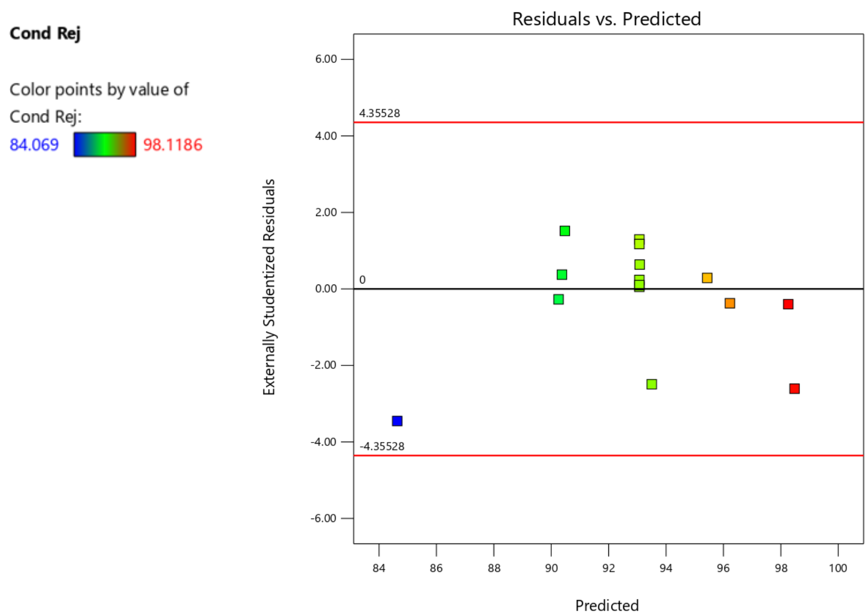

Figure D15

Box-Cox Plot for Reduced Quadratic Model Correlation of Conductivity Rejection

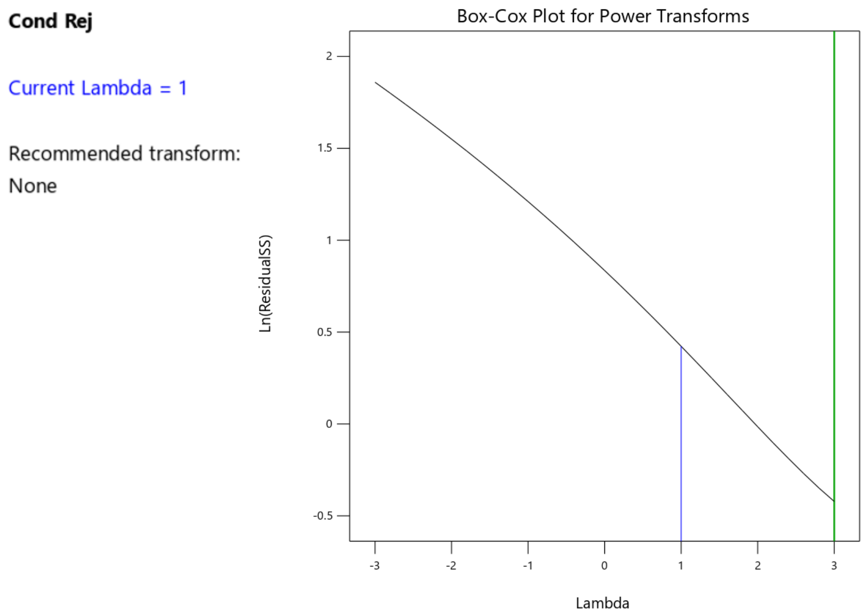

Figure D16

Predicted vs Actual Diagnostic Plot for Reduced Quadratic Model Correlation of Conductivity Rejection

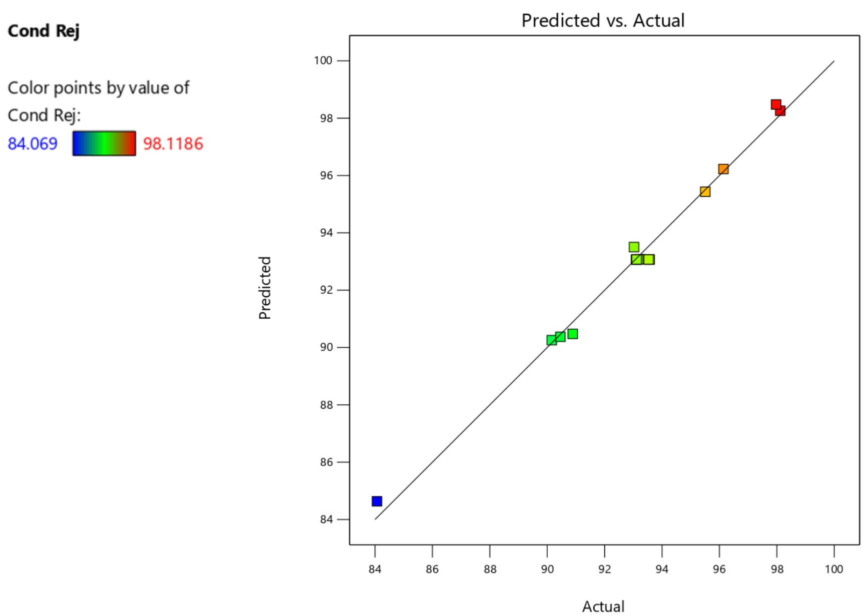

Figure D17

Normal Plot of Residuals for Reduced Linear Model Correlation of COD Rejection

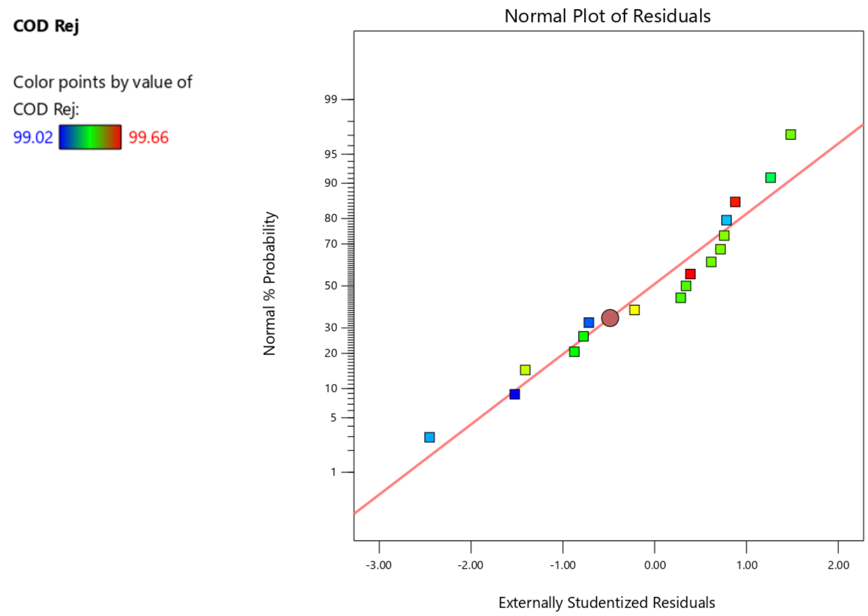

Figure D18

Residuals vs Predicted Diagnostic Plot for Reduced Linear Model Correlation of COD Rejection

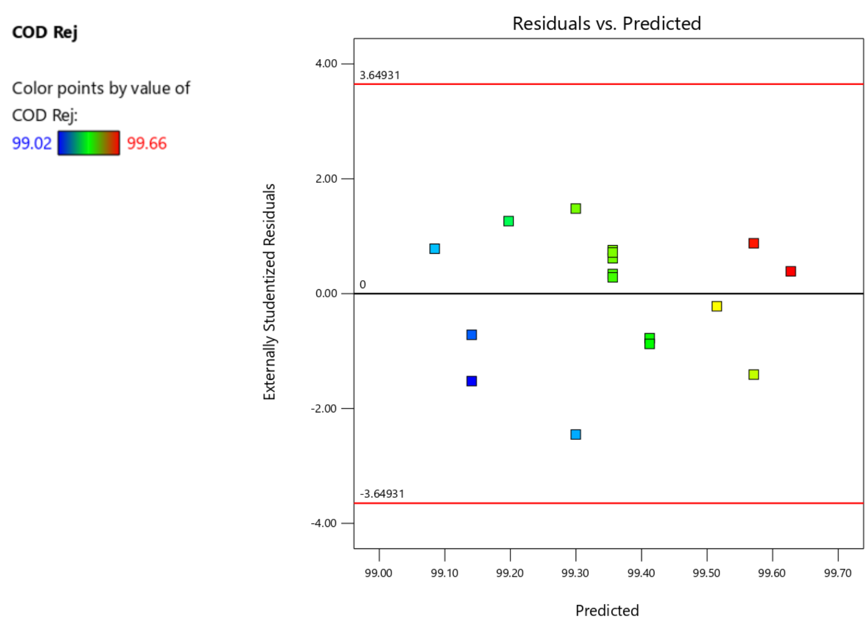

Figure D19

Box-Cox Plot for Reduced Linear Model Correlation of COD Rejection

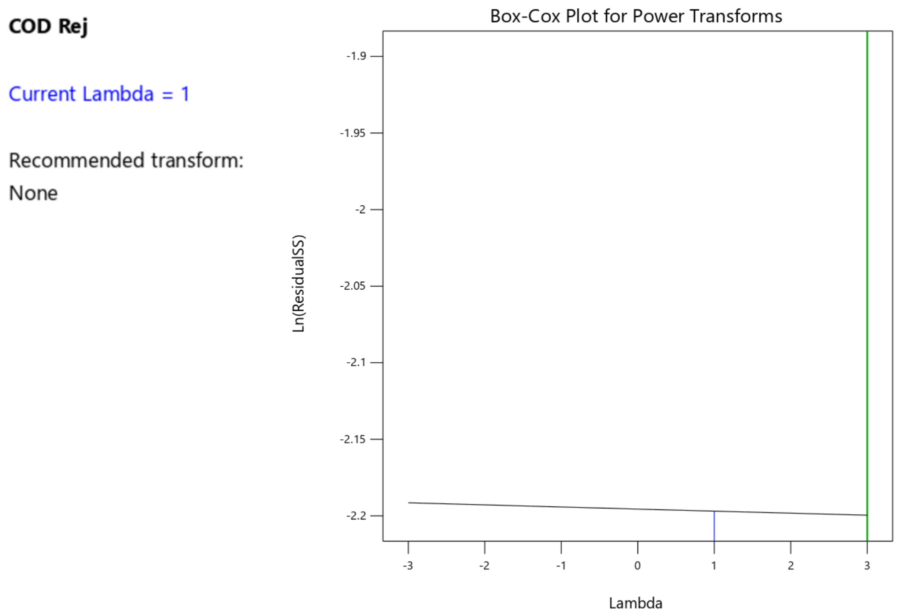

Figure D20

Predicted vs Actual Diagnostic Plot for Reduced Linear Model Correlation of COD Rejection

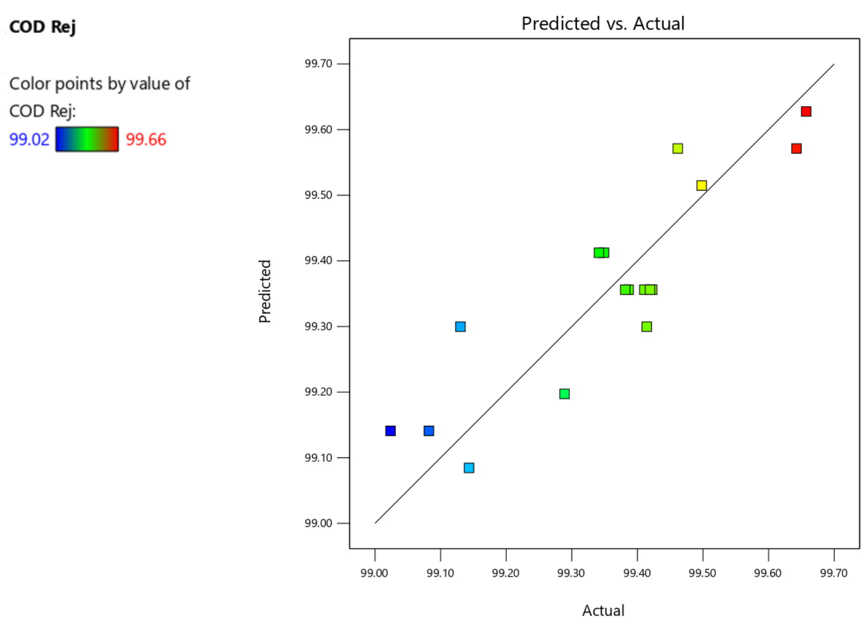

Table D11

Constraints for Numerical Optimization of Vibratory NF of Coffee Extracts

Name	Goal	Lower Limit	Upper Limit	Lower Weight	Upper Weight	Importance
A (C_o)	equal to 25.44	8.48	42.4	1	1	3
B (ΔP)	is in range	1.034	3.79	1	1	3
C (F)	is in range	53.3	54.7	1	1	3
J_v	maximize	12.348	80.6526	1	1	3
$C_{p\ Conductivity}$	minimize	13.2	378	1	1	3
$C_{p\ COD}$	minimize	47.5	439	1	1	3
$\%r_{o\ conductivity}$	maximize	84.069	98.1186	1	1	3
$\%r_{o\ COD}$	maximize	99.0237	99.6573	1	1	3

Table D12

Solutions to Numerical Optimization of Vibratory NF of Coffee Extracts

	C_o (g L^{-1})	ΔP (MPa)	F (Hz)	J_v (L m^{-2} h^{-1})	$C_{p\ Cond}$ (μS cm^{-1})	$C_{p\ COD}$ (mg L^{-1})	$\%r_{o\ cond}$	$\%r_{o\ COD}$	Desirability
1	25.440	3.790	54.700	54.903	112.293	145.833	98.578	99.515	0.742
2	25.440	3.735	54.700	55.201	114.184	147.961	98.413	99.506	0.738
3	25.440	3.790	54.659	52.882	112.511	144.411	98.336	99.518	0.737
4	25.440	3.790	54.424	44.113	113.743	136.380	97.138	99.537	0.699

Appendix E

Supporting Information for Techno-economic and Environmental Assessment

E.1 Modified Scale-up Study

Table E1

Steady State Permeate Conditions for Modified Scale-up Study of Vibratory NF of Coffee Extracts at F = 54.7 Hz, P = 2.76 MPa

Feed Concentration (g L^{-1})	Permeate Flux (L m^{-2} h^{-1})	Permeate Characteristics				
		Conductivity (μS cm^{-1})	pH	Turbidity (NTU)	Abs	COD (mg L^{-1})
50.9	34.31	408	4.219	0.479	0.003	420
	32.97	391	4.284	0.321	0	380
	32.29	467	4.196	0.683	0	450
42.4	41.04	478	4.696	2.67	0.032	210
	39.70	448	4.591	1.43	0.018	900
	41.04	429	4.522	1.27	0.011	310
33.9	59.21	372	4.628	1.01	0	350
	59.88	364	4.478	0.571	0.001	240
	60.55	358	4.382	0.552	0.001	260
25.4	94.40	305	4.439	0.379	0.008	330
	95.21	298	4.442	1.25	0.009	360
	94.19	295	4.45	0.558	0.008	340
21.2	109.00	308	4.358	0.429	0.003	290
	110.34	298	4.301	0.529	0.003	190
	108.32	296	4.268	0.562	0.005	190
17.0	124.47	273	4.135	0.248	0.003	257
	121.11	260	4.15	0.44	0.002	250
	119.76	274	4.23	0.334	0	263
12.7	128.85	99	6.37	0.925	0.003	187
	128.85	93.2	5.83	0.451	0.002	162
	129.18	86.7	5.64	0.429	0.003	162
10.6	139.37	57.9	5.78	0.645	0.001	106
	139.20	50.8	5.6	0.45	0.004	95
	140.82	50.4	5.65	0.318	0.003	92
8.5	144.65	68.5	5.783	1.28	0.005	118
	142.64	64.6	5.531	0.338	0	109
	142.64	63.4	5.463	0.267	0.004	114

Table E2

Steady State Observed Rejection Efficiencies for Modified Scale-up Study of Vibratory NF of Coffee Extracts at F = 54.7 Hz, P = 2.76 MPa

Feed Concentration (g L^{-1})	Rejection Efficiencies (%)			
	$r_{o\ conductivity}$	$r_{o\ turbidity}$	$r_{o\ abs}$	$r_{o\ COD}$
50.9	90.82	99.98	99.93	99.24
	91.21	99.99	100.00	99.31
	89.50	99.97	100.00	99.19
42.4	88.23	99.87	99.24	99.54
	88.97	99.93	99.58	98.01
	89.43	99.94	99.74	99.31
33.9	89.51	99.94	100.00	99.09
	89.74	99.97	99.97	99.38
	89.91	99.97	99.97	99.33
25.4	89.09	99.97	99.75	98.87
	89.34	99.92	99.72	98.76
	89.45	99.96	99.75	98.83
21.2	87.75	99.97	99.90	98.79
	88.14	99.96	99.90	99.21
	88.22	99.96	99.83	99.21
17.0	87.00	99.98	99.88	98.65
	87.62	99.96	99.92	98.69
	86.95	99.97	100.00	98.62
12.7	94.39	99.82	99.83	98.87
	94.72	99.91	99.88	99.02
	95.09	99.92	99.83	99.02
10.6	96.16	99.84	99.93	99.22
	96.63	99.89	99.73	99.30
	96.65	99.92	99.80	99.32
8.5	94.46	99.61	99.56	98.74
	94.78	99.90	100.00	98.84
	94.88	99.92	99.65	98.78

Table E3

Steady State Permeate Conditions for Modified Scale-up Study of Non-Vibratory NF of Coffee Extracts at F = 0 Hz, P = 2.76 MPa

Feed Concentration (g L^{-1})	Permeate Flux (L m^{-2} h^{-1})	Permeate Characteristics				
		Conductivity (μS cm^{-1})	pH	Turbidity (NTU)	Abs	COD (mg L^{-1})
50.9	18.84	451	4.375	0.307	0	440
	17.94	538	4.25	0.202	0	470
	17.04	565	4.402	0.228	0	470
42.4	22.88	515	4.617	0.66	0.002	460
	20.63	506	4.471	0.37	0.009	260
	18.84	526	4.522	0.324	0.004	210
33.9	26.02	455	4.404	0.421	0.001	380
	24.22	450	4.407	0.31	0	370
	21.08	460	4.412	0.326	0	370
25.4	29.60	423	4.569	0.533	0.004	180
	27.81	428	4.522	0.637	0.001	260
	25.12	438	4.566	0.501	0.004	180
21.2	32.74	415	4.4	0.417	0.002	280
	28.71	428	4.404	0.307	0.008	240
	26.46	428	4.417	0.355	0.001	290
17.0	36.33	324	4.26	0.298	0	301
	33.19	332	4.25	0.235	0	322
	31.40	346	4.285	0.222	0	349
12.7	46.99	114.8	5.97	0.222	0	202
	39.88	115.3	5.92	0.229	0.002	192
	36.18	115.8	5.75	0.166	0	189
10.6	52.67	75.8	5.71	0.213	0	120
	47.32	77.6	5.59	0.26	0	130
	41.55	81	5.57	0.173	0	130
8.5	56.30	85.5	5.531	0.194	0.001	127
	51.58	87.5	5.802	0.208	0.001	121
	45.75	90.5	5.84	0.29	0.001	124

Table E4

Steady State Observed Rejection Efficiencies for Modified Scale-up Study of Non-Vibratory NF of Coffee Extracts at F = 0 Hz, P = 2.76 MPa

Feed Concentration ($g\ L^{-1}$)	Rejection Efficiencies (%)			
	$r_{o\ conductivity}$	$r_{o\ turbidity}$	$r_{o\ abs}$	$r_{o\ COD}$
50.9	89.86	99.99	100.00	99.20
	87.90	99.99	100.00	99.15
	87.29	99.99	100.00	99.15
42.4	87.32	99.97	99.95	98.98
	87.54	99.98	99.79	99.42
	87.04	99.98	99.91	99.54
33.9	87.17	99.98	99.97	99.01
	87.31	99.98	100.00	99.04
	87.03	99.98	100.00	99.04
25.4	84.87	99.96	99.88	99.38
	84.70	99.96	99.97	99.11
	84.34	99.97	99.88	99.38
21.2	83.49	99.97	99.93	98.84
	82.97	99.98	99.72	99.00
	82.97	99.97	99.97	98.79
17.0	84.57	99.97	100.00	98.42
	84.19	99.98	100.00	98.31
	83.52	99.98	100.00	98.17
12.7	93.49	99.96	100.00	98.78
	93.46	99.95	99.88	98.84
	93.44	99.97	100.00	98.86
10.6	94.97	99.95	100.00	99.11
	94.85	99.94	100.00	99.04
	94.62	99.96	100.00	99.04
8.5	93.09	99.94	99.91	98.64
	92.93	99.94	99.91	98.71
	92.69	99.91	99.91	98.68

Figure E1

Permeate Flux Correlation Using Film Layer Model for Modified Scale-up Study of Vibratory NF of Coffee Extracts at F = 54.7 Hz, P = 2.76 MPa

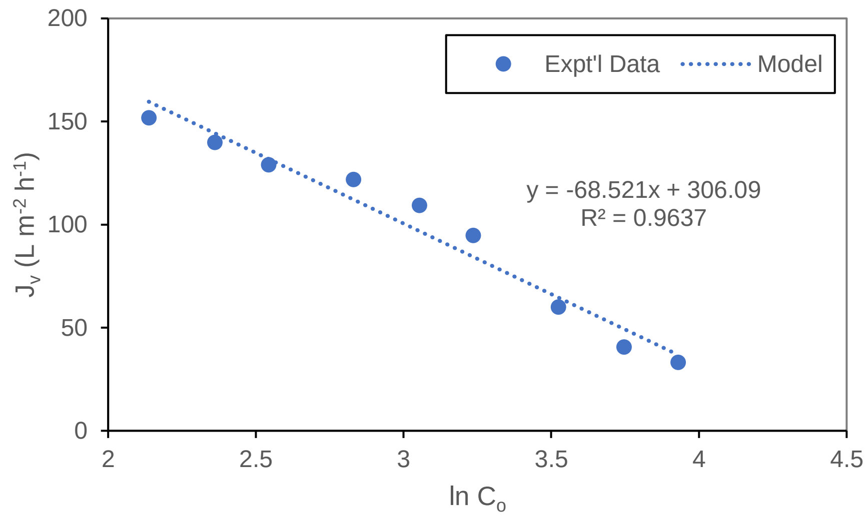

Figure E2

Permeate COD Correlation Using Film Layer Model for Modified Scale-up Study of Vibratory NF of Coffee Extracts at F = 54.7 Hz, P = 2.76 MPa

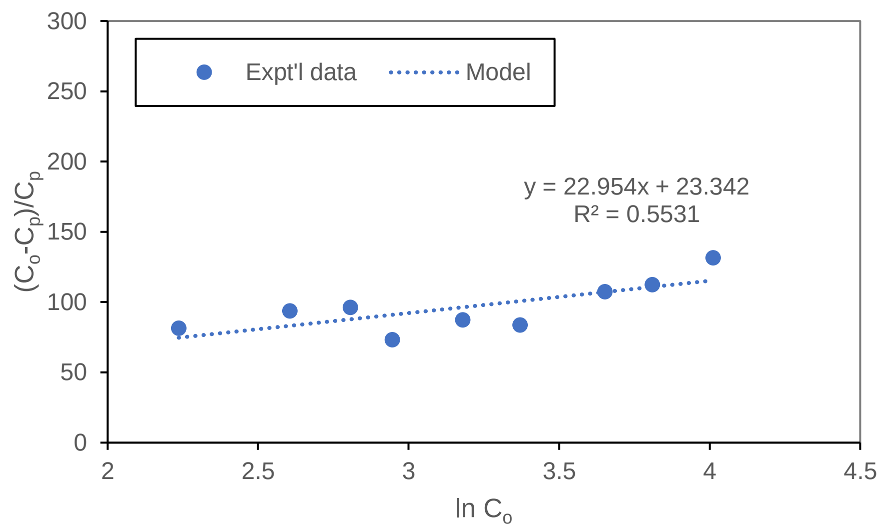

Figure E3

Permeate Conductivity Correlation Using Film Layer Model for Modified Scale-up Study of Vibratory NF of Coffee Extracts at F = 54.7 Hz, P = 2.76 MPa

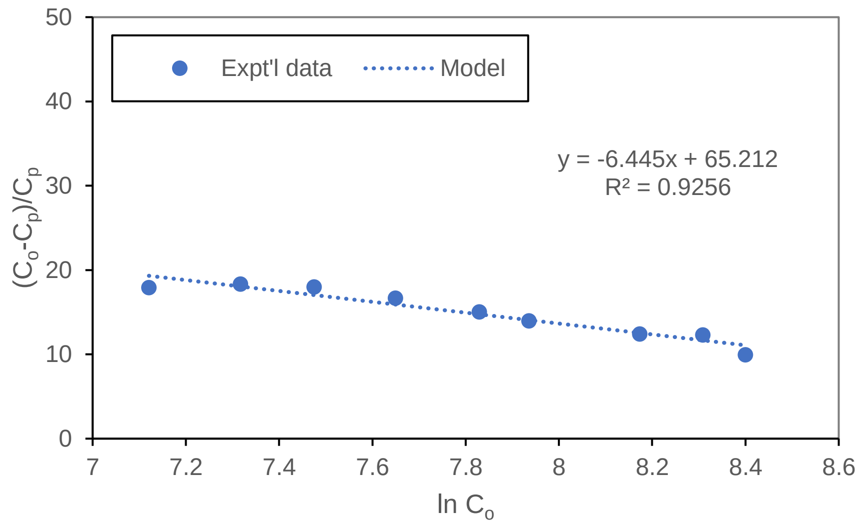

Figure E4

Permeate Flux Correlation Using Film Layer Model for Modified Scale-up Study of Non-Vibratory NF of Coffee Extracts at F = 0 Hz, P = 2.76 MPa

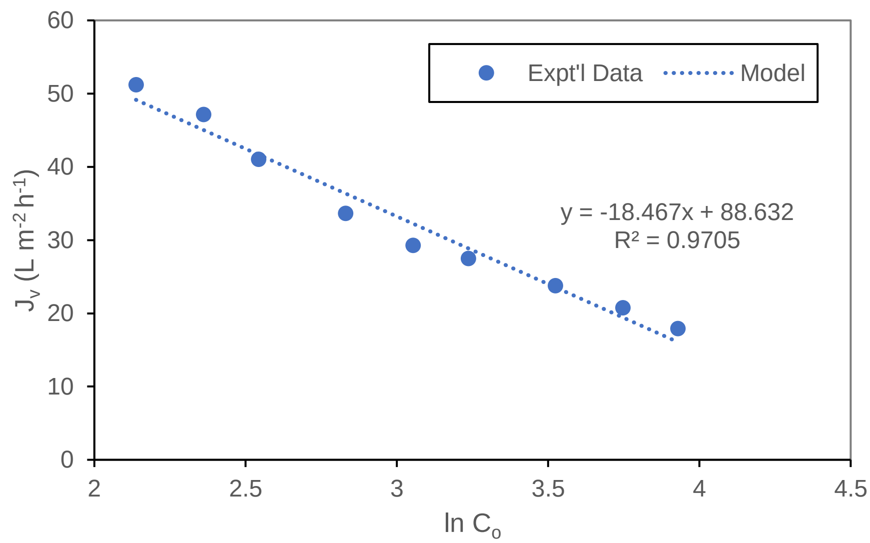

Figure E5

Permeate COD Correlation Using Film Layer Model for Modified Scale-up Study of Non-Vibratory NF of Coffee Extracts at F = 0 Hz, P = 2.76 MPa

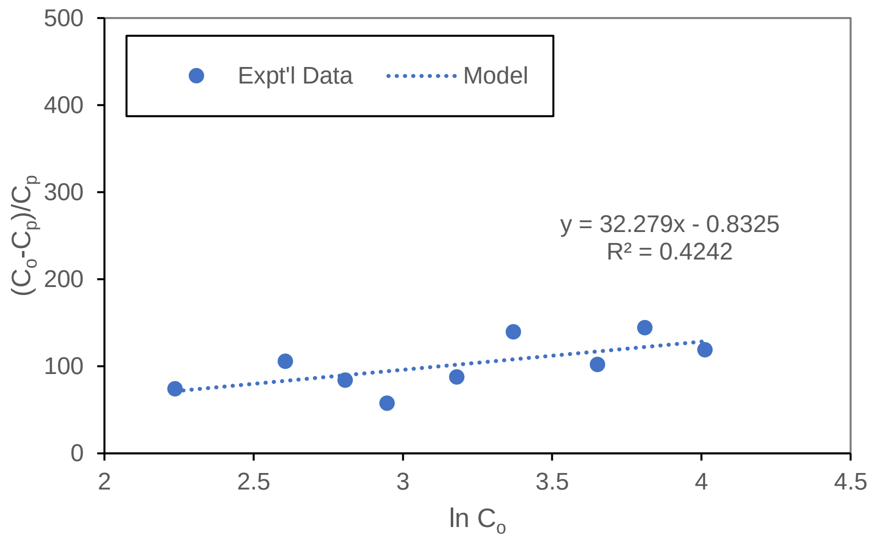

Figure E6

Permeate Conductivity Correlation Using Film Layer Model for Modified Scale-up Study of Non-Vibratory NF of Coffee Extracts at F = 0 Hz, P = 2.76 MPa

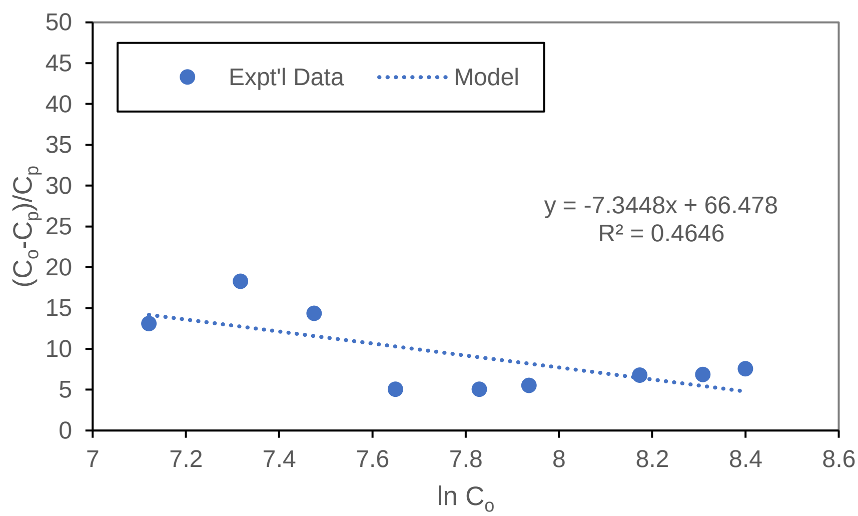

E.2 Life Cycle Emissions and Avoided Emissions for Alternative Cases

Table E5

Life Cycle Emissions (in kg) Associated with Vibratory NF of 8.5 g L^{-1} Coffee Extracts

Emissions	Freshwater	NHW	HW	Electricity	Steam	Total
Total Air Emissions	2.86E+05	9.57E+06	4.20E+03	8.85E+05	0.00E+00	1.07E+07
CO_2	2.84E+05	9.51E+06	4.17E+03	8.71E+05	0.00E+00	1.07E+07
CO	4.67E+01	7.85E+02	3.40E-01	6.31E+02	0.00E+00	1.46E+03
CH_4	3.12E+02	8.40E+03	3.66E+00	4.66E+03	0.00E+00	1.34E+04
NO_X	0.00E+00	1.98E+04	0.00E+00	6.41E+02	0.00E+00	2.05E+04
NMVOC	9.72E+00	2.64E+02	1.15E-01	2.73E+02	0.00E+00	5.47E+02
Particulate	8.80E+02	2.61E+02	1.11E-01	1.74E+02	0.00E+00	1.31E+03
SO_2	3.09E+02	9.54E+03	4.11E+00	8.01E+03	0.00E+00	1.79E+04
Total Water Emissions	6.29E+03	1.24E+05	1.03E+02	1.33E+05	0.00E+00	2.63E+05
VOCs	1.06E-03	3.07E-02	1.34E-05	3.04E-01	0.00E+00	3.36E-01
Total Soil Emissions	3.51E+00	1.05E+02	4.58E-02	9.44E+00	0.00E+00	1.18E+02
Total Emissions	2.93E+05	9.68E+06	4.30E+03	1.02E+06	0.00E+00	1.10E+07

Table E6

Avoided Emissions (in kg) Associated with Vibratory NF of 8.5 g L^{-1} Coffee Extracts

Emissions	Base Case	AC (C_o = 8.5 g L^{-1})	Avoided Emissions	% Avoided
Total Air Emissions	1.80E+07	1.07E+07	7.28E+06	40.4
CO_2	1.79E+07	1.07E+07	7.25E+06	40.5
CO	3.07E+03	1.46E+03	1.61E+03	52.4
CH_4	2.29E+04	1.34E+04	9.48E+03	41.5
NO_X	2.84E+04	2.05E+04	7.94E+03	27.9
NMVOC	7.34E+02	5.47E+02	1.88E+02	25.5
Particulate	1.73E+03	1.31E+03	4.14E+02	23.9
SO_2	2.44E+04	1.79E+04	6.53E+03	26.8
Total Water Emissions	3.55E+05	2.63E+05	9.22E+04	25.9
VOCs	5.84E-01	3.36E-01	2.48E-01	42.5
Total Soil Emissions	2.24E+02	1.18E+02	1.06E+02	47.2
Total Emissions	1.84E+07	1.10E+07	7.37E+06	40.1

Table E7

Life Cycle Emissions (in kg) Associated with Vibratory NF of 1% (wt/wt) Coffee Extracts

Emissions	Freshwater	NHW	HW	Electricity	Steam	Total
Total Air Emissions	2.86E+05	9.57E+06	4.20E+03	8.85E+05	0.00E+00	1.08E+07
CO_2	2.84E+05	9.51E+06	4.17E+03	8.71E+05	0.00E+00	1.07E+07
CO	4.67E+01	7.85E+02	3.40E-01	6.31E+02	0.00E+00	1.46E+03
CH_4	3.12E+02	8.40E+03	3.66E+00	4.66E+03	0.00E+00	1.34E+04
NO_X	0.00E+00	1.98E+04	0.00E+00	6.41E+02	0.00E+00	2.05E+04
NMVOC	9.72E+00	2.64E+02	1.15E-01	2.73E+02	0.00E+00	5.47E+02
Particulate	8.80E+02	2.61E+02	1.11E-01	1.74E+02	0.00E+00	1.31E+03
SO_2	3.09E+02	9.54E+03	4.11E+00	8.02E+03	0.00E+00	1.79E+04
Total Water Emissions	6.29E+03	1.24E+05	1.03E+02	1.33E+05	0.00E+00	2.63E+05
VOCs	1.06E-03	3.07E-02	1.34E-05	3.04E-01	0.00E+00	3.36E-01
Total Soil Emissions	3.51E+00	1.05E+02	4.58E-02	9.45E+00	0.00E+00	1.18E+02
Total Emissions	2.93E+05	9.68E+06	4.30E+03	1.02E+06	0.00E+00	1.10E+07

Table E8

Avoided Emissions (in kg) Associated with Vibratory NF of 1% (wt/wt) Coffee Extracts

Emissions	Base Case	AC (C_o = 1%)	Avoided Emissions	% Avoided
Total Air Emissions	1.80E+07	1.08E+07	7.28E+06	40.37
CO_2	1.79E+07	1.07E+07	7.25E+06	40.46
CO	3.07E+03	1.46E+03	1.61E+03	52.41
CH_4	2.29E+04	1.34E+04	9.48E+03	41.49
NO_X	2.84E+04	2.05E+04	7.94E+03	27.94
NMVOC	7.34E+02	5.47E+02	1.87E+02	25.52
Particulate	1.73E+03	1.31E+03	4.14E+02	23.95
SO_2	2.44E+04	1.79E+04	6.53E+03	26.76
Total Water Emissions	3.55E+05	2.63E+05	9.21E+04	25.94
VOCs	5.84E-01	3.36E-01	2.48E-01	42.54
Total Soil Emissions	2.24E+02	1.18E+02	1.06E+02	47.24
Total Emissions	1.84E+07	1.10E+07	7.37E+06	40.13

Table E9

Life Cycle Emissions (in kg) Associated with Vibratory NF of 2% (wt/wt) Coffee Extracts

Emissions	Freshwater	NHW	HW	Electricity	Steam	Total
Total Air Emissions	2.86E+05	9.57E+06	4.20E+03	9.11E+05	0.00E+00	1.08E+07
CO_2	2.84E+05	9.51E+06	4.17E+03	8.96E+05	0.00E+00	1.07E+07
CO	4.67E+01	7.85E+02	3.40E-01	6.50E+02	0.00E+00	1.48E+03
CH_4	3.12E+02	8.40E+03	3.66E+00	4.79E+03	0.00E+00	1.35E+04
NO_X	0.00E+00	1.98E+04	0.00E+00	6.59E+02	0.00E+00	2.05E+04
NMVOC	9.72E+00	2.64E+02	1.15E-01	2.81E+02	0.00E+00	5.55E+02
Particulate	8.80E+02	2.61E+02	1.11E-01	1.79E+02	0.00E+00	1.32E+03
SO_2	3.09E+02	9.54E+03	4.11E+00	8.25E+03	0.00E+00	1.81E+04
Total Water Emissions	6.29E+03	1.24E+05	1.03E+02	1.36E+05	0.00E+00	2.67E+05
VOCs	1.06E-03	3.07E-02	1.34E-05	3.13E-01	0.00E+00	3.44E-01
Total Soil Emissions	3.51E+00	1.05E+02	4.58E-02	9.72E+00	0.00E+00	1.18E+02
Total Emissions	2.93E+05	9.68E+06	4.30E+03	1.05E+06	0.00E+00	1.10E+07

Table E10

Avoided Emissions (in kg) Associated with Vibratory NF of 2% (wt/wt) Coffee Extracts

Emissions	Base Case	AC (C_o = 2%)	Avoided Emissions	% Avoided
Total Air Emissions	1.80E+07	1.08E+07	7.25E+06	40.2
CO_2	1.79E+07	1.07E+07	7.22E+06	40.3
CO	3.07E+03	1.48E+03	1.59E+03	51.8
CH_4	2.29E+04	1.35E+04	9.35E+03	40.9
NO_X	2.84E+04	2.05E+04	7.92E+03	27.9
NMVOC	7.34E+02	5.55E+02	1.80E+02	24.5
Particulate	1.73E+03	1.32E+03	4.09E+02	23.7
SO_2	2.44E+04	1.81E+04	6.30E+03	25.8
Total Water Emissions	3.55E+05	2.67E+05	8.83E+04	24.9
VOCs	5.84E-01	3.44E-01	2.40E-01	41.0
Total Soil Emissions	2.24E+02	1.18E+02	1.05E+02	47.1
Total Emissions	1.84E+07	1.10E+07	7.34E+06	40.0

Table E11

Life Cycle Emissions (in kg) Associated with Vibratory NF of 3% (wt/wt) Coffee Extracts

Emissions	Freshwater	NHW	HW	Electricity	Steam	Total
Total Air Emissions	2.86E+05	9.57E+06	4.20E+03	9.85E+05	0.00E+00	1.08E+07
CO_2	2.84E+05	9.51E+06	4.17E+03	9.69E+05	0.00E+00	1.08E+07
CO	4.67E+01	7.85E+02	3.40E-01	7.03E+02	0.00E+00	1.53E+03
CH_4	3.12E+02	8.40E+03	3.66E+00	5.18E+03	0.00E+00	1.39E+04
NO_X	0.00E+00	1.98E+04	0.00E+00	7.13E+02	0.00E+00	2.06E+04
NMVOC	9.72E+00	2.64E+02	1.15E-01	3.04E+02	0.00E+00	5.78E+02
Particulate	8.80E+02	2.61E+02	1.11E-01	1.93E+02	0.00E+00	1.33E+03
SO_2	3.09E+02	9.54E+03	4.11E+00	8.92E+03	0.00E+00	1.88E+04
Total Water Emissions	6.29E+03	1.24E+05	1.03E+02	1.47E+05	0.00E+00	2.78E+05
VOCs	1.06E-03	3.07E-02	1.34E-05	3.38E-01	0.00E+00	3.70E-01
Total Soil Emissions	3.51E+00	1.05E+02	4.58E-02	1.05E+01	0.00E+00	1.19E+02
Total Emissions	2.93E+05	9.68E+06	4.30E+03	1.13E+06	0.00E+00	1.11E+07

Table E12

Avoided Emissions (in kg) Associated with Vibratory NF of 3% (wt/wt) Coffee Extracts

Emissions	Base Case	AC (C_o = 3%)	Avoided Emissions	% Avoided
Total Air Emissions	1.80E+07	1.08E+07	7.18E+06	39.8
CO_2	1.79E+07	1.08E+07	7.15E+06	39.9
CO	3.07E+03	1.53E+03	1.54E+03	50.1
CH_4	2.29E+04	1.39E+04	8.96E+03	39.2
NO_X	2.84E+04	2.06E+04	7.87E+03	27.7
NMVOC	7.34E+02	5.78E+02	1.57E+02	21.3
Particulate	1.73E+03	1.33E+03	3.94E+02	22.8
SO_2	2.44E+04	1.88E+04	5.63E+03	23.1
Total Water Emissions	3.55E+05	2.78E+05	7.72E+04	21.7
VOCs	5.84E-01	3.70E-01	2.14E-01	36.7
Total Soil Emissions	2.24E+02	1.19E+02	1.05E+02	46.8
Total Emissions	1.84E+07	1.11E+07	7.25E+06	39.5

Table E13

Life Cycle Emissions (in kg) Associated with Vibratory NF of 4% (wt/wt) Coffee Extracts

Emissions	Freshwater	NHW	HW	Electricity	Steam	Total
Total Air Emissions	2.86E+05	9.57E+06	4.20E+03	1.11E+06	0.00E+00	1.10E+07
CO_2	2.84E+05	9.51E+06	4.17E+03	1.09E+06	0.00E+00	1.09E+07
CO	4.67E+01	7.85E+02	3.40E-01	7.91E+02	0.00E+00	1.62E+03
CH_4	3.12E+02	8.40E+03	3.66E+00	5.83E+03	0.00E+00	1.45E+04
NO_X	0.00E+00	1.98E+04	0.00E+00	8.03E+02	0.00E+00	2.06E+04
NMVOC	9.72E+00	2.64E+02	1.15E-01	3.42E+02	0.00E+00	6.16E+02
Particulate	8.80E+02	2.61E+02	1.11E-01	2.18E+02	0.00E+00	1.36E+03
SO_2	3.09E+02	9.54E+03	4.11E+00	1.00E+04	0.00E+00	1.99E+04
Total Water Emissions	6.29E+03	1.24E+05	1.03E+02	1.66E+05	0.00E+00	2.96E+05
VOCs	1.06E-03	3.07E-02	1.34E-05	3.80E-01	0.00E+00	4.12E-01
Total Soil Emissions	3.51E+00	1.05E+02	4.58E-02	1.18E+01	0.00E+00	1.20E+02
Total Emissions	2.93E+05	9.68E+06	4.30E+03	1.27E+06	0.00E+00	1.12E+07

Table E14

Avoided Emissions (in kg) Associated with Vibratory NF of 4% (wt/wt) Coffee Extracts

Emissions	Base Case	AC (C_o = 4%)	Avoided Emissions	% Avoided
Total Air Emissions	1.80E+07	1.10E+07	7.05E+06	39.1
CO_2	1.79E+07	1.09E+07	7.03E+06	39.2
CO	3.07E+03	1.62E+03	1.45E+03	47.2
CH_4	2.29E+04	1.45E+04	8.31E+03	36.4
NO_X	2.84E+04	2.06E+04	7.78E+03	27.4
NMVOC	7.34E+02	6.16E+02	1.19E+02	16.2
Particulate	1.73E+03	1.36E+03	3.70E+02	21.4
SO_2	2.44E+04	1.99E+04	4.51E+03	18.5
Total Water Emissions	3.55E+05	2.96E+05	5.87E+04	16.5
VOCs	5.84E-01	4.12E-01	1.72E-01	29.4
Total Soil Emissions	2.24E+02	1.20E+02	1.03E+02	46.2
Total Emissions	1.84E+07	1.12E+07	7.11E+06	38.7

Table E15

Life Cycle Emissions (in kg) Associated with Vibratory NF of 5% (wt/wt) Coffee Extracts

Emissions	Freshwater	NHW	HW	Electricity	Steam	Total
Total Air Emissions	2.86E+05	9.57E+06	4.20E+03	1.35E+06	0.00E+00	1.12E+07
CO_2	2.84E+05	9.51E+06	4.17E+03	1.33E+06	0.00E+00	1.11E+07
CO	4.67E+01	7.85E+02	3.40E-01	9.66E+02	0.00E+00	1.80E+03
CH_4	3.12E+02	8.40E+03	3.66E+00	7.12E+03	0.00E+00	1.58E+04
NO_X	0.00E+00	1.98E+04	0.00E+00	9.81E+02	0.00E+00	2.08E+04
NMVOC	9.72E+00	2.64E+02	1.15E-01	4.18E+02	0.00E+00	6.92E+02
Particulate	8.80E+02	2.61E+02	1.11E-01	2.66E+02	0.00E+00	1.41E+03
SO_2	3.09E+02	9.54E+03	4.11E+00	1.23E+04	0.00E+00	2.21E+04
Total Water Emissions	6.29E+03	1.24E+05	1.03E+02	2.03E+05	0.00E+00	3.33E+05
VOCs	1.06E-03	3.07E-02	1.34E-05	4.65E-01	0.00E+00	4.97E-01
Total Soil Emissions	3.51E+00	1.05E+02	4.58E-02	1.45E+01	0.00E+00	1.23E+02
Total Emissions	2.93E+05	9.68E+06	4.30E+03	1.56E+06	0.00E+00	1.15E+07

Table E16

Avoided Emissions (in kg) Associated with Vibratory NF of 5% (wt/wt) Coffee Extracts

Emissions	Base Case	AC (C_o = 5%)	Avoided Emissions	% Avoided
Total Air Emissions	1.80E+07	1.12E+07	6.81E+06	37.8
CO_2	1.79E+07	1.11E+07	6.78E+06	37.9
CO	3.07E+03	1.80E+03	1.28E+03	41.5
CH_4	2.29E+04	1.58E+04	7.01E+03	30.7
NO_X	2.84E+04	2.08E+04	7.60E+03	26.7
NMVOC	7.35E+02	6.92E+02	4.28E+01	5.8
Particulate	1.73E+03	1.41E+03	3.22E+02	18.6
SO_2	2.44E+04	2.21E+04	2.28E+03	9.4
Total Water Emissions	3.55E+05	3.33E+05	2.19E+04	6.2
VOCs	5.84E-01	4.97E-01	8.75E-02	15.0
Total Soil Emissions	2.24E+02	1.23E+02	1.01E+02	45.0
Total Emissions	1.84E+07	1.15E+07	6.83E+06	37.2

E.3 Operating Costs and Savings of Alternative Cases

Table E17

Annual Operating Costs and Savings Associated with Vibratory NF of 8.5 g L^{-1} Coffee Extracts

Process Component	Base Case	AC (C_o = 8.5 g L^{-1})	Savings	% Savings
Feedwater	22,360	17,557	4,803.50	21.5
Non-hazardous Wastewater Discharge	503,500	361,198	142,302.08	28.3
BOD Surcharge	20,622	14,701	5,920.65	28.7
TSS Surcharge	20,835	14,853	5,981.88	28.7
Well Pumps	48,100	37,826.14	10,273.86	21.4
Blowers	296,000	211,311.61	84,688.39	28.6
Recovery System		60,500.96	(60,500.96)	-
Evaporator System	416,460		416,459.72	100.0
Total	1,327,876	717,947.02	609,929.13	45.9

Table E18

Annual Operating Costs and Savings Associated with Vibratory NF of 1% (wt/wt) Coffee Extracts

Process Component	Base Case	AC (C_o = 1%)	Savings	% Savings
Feedwater	22,360.00	17,556.50	4,803.50	21.5
Non-hazardous Wastewater Discharge	503,500.00	361,197.92	142,302.08	28.3
BOD Surcharge	20,621.59	14,700.94	5,920.65	28.7
TSS Surcharge	20,834.83	14,852.96	5,981.88	28.7
Well Pumps	48,100.00	37,826.14	10,273.86	21.4
Blowers	296,000.00	211,311.61	84,688.39	28.6
Recovery System		60,534.17	(60,534.17)	-
Evaporator System	416,446.72		416,446.72	100.0
Total	1,327,863.15	717,980.22	609,882.93	45.9

Table E19

Annual Operating Costs and Savings Associated with Vibratory NF of 2% (wt/wt) Coffee Extracts

Process Component	Base Case	AC (C_o = 2%	Savings	% Savings
Feedwater	22,360	17,557	4,804	21.5
Non-hazardous				
Wastewater Discharge	503,500	361,198	142,302	28.3
BOD Surcharge	20,622	14,701	5,921	28.7
TSS Surcharge	20,835	14,853	5,982	28.7
Well Pumps	48,100	37,826	10,274	21.4
Blowers	296,000	211,312	84,688	28.6
Recovery System	-	94,575	(94,575)	-
Evaporator System	416,453	-	416,453	100.0
Total	1,327,870	752,021	575,849	43.4

Table E20

Annual Operating Costs and Savings Associated with Vibratory NF of 3% (wt/wt) Coffee Extracts

Process Component	Base Case	AC (C_o = 3%)	Savings	% Savings
Feedwater	22,360	17,557	4,804	21.5
Non-hazardous				
Wastewater Discharge	503,500	361,198	142,302	28.3
BOD Surcharge	20,622	14,701	5,921	28.7
TSS Surcharge	20,835	14,853	5,982	28.7
Well Pumps	48,100	37,826	10,274	21.4
Blowers	296,000	211,312	84,688	28.6
Recovery System	-	157,716	(157,716)	-
Evaporator System	416,467	-	416,467	100.0
Total	1,327,883	815,162	512,721	38.6

Table E21

Annual Operating Costs and Savings Associated with Vibratory NF of 4% (wt/wt) Coffee Extracts

Process Component	Base Case	AC (C_o = 4%)	Savings	% Savings
Feedwater	22,360	17,557	4,804	21.5
Non-hazardous Wastewater Discharge	503,500	361,198	142,302	28.3
BOD Surcharge	20,622	14,701	5,921	28.7
TSS Surcharge	20,835	14,853	5,982	28.7
Well Pumps	48,100	37,826	10,274	21.4
Blowers	296,000	211,312	84,688	28.6
Recovery System	-	262,819	(262,819)	-
Evaporator System	416,476	-	416,476	100.0
Total	1,327,893	920,265	407,628	30.7

Table E22

Annual Operating Costs and Savings Associated with Vibratory NF of 5% (wt/wt) Coffee Extracts

Process Component	Base Case	AC (C_o = 5%)	Savings	% Savings
Feedwater	22,360	17,557	4,804	21.5
Non-hazardous Wastewater Discharge	503,500	361,198	142,302	28.3
BOD Surcharge	20,622	14,701	5,921	28.7
TSS Surcharge	20,835	14,853	5,982	28.7
Well Pumps	48,100	37,826	10,274	21.4
Blowers	296,000	211,312	84,688	28.6
Recovery System	-	472,802	(472,802)	-
Evaporator System	416,491	-	416,491	100.0
Total	1,327,907	1,130,248	197,659	14.9

Appendix F

Copyright Permissions

F.1 Chapter 7 Text, Figures, and Tables

Copyright Clearance Center RightsLink®

Home | Help | Email Support | Sign in | Create Account

Optimization of vibratory nanofiltration for sustainable coffee extract concentration via response surface methodology

Author: Michael Vincent O. Laurio, , Kirti M. Yenkie, et al

Publication: Separation Science and Technology

Publisher: Taylor & Francis

Date: Feb 8, 2021

Rights managed by Taylor & Francis

Thesis/Dissertation Reuse Request

Taylor & Francis is pleased to offer reuses of its content for a thesis or dissertation free of charge contingent on resubmission of permission request if work is published.

BACK   CLOSE

F.2 Chapter 8 Text, Figures, and Tables

Thank you for your order!

Dear Mr. Michael Vincent Laurio,

Thank you for placing your order through Copyright Clearance Center's RightsLink® service.

Order Summary

Licensee:	Mr. Michael Vincent Laurio
Order Date:	Mar 16, 2021
Order Number:	5030840652024
Publication:	Clean Technologies and Environmental Policy
Title:	Process scale-up, economic, environmental assessment of vibratory nanofiltration of coffee extracts for soluble coffee production process intensification
Type of Use:	Thesis/Dissertation
Order Total:	0.00 USD

View or print complete details of your order and the publisher's terms and conditions.

Sincerely,

Copyright Clearance Center